



A GREEN SYNTHESIS OF COLLOIDAL SILVER NANOPARTICLES AND THEIR REACTION WITH OZONE

Franco Cataldo^{[a,b]*}, Ornella Ursini^[a], Giancarlo Angelini^[a]

Keywords: silver nanoparticles; colloidal silver; NaBH₄; tannic acid (tannin); ozone; oxidized silver nanoparticles

Colloidal silver nanoparticles were prepared by a conventional reduction of Ag⁺ ions with NaBH₄ and with a novel approach using tannic acid (tannin) as reducing agent of Ag⁺ ions. The formation of colloidal silver was followed by electronic absorption spectroscopy monitoring the growth of the surface-plasmon resonance band of the nanoparticles. Colloidal silver in tannin is more stable than that prepared with NaBH₄ because tannin exerts also a protective colloid function permitting to reach much higher colloidal silver concentration than in the case of NaBH₄. Colloidal silver nanoparticles are readily reactive with ozone producing oxidized silver nanoparticles composed by the mixed oxide Ag₂O₂ formulated as Ag^IAg^{III}O₂. If the ozonization is conducted in gentle conditions the oxidized silver nanoparticles remain as colloidal suspension for a certain time. If instead mechanical shaking is applied, the particles coagulate immediately and separate from the liquid medium as a precipitate.

* Corresponding Authors

E-Mail: franco.cataldo@fastwebnet.it

- [a] CNR-Istituto di Metodologie Chimiche, Area della Ricerca di Montelibretti, Via Salaria Km 29,300, 00016, Monterotondo, Scalo, Rome, Italy
- [b] Lupi Chemical Research srl, Via Casilina 1626A, 00133 Rome, Italy

Introduction

Metal nanoparticles sols such as silver and gold nanoparticles in water and in other media are known since long time as silver and gold colloids.¹⁻⁶ These colloidal solutions are characterized by their color which today we know as due to surface plasmon resonance whose origin is attributed to the collective oscillation of the free conduction electrons induced by an interacting electromagnetic field form incident photon radiation.⁷ Another feature of these solutions regards the Tyndall effect which consists in the light scattering caused by the dispersed metal nanoparticles.⁶ In recent times, the interest on nanomaterials and their applications has re-awakened the attention on metal nanoparticles colloidal dispersion.⁸⁻¹⁰

The simplest way to produce a silver lyosol is by electrospattering, a technique involving the submerged electric arc between two silver electrodes submerged into distilled water. The arc vaporizes the electrodes and the metal vapour is quenched under the form of nanoclusters inside the liquid medium surrounding the electrodes.⁶ The method is general and can be applied also to other metals other than silver. However the lyosol prepared in this way suffers from a certain instability because of the lack of a stabilizing electrolyte or other agent which must be added purposely. Also in recent times variants of the electrospattering have been proposed involving water-submerged spark discharge^{11,12} as well as the submerged arc discharge.¹³

A less common method for the preparation of silver nanoparticles dispersion regards the use of high intensity

ultrasonic waves in order to fragmentate and disperse the metal particles.¹⁴ An approach which is not new, since was reported in literature since long time.¹⁵

The advent of the radiation chemistry led to the radiolytic reduction in solution of metal salts into colloidal solutions.¹⁶⁻¹⁸ This approach is currently in use for the production of metal nanoparticles dispersions.^{19,20} Photolysis²¹ and laser ablation are other approaches using electromagnetic radiation to produce metal nanoparticle dispersions in liquids.²²

The preferred method for the production of metal colloidal solution in general and silver colloids in particular was and remains the chemical approach.^{6-10,23-26} Such a method consists in the addition of Ag⁺ ions to a solution of a reducing agent taking care to work at high dilution. A number of reducing agents are known as effective in the reduction of silver in a colloidal state. Tolaymat et al.⁸ have even made a complete statistics of the various methods used and among the chemical reduction the preferred approach regards the use of NaBH₄ as the reducing agent followed by citrate, amines, formaldehyde and aldehydes, ascorbic acid, sugars and polysaccharides and hydrogen. The advantage of the chemical reduction of silver regards the fact that the reducing agent acts also as a stabilizer of the colloid. It is for example the case of citric acid and citrates or sugars and polysaccharides.⁸ A typical use of citrate reduction of Ag⁺ ions regards the preparation of silver nanoparticles useful for surface enhanced Raman scattering application.²⁷

Tannic acid, known also as gallotannic acid and tannin is extracted from different plant sources or from plant galls and its chemical structure is a mixture of molecules of pentadigalloylglucose and pentagalloylglucose.^{28,29} It forms colloidal solutions in water and it is a reducing agent used to treat leather and also in medicine as astringent.^{28,29} Tannic acid is not toxic and could be suitably combined with colloidal silver to stabilize the resulting lyosol. In this work we will show that tannic acid from renewable sources is an effective reducing agent of Ag⁺ solutions forming colloidal silver nanoparticles which are stabilized by the tannin.

Experimental

Materials and Equipment

Silver nitrate (AgNO_3) and sodium borohydride NaBH_4 were analytical grades from Sigma-Aldrich. Tannic acid was obtained from Rhiedel de Haen. The electronic absorption spectra were recorded on a Shimadzu UV 2450 spectrophotometer.

Colloidal silver from AgNO_3 reduction with NaBH_4

Reference colloidal silver solutions were prepared following the procedure reported in ref.²⁴ A solution of NaBH_4 2.38×10^{-3} M was prepared and, separately, another solution of AgNO_3 1.32×10^{-3} M. Then, 2 to 8 ml of the AgNO_3 solution were added to 40 ml of NaBH_4 under stirring. After the addition, the stirring was stopped and the electronic absorption spectra of the resulting yellow solutions were recorded. The following solutions were prepared:

#1: $[\text{Ag}]_{\text{colloidal}} = 8.25 \times 10^{-5}$ M = 8.9 mg L⁻¹ → Stable

#2: $[\text{Ag}]_{\text{colloidal}} = 1.20 \times 10^{-4}$ M = 12.9 mg L⁻¹ → Stable

#3: $[\text{Ag}]_{\text{colloidal}} = 1.72 \times 10^{-4}$ M = 18.6 mg L⁻¹ → Unstable

#4: $[\text{Ag}]_{\text{colloidal}} = 2.64 \times 10^{-4}$ M = 28.5 mg L⁻¹ → Unstable

The first two appeared indefinitely stable while the last two start to become turbid few hours after preparation and then become completely grey with evident silver sedimentation after 1 day from preparation.

Ozone treatment of the colloidal silver #2

An assay of 20 ml of solution #2 was transferred into a 500 ml flask. The flask was evacuated and the was filled with a mixture of O_3 and O_2 with the former 5% by mol in the gas phase. The colloidal solution was shaken in ozone and immediately it was bleached from the starting yellow color becoming slightly grey and turbid because of the resulting argentic oxide precipitation. In another test, 20 ml of solution #2 in 500 ml flask with O_3/O_2 was not shaken at all but just rolled up on the internal surface of the flask. Ozone reacted immediately with the silver particles causing a discoloration from yellow to water-white but this time there was no separation of oxidized silver because the solution was not shaken. However, on standing, after several hours, Ag_2O_2 separated from the aqueous phase also in this case.

Colloidal silver from AgNO_3 and tannic acid

Tannic acid (35 mg) was dissolved in 150 ml of distilled water. From this stock solution 20 ml were diluted with distilled water to a final volume of 60 ml. Then K_2CO_3 (30 mg) were added to the 60 ml of tannic acid solution. The addition of potassium carbonate causes a slight darkening of the solution. To the 60 ml of tannic acid, the solution of silver nitrate 1.32×10^{-3} M was added. After the addition of

each ml of silver nitrate under stirring the spectrum of the solution was recorded. The following table reports the concentration of colloidal silver [Ag] present in the tannic acid solution after the gradual addition of silver. A gradual darkening of the solution was observed as function of the amount of silver added. The solution became brown and gradually dark-brown.

Table 1. Colloidal silver concentration in tannic acid solution

Entry	[Ag], mol L ⁻¹	[Ag], mg L ⁻¹
#5	1.63×10^{-5}	1.8
#6	3.22×10^{-5}	3.5
#7	4.77×10^{-5}	5.1
#8	7.76×10^{-5}	8.4
#9	1.06×10^{-4}	11.5
#10	1.33×10^{-4}	14.4
#11	1.60×10^{-4}	17.2
#12	1.85×10^{-4}	19.9
#13	2.08×10^{-4}	22.5
#14	2.42×10^{-4}	26.1

Ozone treatment of the colloidal silver #14 in tannic acid

The solution #14 of colloidal silver in tannic acid is stable and dark-brown. To run the ozonolysis experiment, 30 ml of the solution #14 was diluted with 30 ml of distilled water. The resulting solution was charged into a 500 ml flask which was evacuated and the O_3/O_2 mixture was added into the flask which was shaken. This operation causes the immediate discoloration of the solution from brown to transparent but it appeared light turbid and grey for the separation of oxidized silver: Ag_2O_2 . The same ozonolysis experiment was repeated again with a new diluted sample of #14 avoiding, this time, to shake the solution but just rolling the solution on the walls of the flask filled with the O_3/O_2 mixture. Also in this case the discoloration of the solution was complete without oxidized silver particles separation. Consequently the solution was water-white and not light grey as in the previous case when it was shaken. However, on standing, after several hours, Ag_2O_2 separated from the aqueous phase also in this case.

Results and Discussion

Colloidal silver from AgNO_3 reduction with NaBH_4

The reduction of AgNO_3 with NaBH_4 is the most popular approach for the preparation of silver nanoparticles.^{8,24} We have repeated this preparation to use it as a reference for our study on the action of tannic acid as reducing and stabilizing agent for silver nanoparticles. The electronic absorption spectra of Fig. 1 show the surface-plasmon resonance feature of the yellow solutions #3 and #4 prepared by the reduction of Ag^+ with NaBH_4 . The thick black and red curves were recorded respectively on solutions #3 and #4 immediately after preparation. The peaks are located respectively at 392.5 and 389.6 nm. Similar spectra were obtained from solutions #1 and #2 not shown in Fig. 1 with the surface-plasmon resonance peaks again at about 393 nm.

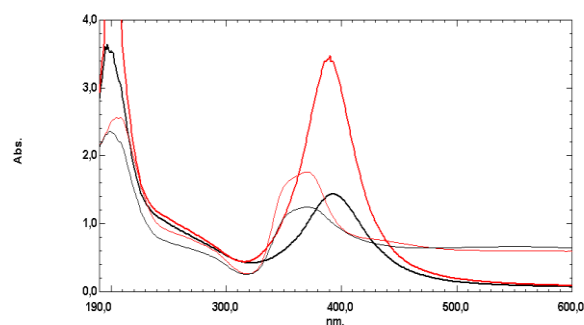
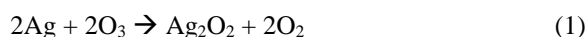


Figure 1. Electronic absorption spectra showing the surface-plasmon resonance of silver nanoparticles obtained by reduction of Ag^+ with NaBH_4 . The thick black and red curves were recorded respectively on solutions #3 and #4 immediately after preparation. The peaks are located respectively at 392.5 and 389.6 nm. The two solutions are unstable and after few hours from the preparation appear cloudy because of the separation of silver in larger particles. The two thin black and red curves refer to these aged #3 and #4 solutions. Note the growth of the baseline from 400 to 600 nm due to intense light scattering. Note also the alteration of the surface-plasmon resonance spectra which appear blue shifted to 370 nm and irregularly broadened.

However, the two solutions #1 and #2 having an $[\text{Ag}]_{\text{colloidal}}$ of 83 and 120 $\mu\text{mol L}^{-1}$ respectively are indefinitely stable while the two solutions #3 and #4 $[\text{Ag}]_{\text{colloidal}}$ of 172 and 264 $\mu\text{mol L}^{-1}$ respectively are unstable and after few hours from the preparation appear cloudy because of the separation of silver in larger particles. The two thin black and red curves shown in Fig. 1 were taken after the “ageing” of the #3 and #4 solutions respectively, when silver started to separate under the form of macroscopic particles and to precipitate. The evidence of silver separation from the solution is clearly suggested by the growth of the baseline of Fig. 1 (thin black and red lines) in the spectral range comprised from 400 to 600 nm due to intense light scattering. Note also the alteration of the surface-plasmon resonance spectra which appear blue shifted to 370 nm and irregularly broadened when silver clusters start to precipitate from the formerly colloidal suspension.

Action of O_3 on colloidal silver solution prepared from Ag^+ and NaBH_4

Metallic silver is reactive with ozone forming argentic oxide³⁰ which is known to be a mixed Ag(I) and Ag(III) oxide^{31,32} $\text{Ag}^{\text{I}}\text{Ag}^{\text{III}}\text{O}_2 = \text{Ag}_2\text{O}_2$ according to:



Ag_2O_2 is a black and insoluble compound.³⁰⁻³² When ozone is added to the colloidal silver nanoparticles its reaction with metallic silver according to the above mentioned reaction (1) leads to the immediate destruction of the surface-plasmon resonance band at 393 nm as shown in Fig. 2.

This is completely in line with the theoretical expectation since that band is due to the interaction between the conduction band electrons of the metal with the incident electromagnetic radiation. Since the metal is oxidized to the oxide Ag_2O_2 , the conduction band electrons are no more available to interact with the electromagnetic radiation with the consequent disappearance of the band at 393 nm.

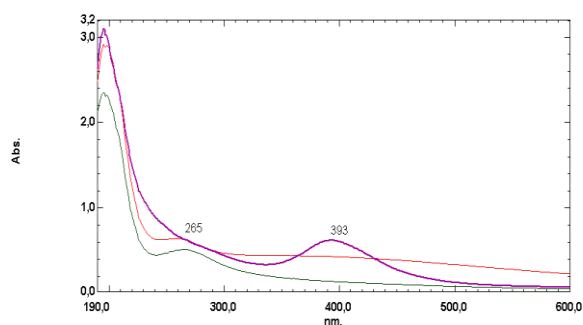


Figure 2. Electronic absorption spectra of the colloidal silver solution #2 showing the surface-plasmon resonance feature at 393 nm (thick violet curve). The thin red line is the resulting spectrum after the addition of O_3 under mechanical shaking. The band at 393 nm is lost and a broad light scattering can be observed by the high baseline between 300 and 600 nm due to the separation of large oxidized silver particles. The thin green curve shows the product derived from the addition of O_3 to solution #2 without shaking; the band at 393 nm is lost but the oxidized silver particles do not aggregate and do not precipitate remaining in the colloidal state.

Fig. 2 shows the spectrum of colloidal silver solution #2 before the ozone treatment with the band at 393 nm and after the ozone treatment, when that band disappeared and only a small and broad band at 265 nm can be observed. Fig. 2 documents also the addition of ozone to colloidal silver solution #2 under shaking, then the oxidized silver particles aggregate in larger particles and precipitate forming a turbid solution as testified by the increase of the baseline of the spectrum (red curve of Fig. 2) due to extensive light scattering caused by the separating solid particles. If instead O_3 is reacted gently with colloidal silver solution #2 avoiding mechanical shaking, then the colloidal silver particles are oxidized but remain in colloidal suspension as shown by the green curve of Fig. 2 where no increase in the baseline is observed after the disappearance of the 393 nm band suggesting the absence of any aggregation and precipitation of the ozone-oxidized silver particles for a certain time.

Colloidal silver from AgNO_3 reduction with tannic acid

Tannic acid or tannin is essentially an hydroxylated polyphenol. Fig. 3 shows the electronic absorption spectrum of tannic acid solution (thick black line) which is characterized by an absorption maximum at 210 nm followed by the benzenoid band at 275 nm. In basic solution, after the addition of potassium carbonate, the benzenoid band of tannin appears at 323 nm (thick red line). As detailed in the experimental, silver ions were added to the alkalized tannin solution and the spectra were taken immediately after each Ag^+ addition and displayed in Fig. 3.

The growth of the colloidal silver band at about 410 nm (Fig. 3, see arrow pointing upward) is accompanied by the reduction of the intensity of the band at 323 nm due to the tannin (Fig. 3, see arrow pointing downward). The absorbance data at 410 and 323 nm are plotted in Fig. 4 and show the linear response to the Ag^+ addition.

The consequence of the Ag^+ reduction with tannic acid (which is a polyphenol molecule) is the growth of a new band at about 410 nm which is assigned to the surface-plasmon resonance of the silver nanoparticles.

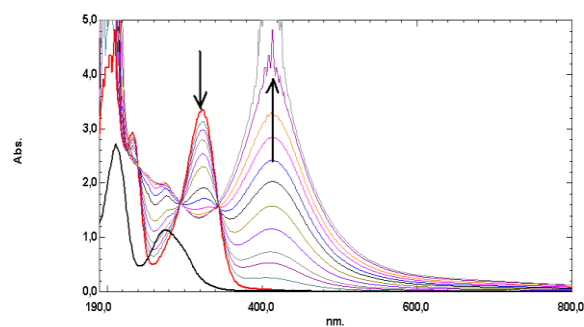


Figure 3. Electronic absorption spectra of pure tannic acid (thick black curve), tannic acid in presence of K_2CO_3 (thick red curve). The addition of silver ions to the tannic acid solution causes a gradual reduction of the band at 323 nm (as indicated by the arrow pointing downward) and the increase of a new band at about 413 nm due to the surface-plasmon resonance of the silver nanoparticles formed by the reduction of Ag^+ (as indicated by the arrow pointing upward).

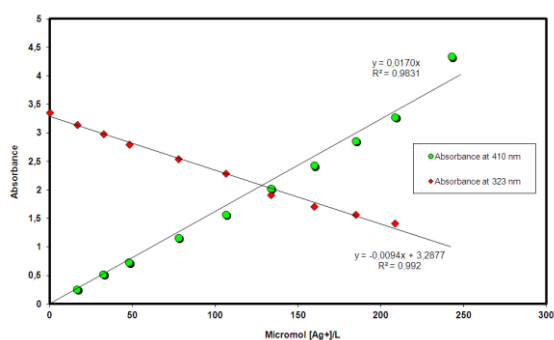


Figure 4. The addition of Ag^+ to the alkalized tannin solution causes a linear grow of the absorbance at about 410 nm due to the formation of metallic silver nanoparticles. At the same time, to the growth of the band at 410 nm corresponds the reduction of the absorbance at 323 nm due to the tannin. Note that the slope of $[Ag]_{410nm} \approx -2[tannin]_{323nm}$.

It is curious to note that the slope of $[Ag]_{410nm} \approx -2[tannin]_{323nm}$ suggesting a possible stoichiometry between silver reduction and amount of tannin oxidized.

From the absorbance and $[Ag]_{410nm}$ concentration data of Fig. 4 using the Lambert and Beer law:

$$\varepsilon = A/bC \quad (2)$$

it is possible to calculate the molar extinction coefficient (in $L mol^{-1} cm^{-1}$) of the surface-plasmon resonance band of colloidal silver in tannin, being $b = 1$ cm the optical pathlength and C the concentration in $mol L^{-1}$ of colloidal silver. All the experimental data of Fig. 4 lead to an $\varepsilon = 15886 L mol^{-1} cm^{-1}$ ($\pm 5.6\%$).

Another feature of the reaction between Ag^+ and tannin regards the red shift of the surface-plasmon resonance band of the resulting colloidal silver. In fact, after the first silver addition the band of colloidal silver appears at 404 nm and is gradually shifted by the continuous silver ions addition to about 414 nm. These experimental data are shown in Fig. 5 and can be fitted with the power law:

$$\lambda = 397.1[Ag]^{0.0077} \quad (3)$$

where λ is the position of the surface-plasmon resonance transition peak and $[Ag]$ is the amount in ($\mu mol L^{-1}$) of the silver ions added (assuming a complete conversion to colloidal metallic silver). Eq.3 implies that the limiting value of the maximum absorption of the surface-plasmon resonance is about 397 nm for the system silver/tannin and then it is red shifted by the continuous addition of silver.

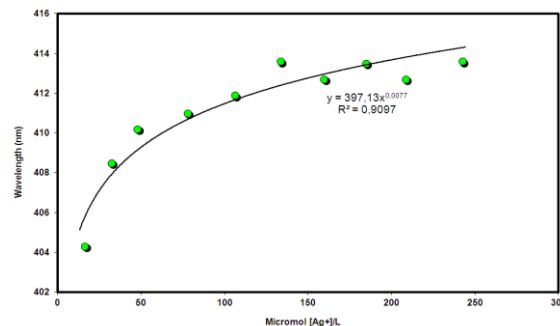


Figure 5. The addition of Ag^+ to tannin causes a gradual red shift of the surface-plasmon resonance of the resulting colloidal silver. This phenomenon is due to the growth of the dimension of the colloidal particles as function of the silver addition.

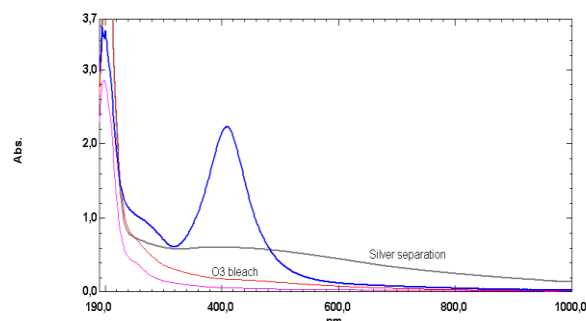
This phenomenon is due to the growth of the dimensions of the colloidal particles as function of the silver addition and it is well known and has been observed also in other cases of colloidal silver systems.^{16,20} After all, the continuous addition of Ag^+ causes an increase in the dimensions of the colloidal particles which is reflected in the red shift of the surface-plasmon resonance band. Fig 5 shows that large part of the experimental values are comprised between 410 and 413 nm so that the spherical particles of colloidal silver may have a diameter comprised between 10-20 nm.²⁰

The threshold of colloidal instability in the system formed from the reduction of Ag^+ with $NaBH_4$ lies above $120 \mu mol L^{-1}$ or above $13 mg L^{-1}$ of silver. In the case of silver colloid prepared by the action of tannin on Ag^+ , we have reached a concentration of colloidal silver of $242 \mu mol L^{-1}$ corresponding to $26 mg L^{-1}$ of silver, the double of the previous system without finding a threshold of instability which, evidently lies at higher concentrations. This implies that tannin is not only an effective reducing agent for the production of colloidal silver but it is also a powerful stabilizer of the colloidal silver, in other words it works also as a protective colloid.

Action of O_3 on colloidal silver solution prepared from Ag^+ and tannin

Ozone was used to oxidize the colloidal silver particles to Ag_2O_2 . In principle, the surface oxidation should improve the interaction between the colloid and the aqueous phase enhancing its stability. However, mechanical shaking of the solutions led to the separation of silver or Ag_2O_2 from the solution. Furthermore, tannin is a protective colloid towards colloidal silver. However, as shown in Fig. 6 the addition of O_3 with mechanical shaking to silver colloid produced from Ag^+ and tannin causes not only the disappearance of the surface-plasmon resonance band at about 413 nm but the separation of oxidized silver particles (grey line with high baseline and broad peak at about 400 nm). Instead the

ozonolysis of the silver colloid without shaking leads only to the bleaching of the surface-plasmon resonance band but not to the coagulation and separation of the resulting oxidized



silver particles (red and pink lines).

Figure 6. Electronic absorption spectrum of colloidal silver in tannin (blue curve). The addition of O₃ with mechanical shaking causes not only the disappearance of the surface-plasmon resonance band at about 413 nm but the separation of oxidized silver particles (grey line with high baseline and broad peak at about 400 nm). Instead the ozonolysis of the silver colloid without shaking leads only to the bleaching of the surface-plasmon resonance band but not to the coagulation and separation of the resulting oxidized silver particles (red and pink lines).

Conclusions

Tannic acid (tannin) an extract from plants and gall nuts is an almost non-toxic (LD₁₀₀ = 6.0 g kg⁻¹ per os, mice)²⁹ reducing agent from renewable sources. It is effective in the reduction of Ag⁺ ions yielding colloidal silver solutions which are very stable even after very long storage time at relatively high silver concentration. A concentration of 242 μmol L⁻¹ corresponding to 26 mg L⁻¹ of silver is completely stable for months and probably higher colloidal silver concentrations can be reached without problems. On the contrary, colloidal silver prepared by a conventional reducing agent like NaBH₄ is already unstable at concentrations above 120 μmol L⁻¹ corresponding to 13 mg L⁻¹. It is evident that tannin is not only a reducing agent but it exerts also a protective colloidal function against the colloidal silver particles which are maintained in the colloidal state even at relatively high concentrations. This aspect may be important in the potential use of colloidal silver stabilized with tannin as medicine or as disinfectant and sterilant. The colloidal silver prepared with tannin exhibits the typical surface-plasmon resonance band at about 413 nm with a molar extinction coefficient of 15886 L mol⁻¹ cm⁻¹. A dependence of the surface-plasmon resonance band position in the electronic spectrum with the amount of colloidal silver has been found also in the case of colloidal silver prepared with tannin, as observed also in other systems. The exposure of colloidal silver particles to ozone leads to a quick bleaching of the surface-plasmon resonance band and the solution turns from yellow to water-white. The reason of this is due to the high reactivity of silver with ozone which leads to the formation of Ag₂O₂.³⁰⁻³² Consequently, the colloidal silver nanoparticles are converted into oxidized silver nanoparticles once exposed to ozone. If the ozonolysis is conducted in gentle conditions without shaking, the oxidized silver nanoparticles remain in the colloidal suspension for a while. Thus, it is quite easy to prepare a colloidal solution of oxidized silver nanoparticles:

it is only necessary to expose to ozone the colloidal silver particles. If instead the action of ozone on colloidal particles is conducted by shaking the solution with the gas, then the oxidized silver nanoparticles immediately coagulate together and separate from the solution as a dark-grey precipitate.

References

- Lettermoser, A., *J. Prakt. Chem.*, **1903**, 68, 357.
- Schaum, K., Lane, H., *Kolloid Z.*, **1921**, 28, 243.
- Guthier, A., Huber, J., Kuppinger, O., *Ber. Deutsch. Chem. Ges.*, **1922**, 55, 748.
- Britzinger, H., *Kolloid Z.*, **1937**, 78, 22.
- Wiegel, E., *Z. Phys.*, **1954**, 136, 642.
- Voyutsky, S. "Colloid Chemistry" Mir Publishers, Moscow, **1978**, Chapter 8.
- Link, S. El-Sayed, M.A. *J. Phys. Chem., B*, **1999**, 103, 4212.
- Tolaymat, T.M., El Badawy, A.M., Genaidy, A., Scheckel, K.G., Luxton, T.P., Suidan, M. *Sci. Total Environ.*, **2010**, 408, 999.
- Dallas, P., Sharma, V.K., Zboril, R., *Adv. Colloid Interface Sci.*, **2011**, 166, 119.
- Murphy, C.J., Gole, A.M., Hunyadi, S.E., Orendorff, C.J., *Inorg. Chem.* **2006**, 45, 7544.
- Tien, D.C., Tseng, K.H., Liao, C.Y., Tsung, T.T., *Med. Eng. Phys.*, **2008**, 30, 948.
- Tien, D.C., Tseng, K.H., Liao, C.Y., Tsung, T.T., *J. Alloys Compds.*, **2009**, 473, 298.
- Ashkarran, A.A., *Current Appl. Phys.*, **2010**, 10, 1442.
- Darroudi, M., Zak, A.K., Muhamad, M.R., Huang, N.M. Hakimi, M. *Mater. Lett.*, **2012**, 66, 117.
- Suslik, K. S. "Ultrasound. Its Chemical, Physical and Biological Effects" VCH Publishers, Weinheim, **1989**.
- Henglein, A., *Chem. Mater.*, **1998**, 10, 444.
- Henglein, A., Meisel, D., *Langmuir* **1998**, 14, 7392.
- Henglein, A., *Langmuir* **1999**, 15, 6738.
- Choi, S.H., Lee, S.H., Hwang, Y.M., Lee, K.P., Kang, H.D., *Radiat. Phys. Chem.*, **2003**, 67, 517.
- Li, T., Park, H.G., Choi, S.H. *Mater. Chem. Phys.*, **2007**, 105, 325.
- Linnert, T., Mulvaney, P., Henglein, A., Weller, H., *J. Am. Chem. Soc.*, **1990**, 112, 4657.
- Darroudi, M., Ahmad, M.B., Zamiri, R., Abdullah, A.H., Ibrahim, N.A., Sadrolhosseini, A.R., *Solid State Sci.*, **2011**, 13, 520.
- Guzmán, M.G., Dille, J., Godet, S. *Int. J. Chem. Biomol. Eng.*, **2009**, 2:3, 104.
- Solomon, S.D., Bahadory, M., Jeyarajasingam, A.V., Rutkowsky, S.A., Boritz, C., Mulfinger, L. *J. Chem. Educ.*, **2007**, 84, 322.
- Petica, A., Gavrilu, S., Lungu, M., Buruntea, N., Panzaru, C., *Mater. Sci. Eng. B*, **2008**, 152, 22.
- Rai, M., Yadav, A., Gade, A., *Biotechnol. Adv.*, **2009**, 27, 76.
- Lucotti, A., Casari, C.S., Tommasini, M., Li Bassi, A., Fazzi, D., Russo, V., Del Zoppo, M., Castiglioni, C., Cataldo, F., Bottani, C.E., Zerbi, G., *Chem. Phys. Lett.* **2009**, 478, 45.
- Steglich, W., Fugmann, B., Lang-Fugmann, S. (eds.) "Rompp Encyclopedia of Natural Products" Georg Thieme Verlag, Stuttgart, **2000**, p.630-631.

²⁹Budavari, S. (ed.) “*The Merck Index*” 12th Ed. Merck Research Laboratories, Whitehouse Station, **1996**, p.9221.

³⁰Thompson, N.R., “*Silver*” Chapter 28 in “*Comprehensive Inorganic Chemistry*” edited by Bailar, J.C., Emeleus, H.J., Nyholm, R., Trotman-Dickenson, A.F., Pergamon Press, Oxford, **1973**, Vol. 3, p. 119.

³¹Waterhouse, G.I.N., Bowmaker, G.A., Metson, J.B., *Appl. Surf. Sci.* **2001**, *183*, 191.

³²Waterhouse, G.I.N., Metson, J.B., Bowmaker, G.A., *Polyhedron* **2007**, *26*, 3310.

Received: 30.03.2013.

Accepted: 26.04.2013.



CHROMIUM ADSORPTION KINETICS FROM AQUEOUS METAL SOLUTIONS USING CHITOSAN

Uzma Nadeem

Keywords: chitosan; intraparticle diffusion rate model; adsorption; chromium(VI); hazardous; wastewater

The paper discusses the kinetics of chromium(VI) ions adsorption from aqueous solutions using chitosan at 25 °C and pH 5. The intraparticle diffusion rate constants (K_{id} and C_i) determined for chitosan are 0.487 mg g⁻¹ min^{-1(1/2)} and 11.66 mg g⁻¹ respectively. The results show that the intraparticle diffusion model fits the sorption of chromium(VI) with higher coefficient of determination (R^2), thereby indicating the intraparticle diffusion may be rate limiting step for chromium(VI) adsorption. The results from this study indicate that chitosan is a good adsorbent for the removal of chromium(VI) from wastewater.

Corresponding Author*

Tel.: (+91) (011) 9711870215

E-Mail: uzmanadeem3@gmail.com

[a] Department of Chemistry, University of Delhi, Delhi-110007, India

Introduction

Heavy metal ions are toxic pollutants, some of these are cumulative poisons capable of being assimilated, stored and concentrated by organisms that are exposed to low concentration of these substances for long period or repeatedly for short period.¹ The anthropogenic sources of heavy metals include waste from the electroplating and metal finishing industries, metallurgical industries, tannery operations, chemical manufacturing, mine drainage, battery manufacturing, leachates from landfills and contaminated groundwater from hazardous waste sites.^{2,3} The use of chromate and dichromate in metal plating and as corrosion control agents in cooling waters is quite extensive. It is well known that chromium(VI) is toxic to living systems and must be removed from wastewater before it can be discharged. Current treatment for the removal of chromium(VI) involves acid catalyzed chemical reduction to chromium(III). The chromium(III) is then precipitated as hydroxide at alkaline conditions using either caustic or lime.⁴ Unfortunately this method is expensive and requires the use of contaminating products for desorption of metals for cleaning up of the inorganic matrix. Physico-chemical methods presently in use have several disadvantages such as unpredictable metal ion removal, high reagent requirements, formation of sludge and its disposal in addition to high installation and operational costs.⁵ Natural materials that are available in large quantities or certain waste from agricultural operations may have potential to be used as low cost adsorbents, as they represent unused resources, widely available and are environmental friendly.⁶ In recent years studies on polymers, which bind metal ions, have increased significantly. Studies on the polymer metal complexes are of great practical importance. Complexing ability of polymers is used in nuclear chemistry, electrochemistry, hydrometallurgy and environmental protection. Of particular significance among many methods of metal ion separation is one which combines two processes: complexing of polymer with metal ions and ultra-filtration of the complexes through membranes of appropriate selectivity. Chitosan is a natural product derived from chitin, a polysaccharide found in outer skeleton of crustacean shells, shell fish like shrimp, prawn, crab etc., and also obtained from fungal sources. Chitin is

the second most bountiful natural polysaccharide after cellulose on earth. Chitosan is a linear polymer of $\beta(1-4)$ linked 2-amino-2-deoxy- β -D-glucopyranose and is easily derived by N-deacetylation, to a varying extent that is characterized by the degree of deacetylation (DDA) and is consequently a copolymer of N-acetylglucosamine and glucosamine units.^{7,8} Chitosan forms chelates with metal ions by releasing hydrogen ions.⁹ Chitosan has undoubtedly been one of the most popular adsorbents for the removal of metal ions from aqueous solution and is widely used in waste treatment applications.¹⁰⁻¹³ Chitin and its de-acetylated derivatives, chitosan, have unique properties, which make them useful for a variety of applications.¹⁴⁻¹⁶ The traditional source of chitin is selfish waste from shrimps, Antarctic krill, crab and lobster processing.^{17,18} Chitosan is a natural, cationic, hydrophilic, nontoxic, biocompatible and biodegradable polysaccharide suitable for application in biosorption of heavy metal. Chitosan is slightly soluble at low pH and poses problems for developing commercial applications. It is also soft and has a tendency to agglomerate or form a gel in aqueous solution.¹⁴ Low pH would favour protonation of the amino sites resulting in a reversal of charge and would greatly diminish the metal chelating ability of chitin and chitosan. This suggests that a neutral pH more of the metal ions should be adsorbed by chitosan. The amino sugars of chitin and chitosan are the major effective binding sites for metal ions, forming stable complexes by co-ordination.¹⁹ The nitrogen electrons present in the amino and N-acetyl amino groups can establish dative bonds with transition metal ions. Some hydroxyl groups in these biopolymers may function as donor. Hence, deprotonated hydroxyl groups can be involved in the co-ordination with metal ions.²⁰

In this study, chitosan is used to remove chromium(VI) from wastewater. A kinetic study was carried out for chromium(VI) removal from aqueous metal solution by using chitosan.

Experimental

Adsorbent and reagents

Chitosan (India Sea Food, Kochi M.W. 10⁷), Potassium dichromate ($K_2Cr_2O_7$) (Qualigens, India), hydrochloric acid (HCL) (Merck, Limited, Mumbai, India), Sodium hydroxide (NaOH) (Thomas baker (Chemicals) Pvt. Limited, Mumbai,

India], demonized water. All the reagents used were of good quality grade. Standard stock solution (1000 mg L^{-1}) of chromium(VI) was prepared by dissolving salt of $\text{K}_2\text{Cr}_2\text{O}_7$ in deionized water and required concentration of chromium(VI) ions was prepared by diluting stock solution with deionized water.

Kinetics of metal sorption

Kinetic sorption studies for chromium(VI) were carried out for chitosan at pH 5, temperature $25 \text{ }^\circ\text{C}$ for initial concentration 10 mg L^{-1} . 300 mL of standard solution of metal was transferred into various 500 mL flask. The fixed amount of chitosan (1.0 g) was weighed into the flasks and agitated in a shaker for the different contact time (5, 10, 15, 20, 30, 40, 100, 160 and 180 min.). After each agitation time, the content of each flask was centrifuged and the residual concentration of metal in supernatant solution was analyzed using atomic absorption spectrophotometer (ECIL-4141). Blank solutions were also prepared and analyzed.

Data analysis

The amount of chromium(VI) adsorbed (a_t) in mg L^{-1} from each metal solution by chitosan at time t was calculated by using the following equation:

$$a_t = C_0 - C_t \quad (1)$$

The percentage of metal removed (% R) from the aqueous solutions by the chitosan was calculated using equation:

$$R = \frac{C_0 - C_t}{C_0} \times 100 \quad (2)$$

where, C_0 and C_t are the initial metal ion concentration and metal ion concentration at time t respectively in mg L^{-1} .

Adsorption dynamic

Adsorption kinetics of chromium(VI) on chitosan was evaluated using the intraparticle diffusion model.^{21,22} Weber-Morris found that in many adsorption cases, solute uptake varies almost proportionally with $t^{1/2}$ rather than with the contact time t .

$$q_t = k_{id}t^{0.5} + C_i \quad (3)$$

where,

k_{id} ($\text{mg g}^{-1} \text{ min}^{-1/2}$) = measure of diffusion coefficient.

C_i = intraparticle diffusion constant i.e. intercept of the line (mg g^{-1}). It is directly proportional to the boundary layer thickness.

The plots of $q_t \sim t^{1/2}$ gave a straight line are shown in Fig. 1 and is not going through the origin represents that the adsorption kinetics may be controlled by film diffusion and intraparticle diffusion simultaneously.

Results and discussion

Sorption kinetics

Kinetics of metal sorption governs the rate, which determines the residence time and it is one of the important characteristics defining the efficiency of an adsorbent.²³ Sorption kinetics can be controlled by several independent processes that could act in series or in parallel, such as bulk diffusion, external mass transfer (film diffusion), chemical reaction (chemisorptions) and intraparticle diffusion.²⁴ From the Fig. 1, it can be determined that the adsorption of metal was quite rapid initially, however the adsorption rate becomes slower with passage of time up to 100 min. The initial faster rate of removal of metal ions may be due to the availability of the uncovered surface area of the adsorbent, since adsorbent kinetics depends on the surface area of the adsorbent.²⁵

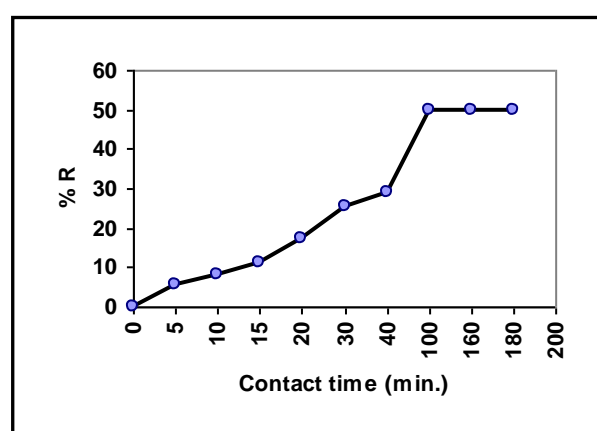


Figure 1. Effect of contact time on % removal of chromium(VI) by chitosan

Kinetic modeling

Kinetic equations have developed to explain the transport of metals onto various adsorbents. These equations include the pseudo first order equation²⁶, the pseudo second order equation²⁷, the Elovich equation²⁸ and the intraparticle diffusion model.²² These kinetic models are only concerned with the effect of the observable parameters on the overall rate of sorption.²⁹ However for this study the intraparticle diffusion model was chosen to analyse the rate of sorption of chromium(VI) on chitosan.

Table 1. Intraparticle diffusion model rate constant (Eq.3) for chromium(VI) using chitosan as adsorbent at $25 \text{ }^\circ\text{C}$

Kinetic model Relationship	R^2	Constants	Values
$y=0.487x+11.66$	0.91	k_{id} C_i	$0.487 \text{ mg g}^{-1} \text{ min}^{-1/2}$ 11.66 mg g^{-1}

Figure-2 presents the intraparticle diffusion kinetic model for chromium(VI) ions. Linear regression (R^2) is frequently used to determine the best fitting kinetic model for metal sorption. In this study kinetic of chromium(VI) ions was evaluated using the intraparticle diffusion model. The coefficient of determination (R^2) was used as the fitting parameter.

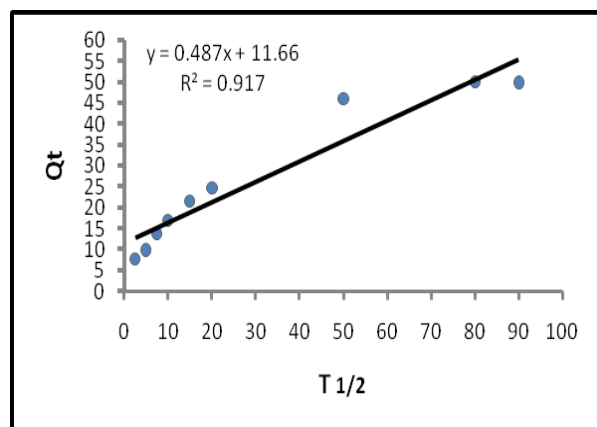


Figure 2. Intraparticle diffusion kinetic model for chromium(VI) ions

Table 1 represents the values of the parameters calculated from the linearized form of the intraparticle diffusion model equation. The R^2 values for chromium(VI) ions can be stated that sorption of chromium(VI) on chitosan, to a certain extent and can be explained by using the intraparticle diffusion model. It therefore, means that for sorption of chromium(VI), intraparticle diffusion may be the rate-limiting step since it obeys the intraparticle diffusion model. It has been reported that sorption of chromium(VI) follows the intraparticle diffusion model.³⁰

Conclusion

This study indicated that chitosan is a good adsorbent for removal of chromium(VI) from aqueous solutions. The kinetics of the adsorption of metal was rapid in the initial stage followed by slow rate. The adsorption data showed that the applicability of the intraparticle diffusion model for chromium removal.

Acknowledgements

The authors are thankful for the financial assistance received from the University Grants Commission (UGC).

References

- ¹Weng, C. H., Huang, C. P., *J. Env. Eng. ASCE*, **1994**, 120, 1470-1487.
- ²Reed, B. F.; Annachalam, S.; Thomas, B.; *Environ. Prog.* **1994**, 13, 60-65.
- ³Neal, B.G.; Lawrence, E.B.; Wandt, J.L.; *Combust. Sci. Tech.* **1990**, 74, 211-214.

- ⁴Udaibhaskar, P.; Iyengar, L.; Prabhakara Rao, A. V. S.; *J. Appl. Polym. Sci.*, **1990**, 39, 739-747.
- ⁵Deepa, K.K.; Sathishkumar, M.; Binupria, A. R.; Murugesan, G. S.; Swaminathan, K.; Yen, S.E.; *Chemosphere*, **2006**, 62, 833-840.
- ⁶Deans, J. R.; Dixon, B. G.; *Water Research*, **1992**, 26, 469-472.
- ⁷Dutta, P. K.; Dutta, J.; Tripathi, V. S.; *J. Sci. Indus. Res.*, **2004**, 63, 20-31.
- ⁸Dutta, P. K.; Dutta, J.; Chattopadhyaya, M.C.; Tripathi, V. S., *J. Polym. Mater.*, **2004**, 21, 321-333.
- ⁹Kaminski, W.; Modrzejewska, Z.; *Sep. Sci. Technol.* 32 (1997) 2659.
- ¹⁰Babel, S.; Kurniawan, T. A.; *J. Hazar. Mater.*, **2003**, B97, 219-243.
- ¹¹Wu, F.C.; Tseng, R. L.; Juang, R. S.; *J. Hazar. Mater.*, **2000**, B73, 63-75.
- ¹²Chu, K. H.; *J. Hazar. Mater.*, **2002**, B90, 77-95.
- ¹³Rengaraj, S.; Yeon, K. H.; Moon, S. H.; *J. Hazar. Mater.*, **2001**, B87, 273-287.
- ¹⁴Guibal, E.; Vooren, M. V.; Dempsey, B. A.; Roussy, J.; *Separation Science and Technology*, **2006**, 41, 2487-2514.
- ¹⁵Kumar, M. N. V. R.; *Reactive Func. Polymer*, **2000**, 46, 1-27.
- ¹⁶Verma, A. J.; Deshpande, S. V.; Kennedy, J. F.; *Carbohydrate Polymer*, **2004**, 55, 77-93.
- ¹⁷Muzzarelli, A. A.; Chitin, Pergamon Press, New York, 1977.
- ¹⁸Shahidi, F.; Synowiecki, J.; *Jour. Agricultural Food Chemistry*, **1991**, 39, 1527-1532.
- ¹⁹Chui, V. W. D.; Mok, K. W.; Ng, C. Y.; Luong, B. P.; Ma, K. K.; *Environ. Int.*, **1996**, 22, 463-468.
- ²⁰Lerivrey, J.; Dubois, B.; Decock, P.; Micera, J.; Kozlowski, H.; *Inorg. Chim. Acta.*, **1986**, 125, 187-190.
- ²¹Weber, W. J.; Morris, J. C.; *J. Sanit. Eng. Div. Am. Soc. Civ. Eng.* **1963**, 89, 31-60.
- ²²Srivastava, S. K.; Yagi, R.; Pant, N.; *Water Res.*, **1989**, 23, 1161-11.
- ²³Krishnan, K. A.; Anirudhan, T. S.; *Water SA*, **2003**, 29, 147-156.
- ²⁴Ho, Y. S.; Ng, J. C. Y.; McKay, G.; *Sep. Purif. Method.*, **2000**, 29, 189.
- ²⁵Qadeer, R.; Akhtar, S.; *Turk. J. Chem.*, **2005**, 25, 95-99.
- ²⁶Lagergren, S.; *Kunglila svenska vertenskapsakademiens., Hand lingen*, **1898**, 24, 1-39.
- ²⁷Ho, Y. S.; McKay, G.; *Pro Safety and Environ. Protec.*, **1998**, 76B, 332-340.
- ²⁸Chien, S. H.; Clayton, W. R.; *Soil Sci. Soc. Am. J.*, **1980**, 44, 265-268.
- ²⁹Ho, Y. S.; *Water Res.*, **2006**, 40, 119-125.
- ³⁰Demirbas, E.; Kobya, M.; Senturk, E.; Ozkan, T.; *Water SA.*, **2004**, 30, 533-539.

Received: 31.03.2013.

Accepted: 05.05.2013.



EQUILIBRIUM AND THERMODYNAMIC STUDIES OF THIONINE ADSORPTION FROM AQUEOUS SOLUTION ONTO RICE HUSK

Hamid Dezhampah^{[a]*}, Ali Mohammad-khah^[a], Naghi Aghajani^[a]

Keywords: rice husk, thermodynamic, thionine, isotherm, adsorption

In this study, the removal of thionine dye from aqueous solutions using low-cost materials as adsorbent by a batch system was investigated. Experiments were carried out as a function of contact time, initial concentration, pH and temperature. The equilibrium adsorption of thionine dye on rice husk adsorbent was analyzed by Langmuir, Freundlich and Temkin models. The results indicate that the Langmuir model provides the best correlation of the experimental data. Various thermodynamic parameters such as enthalpy ΔH° , entropy ΔS° and free energy ΔG° were evaluated. Thermodynamic parameters values revealed that the adsorption of thionine onto rice husk is endothermic, spontaneous, with an increased randomness in nature. The results revealed that the thionine is considerably adsorbed on rice husk and it could be an economical method for the removal of thionine from aqueous systems.

Corresponding Author*

Tel: + 98-131-3243630-5

Fax: + 98-131-3233262

E-Mail: h.dpanah@guilan.ac.ir, h.dpanah@yahoo.com

[a] Laboratory of physical Chemistry, Department of Chemistry, Faculty of Science, University of Guilan P.O. Box 1914, Rasht 0098, Iran.

Introduction

To remove dyes and other colored contaminants from wastewaters, several physical, chemical, physico-chemical and biological such as coagulation and flocculation, membrane separation, different advance oxidation processes, ozonations, electro-coagulation, and adsorption.¹⁻⁵ Among these methods, adsorption currently appears to offer the best potential for overall treatment methods have been developed.⁶

Adsorption is one of the promising alternative techniques used for the removal of dyes from water and wastewater,⁷ and activated carbon is the most widely used adsorbent.⁸ However, the production of activated carbon is complex and expensive, making this technology economically inefficient. Accordingly, the critical challenge of applying the adsorption method to dye removal is finding a low-cost adsorbent that is profoundly available with a high removal capacity so adsorption can successfully compete with other dye removal techniques. This is the driving force behind further studies attempting to find an efficient low-cost adsorbent. Waste materials have recently been viewed as potential low-cost adsorbents, and many reports have been published showing their ability to adsorb various contaminants including dyes.⁷⁻¹⁵ Rice husk, an agricultural waste, is proposed as a no-cost and profoundly accessible potential dye adsorbent.

Rice husk is agricultural waste, accounting for about one fifth of the annual gross rice, 545 million metric tons, of the world. Rice husk contains abundant floristic fiber, protein and some functional groups such as carboxyl, hydroxyl and

amidogen,¹⁶ which make the adsorption processes possible and it has been successfully used to remove colored components¹⁷ or metal ions.¹⁸

Due to the biological and chemical stability of dyestuffs in a number of conventional water treatment methods, adsorption is considered as an attractive and favorable alternate for the removal of dyes and other chemicals from wastewater streams.¹⁹⁻²³ For an efficient adsorption process, rapid removal of the pollutants as well as a high ultimate adsorption capacity of the adsorbent is needed.

The main purpose of the present study is the removal of thionine onto rice husk adsorbent from aqueous solutions under different experimental conditions. The effects of solution pH, dye concentration, contact time and solution temperature were studied for thionine removal. The equilibrium sorption behavior of the adsorbents has been studied using the adsorption isotherm technique. Experimental data have been fitted to various isotherm equations to determine the best isotherm to correlate the experimental data. Thermodynamics of the adsorption process have been studied and the changes in Gibbs free energy, enthalpy and the entropy have been determined.

Experimental

Adsorbent

The milled rice husk was obtained from rice farms in the north of Iran, Guilan, Iran and was used as an adsorbent. The milled rice husk sieved through the sieves, 50-80 mesh size particles. Then rice husk in above particle size rinsed with distilled water to remove dust and soluble impurities and was then dried at 70 °C for 12 hours in an oven before use (The heat treatment of rice husk was carried out for removing any volatiles such as moisture). The dried husks were stored in a desiccator until used.

Adsorbate

Thionine acetate was product of Sigma-Aldrich and was used as received without further purification (Fig. 1).

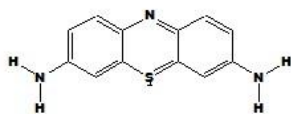


Figure 1. Chemical structure of thionine

A stock solution of dye was prepared by dissolving 0.025 g of it in 50 mL of double distilled water. Working solutions of different concentrations ($10\text{--}50\text{ mg L}^{-1}$) were prepared by further dilutions. The concentration of the dye thionine was determined using a UV-vis spectrophotometer (Janway 6100) at a wavelength corresponding to the maximum absorbance of the dye. Calibration curve was plotted based on the absorbance versus concentration of the dye solution at the maximum wavelength of the dye using Beer's law. A Metrohm pH meter (model 827) with a combined double junction glass electrode was used for showing pH values. pH adjustments were carried out using dilute NaOH and HCl solutions.

Adsorption Experiment

Adsorption experiments were conducted by varying pH, contact time, adsorbent dose, temperature, and adsorbate concentration. The experiments were carried out in 250 mL Erlenmeyer flasks and the total volume of the reaction mixture was kept at 100 mL. The pH of the solution was maintained at a desired value by adding 0.1 M NaOH or HCl. The flasks were shaken for the required time period in a water bath shaker. For the thermodynamic study, the experiment was performed using 0.20 g rice husk added to 100 mL of thionine solution in 250 mL flasks at the different temperature. The flasks were shaken at 120 rpm for 60 min at pH 6. The initial thionine concentration used in this study was 20 mg L^{-1} . A mixture of 0.2 g of rice husks with 100 mL thionine solutions of 20 mg L^{-1} concentrations was shaken at 120 rpm for 60 min at $25\text{ }^{\circ}\text{C}$. The initial pH of the solution was adjusted to 6. All experiments were performed in duplicate. The filtrate samples were analyzed for the determination of the final concentration of thionine by using an UV-vis spectrophotometer (Janway 6100) set at a wavelength of 598 nm, maximum absorbance. The thionine concentration retained in the adsorbent phase was calculated according to:

$$q_e = \frac{(C_0 - C_e)V}{W} \quad (1)$$

where

C_0 and C_e are the initial and the equilibrium concentrations (mg L^{-1}) of thionine solution, respectively; V is the volume (L), and W is the weight (g) of the adsorbent.

Results and discussions

Effect of pH

The effect of pH on the removal efficiency of thionine was studied at different pH ranging from 2.0 to 12.0 and results are shown in Fig. 2. It can be seen that adsorption of thionine was minimum at solution pH 2 and increased with pH up to 6.0 and then remained nearly constant over the initial pH ranges of 6–12. The observed low absorption rate of thionine on the rice husk at $\text{pH} < 6$ may be because the surface charge becomes positively charged, thus making (H^+) ions compete effectively with dye cations causing a decrease in the amount of dye adsorbed. To decrease in acidity of the solution, the functional groups on the adsorbent surface become deprotonated resulting in an increase in the negative charge density on the adsorbent surface and facilitate the binding of dye cation.

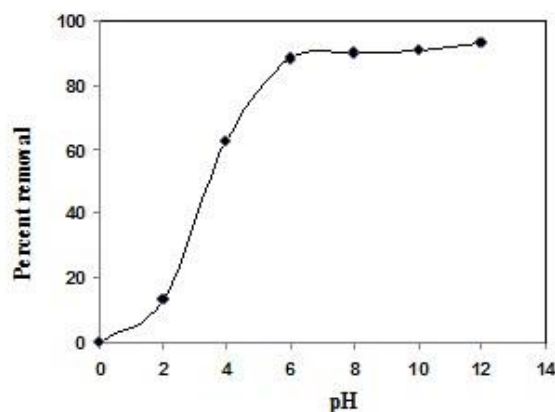


Figure 2. Effects of pH on thionine dye removal at various concentrations (adsorbent dosage: 0.20 g; contact time: 120 min; temperature: 25°C).

The increase in dye removal capacity at higher pH may also be attributed to the reduction of H^+ ions which compete with dye cations at lower pH for appropriate sites on the adsorbent surface. However with increasing pH, this competition weakens and dye cations replace H^+ ions bound to the adsorbent surface resulting in the increased dye uptake.

Effect of Adsorbent Dose

Fig. 3 shows the effect of adsorbent dose (rice husk) on the removal of thionine ($C_0=20\text{ mg L}^{-1}$) at $25\text{ }^{\circ}\text{C}$. It can be seen that the thionine removal increases with increase rice husk up to 0.40 g, thereafter remained fairly constant despite an increase in the amount of the rice husk to 0.4 g. At the equilibrium time, the % removal increased from 34.67 to 80% for an increase in rice husk dose from 0.05 to 0.40 g. The increase in % removal was due to the increase of the available sorption surface and availability of more adsorption sites.

Table 1: Thermodynamic parameters for the adsorption of thionine onto rice husk

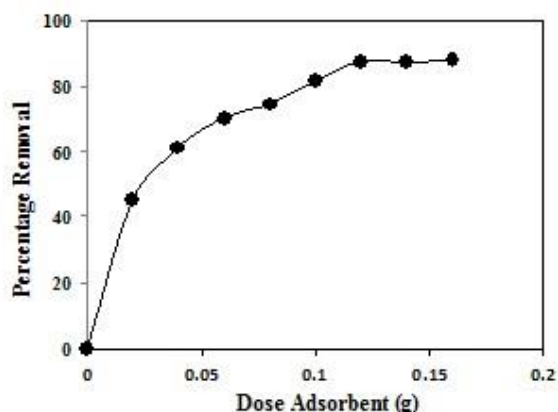
Initial thionine concn. (mg L ⁻¹)	ΔH° , kJ mol ⁻¹	ΔS° , J mol ⁻¹ K ⁻¹	ΔG° , kJ mol ⁻¹			
			15 °C	25 °C	35 °C	45 °C
20	21.940	86.711	-3.319	-4.073	-4.794	-5.607

Table 2. Isotherm models constants and correlation coefficients for adsorption thionine onto rice husk.

Adsorbent	Langmuir Isotherm			Freundlich isotherm			Temkin isotherm		
	a (mg g ⁻¹)	B (L mg ⁻¹)	R^2	K_F	n	R^2	A (L g ⁻¹)	B	R^2
Rice Husk	8.67	0.55	0.99	2.85	2.22	0.94	5.19	3.11	0.96

Effect of contact time on dye removal

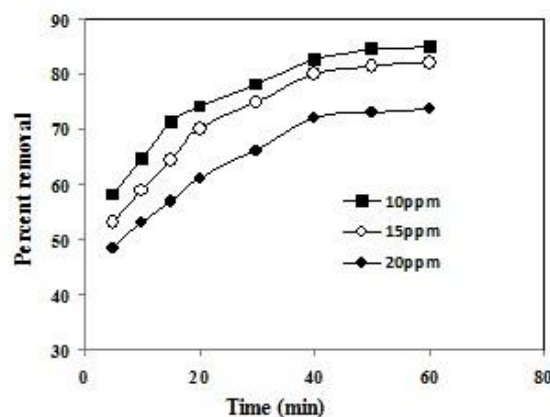
Adsorption of thionine was measured at given contact times for the different initial thionine concentrations from 10 to 20 mg L⁻¹. From Fig. 4, the plot reveals that the percent thionine removal is higher at the beginning; this is probably due to a larger surface area of the rice husk being available at the beginning for the adsorption of thionine. As the surface adsorption sites become exhausted, the uptake rate is controlled by the rate at which the adsorbate is transported from the exterior to the interior sites of the adsorbent particles. Most of the maximum percent thionine removal was attained after about 90 min of shaking time at different concentrations. The increasing contact time increased the thionine adsorption and it remained constant after equilibrium was reached in 40 min for different initial concentrations.

**Figure 3.** Effects of contact time of the dye removal at various concentrations (adsorbent dosage: 0.2 g; pH: 7.0; temperature: 25 °C).

Effect of initial dye concentration

The effect of the initial concentration in the range of 5 to 30 mg L⁻¹ on adsorption was investigated and is shown in Fig. 5. It is evident from this figure that the percentage thionine removal decreased with the increase in initial concentration of thionine. The initial dye concentration provides the necessary driving force to overcome the resistances to the mass transfer of thionine between the aqueous phase and the solid phase. The increase in initial dye concentration also enhances the interaction between thionine and rice husk. Therefore, an increase in the initial concentration of the enhances the adsorption uptake of the. This is due to the increase in the driving

force of the concentration gradient produced by the increase in the initial thionine concentration. While the percentage thionine removal was found to be 89.59% for a 5 mg L⁻¹ initial concentration, this value was 59.10% for 30 mg L⁻¹.

**Figure 4.** Influence of rice husk dosage on thionine removal under different solution concentration (contact time: 120 min; pH: 7.0; temperature: 25°C).

Thermodynamic studies

The thermodynamic parameters such as Gibbs free energy change (ΔG°), enthalpy (ΔH°) and entropy (ΔS°) were calculated using the following equations.²⁴

$$\Delta G^\circ = -RT \ln K \quad (2)$$

$$\ln K = -\frac{\Delta H^\circ}{RT} + \frac{\Delta S^\circ}{T} \quad (3)$$

where K_C is the distribution coefficient for adsorption and is determined as:

$$K = \frac{C_{Ae}}{C_e} \quad (4)$$

where

C_{Ae} is the equilibrium dye concentration on the adsorbent (mg L⁻¹) and

C_e is the equilibrium dye concentration in solution (mg L⁻¹).

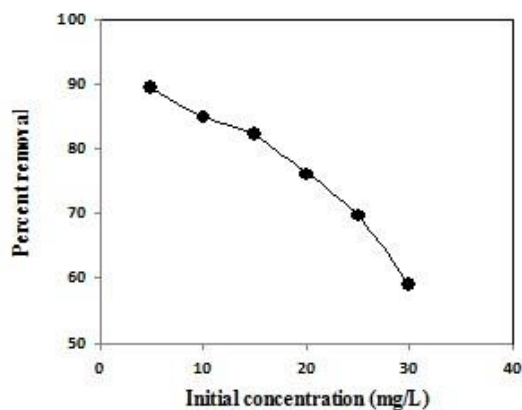


Figure 5. Effect of initial concentration thionine on its sorption onto rice husk (adsorbent dosage: 0.20 g; contact time: 120 min; temperature: 25 °C).

In order to explain and confirm the mechanism of thionine adsorption onto rice husk, the thermodynamics of adsorption were evaluated using ΔG° , ΔH° and ΔS° , given by Eqs. (2) and 3). As seen in Table 1, the value of ΔG° for all tested temperatures was calculated to be negative, which suggests that the adsorption of thionine onto rice husk is spontaneous and indicates that rice husk has a high affinity for the adsorption of thionine from solution under experimental conditions.²⁵ Values of ΔG° between -20 and 0 kJ mol^{-1} indicate a physical adsorption process;²⁶ thus, the results of thermodynamic investigation reconfirmed the hypothesis of physisorption of thionine onto rice husk. Furthermore, the values of ΔH° and ΔS° in the present experiment were 21.94 J mol^{-1} and 86.71 $\text{J mol}^{-1} \text{K}^{-1}$, respectively. A positive value of ΔH° proves the adsorption phenomenon is endothermic.²⁷ Also, the positive value of ΔS° (86.71 $\text{J mol}^{-1} \text{K}^{-1}$) reflects the affinity of the treated rice husk for thionine and an increased randomness at the solid-solution interface during adsorption.^{28, 29}

Adsorption isotherms

The adsorption isotherm indicates how the adsorbed molecules distribute between the liquid phase and the solid phase when the adsorption process reaches an equilibrium state. The analysis of the isotherm data by fitting them to different isotherm models is an important step in finding a suitable model that can be used for design purpose. The adsorption capacity of this system was investigated with the Freundlich, Langmuir and Temkin adsorption isotherms. The thionine sorption isotherm followed the linearized Freundlich model, as shown in Fig. 6. The relation between the thionine uptake capacity q_e (mg g^{-1}) of adsorbent and the residual thionine concentration C_e (mg L^{-1}) at equilibrium is given by

$$\ln q_e = \ln K_F + \frac{1}{n} \ln C_e \quad (5)$$

where the intercept, $\ln K_F$, is a measure of adsorbent capacity, and the slope $1/n$ is the sorption intensity.

The isotherm data fit the Freundlich model well ($R^2=0.94$). The values of the constants K_F and $1/n$ were calculated to be 2.85 and 0.45, respectively. Since the value of $1/n$ is less than 1, it indicates a favorable adsorption. The Freundlich isotherm is more widely used, but provides no information on the monolayer adsorption capacity, in contrast to the Langmuir model.

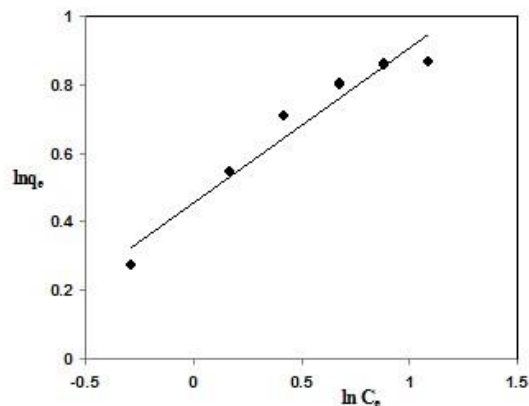


Figure 6. Freundlich adsorption isotherm thionine-rice husk system.

The Langmuir equation relates the solid phase adsorbate concentration (q_e) or uptake to the equilibrium liquid concentration (C_e) as follows:

$$q_e = \frac{abC_e}{1 + bC_e} \quad (6)$$

where a and b are the Langmuir constants, representing the maximum adsorption capacity for the solid phase loading and the energy constant can be seen from Fig. 7. The isotherm data fits the Langmuir equation more poorly ($R^2=0.99$) than the Freundlich and Temkin equations. The values of a and b were determined from Fig. 7 to be 8.67 mg g^{-1} and 0.55 L mg^{-1} , respectively.

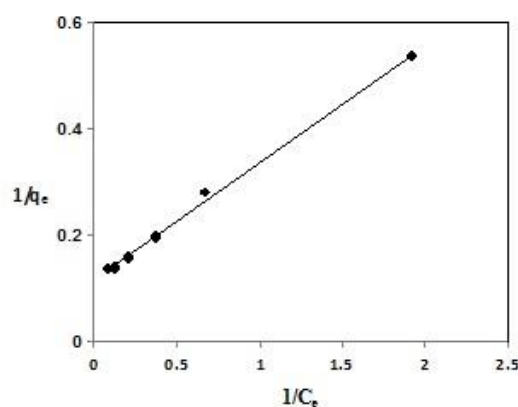


Figure 7. Langmuir adsorption isotherm thionine-rice husk system.

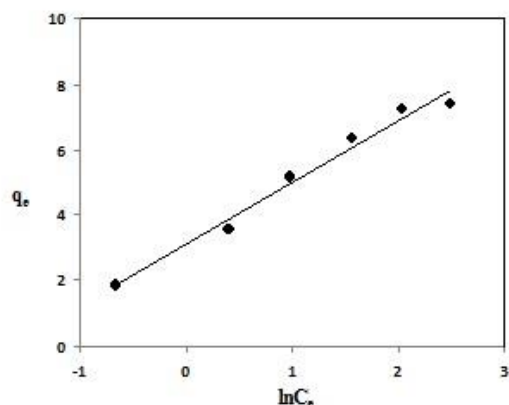


Figure 8. Temkin adsorption isotherm thionine-rice husk system.

The Temkin isotherm has been used in the following form:

$$q_e = B \ln A + B \ln C_e \quad (7)$$

where

$$B = RT/b,$$

T is the absolute temperature in Kelvin and

R is the universal gas constant ($8.314 \text{ J mol}^{-1} \text{ K}^{-1}$).

A is the equilibrium binding constant and

B is corresponding to the heat of sorption.

The sorption data can be analyzed according to Eq. (7). Therefore, a plot of q_e versus $\ln C_e$ enables one to determine the constants A and B . The values of the Temkin constants A and B were determined from Fig. 8 and were found to be 5.19 L g^{-1} and 1.88 , respectively. The correlation coefficient of 0.96 obtained showed that adsorption of thionine also followed the Temkin model.

The Langmuir isotherm is obeyed better than the Freundlich and Temkin isotherms, as is evident from the values of the regression coefficients. The resulting values of the parameters K_F , n , a , b , A , B , R^2 , for all the experiments in solutions with pH equal to 6.0 for maximum removal of thionine are presented in Table 2.

Conclusion

The results of this study indicate that the rice husk adsorbent can be successfully used for the adsorption of thionine dye from aqueous solutions. Adsorption is a strong choice for removal of dye from wastewater. The adsorption of thionine on rice husk reached equilibrium in 40 minutes. The equilibrium sorption data fitted the Langmuir isotherm model better than the Freundlich and Temkin models. The negative values of ΔG° and positive ΔH° obtained indicated that the thionine dye adsorption process is a spontaneous and an endothermic. Rice husk showed high adsorption capacities and it can be successfully used for treatment of thionine containing wastewater. Since this method involves less capital cost and is highly efficient, it is practically feasible for developing countries.

The results of this investigation will be useful for the removal of cationic dyes from industrial effluents.

Acknowledgements

We gratefully acknowledge the Research Council of University of Guilan for supporting this work.

References

- Faria, P. C. C., Orfao, J. J., Pereira, M. M. F. R., *Water Res.*, **2004**, *38*, 2043.
- Qin, Q., Liu, J. Ma., K., *J. Hazard. Mater.*, **2009**, *162*, 133.
- Namasivayam, C., Radhika, R., Suba, S., *Waste Manage.*, **2001**, *21*, 381.
- Mall, D. V. C., Srivastava, N. K., *Dyes Pigm.*, **2006**, *69*, 210.
- Jain, R., Gupta, V. K., Sikarwar, S., *J. Hazard. Mater.*, **2010**, *182*, 749.
- Muthukumar, M., Sargunamani, D., Selvakumar, N., Venkata Rao, J., *Dyes Pigm.*, **2004**, *63*, 127.
- Gupta, V. K., Suhas, *J. Environ. Manage.*, **2009**, *90*, 2313.
- Wu, F. C., Tseng, R. L., Juang, R. S., *J. Colloid Interface Sci.*, **2005**, *283*, 49.
- Rafatullah, M., Sulaiman O., Hashim, R., Ahmad, A., *J. Hazard. Mater.*, **2010**, *177*, 70.
- Song, S., Fan, J., He, Z., Zhan, L., Liu, Z., Chen, J., Xu, X., *Electrochim. Acta.*, **2010**, *55*, 3606.
- Deniz, F., Saygideger, S. D., *Bioresour. Technol.*, **2010**, *101*, 5137.
- Safa, Y., Nawaz Bhatti, H., *Chem. Eng. J.*, **2011**, *167*, 35.
- Tehrani-Bagha, A. R., Nikkar, H., Mahmoodi, N. M., Markazi, M., Menger, F. M., *Desalination* **2011**, *266*, 274.
- Moussavi, G., Khosravi, R., *Chem. Eng. Res. Design*, **2011**, *89*, 2182.
- Vargas, A. M. M., Cazetta, A. L., Martins, A. C., Moraes, J. C. G., Garcia, E. E., Gauze, G. F., Costa, W. F., Almeida, V. C., *Chem. Eng. J.*, **2012**, *181*, 243.
- Dong, Y., Han, Z., Liu, C., Du, F., *Sci. Total Environ.*, **2010**, *40*, 2245.
- Dogan, M., Ozdemir, Y., Alkan, M., *Dyes Pigm.*, **2007**, *75*, 701.
- Suna, D., Zhang, X., Wu, Y., Liu, X., *J. Hazard. Mater.*, **2010**, *181*, 335.
- Tan, I. A. W., Ahmad, A. L., Hameed, B. H., *Desalination*, **2008**, *225*, 13.
- Nakbanpote, W., Goodman, B. A., Thiravetyan, P., *Colloid Surf. A: Physicochem. Eng. Aspects*, **2007**, *304*, 7.
- Han, R., Ding, D., Xu, Y., Zou, W., Wang, Y., Li, Y., Zou, L., *Bioresour. Technol.*, **2008**, *99*, 2938.
- Naiya, T. K., Bhattacharya, A. K., Das, S. K., *Environ. Prog. Sustain. Ener.*, **2009**, *28*, 538–546.
- Mohapatra, M., Khatun, S., Anand, S., *Chem. Eng. J.*, **2009**, *155*, 184.
- Anirudhan, T. S., Radhakrishnan, P. G., *J. Chem. Thermodyn.*, **2008**, *40*, 702.
- Crini, G., *Dyes Pigments*, **2008**, *77*, 415.

- ²⁶Almeida, C. A. P., Debacher, N. A., Downs, A. J., Cottet, L.C., Mello, A. D., *J. Colloid Interface Sci.*, **2009**, 332, 46.
- ²⁷Cheung, W. H., Szeto, Y. S., McKay, G., *Bioresour. Technol.*, **2007**, 98, 2897.
- ²⁸Liu, Y., Liu, Y. J., *Sep. Purif. Technol.*, **2008**, 61, 229.
- ²⁹Jain, S., Jayaram, R. V., *Desalination* **2010**, 250, 921.

Received: 27.03.2013.
Accepted: 06.05.2013.



CHROMATOGRAPHY OF ANTICANCER DRUGS

Tibor Cserhádi and Mária Szógyi

Keywords: synthetic anticancer drugs; natural anticancer agents; liquid and gas chromatographic technologies; electrically driven systems.

The objectives of the series of reviews are the collection, concise description, comparison and evaluation of the various chromatographic methodologies applied for the separation and quantitative determination of anticancer drugs in various accompanying matrices.

* Corresponding Authors

E-Mail: szogyim@t-online.hu

[a] Research Center for Natural Sciences, Hungarian Academy of Sciences, Budapest, Hungary

Introduction

Chromatographic techniques have been developed and successfully applied for the analysis of a considerable number of organic and inorganic compounds present at trace level in sometimes complicated accompanying matrices. The rapid development of new chromatographic instrumentation and separation strategies resulted in the increase of the number of chromatographic technologies with higher separation capacity. Because of their considerable importance in human health care a high number of synthetic and natural compounds were investigated for possible anticancer activity. The different character of synthetic and natural products made necessary the separated discussion of the chromatographic techniques applied for the investigation.

Chromatographic investigation of synthetic anticancer drugs

Liquid chromatography (LC) of synthetic anticancer drugs: Because of their high separation capacity various liquid chromatographic (LC) methods such as normal and reversed phase performance liquid chromatography (RP-HPLC), ultra performance liquid chromatography (UPLC), size exclusion chromatography (SEC), gel permeation chromatography (GPC) have been frequently employed for the analysis of synthetic anticancer drugs and for their formulation. The oxidative damage to guanine nucleosides following combination chemotherapy with 5-fluorouracil and oxiplatin has been recently investigated using UPLC. It was established that chemotherapy increases the concentration of metabolites. It was further established, that smoking, sex, and age exerts a marked influence on the oxidative damage.¹

The analytical methods used for the determination of metallodrugs in biological samples have been recently collected and critically evaluated. Future trends have also been discussed in detail.² The stability of 5-fluorouracil a widely used chemotherapeutic agent has been investigated under various conditions using HPLC and infrared spectroscopy (IR). HPLC measurements were carried out on a C18 reversed phase column the mobile phase consisted of

40 mM KH_2PO_4 . Analytes were detected at 260 nm. The relationship between the detector response and the concentration of the analyte was linear between 20 and 550 $\mu\text{g mL}^{-1}$. The coefficient of correlation was 0.9995. The relative RSD values of intra-day and inter-day were $>0.2\%$ and $>1\%$. Investigations indicated that the decomposition rate of the analyte was higher in alkaline than in acidic conditions. UV radiation exerts a minimal influence on the stability of the drug.³ The effect of adriamycin treatment on the mouse splenic protein levels was studied in detail using reversed-phase liquid-chromatography-tandem mass spectrometry. The measurements indicated that the drug exerts a marked effect of the protein levels.⁴ The application of thermochemotherapy mediated by a new solar planet-structured magnetic nanocomposites has been recently reported. Docetaxel (an anticancer drug) was encapsulated and the efficacy of encapsulation and the drug release was followed by HPLC. It was stated that the method can be employed as an effective mediator for magnetic thermochemotherapy.⁵ A new, specific and sensitive LC-MS/MS analytical method was developed for the simultaneous determination of eleven thiopurine nucleotides. Synthetic products such as eleven mono-, di- and triphosphates of thioguanosine, methylthioinosine, methylthioinosine, thioinosine, and methylthioguanosine. It was further established that the RSD value was below 8%, the recovery varied between 92% and 107%. It was further found that the method can be successfully employed for the better understanding of thiopurine metabolism.⁶

The behaviour of the anticancer drug doxorubicin (DOX) and its loaded form with poly(alkylcyanoacrylate) nanoparticles was studied by using HPLC technology. The method made possible the extraction of Dox and its metabolites by liquid-liquid extraction. The efficacy of extraction of total Dox (free Dox and Dox associated with nanoparticles) was 71 and 78 %. It was concluded from the data, that the within-day and between day precisions of the method were 97.1 – 102.9% and 97.3 – 101.7%. It was further suggested that the method is suitable for the determination the pharmacokinetic and biodistribution of DOX associated with nanoparticles.⁷ Both SEC and HPLC were employed for the development and characterization of a niosomal formulation of doxorubicin aimed at brain targeting. Loaded and unloaded niosomes were separated by SEC. It was stated that niosomal formulations improve doxorubicin brain delivery.⁸ Doxorubicin-loaded Fe_3O_4 magnetic nanoparticles were prepared and modified with biocompatible copolymers. The anticancer drug doxorubicin hydrochloride was encapsulated into poly (D,L-lactic co-

glycolic acid) poly(ethylene glycol) (PLGA-PEG). The copolymers were characterized with ^1H NMR spectroscopy, gel permeation chromatography, Fourier transform infrared spectroscopy, differential scanning calorimetry, X-ray powder diffraction, scanning electron microscopy and vibrating sample magnetometry. The drug encapsulation efficacy were 69.5%, 73% and 78% for PLGA, PEG(2000), PLGA, PED(3000) and PLGY PEG(4000), respectively. It was proposed that these nanoparticles can be employed for biomedical investigations.⁹ A LC/MS/MS method was developed and successfully applied for the determination of doxorubicin and its primary metabolite (doxorubicinol) in cultured human leukemia cells. Solid phase extraction was employed for the clean up and enrichment of analytes. The calibration range was 5.00-1000 mg mL⁻¹ and 0.50-50 ng mL⁻¹ for doxorubicin and its metabolite, respectively. It was established that the anticancer drug and its primary metabolite can be simultaneously determined by LC/MS/MS.¹

A new type of alendronate conjugated amphiphilic hyperbranched polymer based on Boltom H-40 and poly(ethylene glycol) for bone targeted drug delivery was synthesized. The star copolymer was investigated by FTIR and GPC. The investigations indicated that this type of micelles are highly promising bone-targeted drug carriers for skeletal metastases.¹¹ Dendron-like poly(ϵ -benzyloxycarbonyl-L-lysine)/linear PEO block copolymers were synthesized and their behaviour under various conditions was investigated. The physicochemical characteristics were investigated by FTIR, ^1H -NMR, GPC, differential scanning calorimetry, polarized, optical microscopy, and wide range X-ray.¹²

A new type of cyclodextrin-overhanging hyperbranched core-couple-shell miktoarm architectures were developed. The polymers were characterized by ^1H -NMR, FTIR, SEC.¹³ Affinity chromatography was employed for the determination of the effect of spectrin α II and β II tetramers on the platinum anticancer drug resistance in ovarian serous adenocarcinoma. The measurements indicated that proteins Spectrin α II and β II may contribute to drug resistance.¹⁴ The effect of sodium thiosulphate on the metabolism of cisplatin in human plasma has been investigated by using size exclusion chromatography coupled to an inductively coupled plasma atomic emission spectrometer. It was established that the results can be used to develop feasible strategies to reduce the side effects of Pt-based anticancer drugs in patients.¹⁵

Biocompatible amphiphilic block copolymers with various molecular weight were synthesized and applied for the development of anticancer drug nanocarriers. The new copolymers were characterized by nuclear magnetic resonance and gel permeation chromatography. It was established that the new copolymers can be employed for the development of drug delivery systems with various molecular weight and with drug various drug loading capacity.¹⁶ The anticancer drug methotrexate (MTX) was incorporated in layered ceramic nanoparticles of layered double hydroxides (LDHs). The nanoassemblies showed marked elevated chemical and thermal stability as determined with HPLC measurements. It was assumed that the high cellular uptake may be due to the enhanced drug efficacy.¹⁷ Pharmacokinetics of the peptide mediated delivery on the anticancer drug ellipticine has been

investigated in detail. The complex of the amino acid pairing peptide (EAK16II) with the hydrophobic anticancer agent ellipticine was prepared and the pharmacokinetics parameters were determined by HPLC. The measurements indicated that EAK prolongs the residence time of the drug and increases the bioavailability.¹⁸ The synthesis and characterization of poly(ethylene glycol)-b-poly(ϵ -caprolactone) copolymers with functional side groups on the polyester block was reported. The new polymers were characterized with differential scanning calorimetry, ^1H NMR, GPC, fluorescence spectroscopy, transmission electron microscopy, and dynamic light scattering. The weak drug entrapment efficacy and drug-loading ability of these copolymers were established.¹⁹

The oral bioavailability and gender-related pharmacokinetics of celestrol, an anti-inflammatory and antitumor agent was investigated by LC/MS/MS. The measurements indicated that the LC/MS/MS method was selective, and precise. It was further found that formulation markedly increased the bioavailability, and female rats showed significantly better absorption than males.²⁰ Surface modification of paclitaxel-loaded polymeric nanoparticles was achieved and the in vitro cellular behaviour and in vivo pharmacokinetics was studied in detail. Samples were analysed with atomic force microscopy, dynamic light scattering, and cell confocal microscopy. It was concluded from the results that the surface modification of polymeric nanoparticles results in modified pharmacokinetic behavior.²¹

LC/MS/MS technology was employed for the simultaneous determination of seven commonly used anticancer drugs. The anticancer agents included in the investigations were: cyclophosphamide, ifosfamide, irinotecan, eloposide, gemcitabine, carboplatin and perimetrexet. The separation of analytes was carried out on a C18 column (2.1 mm x 100 mm), 3 mm particle size. Positive electrospray ionization was employed as the ionization source. Mobile phase consisted of acetone-water (0.1% formic acid and 10 mM ammonium acetate). The flow rate ranged 0.1 – 0.25 mL min⁻¹. Linear coefficients were always over 0.992. The recovery ranged from 50 to 81.0%. The method was successfully applied to samples from cancer patients.²² An LC-MS method and radiometric detection was developed for the study of the disposition, metabolism, and excretion of the orally active pantoic acid inhibitor in cancer patients. Recovery of radioactivity in excreta was 87% (44 – 77% in feces and 29–51% in urine). Approximately 40 metabolites were detected, in was found that biotransformation begins at the hydroxamic acid side chain and ethyl-methyl indole moiety. It was further established that panobinostat and metabolites are excreted by both kidney and liver.²³

Liquid chromatography combined with electrospray ionization mass spectrometry was employed for the investigation of chronic doxorubin cardiotoxicity in rats. The measurements indicated that doxorubicin influences the cardiac cytochrom P450-mediated arachidonic acid metabolism.²⁴

Ultra performance liquid chromatography (UPLC) followed with electrospray ionization quadrupole time of flight mass spectrometry was applied for the investigation of the metabolites of the antitumor drug noscapine. The

method detected some new primary phase metabolites such as an N-demethylated product, two hydroxylated derivatives, one bis-demethylated derivative. Several novel glucuronides have also been detected.²⁵ A high performance liquid chromatographic method coupled with electrospray mass spectrometry (LC-ESMS) was developed for the investigation of the structural and functional diversity in DNA-targeted hybrid anticancer drugs. It was stated that the new method can be successfully employed for the determination of structure-activity relationships and for the identification of target compounds.²⁶

The structure of the new anticancer agent EAPB0203 and its metabolites were investigated in detail. Measurements were carried out using liquid chromatography-mass spectrometry and LC/MS/MS. The structures of the metabolites were identified by one and two dimensional H-NMR.²⁷ A new immunoassay method was developed for the determination of 5-fluorouracil (5-FU) in patients with gastric cancer. The results were compared with those obtained with the application of GC-MS. It was established that the results of the immunoassay method and GC/MS were comparable and can be employed simultaneously for the determination of 5-FU in the plasma of patients with gastric cancer. It was further established that the immunoassay method is simpler and easier to carry out than the traditional GC/MS procedure.²⁸

Chiral chromatography combined with other physicochemical analytical procedures has been successfully applied for the investigation of the chemistry and pharmacology of Imexon and related cyanoaziridines. The measurements indicated that the activity of these new compounds was relatively low compared with the activity of the original compounds.²⁹

The interaction between of RAPTA-T, a new ruthenium-based anticancer agent and human ovarian cells was investigated in detail. SEC has been employed for the determination of the distribution profile of metaldrug within the cancer cells. Multidimensional protein identification technology was employed for the elucidation of the cellular response mechanism. It was established that the investigation methods employed may help the elucidation of the interaction between the cancer cells and the anticancer drug.³⁰ A combining data acquisition method followed with multi-period ion scan and high resolution characteristics extracted ion chromatograms were employed for in-vivo drug metabolites screening and identification of the metabolites of the potential antitumor agent 3,6,7-trimethoxyphenantroindolizine (CAT) in rat urine. It was established that the method is suitable for the detection of 21 metabolites and for the identification of 9 metabolites in rat urine. Furthermore the method allowed the differentiation between N-oxidized and hydroxylated metabolites.³¹ A new type of folic acid conjugated amphiphilic 4-arm star-shaped PLGA-PEG-NH₂ were synthesized and tested as nanocarrier for doxorubicin. The characteristics of the preparation were assessed by H-1 NMR, dynamic light scattering and GPC. It was established that the new nanocarrier can be successfully applied for the deliver of doxorubicine.³² The composition of the ethanolic extract of the chemopreventive Taiwanese mushroom *Antrodia camphorata* was investigated by HPLC. The measurements indicated that the triterpenoid rich fraction contained antileukemia components such as anticin, dehydroeburicoic acid, and zhankuic acid. It was found that

the bioactive components decrease tumor weight and size without decreasing body weight. The preparation was proposed for the treatment of leukaemia.³³

Capillary electrophoresis (CE) combined with laser-induced fluorescence detection (LIF) has been employed for the study of the interaction of the antitumor agent ellipticine with DNA. The background electrolyte contained 20% dimethyl sulfoxide and 50 mM sodium acetate (pH 4.5). It was established that the peak of ellipticine decreased in the presence of DNA indicating the interaction of ellipticine with DNA.³⁴

A HPLC/MS method was developed for the determination of CM1, the active agent derived from the prodrug CA1P, in human plasma and urine, and of CA1P and three glucuronides CA1G1, CA1G2, and CA1DG in human urine were analysed. Plasma CA1 was preconcentrated by solid phase extraction (SPE). Urine samples were investigated without extraction. The intra-day and inter-day accuracy and precision were lower than 15%. Mean recovery of CA1 from plasma was 101% and 97% from urine. Mean urine recovery was of CA1P was 98%, CA1G1 96%, CA1G2 93% and CM1DG 93%.³⁵ A new GnRH-based multifunctional drug delivery system containing daunorubicin and methotrexate was developed and the in vitro stability, degradation in human serum, and in the presence of rat liver homogenate was investigated by LC/MS. It was concluded from the results that multifunctional bioconjugate resulted in higher in vitro cytostatic effect than the monofunctional bioconjugate contain either methotrexate or daunorubicin.³⁶

Fluorinated, and pegylated polyaspartamide copolymers were synthesized to increase the solubility and efficacy of flutamide. The characteristics of copolymers were determined by SEC, pyrene colorimetric assay, light scattering analysis and scanning electron microscopy. The results indicated that the inclusion of flutamide in polymer matrices markedly modifies the efficacy of the complexed bioactive compound.³⁷ The characteristics of the newly synthesized anticancer agent, 7-(4-fluorobenzylamino)-1,3,4,8-tetrahydropyrrolo[4,3,2-d,e]quinolin-8(1H)-one (FBA-TPQ) were investigated employing various physicochemical and biophysical investigation methods such as rapid resolution liquid chromatography, determination of FBA-TPQ in plasma and tissue samples, stability in plasma, plasma protein binding, metabolism by S9 enzymes, plasma pharmacokinetics, and tissue distribution. It was concluded from the data that FBA-TPQ is a potential therapeutic agent for pancreatic cancer.³⁸

The pharmacokinetics and antitumor activity of XMT-1001, a new polymeric topoisomerase I inhibitor was investigated in mice bearing HT-29 human colon carcinoma xenografts. LS/MS method was employed for the determination of the chromatographic profile of the drug and its conjugate release products. It was established that the efficacy of drug was markedly modified by formulation.³⁹

An LC-MS/MS technology was developed and applied for the simultaneous determination of highly hydrophobic pyrimidine anticancer agents in human plasma and the efficacy of three derivatization reagents were compared. The anticancer agents included in the experiments were tegafur, 5-fluorouracil and gimeracil. Derivatization agents employed were p-bromophenacyl bromide, dansyl chloride

and diazomethane. The experiments revealed that the *p*-bromophenacyl was the best derivatization agent. The method was employed for the pharmacokinetic study of tegafur, 5-fluorouracil and gimeracil in cancer patients.⁴⁰ The purification and characterization of lunasin, a peptide isolated from soy bean has been recently reported. The interest in lunasin is due to its marked anticancer and anti-inflammatory activity. A combined method was developed for the purification of lunasin from soybean. The method includes anion exchange chromatography, ultrafiltration and reversed-phase chromatography. It was stated that the procedure facilitates the development of lunasin as a potential nutraceutical of therapeutic anticancer agent.⁴¹

The safety and pharmacokinetics of α -tocopheryloxy acetic acid (α -TEA) was investigated using LC/MS technologies. The measurements were motivated by the antitumor activity of α -TEA. According to the results α -TEA showed no toxic effect, the half life of orally administered α -TEA was 52 h. No clinical signs of toxicity was detected. No significant sex specific differences were established.⁴²

A novel LC-MS/MS procedure was developed for the quantification of E7080 (lenvatinib) and metabolites in various human biological matrices such as human plasma, whole blood, urine and faeces. Plasma, urine, and faeces samples were extracted with acetonitrile. Analyses were carried out on an octadecyl-silica column (50 mm x 2.1 mm). Analytes were separated using gradient elution consisting of water-acetonitrile mixtures and detected with API300 triple quadrupole mass spectrometer with turbo ion spray interface operating in positive ion mode. Calibration curves were in each case linear, accuracy varied between $\pm 20\%$. It was found that the method can be successfully employed for the analysis of E7080 and its metabolites in various human biological matrices.⁴³

A liquid chromatography-tandem mass spectrometry (LC-MS/MS) analytical procedure was applied for the separation and quantitative determination of felotaxel (SHR110008) in tumor-bearing mice. Samples (plasma, urine, faeces, brain heart, liver, lung) were extracted with ethyl acetate. Calibration curves were linear ($r^2=0.995$). The accuracy and precision varied between 86.1–107.2 % and 1.1–9.2%. Recoveries ranged from 73.9 to 96.1 %.⁴⁴

A HPLC method was employed for the analysis of doxorubicin (Dox) loaded poly(alkyl cyanoacrylate, PACA) nanoparticles. The measurements indicated that Dox and its main metabolites doxorubicinol and doxorubicinon are well separated from the target compound. It was further established that recovery varied between 71 and 78%. The between-day and within-day precision of the method varied from 97.1 to 102.9% and from 97.3 to 1.02 %.⁴⁵ Another LC-MS method was developed for the investigation of pharmacokinetics of the anticancer drug CYC-116 in rat plasma. Analytes were separated on an octadecylsilica column (150 x 04.6 mm, particle size, 5 μm) using isocratic separation mode. The flow rate was 0.8 mL min⁻¹. Isocratic mobile phase consisted of acetonitrile-water-formic acid: 23.5; 76.5; 0.1 v/v/v). Analytes were extracted by liquid-liquid extraction using ethyl acetate. MS analysis was carried out employing a quadrupole mass spectrometer. The calibration curve was linear in the concentration range investigated. The intra- and interday precisions were less

then 11.8–6.6 %. It was stated that the method can be successfully applied for the study of the pharmacokinetics of CYC-116 in rats after oral administration.⁴⁶

A LC/MS/MS procedure was developed for the simultaneous determination of eleven thiopurine nucleotides (mono-, di- and triphosphates of thioguanosine, methylthioinosine, methylthioguanosine, and thioinosine). Target compounds show marked anticancer and immunosuppressive activity. It was established that the method facilitates the understanding of the thiopurine metabolism in one run.⁴⁷

The application of thermochemotherapy mediated by novel solar-planet structured magnetic nanocomposite for glioma treatment has been reported. The efficacy of the encapsulation of docetaxel and drug release was followed by HPLC. It was concluded from the results that this novel method can be successfully employed for the comprehensive treatment of glioma.⁴⁸

The stability of 5-fluorouracil under different environmental conditions was investigated by using HPLC and infrared spectroscopy (IR). Analytes were separated on an octadecylsilica column using 40 mM KH₂PO₄ as mobile phase. Target compounds were detected at 260 nm. Significant linear correlation was found between the concentration of detector response and the amount of analytes in the samples ($r^2=0.9995$). The R. S. D. values for intra-day and inter-day were <0.2% and <1%, respectively. The measurements indicated that the analyte is sensitive to oxidative conditions and stable when exposed to UV irradiation.⁴⁹

Another LC-MS/MS technique was developed and successfully employed for the simultaneous determination of doxorubicin and its metabolite in cultured human leukemia cells. Samples were enriched using solid phase extraction, the validated calibration ranges were 5.00 – 1000 mg mL⁻¹. The data indicated that the method is precise and can be applied for the simultaneous determination of the drug and its metabolite.⁵⁰

Niosomal formulations were developed, characterized and applied as potential brain targeted system. Light scattering and transmission electron microscopy were applied for the characterization of vesicles. SEC or dialysis was applied for the investigation of the physicochemical parameters of vesicles. It was concluded from the results that the method is suitable to improve the doxorubicin brain delivery.⁵¹ A novel (NAG)-PEG-doxorubicin targeted conjugates were designed, developed, synthesized for its capacity as anticancer delivery agent. The product was characterized by ¹H-NMR, UV spectroscopy and HPLC. It was concluded from the results that the new products can be applied in targeted anticancer therapy.⁵² The in vivo performance and in vitro cytotoxicity of 10-hydroxycamptothecin (10-HCPT) was investigated in detail. The effect of 10-HCPT nanosuspension and 10-HCPT solution was compared and critically evaluated. HPLC-FD was employed for the analysis of serum samples and tissue homogenizates. It was further found that 10-HCPT increases the cytotoxicity of the original anticancer agent. Increase the anti-tumor activity of poorly soluble bioactive compound.⁵³ The solubility of paclitaxel (PTX) was improved by using various coprecipitation processes including poly (L-lactic

acid, PLLA). The components of the formulation were mixed and coprecipitated by a supercritical antisolvent (SAS) process using dichloromethane (DCM) and mixtures of DCM and ethanol, or DCM and dimethyl sulfoxide (DMSO). The end product was characterized by X-ray diffraction (XRD), scanning electron microscopy (SEM), laser diffraction, particle size analysis, and HPLC. The experimental conditions for the optimal system were: DCM/EtOH 50:50 %, 35 °C, 10-12 MPa, PLLA concentration, 5 g L⁻¹; solution flow rate 0.5 ml min⁻¹.⁵⁴

The anticancer applications of mesoporous materials functionalized with the natural betulinic acid (BA) has been investigated in detail. Dehydrated CMC-41 was functionalized with 3-chloropropyltriethoxysilane (CPTS) and 3-aminopropyltriethoxysilane (APTS). The end product was characterized by powder X-ray diffraction, X-ray fluorescence, nitrogen gas sorption, multinuclear MAS NMR spectroscopy, thermogravimetry, UV spectroscopy, IR, SEM, and HPLC.⁵⁵

The characteristic of methoxy stilbenes as potent, specific, untransported and cytotoxic inhibitory of breast cancer resistance protein has been studied in detail. It was established by HPLC and mass spectrometry titration that methoxystilbenes are not transported. It was further suggested that the methoxy derivatives of stilbene can be applied to influence drug-efflux activity.⁵⁶ The light-mediated release of the anticancer drug methotrexate was investigated employing three different analytical methods such as UV/vis spectrometry, ¹H NMR spectroscopy and HPLC. The measurements indicated that the drug is released by the photochemical mechanism in an actively controlled manner. It was further found that the release of methotrexate depended on the linker design, light wavelength, exposure time, and the pH of the medium.⁵⁷

An octadecyl-silica column was applied for the separation and quantitative determination of some new benzimidazole derivatives with marked cytotoxic activity. The stability of the target compounds was investigated in aqueous solution of 0.2% dimethyl sulfoxide. The mobile phase of the HPLC measurements consisted of acetate buffer (pH 4.5):acetonitrile. The flow rate was 1.0 mL min⁻¹. The correlation coefficients were over $r^2 = 0.9995$. The new method was proposed for the HPLC analysis and stability test of these novel benzimidazole derivatives.⁵⁸

During the study of the pharmacokinetics of the amino-pairing peptide EAK16-II (EAK) it was established that EAK is suitable for the stabilization of EAK-EPT (ellipticine) complexes in vivo. The characteristics of the EAK-EPT complexes were investigated by transmission electron microscopy TEM), HPLC and zero potential measurements. EPT was extracted from rat plasma with dexamethasone sodium phosphate. The measurements found significant differences between EPT and EAK-EPT complexes indicating that EAK can be applied as a carrier to increase the bioavailability of EPT.⁵⁹

The design and synthesis of photoactivatable metallodrugs has been recently published. The compounds included in the experiments were: inert (Ru(II) half sandwich compounds, [Ru([9]aneS(3)(bpy)(py)]PF₆] ([9]aneS(3)=1,4,7-trithia-cyclonane, bpy=2,2'-bipyridine, py=pyridine), [Ru([9]aneS(3))(en)(py)]PF₆] (en=1,2-diaminoethane), and

[Ru([9]aneN(3))(en)(dmsO-S)]PF₆], [9]aneN(3)=1,4,7-triazacyclononane), is reported along with the X-ray crystal structure of [Ru([9]aneS(3)(bpy)(py)]PF₆]. It was established that these complexes are promising for further investigation as potential photochemotherapeutic agents.⁶⁰

A new potential PET (positron emission tomography) agent was synthesized for imaging steroid sulfatase (STS) in cancers. Solid phase extraction combined with HPLC was employed for the purification the target tracer.⁶¹ The murine pharmacokinetics, pharmacodynamics and metabolism of (3-(1H-indol-2-yl-phenyl)(1H-indol-2yl-methanone) (indole-15). The concentration of indole-15 was determined by HPLC and LC/MS/MS. The investigation of metabolites indicated that the original compound undergoes extensive oxidative metabolism with following sulfation. It has been proposed that indole-15 can be employed in clinical trials.⁶² A specific and sensitive enzyme-linked immunosorbent assay (ELISA) was developed for the analysis of Vindesine (VDS) and the results were compared with those obtained by HPLC. Anti-VDS antibody was obtained by immunizing rabbits with VDS conjugated with bovine serum albumin using N-[β-4-(diazophenyl)ethyl]maleinimide. The enzyme marker was produced by coupling VDS with horse radish peroxidase using N-4-diazophenylmaleinimide. The method was highly specific the cross reactivity was 0.18% for vincristine and 0.11 % for vinblastine. It has been stated that the method can be successfully employed for the pharmacokinetics studies of (VDS).⁶³ The mass balance, excretion and metabolism of the small molecule flavonoid tumour vascular disrupting agent ASA404 was investigated using various chemical, physicochemical methods such as HPLC, liquid scintillation counting, mass spectrometry, glucuronidase. The mean recoveries were: urine, 59.9%; faeces, 33.3%. It was found that the method is suitable for the detection and analysis of two new metabolites did not detected before.⁶⁴

A new HPLC method was developed for the study of new anticancer agents in intravenous solutions. Compounds included in the experiments were the derivatives of daunorubicin containing various amidine group such as piperidine (DD-1), morpholine (DD-2), pyrrolidine (DD-3), or hexahydroazepine (DD-4) moiety. It was found that the environmental conditions exert marked effect on the stability of the preparation.⁶⁵ A TAT peptide fragment (YGRKKRQRRR) was conjugated to a platinum(IV) analogue of oxiplatin as a vehicle for membrane penetration. The mono- and difunctionalized conjugates were separated by preparative HPLC and characterized by analytical HPLC, ESI-MS, and H-1 NMR spectroscopy. The results indicated that the biological activity of conjugates was higher than that of the untargeted analogues.⁶⁶ The influence of miRNAs a regulator in some biological processes such as development, cellular differentiation, and carcinogenesis was investigated in detail. The promising anticancer drug 3,6-dihydroxyflavone (3,6-DHF) was selected as model compound. HPLC was employed for the detection of the bioavailability of 3,6-DHF. Cell apoptosis was determined by flow cytometry or terminal deoxynucleotidyl transferase UTP nick end-labeling assay. The investigations indicated that the oral administration of 3,6-DHF suppressed the breast carcinogenesis induced by 1-methyl-1-nitrosourea (MNU) in rats. It was further found that 3,6-DHF is a potent natural chemopreventive agent, and miR-34a and miR-21 play a considerable role in MNU-induced breast

carcinogenesis.⁶⁷ Long conjugated 2-nitrobenzyl-derivative caged anticancer prodrug with visible light regulated release was synthesized. Styryl conjugated 2-nitrobenzyl derivatives were introduced in the molecules as phototrigger to regulate the release of the anticancer drug chlorambucil. UV absorption, FT-IR and HPLC technologies were applied for the study of the regulated release of the parent molecule.⁶⁸ The efficacy of a non-hypercalcemic vitamin-D-2 derived anti cancer agent (MT19c) was investigated. The investigation indicated that the new compound makes possible of the future potential application of this compounds as anticarcinogen agent.⁶⁹

Reversed phase thin layer chromatography has also found applications in the chromatographic analysis of bioactive compounds. Stationary phases consisted of octadecyl silica and silica surface modified with cyano groups. Methanol-water and acetonitrile-water mixtures served as stationary phases. Significant correlations were found between the lipophilicity determined with RP-TLC and calculated with principal component analysis. The chromatographic parameters of bioactive compounds included in the experiment were correlated with the biological activity of the analytes (quantitative structure-retention relationship and quantitative structure-activity relationship). The measurements indicated that there is a significant correlation between the lipophilicity and molecular descriptors of phytol derivatives. It was assumed that the chromatographic behaviour of phytol derivatives may influence their penetration and partitioning over biomembranes.⁷⁰

Abbreviations

APTS	3-aminopropyltriethoxysilane
CA	Capillary electrophoresis
CPTS	3-chloropropyltriethoxysilane
DCM	dichloromethane
DHF	3,6-dihydroxyflavone
DMSO	dimethyl sulfoxide
FTIR	Fourier transformed infrared spectroscopy
GPC	gel permeation chromatography
HPLC	high performance liquid chromatography
MNU	1-methyl-1-nitrosourea
IR	infrared spectroscopy
PET	positron emission tomography
PLLA	poly-L-lactic acid
PTX	paclitaxel
LIF	Laser-induced fluorescence detection
RP-HPLC	LC-MS/MS reversed-phase high performance liquid chromatography-tandem mass spectrometry
RSD	relative standard deviation
SEM	scanning electron microscopy
SEC	size exclusion chromatography
SPE	solid phase extraction
UPLC	ultra performance liquid chromatography
XRD	X-ray diffraction

References

- Afzal, S., Jensen, S. A., Sorensen, J. S., Henriksen, T., Weimann, A., Poulsen, H. E., *Cancer Ther. Pharmacol.*, **2012**, *59*, 301-307.
- Timerbaev, A., Sturup, S., *Current Drug Metabol.*, **2012**, *13*, 272-283.
- Yadav, N., Singh, P., Mehrotra, R., *Curr. Pharm. Anal.*, **2012**, *8*, 49-55.
- Evans, A. R., Myriyala, S., St Clair, D. K., Butterfield, D. A., Robinson, R. A. S., *J. Proteome Res.*, **2012**, *11*, 1054-1064.
- Zhao, L. Y., Yang, B., Wang, Y. Y., Yao, Z., Wang, X. W., Feng, S. S., Tang, J. T., *J. Nanosci. Nanotechnol.*, **2012**, *12*, 1024-1031.
- Hofmann, U., Heinkele, G., Angelberger, S., Scheffeler, E., Lichtenberger, C., Jaeger, S., Reinisch, W., Schwab, M. *Anal. Chem.*, **2012**, *84*, 1294-1301.
- Alhareth, K., Vauthier, C., Gueutin, C., Ponchel, G., Moussa, F., *J. Chromatogr. B.*, **2012**, *887*, 128-132.
- Bragagni, M., Mennini, N., Ghelardini, C., Mura, P., *J. Pharm. Pharmaceut. Sci.*, **2012**, *15*, 184-196.
- Akbarzadeh, A., Mikaeili, H., Zarghami, N., Mohammad, R., Barkhordari, A., Davaran, S., *Int. J. Nanomed.*, **2012**, *7*, 511-526.
- Xu, J. H., Liu, Y., Yu, Y., Ni, Q. J., Chen, Y., *Anal. Lett.*, **2012**, *45*, 1980-1994.
- Chen, H. Y., Li, G. L., Chi, H. R., Wang, D. L., Tu, C. L., Pan, L. Y., Zhu, L. J., Qiu, F., Guo, F. L., Zhu, X. Y., *Bioconjugate Chem.*, **2012**, *23*, 1915-1924.
- Xu, Y. C., Dong, C. M., *J. Polymer Sci. Part A, Polym. Chem.*, **2012**, *50*, 1216-1225.
- Tian, W., Lv, X. Y., Mu, C. G., Zhang, W. H., Kong, J., Liu, Y. Y., Fan, X., D., *J. Polym. Sci. Part A*, **2012**, *50*, 759-771.
- Maeda, O., Shibata, K., Hosono, S., Fujiwara, S., Kajiyama, H., Ino, K., Nawa, A., Tamakoshi, K., Kikkawa, F., *Int. J. Cancer*, **2012**, *130*, 113-121.
- Sooriaar A. Ch, Ch., Narendran, A., Galler, J., *Metallomix* **2012**, *4*, 960-967.
- Yun, J. M., Park, S. Y., Lee, S. S., Youn, Y. S., Park, G. Y., Lim, C., Lee, B. J., Song, H. T., Oh, Y. T., Oh, K. T., *Macromol. Res.*, **2012**, *20*, 944-953.
- Choi, G., Kim, S. Y., OH, J. M., Choi, J. H., *J. Am. Ceram. Soc.*, **2012**, *95*, 2758-2765.
- Ma, W. N., Lu, S., Pan, P., Sadatmousavi, P., Yuan, Y. F., Chen, P., *Plos One*, **2012**, *7*, DOI:10.1371.
- Chen, W. H., Hua, M. Y., Lee, R. S., *J. Appl. Polym. Sci.*, **2012**, *125*, 2902-2913.
- Zhang, J., Li, C. Y., Xu, M. J., Wu, T., Chu, J. H., Liu, S. J., Ju, W. Z., *J. Ethnopharm.*, **2012**, *144*, 195-200.
- Tao, Y. H., Han, J. F., Dou, H. Y., *Polymer* **2012**, *53*, 5078-5086.
- Zhou, J. Y., Gao, S. H., Zhang, F., Jiang, B., Zhang, Q., Cai, F., Li, J. X., Chen, W. S., *J. Chromatogr. B.*, **2012**, *906*, 1-8.
- Clive, S., Woo, M. M., Nydam, T., Kelly, L., Squier, M., Kagan, M., *Cancer Chemother. Pharmacol.*, **2012**, *70*, 513-522.
- Alsaad, A. M. S., Zordoky, B. N. M., *Drug Metab. Dispos.*, **2012**, *40*, 2126-2135.
- Fang, Z. Z., Krausz, K. W., Li, F., Cheng, J., Tanaka, M., Gonzalez, F., *J. British J. Pharmacol.*, **2012**, *167*, 1271-1286.
- Ding, S., Qiao, X., Kucera, G. L., Bierbach, U., *J. Med. Chem.*, **2012**, *55*, 10198-10203.
- Lafaille, F., Banaigs, B., Inguibert, N., Enjalbal, C., Doulain, P. N., Bonnet, P. A., Masquefa, C., Bressole, F. M. M., *Anal. Chem.*, **2012**, *84*, 9865-9872.

- ²⁸Matsumoto, H., Higashida, M., Kubota, H., Murakami, Tsutsumi, K., Nakashima, H., Oka, Y., Okumura, H., Nakamura, M., Tirai, H., *Anticancer Res.*, **2012**, 32, 5111-5114.
- ²⁹Remers, W. A., Dorr, R. T., *Current Med. Chem.*, **2012**, 19, 5745-5763.
- ³⁰Wolters, D.A., Stefanopoulou, M., Dyson, P., *J. Metallomics.*, **2012**, 4, 1185-1196.
- ³¹Tian, Y.P., He, J.M., Zhang, R. P., Lv, H.N., Ma, S. G., Chen, Y. H., Yu, S., S., Chen, X. G., Wu, Y., *Anal. Chim. Acta*, **2012**, 731, 60-67.
- ³²Ma, G. L., Zhao, S. X., Jin, X., Chen, M. M., Zhang, Z. P., Song, C. X., *Chem. J. Chin.*, **2012**, 33, 1854-1859 (in Chinese, Abstract in English).
- ³³Du, Y. C., Chang, F. R., Wu, T. Y., Hsu, Y.M. El-Shazly, M., Chen, C. F., Sung, P. J., Lin, Y., Y. Lin, Y. H., Wu, Y.C., Lu, M. C., *Phytomedicine* **2012**, 19, 788-796.
- ³⁴Ryvolova, M., Adam, V., Eckschlager, T., Stiborova, M. *Electrophoresis* **2012**, 33, 1545-1549.
- ³⁵Stratford, M. R. L., Folkes, L. L. J. *Chrom. B., Anal. Technol Biomed. Life Sci.*, **2012**, 898, 1-6.
- ³⁶Leurs, U., Lajko, E., Mezo, G., Orban, E., Ohlschlager, P., Marquardt, A., Kohidai, L., Manea, M., *Eur. J. Med. Chem.* **2012**, 52, 173-183.
- ³⁷Piccionello, A. P., Pitarresi, G., Pace, A., Triolo, D., Picone, P., Buscemi, S., Giammona, G., *J. Drug Targ.*, **2012**, 20, 433-444.
- ³⁸Zhang, X. R., Xu, H. X., Zhang, X., Voruganti, S., Murugesan, S., Nadkarni, D. H., Velu, S. E., Wang, M. H., Wang, W., Zhang, R. W., *Marine Drugs* **2012**, 10, 1138-1155.
- ³⁹Walsh, M. D., Hanna, S. K., Sen, J., Rawal, S., Cabral, C. B., Yurkovetskiy, A. V., Fram, R. J., Lowinger, T. B., Zamboni, W. C., *Clin. Canc. Res.*, **2012**, 18, 2591-2602.
- ⁴⁰Liu, H. Y., Ding, L., Yu, Y., Chu, Y., Zhu, H., *J. Chromatogr. B., Anal. Technol. Biomed. Life Sci.*, **2012**, 893, 49-56.
- ⁴¹Seber, L. E., Barnett, B. W., McConnell, E. J., Hume, S. D., Cai, J., Boles, K., Davis, K. R., *Plos One* **2012**, 7, article number: e35409 DOI: 10.1371.
- ⁴²Hahn, T., Akporiyaye, E. T., *Anti-Cancer Drugs*, **2012**, 23, 455-464.
- ⁴³Dubbelman, A. C., Rosing, H., Thijssen, B., Gebretensae, A., Lucas, L., Chen, H., Shumaker, R., Schellens, J., H., M., Beijnen, J. H., *J. Chromatogr. B., Anal. Technol. Biomed. Life Sci.*, **2012**, 887, 25-34.
- ⁴⁴Ding, Y., Lu, C. T., Yang, Y., Yin, X., Yang, L., Wang, C., Ma, Z. Y., Zhu, Y. R., Dung, R. K. Jia, Y. Y., Wen A. D., *J. Chromatogr. B. Anal. Technol. Biomed. Life Sci.*, **2012**, 887, 61-66.
- ⁴⁵Alhareth, K., Vauthier, C., Gueutin, C., Ponchel, G., Moussa, F., *J. Chromatogr. B., Anal. Technol. Biomed. Life Sci.*, **2012**, 887, 128-132.
- ⁴⁶Su, J., Chen, X. H., Li, Q., Yu ZG., Guan, X. G., Geng, L. L., Bi K. S., *Chromatographia* **2012**, 75, 263-268.
- ⁴⁷Hofmann, U., Heinkele, G., Angelberber, S., Schaeffeler, E., Lichtenberger, CV., Jaeger, S. Reinisch, W., Schwab, M., *Anal. Chem.*, **2012**, 84, 1294-1301.
- ⁴⁸Zhao, L. Y., Yang, B., Wang, Y., Y., Yao, Z., Wang, X. W., Feng, S. S., Tang, J. T., *J. Nanosci. Nanotechnol.*, **2012**, 12, 1024-1031.
- ⁴⁹Yadav, N., Singh, P., Mehrotra, R., *Curr. Pharm. Anal.*, **2012**, 8, 49-55.
- ⁵⁰Xu, J. H., Liu, Y., Y., Ni Q. J., Chen, Y., *Anal. Lett.*, **2012**, 45, 1980-1994.
- ⁵¹Bragagni, M., Mennini, N., Ghelardini, C., Mura, P., *J. Pharm. Pharm. Sci.*, **2012**, 15, 184-196.
- ⁵²Pawar, S. K., Badhwar, A. J., Kharas, F., Khandare, J. J., Vavia, P. R., *Int. J. Pharm.*, **2012**, 183-193.
- ⁵³Pu, X. H., Sun, J., Quin, Y. M., Zhang, X., Zhang, P., Yan, Z. T., He, Z. G., *Curr. Nanosci.*, **2012**, 8, 762-766.
- ⁵⁴Li, W. F., Liu, G. J., Li, L. X., Wu, J., Lu, Y. X., Jiang, Y. B., *Chinese J. Chem. Eng.*, **2012**, 20, 803-813.
- ⁵⁵Sanchez-Munoz, S., Gomez-Ruiz, S., Perez-Quintanilla, D., Morante-Zarero, S., Sierra, I., Prahhar, S., Paschke, R., Kauderovic, G. N., *Chemmedchem*, **2012**, 7, 670-699.
- ⁵⁶Waldameri, G., Rangel, L. P., Spatafora, C., Guitton, J., Gauthier, C., Arnaud, O., Ferreira-Pereira, A., Falson, P., Winnischoffer, S., M., B.Rocha, M. E. M., Tringali, C., di Pietro, A., *ACS Chem. Biol.*, **2012**, 7, 321-329.
- ⁵⁷Choi, S., K., Verma, M., Silpe, J., Moody, R. E., Tang, K., Hanson, J. J., Baker, J. R., *Bioorg. Med. Chem.*, **2012**, 20, 1281-1290.
- ⁵⁸Blaszczak-Swiatkiewicz, K., Mirowski, M., Kapinska, A., Mikiciuk-Olasik, E., *Acta Biochim. Polonica*, **2012**, 59, 279-288.
- ⁵⁹Ma, W. N., Lu, S., Pan, P., Sadatmousavi, P., Yuan, Y., F., Chen, P., *Plos One* **2012**, 8, Article number: e43684.
- ⁶⁰Ragazzon, G., Bratsos, I., Alesso, E., Salassa, L., Habtemarian, A., McQuitty, R., Clarkson, G., J., Sadler, P. J., *Inorg. Chem. Acta* **2012**, 393, 230-238.
- ⁶¹Wang, M., Xu, L., Gao, M. Z., Iller, K. D., Sledge, G. W., Zheng, Q. H., *Steroids* **2012**, 77, 864-870.
- ⁶²Yang, J., Ahn, s., Wu, Z. R., Hwang, D. J., Miller, D. D., Dalton, J. T. *Int. J. Oncol.* **2012**, 41, 337-344.
- ⁶³Nakano, Y., Saita, T., Fujito, F., *J. Pharm. Soc. Japan* **2012**, 132, 727-732. (in Japanese, abstract in English).
- ⁶⁴McKaege, M. J., Fong, P. C., Hong, X., Flarakos, J., Mangold, J., Du, Y., Tanaky, C., Schran, H., *Cancer Chemother. Pharmacol.*, **2012**, 69, 1145-1154.
- ⁶⁵Cielecka-Piontek, J., Jelinska, A., Dolham, A., Zalewski, P., Burek, D., Piekarski, M., Krause, A., Uszak, J., Oszczapowich, I., Lukawszka, M., *Asian J. Chem.* **2012**, 24, 769-772.
- ⁶⁶Abramkin, S., Valiahdi, S. M., Jakupec, M. A., Galanski, M., Metzler-Nolte, N., Keppler, B. K., *Dalton Trans.*, **2012**, 41, 3001-3005.
- ⁶⁷Chang, H., Fu, Y. J., Yuan, L. J., Yi, L., Xu, H. X., Zhou, Y., Zhu, J. D., Zhang, Q., Y., Mi, M. T., *Breast Cancer Res.* **2012**, 14, article number: R80 DOI:10.1186/ber3194.
- ⁶⁸Bao, C. Y., Jin, M., Li, B., Xu, Y. D., Jim, J. Y., Zhu, L. Y. *Org. Biomol. Chem.*, **2012**, 10, 5238-5244.
- ⁶⁹Moore, R. G., Lange, T. S., Robinson, K., Kim, K.K., Uzun, A., Horan, T. C., Kavar, N., Yano, N., Chu, S. R., Mao, Q. F., Brard, DePaepe, M. E., Padbury, J. F., Arnold, L. A., Brodsky, A., Shen, T. L. Singh, R. K., *Plos One* **2012**, 7, article number: e34443, DOI: 10.1371/journal.phone.003443.
- ⁷⁰Singh, R., Meena, A., Negr, A. S. Shanker, K., *JPC-J. Planar Chrom. Mod. TLC* **2012**, 25, 10-18.

Received: 05.05.2013.

Accepted: 06.05.2013.



SYNTHESIS, CRYSTALLOGRAPHICAL AND THEORETICAL INVESTIGATION OF 7-BENZYL-3H-1,2,4-TRIAZOLO[3,1-i]-PURINE

Asieh Yahyazadeh^{[a]*}

Keywords: diaminomaleodinitrile, purine, iminopurines, triazolopurines, theoretical investigation

The title compound has been prepared in high yield from 9-benzyl-purine derivative by reaction with diethoxymethyl acetate (DEMA). The structure of the tricyclic compound, 7-(2-chlorobenzyl-3H-1,2,4-triazolo[3,1-i]purine (**2**), was confirmed by X-ray analysis. Semiempirical calculations for predicting geometrical parameters are in excellent agreement with the X-ray crystal structure.

Corresponding Authors*

Tel/Fax +981313233262

E-Mail: Yahyazadehphd@yahoo.com,

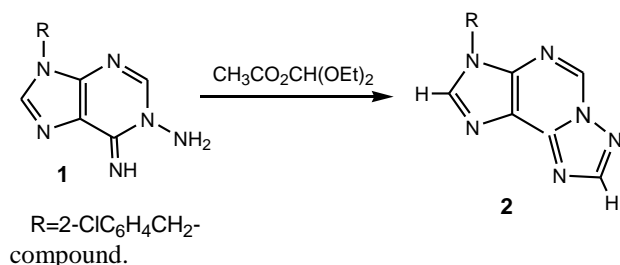
Yahyazadeh@guilan.ac.ir

[a] Department of Chemistry, University of Guilan, P.O. Box 41335-1914, Rasht, Iran

Introduction

Fused triazoles have been found to exhibit a wide range of biological activities.¹⁻³ Most of these compounds show significant *in vivo* antitumor and antiviral activity and, in addition, possess fluorescent properties which makes them of interest as biological probes.⁴⁻⁷

As a class of compounds the s-triazolo[3,1-i]purines have been prepared from the corresponding 6-hydrazinopurines by reaction with diethoxymethyl acetate (DEMA).⁸⁻¹¹ As part of our ongoing study of the use of diaminomaleodinitrile as a cheap starting material for a range of imidazole, purine, dihydropurine and pyrimidine derivatives. We have previously described the synthesis of some derivatives of 1-amino-9-aryl-(or benzyl)-6-iminopurines.⁵⁻⁹ We decided to investigate the reaction of 1-amino-9-benzyl-6-iminopurine (**1**) with cyclizing agent diethoxymethyl acetate to see whether this might provide a route to 7-(2-chlorobenzyl)-3H-1,2,4-triazolo[3,1-i]purine



Scheme 1.

Results and Discussion

1-Amino-9-(2-chlorobenzyl)-6-iminopurine (**1**) was prepared via a multistep synthesis from ethyl (Z)-N-(2-amino-1,2-dicyanovinyl)formimidate,⁶⁻¹⁰ by a treatment with benzylamine in a 1:1 molar ratio in ethanol in the presence of a catalytic amount of anilinium hydrochloride to give the corresponding formamidine. Cyclisation of the formamidine in the presence of a strong base, aqueous KOH solution, provided the corresponding 5-amino-1-benzyl-4-cyanoimidazole, which are readily converted to 1-amino-9-benzyl-6-iminopurine by treatment with HC(OEt)₃ and Ac₂O followed by reaction with hydrazine hydrate.¹¹⁻¹⁵

On heating **1** with an excess of diethoxymethyl acetate (DEMA), 7-benzyl-3H-1,2,4-triazolo[3,1-i]purine **2** is obtained in good yield. Compound **2** was refluxed in diethoxymethyl acetate for 4-5 hours, after which time TLC showed that all starting material had been consumed. Removal of the solvent and addition of water to the residue followed by extraction with chloroform gave pure compound **2** in 87% yield as pale yellow crystal and after recrystallization from chloroform-hexane that was characterized fully.

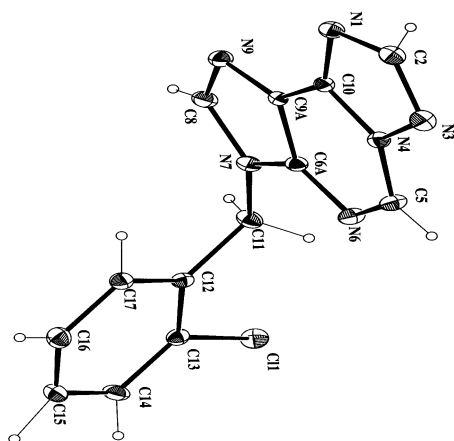
The microanalysis and mass spectra of the isolated triazolopurine **2** was satisfactory. The ¹H NMR spectra had some interesting features. The H-8 of the imidazole ring shifted to higher field at 8.78, with H-2 of the purine ring at 8.90 ppm and H-5 at 9.82 ppm. The ¹³C NMR spectra of the compound **2** had the expected number of bands, with the C-8 carbon having a chemical shift at δ 141.8, C-5 at δ 147.7 and C-2 at δ 158.9 ppm. The infrared spectrum confirmed the presence of the C=N stretching vibration in the region of 1600-1680 cm⁻¹.

Crystals of compound **2** suitable for a single crystal X-ray structure determination was obtained and the results (Fig. 1.) confirmed the expected structure. As far as we are aware the X-ray structure of a **2** has not been reported previously. However, the structure is almost analogous to that established for 3-methyl-3H-1,2,4-triazolo[5,1-i]purine reported by Asano *et al.*¹⁶

Table 1. X-ray structure data, AM1 and PM3 computational studies of 7-(2-chlorobenzyl-3*H*-1,2,4-triazolo[3,1-*i*]purine (**2**).

X-ray crystal structure		Theoretical data		X-ray crystal structure		Theoretical data	
Bond	Angle (o)	AM1	PM3	Bond	Angle (o)	AM1	PM3
C10-N1-C2	101.9(4)	103.22	103.4	N9-C9a-C10	132.9(4)	132.3	133.0
N3-C2-N1	118.1(4)	114.6	110.8	C6a-C9a-C10	116.0(4)	117.2	116.9
C2-N3-N4	100.8(4)	104.2	105.9	N1-C10-N4	109.8(4)	108.5	106.6
C5-N4-N3	124.9(4)	129.6	127.6	N1-C10-C9a	136.4(4)	135.5	137.1
C5-N4-C10	125.5.6(4)	121.0	123.3	N4-C10-C9a	113.7(4)	115.8	116.1
N3-N4-C10	109.4(4)	109.2	108.9	N7-C11-C12	114.5(4)	117.1	115.7
N6-C5-N4	121.3(4)	121.3(4)	120.4	C17-C12-C13	117.7(4)	118.5	118.5
C5-N6-C6a	115.5(4)	116.0	117.9	C17-C12-C11	122.2(4)	123.1	123.7
N6-C6a-N7	127.0(4)	129.3	128.7	C13-C12-C11	120.0(4)	119.2	120.1
N6-C6a-C9a	127.8(5)	125.2	125.1	C14-C13-C12	121.6(5)	120.8	121.1
N7-C6a-C9a	105.2(4)	105.4	106.0	C14-C13-C11	119.4(4)	118.3	118.6
C6a-N7-C8	106.2(4)	105.8	107.1	C12-C13-C11	118.9(4)	120.8	120.2
C6a-N7-C11	127.0(4)	126.9	127.2	C15-C14-C13	120.4(5)	119.7	119.5
C8-N7-C11	126.7(5)	127.0	126.5	C14-C15-C16	119.4(5)	119.9	119.8
N9-C8-N7	113.4(5)	113.5	112.9	C15-C16-C17	120.8(5)	120.2	120.4
C8-N9-C9a	104.3(4)	104.8	107.7	C12-C17-C16	120.0(5)	120.7	120.4
N9-C9a-C6a	110.9(4)	110.3	109.0	N9-C9a-C10	132.9(4)	132.3	133.0

It can be seen from this that the C-N double bonds are localised between C8-N9, C9a-C6a, N6-C5 and N3-C2. The three rings from a plane with the 2-chlorobenzyl group bent out of the plane as anticipated. From an examination of the ¹H NMR chemical shifts of the three ring protons it is clear that the proton on C5 is the most highly deshielded (9.65 ppm) followed by the proton on C2 (8.72 ppm) with the proton on C8 being least deshielded (8.61 ppm).

**Figure 1.** X-ray structure of 7-(2-Chlorobenzyl)-3*H*-1,2,4-triazolo[3,1-*i*]purine **2** with atomic numberings

Computational studies

The most promising semiempirical SCF-MO methods for predicting geometries and electronic properties were AM1 and PM3, as implemented in MOPAC program.¹⁴ MOPAC 6.0 was used exclusively for the work presented herein. The geometry of the 7-(2-chlorobenzyl)-3*H*-1,2,4-triazolo[3,1-*i*]purine **2** has been studied with using

semiempirical molecular orbital methods. This compound has C1 point group and ΔH formation 194.489 kcal mol⁻¹ with dipolment 4.289 Debye.

Table 2. X-ray structure data, AM1 and PM3 computational studies of 7-(2-chlorobenzyl-3*H*-1,2,4-triazolo[3,1-*i*]purine (**2**).

X-ray crystal structure		Theoretical data	
Bond	Length (Å)	AM1	PM3
C11-C13	1.754(5)	1.703	1.687
N1-C10	1.326(6)	1.354	1.352
N1-C2	1.357(7)	1.407	1.391
C2-N3	1.314(7)	1.364	1.340
N3-N4	1.378(6)	1.347	1.377
N4-C5	1.368(7)	1.402	1.415
N4-C10	1.384(6)	1.457	1.422
C5-N6	1.292(7)	1.319	1.318
N6-C6a	1.351(6)	1.387	1.388
C6a-N7	1.366(6)	1.402	1.403
C6a-C9a	1.387(6)	1.451	1.413
N7-C8	1.371(7)	1.412	1.409
N7-C11	1.461(6)	1.432	1.467
C8-N9	1.305(7)	1.339	1.392
N9-C9a	1.370(6)	1.393	1.392
C9a-C10	1.419(6)	1.426	1.422
C11-C12	1.513(7)	1.503	1.499
C12-C17	1.390(7)	1.397	1.394
C12-C13	1.393(6)	1.406	1.400
C13-C14	1.373(7)	1.397	1.391
C14-C15	1.366(8)	1.393	1.389
C15-C16	1.375(9)	1.393	1.390
C16-C17	1.395(8)	1.394	1.391

All calculations were performed using AM1 and PM3 at high precision, and then the geometrical predictions have been compared with known X-ray crystal structure for this compound and have been found to be in excellent agreement¹⁵⁻²⁰. For comparison the main calculated bond length and angles of the compound **2** were shown in Tables 1 and 2.

Experimental

All solvents purified and dried using established procedures. The ¹H NMR spectra were recorded on Hitachi-Perkin-Elmer R24B (60 MHz) or Bruker XL 300 (300 MHz) instruments (with J-values given in Hz), ¹³C NMR spectra (with DEPT 135) either on a Bruker WP 80 or XL300 instrument, and IR spectra on a Shimadzu IR-435 spectrophotometer. Mass spectra were recorded on a Kratos Concept instrument. The melting points were measured on an Electrothermal digital melting point apparatus and are uncorrected. The single crystal X-ray crystallography measurements were made on a Siemens R3m/v diffractometer with graphite-monochromated Mo-K α X-radiation. The data were collected at a temperature -40 \pm 1 $^{\circ}$ C using the $\omega/2\theta$ scanning technique to a maximum of 2 θ value of 46.1 $^{\circ}$. The structure was solved by direct methods using SHELXS-86 and DIRDIF.²¹⁻²²

1-Amino-9-(2-chlorobenzyl)-6-aminopurine (1)

To a stirred solution of the 1-benzyl-4-cyano-5-[(ethoxymethylene)amino]imidazole¹⁵ (0.30 g) in dry methanol (8-10 cm³) under an argon atmosphere at room temperature was added hydrazine monohydrate (1M equivalent). After 15-20 minutes, the separated precipitate was filtered off, washed with a mixture of dry diethyl ether/hexane (1:1), and dried under vacuum to give (**1**) as a white crystalline solid. M.p. 170-172 $^{\circ}$ C. ν_{\max} (mujol mull) 3300 m, 3285 s, 3150 m, 3140 s, 3095 s (NH str.), 3040 s, 2980 m, 1650 s (C=N str.), 1600 m (N-H bend), 1560 s, 1550 s, 1510 m, 1480 m, 1450 m, 1380 m, 1350 m, 1220 s, 1205 m, 1180 s, 1145 s, 1075 s, 1045 m, 945 s, 860 m, 820 s, 760s cm⁻¹; δ_{H} (300 MHz, d₆-DMSO, TMS Int. Ref.) 5.68 (s, 2H, H10), 5.94 (s, 2H, NH₂), 7.25 (dd, 1H, ³J_{16,15} 7 Hz, ⁴J_{16,14} 1Hz, H16), 7.6 (overlapping 2 x dt, 2H, ⁴J_{14,16} 1Hz, ³J_{15,13} 1Hz, ³J_{14,13} 8Hz, ⁴J_{14,15} 2Hz, H14 & H15), 7.8 (dd, 1H, ³J_{13,14} 7Hz, ⁴J_{13,15} 1Hz, H13), 8.22 (s, 1H, H8), 8.26 (s, 1H, H2) ppm; δ_{C} (75 MHz, d₆-DMSO) 48.5 (C10, by DEPT 135), 126.2 (C5), 131.8 (C15), 133.1 (C16), 133.7 (C14), 133.8 (C13), 136.0 (C12), 138.0 (C11), 143.7 (C8), 145.9 (C4), 152.2 (C2), 158.2 (C6) ppm; m/z (EI) 275 (M+1)⁺ 24.0%, 274 (M)⁺100%, 154 [(M+1)-C₄H₄N₅]⁺ 73.3 %, 136 (53.3%), 107 (13.4%); (Calcd. for C₁₂H₁₁N₆Cl : C, 52.6; H, 4.1; N, 30.6, Cl, 12.9.; Found : C, 52.6; H, 4.4; N, 29.4; Cl, 13.1).

3-(2-Chlorobenzyl)-3H-1,2,4-triazolo[3,2-i]purine (2)

A stirred solution of 1-amino-9-(2-chlorobenzyl)-6-aminopurine (1.45 g, 5.3 mmol) in diethoxymethyl acetate (15 cm³) was refluxed for 5h. After TLC (CHCl₃/EtOH 1:1) showed that no starting material remained, most of the solvent was removed under vacuum, then a mixture of

EtOH and CHCl₃ (1:1) was added to give a pale yellow precipitate. This was filtered, washed with diethyl ether to give compound **2** (1.30g, 4.6 mmol, 87%). M.p. 219-220 $^{\circ}$ C ν_{\max} (Nujol mull) 3120 s, 3080 s, 2980 w, 2940 w, 1680 s (C=N str.), 1600 w, 1575 w, 1540 w, 1495 s, 1470 s, 1440 m, 1430 s, 1360 s, 1340 m, 1320 s, 1270 m, 1210 m, 1180 s, 1160 s, 1055 m, 920 s, 870 m, 760s, 690 m, 640 s cm⁻¹; δ_{H} (300 MHz, d₆-DMSO, TMS Int. Ref.) 5.7 (s, 2H, H11), 7.3 (d, 1H, ³J_{16,17} 7Hz, H17), 7.5 (t, 1H, ³J_{16,17} and ³J_{16,15} 7.6 Hz, H16), 7.6 (t, 1H, ³J_{15,16} and ³J_{15,14} 7.6 Hz, H15), 7.8 (d, 1H, ³J_{14,15} 7.7 Hz, H14), 8.6 (s, 1H, H8), 8.72 (s, 1H, H2) 9.65 (s, 1H, H5) ppm; δ_{C} (75 MHz, d₆-DMSO) 49.1 (C11), 131.7(C17), 133.4(C16), 133.6(C15), 133.8(C14), 136.0 (C12), 137.5 (C13), 141.8 (C8), 145.5 (C9a), 147.7 (C5), 151.8 (C6a), 153.4 (C10), 158.9 (C2) ppm; m/z (EI) 285 (M+1)⁺ 100%, 284 (M)⁺ 9.2%, 249 (M-Cl)⁺ 5.3 %, 165 (5.5%), 154 (40%); [Calcd for C₁₃H₉N₆Cl : C, 55.0; H, 3.16; N, 29.6, Cl, 12.3% Found : C, 55.7; H, 3.2; N, 29.9; Cl, 12.6).

Acknowledgments

We are thankful to the Guilan University Research Council for the partial support of this work.

References

- Lockhart, C. C. and Sowell, J. W. Sr, *J. Heterocyclic Chem.* **1996**, *33*, 659.
- Ganapati, A. and Townsend, L. B. *J. Chem. Soc., Perkin. 1*, **1981**, 2387.
- Huang, G. F., Maeda, M., Okamoto, T. and Kawazoe, Y., *Tetrahedron.* **1975**, *31*, 1363.
- Huang, G. F., Okamoto, T., Maeda, M., Kawazoe, Y., *Chem. Pharm. Bull.*, **1974**, *22*, 1938.
- David, F. and Leonard, J., *J. Org. Chem.*, **1974**, *39*, 3438.
- Hand, E. S. and Baker, D. C., *J. Chem.*, **1984**, *62*, 2570.
- Gatta, F., Rosaria, M., Giudice, D. and Borioni, A., *J. Heterocyclic Chem.*, **1994**, *31*, 1171.
- Asano, S., Itano, K., Yamagata, Y. and Kohda, K., *J. Heterocyclic Chem.* **1996**, *33*, 1115.
- Kohda, K., *Tetrahedron*, **1993**, *49*, 8795; Kohoda, K., Yasuda, M., Ukai, H., Baba, K., Yamagata, Y. and Kawazoe, Y., *Tetrahedron*, **1989**, *45*, 6367.
- Kohoda, K., Baba, K. and Kawazoe, Y., *Chem. Pharm. Bull.* **1986**, *34*, 2298.
- Yahyazadeh, A. and Sharifi, Z., *Phosphorus, Sulfur, Silicon*, **2006**, *6*, 1339.
- Schmidt, A. P., Lara, D. R. and Souza, D. O., *Pharmacol.* **2007**, *116*, 401.
- Piguel, S. and Legraverend, M., *J. Org. Chem.* **2007**, *72*, 7026.
- Yahyazadeh, A., *J. Pharm. Research* **2009**, *2*, 3.
- Yahyazadeh, A. and Booth, A. L. *Synth. Commun.* **2002**, *32*, 3241.
- Asano, S., Itano, K., Yamagata, Y. and Kohda, K., *Nucleosides & Nucleotides.* **1994**, *13*, 1453.
- Stewart, J. J. P., MOPAC, A Semiempirical Molecular Orbital Program QCPE 455, **1983**, version 6, 1990.

- ¹⁸Atkinson, I. M., Lindoy, L. F., Matthews, O. A., Meehan, G. V., Sobolev, A. N. and White, A. H. *Aust. J. Chem.* **1994**, *47*, 1155.
- ¹⁹Peng, G., Nichols, J., McCullough, Jr. E. A. and Spence, J. T., *Inorg. Chem.* **1994**, *33*, 2857.
- ²⁰Jin, H. L., Sunkyung, L. and Sun, C. J., *Mol. Graph. Mod.*, **2010**, *28*, 883.

- ²¹Sheldrick, G. M., SHELX86, *University of Gottingen*, **1986**.
- ²²Sheldrick, G. M., in "Crystallographic Computing" 3rd ed. G. M. Sheldrick, C. Kruger and R. Goddard, OUP, p. 175.

Received: 09.03.2013.
Accepted: 05.05.2013.



CRUSH SYNDROME INFLUENCE ON THE ULTRASTRUCTURE OF HEPATOCYTES AND NEURONES

Karapetyan, G. R.^[a], Kukurtchyan, N. S.^[a], Kevorkian, G. A.^[a]

Keywords: Crush syndrome, PRP-1, TEM, neurone, hepatocyte, mitochondria (Mch).

The aim of this study was to find the dynamic of ultrastructural changes of liver at CS and the role of PRP-1 (proline rich peptide) as a protector. Our investigation demonstrated that Mch (mitochondria) of brain are more subject to changes at 2 h of compression than liver Mch, but one time administration of the PRP-1 in a dosage of 10 µg/100 g of the animal weight before decompression period prevent the development of the destructive changes of the hepatocytes of the liver and neurons of the rat cortex (injection of PRP on the background of CS prevent progress of ultrastructural changes typical at 4 h of decompression, and leads to Mch fission).

Corresponding Authors: Karapetyan G.R.

Fax: +374 -10-28 19 51

E-Mail: sapootraa_A@yahoo.com

[a] H. Buniatian Institute of Biochemistry, of National Academy of Sciences of Republic Armenia, Paruir Sevag str. 5/1, 0014, Yerevan, Republic of Armenia.

INTRODUCTION

Earthquake is one of the most dangerous nature cataclysms.¹ Sudden buildings destroy as well as the damages and death of the people caused by the earthquake is more than 90 %. At last 20 years developed the knowledge basis and the tactics chose at such cases.² In current study we were chosen the experimental model of traumatic stress - crush syndrome (CS).³

CS is a special type of traumatic injury of the organism with a specific clinical development of the pathogenesis with a high lethality (up to 70 %).⁴

Today one of the most actual questions is studying the pathology of Crush syndrome (CS) and searching the ways prevent the metabolism disturbances caused by toxins formed in ischemic muscle during decompression. CS follows by acute hemodynamic shock, myoglobinuria, acute renal insufficiency and lethal endotoxicity.⁵

CS is characterized by serious changes in the most parameters of homeostasis, which lead to improve of the patients' treatment. It is already developed the general conceptions of the medical help to the patients with CS. However it could lead to complications especially in excretory and detoxification functions of the organism. There are numerous data indicating that the main intoxication of the organism occurs during decompression, in which toxic metabolic products (toxic peptides) as product from proteolysis of myoglobin are released into the blood from damaged tissue and kidney and accumulated at the targeted organ. Liver damages are wide-spread cause of people disease and death.⁶⁻⁸

An assumption may be suggested that the ultrastructural manifestations of the cell pathology of various organs may occur in all the stages of developing crush syndrome. The

manifestations mentioned have to do both with the cells' and non-cellular structures' components of membranous structure (plasmolemma, mitochondria, nuclear shell) and those of non-membranous structure.

In this work as a protector we have chosen the prolin rich peptide (PRP-1) which is an immunomodulator and neuroprotector with a wide profile of action.⁹ The following important properties of PRP-1 were identified: inhibition of the proapoptotic capasas 3 and 9, activation of 2 and 6 capasas,¹⁰ stimulation of the immuncompetent cells (T, B and macrofagus),¹¹ involving in the mechanisms of interleukin expression (TNF, IL-1, IL-6) in fibroblasts, macrophages and astrosites, neuroprotection against many toxic products produced in organism, has an antimicrobial and antivirus influence.¹²

As at CS we observe the toxic products produced by organism itself (in the ischemic muscle during compression and released into the blood stream during decompression), so in this model, we decided to use PRP-1, taking into consideration all its properties, especially its neuroprotection effect against many toxic products produced in the organism.

Experimentally proved that under compression, white rats that received intraperitoneal PRP-1 before decompression period survived up to 100% (without PRP-1 administration the death of the animals was up to 25-30%), and the damage corrected by PRP-1, in some cases reached to intact level.

It was shown that PRP lead to increase of glucose utilization in the brain during different periods of decompression, which was different in the myocardium and kidneys.

Previous morphological studies were carried out with an hour compression and 1-3 days decompression period, respectively. However, the question of the brain and liver ultrastructure at longer period of compression still remains unknown.

The aim of this study was to find the dynamic of ultrastructural changes of liver at CS and the role of PRP-1 as a protector.

MATERIAL AND METHODS

Reagent: powder paraformaldehyde; OsO₄; Sodium cacodylate trihydrate; 90° ethyl alcohol, acetone, Epon 812, Epon Hardener MNA, Epon Hardener DDSA, Epon accelerator DNP-30, uranyl acetate, citrate Na, Nitrate Pb, photo plates.

All reagent used were of analytical grade and purchased from Sigma Chemical Co. (USA).

Animals: All procedures involving animals were approved by the Institutional Review Board/ Institutional Animal Care and Use Committee (H. Buniatian Institute of Biochemistry, Yerevan, NAS RA) conformed to the European Communities Council directives (86/609/EC). For all experiments, two-month-old male rats weighing 150-200 g obtained from our breeding colony were used. Animals were maintained at normal room temperature with free access to food and tap water. The experimental model of Crush syndrome (CS) was induced by compression of femoral soft tissues using a special press with a compression force 100 kg kg⁻¹ of body weight for 2 h.

Rats were divided randomly into four groups ($n=5$ in each group). Group I – intact animals; Group II – control (2 h compression); and 2 experimental Groups (III and IV): 4 h decompression; PRP-1 injection and 4 h decompression at the end of using PRP-1 (10 µg/100 g of animal weight).

Treatment of material: The bioplates taken immediately after decapitation put in cold 4 °C mix of paraformaldehyde on cacodylate buffer and glutaraldehyde for 12 hours with following post fixation in 1 % OsO₄ solution during 2 hours; dehydration in ascending series of spirits; saturation in a mixture of acetone and epon resins of different proportions and pouring in gelatinous capsules into epon.

Obtaining of ultrathin slices and its treatment: The ultrathin slices (up to 500 Å) were made using ultracut LKB (Swedish) and Reichert (Austria). Ultrathin slices were double contrasted with uranyl acetate and lead citrate.

Observation under TEM: Obtained ultrathin slices were observed under the transmission electron microscope (Phillips CM 10) with resolution X 10-20.000.

Statistical Analysis: Data were expresses as the mean ± S.E.M. All data were analyzed using a one-way analysis of variance (ANOVA) (SigmaStat 3.5 for Windows). Differences were considered as significant at $P < 0.05$.

RESULTS

As have shown the results of our study, in control group of animals (2 h compression) the ultrastructural changes of neurons of cortex and hepatocytes of liver (in particular Mch, Nc, GER and SER) are quite different from ultrastructure of intact group. Thus the specific alterations between organelles of neurons and hepatocytes are also observed. So, it was shown that GER of neurons is in

process of fragmentation and vesiculation, while in hepatocytes it is presented as separate tubules fragments. This indicates on the fact of hypersensibility of cells to the influence of catecholamine's level increasing caused by stress.

Endoplasmatic reticulum is one of the major organelles demonstrate expressed symptoms of a stress and dysfunction at pathology.¹³ Disfunction of ER can cause to organ dysfunction at a strong inflammation caused by endotoxins.¹⁴

As about Mch, at 2 h compressions of soft tissues, in neurons of a brain the tendency of 2-3 organelles fusion is observed (Fig. 1). Thus the cristae are of varies shapes: tubular or in a process of fragmentation.

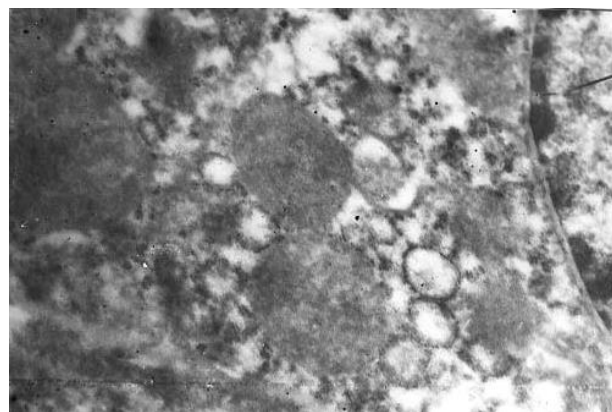


Figure 1. The ultrastructure of neurons at 2 h compression. X 20.000.

In hepatocytes of liver Mch are in groups where the organelles are close contacted to each other, thus no fusion is observed. As about inner membrane of Mch, we can indicate that cristae are generally tubular, practically no process of fragmentation is observed.

Mch are also critical metabolic organelles known as «power system of cells».^{15,16} In addition to their role in cellular bio-energetic, Mch initiate the general forms of the programmed cellular death (apoptosis) through realizing of proteins, such as cytochrome C from an inner membrane.¹⁷

Hepatocytes consist double nuclei, compare to neurons of cortex.

In the first experimental group of animals (2 h compression - 4 h decompression) the ultrastructural changes are developed acutely both in neurons, and in hypatocytes.

As have shown the results of our study in the following group total GER vesiculation process is observed, while SER is presented both in a type of fragmented tubules and by fields consists of vesicles.

Such organelles condition at 4 h decompression caused by the influence of toxins and toxic peptides,¹⁸ produced by ischemic muscle at the 2 h compression and released to the blood at the decompression period, which lead to development of disorder of microcirculation, which in its turn caused the development of acute hypoxia and as a result ischemia of different tissues and organs.¹⁹⁻²²

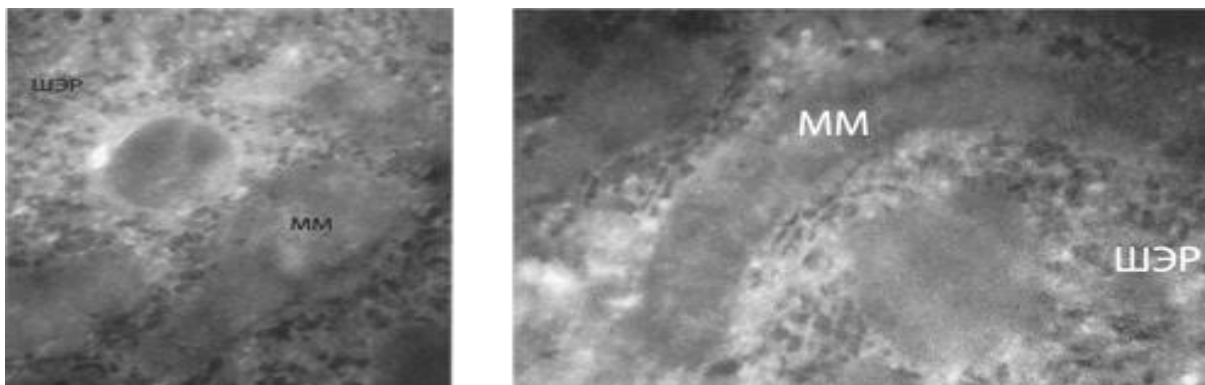


Figure 2. Megamitochondria formation in hepatocytes at 4 h decompression. X 60.000.

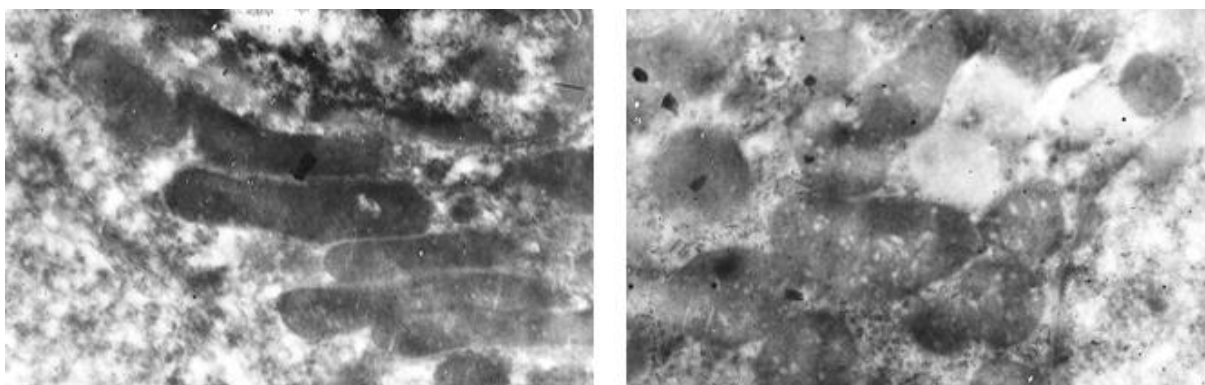


Figure 3. The ultrastructure of neurons Mch at PRP-1 injection. X 25.000.

Such toxic peptides composed of 5-7 amino acids realize into the blood and reach to the target organs lead to the destructive changes and functional disorders.

It's important to mention that Mch of cortex can form conglomerates consist of a great number of fused Mch. Mch matrix has a swollen character. The inner membrane of Mch also has specific alterations. The number of tubular cristae decreased, as well as the number of fragmented cristae, however the process of vesiculation is presented. The Mch of liver hepatocytes are also significantly altered. At 4 h decompression the Mch fuse and the tendency of megamitochondria formation is observed (Fig. 2).

The matrix of Mch is in the process of swollen. The cristae are presented as in a form of tubuls as well as in fragmentation type; it is shown the increasing process of vesiculation tendency.

Increasing of the Mch fussion and fission processes lead to desorganisation of inner membrane of Mch and formation of the tubular and vesiculated cristae.

The ultrastructural architecture of the Mch mostly depends on the quantity and form of cristae. A great number of criastae is observed in tissues with a high need in energy. Such variety in cristae architecture could be explained by different metabolism of organells.²³

As about nuclei we have to mention that as in neurons and in hepatocytes they are swollen with diffused chromatin.

As have shown the results of our study in the second experimental group of animals (2 h compression- PRP-1 injection – 4 h decompression) no ultrastructural changes occur in hepatocytes as well as in neurons. It was shown , that one time PRP-1 administration directly in muscle before decompression neutralize the toxic peptides produced in the ischemic muscle during compression. And inhibit its negative influence on the target organs, in our case on liver and cortex. It was shown that GER in neurons is in a form of tubules and vesicles, while in hepatocytes it's presented by nets. This indicate on the positive effect of PRP-1 on both organs, however its better occurred in hepatocytes, which is caused by sensitivity of neurons to catecholamine's influence, while hepatocytes are less sensitive.

Compare with the Mch of the second group the organelles of the first group do not form conglomerates, and in spite of the fact that there are still observed the fused organelles, but the neurons with single Mch are more common (Fig. 3).

It is important to mention about the influence of the PRP-1 on the inner membrane of Mch. Based on the dates obtained via electron grammas (from tissues and fraction) we indicate increasing of the quantity of tubular and decreasing of vesicular cristae.

As about the Mch of liver hepatocytes we have to say that single injection of PRP-1 lead to the positive changes in the ultrastructure of Mch. It was shown that Mch are closely contact to each other however no process of fusion

was observed. The cristae of Mch were presented in tubules.

DISCUSSION

Today one of the most actual questions is the nature of the toxic damages of organs. It could have as direct and indirect effect, be a result of acute and chronic influence.^{7,24-26}

Organs toxic injuries are widespread cause of the diseases and death in populations.^{6,27-31}

The detoxication reactions are performed by the ferments of endoplasmatic reticulum and Mch,³² that's why any changes in its ultrastructure could have negative effect on the detoxication function of the liver and on the whole its function and on organism. The role of Mch in detoxication is presented by the use of fluorescent microscopy.³²

The influence of hepatotoxic matter lead to damages of parenchyma of liver and destroying of its metabolic fermentative functions. One of the common reasons of death at CS is hyperglycemia at decompression period. At CS develop the immobilization stress activated by toxic peptides form in ischemic muscle.³³ At the compression period the catecholamine level increase which leads to cramp of arterioles and precapillaries lead to falling down the speed of blood flow, endovascular aggregation of erythrocytes and development of thrombus formation. At post compression period toxic products of different etiology produced in ischemic muscles and kidneys realized to the blood and spread to the organism. Such toxic peptides (the toxic products of methabolism) consist of 5-9 amino acids. Which of these toxic peptides is more aggressive from toxic point of view is still unknown.¹⁸

As have shown the results of our study at CS take place the process of aggregation of erythrocytes in sinusoids, which become more critical at 4 h decompression period. Progression of microcirculation dysfunction lead to development of acute hypoxia and as result to ischemia of different organs and tissues.¹⁹⁻²¹ Ischemic damage of different organs and tissues is still one of the most actual problems in medicine and biology. One of the most important factors in the pathogenesis of CS is cells energy deficit, which lead to disruption of intra and extra cellular transport, as well as damage of protein synthesis apparatus of cells.^{3,34} Typical for the 24 h decompression after 1 h compression is damages of the organelles ultrastructure, such as destroying of cristae of Mch. Fragmentation of GER, observation of ribonucleotides masses in cytoplasm as well as partial necrosis foci in hepatocytes.

According to literature dates obtained by different authors, it could be mentioned that alterations ultrastructure of Mch indicate the functional condition of the organelles, depend on the level of energy metabolism.^{35,36} Mch change their forms dynamically by fusion and fission processes.³⁷

Structural changes of Mch divided into 2 main categories: simple swelling³⁸ and formation of mega mitochondria (MM).^{39,40} There are different points of view

concerning the ways of MM formation. Some authors consider, that MM form as a result of nearby Mch fusion,⁴¹⁻⁴³ the others suggest that MM are formed by growth of single Mch, and not by fusion of small Mch.⁴⁴

The process of formation of atypical by the structure and size Mch in cells are related to the different diseases or physiological condition of the organism, such as erythroleucosis in bone marrow, in endometric cells before ovulation process, etc.^{40,45} For each disease Mch have its unique typical just for current disease form. However such giant Mch could accumulate in post mitotic cells depend on the disease type, as well as on the age dependant alterations. It must be mentioned that such organelles have a low inner membrane potential and have no ability to fuse to the other giant or normal Mch.⁴⁶ As have shown the results of our study the morphology of Mch is different depend on CS. So, at 2 h compression there is no viewable alteration in Mch structure however their physiological condition is changed. They are presented in groups where the organelles are closely contacted to each other. As a response to the pain the level of catecholamine in blood increase making Mch more tension, which could be explained by increasing of energy need in hepatocytes. However, increasing of catecholamine level in blood does not influence on the structural safeness of Mch. At 4 h decompression organelles condition become more critical. In spite of the fact that organelles are presented as groups, the size and forms of Mch are very different, and the polymorphism of Mch is observed. Organelles are swollen; in some cases the tendency of MM formation is observed. In literature dates is known that at ischemia, partial hepatoectomy etc, take place the process of Mch swelling.³⁸ It must be mentioned that 24 h after hepatoectomy not only swelling of Mch but also cristae number reducing tendency is observed, which however recovered 96 hr, after partial hepatoectomy.⁴⁷ So if at 2h compression cristae had tubular or vesicle type, then at 4h decompression it is observed almost completely reduction of the cristae, which has its influence on the functional activity of Mch. It's known that at chronically liver diseases take place MM formation with reduction of cristae.⁴⁸ However at 4 h decompression at CS the influence of stress factor has a short time and unlike the dates mentioned above we observe just a tendency of MM formation with reduction of cristae, while the normal size Mch with reduced cristae are often observed, which is suggested as an nonspecific adaptive cellular response to the influence of toxin produced by ischemic muscles. It is well known that alterations in Mch ultrastructure such as remodeling of cristae are included in initiation of cell death.⁴⁹ Mch lost their cristae normal morphology can't realize their function and falling out of cell energy supplying function, lead to disruption of energy dependent processes of metabolism such as liver detoxication function.

Under the influence of PRP-1 on the background of CS the results are quite different from the CS. It was shown that PRP-1 has a protective influence on the ultrastructure of all organelles. Nuclei are in the range of norm, while at CS it was in the process of fragmentation. The inner membrane of Mch persist its safeness. The cristae are presented by the type of tubule or vesicle, compare with CS group, where the practically totally reduction of cristae was observed. As about GER we have to mention that it's

presented by whole nets, while in CS group there was a fragmentation and vesiculation process.

The results of present study update the information about the influence of traumatic stress on the ultrastructure of neurones and hepatocytes, as well as give new dates about PRP-1 as a corrector. Obtained dates have an important theoretical significance because of the increasing number of toxically injures in population. Morphological reconstruction observed at different stresses indicate to the necessity of new drugs developments lead to prevent neurons and hepatocytes ultrastructure injures.

CONCLUSION

CS as a specific type of traumatic damages lead to the whole complex of ultrastructural pathology. Our investigation demonstrated that Mch of brain are more subject to changes at 2 h of compression than liver Mch, but one time administration of the PRP-1 in a dosage of 10 µg/100g of the animal weight before decompression period prevent the development of the destructive changes of the hepatocytes of the liver and neurones of the rat cortex (injection of PRP on the background of CS prevent progress of ultrastructural changes typical at 4 h of decompression, and leads to Mch fission).

REFERENCES

- 1Briggs, S. M., *Surg. Clin. North Am.*, **2006**, 86(3), 537-44.
- 2Ashkenazi, I., Isakovich, B., Kluger, Y., Alfici, R., Kessel, B., Better, O. S., *Prehosp. Disaster Med.*, **2005**, 20(2), 122-133.
- 3Kevorkian, G. A., Kanayan, A. S., Voskarian, L. H., Khachatrian, H. F., *J. Neurochem.*, **1998**, 71, 70.
- 4Wang, L., He, Q., Li, G. S., *Zhongua Neike Zazhi*, **2008**, 47(9), 711-4.
- 5Kevorkian, G. A., Guevorkian, A. G., Kukurtchyan, N. S., Galoyan, A. A., *J. Neurochem.*, **2003**, 87(1), 145-149.
- 6Lewis, J. H., *Curr. Pract. Med.*, **1999**, 2, 49-58.
- 7Mochizuki, M., Shimizu, S., Urasoko, Y., Umeshita, K., Kamata, T., Kitazawa, T., Nakamura, D., Nishihata, Y., Ohishi, T., Edamoto, H., *J. Toxicol. Sci.*, **2009**, 34(2), 175-81.
- 8Zimmerman, H. J., Maddrey, W. C., *Diseases of the liver*, 7th ed. Schiff, L. and Schiff, E. R. eds., **1993**, 707-783.
- 9Galoyan, A. A., *Proc. Int. Conf. Biochem. Mol. Biol., Aspects of the Brain Immune System*. Sep. 15-19, Yerevan-Tsakhkadzor, Encyclopedia Armenica, Armenia, **2001**, 22-34.
- 10Galoyan, A. A., Terio, T., Berg, M., Marks, N., *Neurochemistry (RAS and NAS RA)*, **2000**, 17, 185-188.
- 11Galoyan, A. A. and Aprikian, V. S., *Neurochem. Res.*, **2002**, 27, 305-312.
- 12Galoyan, A. A., *Neurochem. Res.*, **2000**, 25, 1343-1355.
- 13Margaret G. Gregor and Gokhan S. Hotamisligil., *The Journal of Lipid Research*, **2007**, 48, 1905-1914.
- 14Kozlov A. V., Duvigneau JC, Miller I., Nurnberger S., Gesslbauer B., Kungl A., Ohlinger W., Hartl RT., Gille L., Staniek K., Gregor W., Haindl S., Redl H., *Biochim Biophys Acta.*, **2009**, 1792 (6): 521-30.
- 15Wei, Y., Wang, D., Topczewski, F., and Pagliassotti, M. J., *Am J. Physiol. Endocrinol. Metab.*, **2006**, 291(2), E275-81.
- 16Wei Y., Rector, R. S., Thyfault, J. P., Ibdah, J. A., *World J. Gastroenterol.*, **2008**, 14(2), 193-9.
- 17Sun, M. G., Williams, J., Munoz-Pinedo, C., Perkins, G. A., Brown, J. M., Ellisman, M. H., Green, D. R., Frey, T. G., *Nat. Cell Biol.*, **2007**, 9(9), 1057-65.
- 18Kevorkian, G., Kanayan, A., Hayrapetyan, H., Guevorkian A., Melkonyan, L. and Galoyan, A., *FEBS J.*, **2006**, 273, 255.
- 19Lameire, N. H., De Vrise, A. S., Vanholder, R. *Curr. Opin. Crit. Care*, **2003**, 9(6), 481-490.
- 20Malinoski, D. J., Slater, M. S., Mullins, R. J., *Crit. Care Clin.*, **2004**, 20(1), 171-192.
- 21Ismailov, R. M., Shevchuk, N. A., Khusanov, H., *Biomed. Eng. Online*, **2005**, 4(1), 24.
- 22 Gevorkian R., Melkonyan L., Hayrapetyan H., Guevorkian A., Galoyan A., *The FEBS Journal*, **2006**, 273, 77-78.
- 23John, G. B., Shang, Y.-L., Li, L., Renken, C., Mannella, C. A., Selker, J. M. L., Rangell, L., Bennett, M. J. and Zha, J.-P., *Mol. Biol. Cell*, **2005** 16(3), 1543-1554.
- 24Maddrey WC, *J. Clin. Gastroenterol.*, **2005**, 39 (4 Suppl 2): S83-9.
- 25Doi H., Horie T., *Chem. Biol. Interact.*, **2010**, 183 (3), 363-368.
- 26 Kalender S., Uzun FG., Durak D., Demir F., Kalender Y., *Food and Chemical Toxicology*, **2009**, 48 (2), 633-638.
- 27Bass, N. M., Ockner, B. A., *Hepatology: a textbook of liver disease*, 3rd ed., Philadelphia, **1996**, 962-1017.
- 28Holland, E. G., Degruy, F. V., *Am. Fam. Physician*. **1997**, 56(7), 1781-1792.
- 29Schiodt, F. V., Rochling, F. A., Casey, D. L., Lee, W. M., *New Engl. J. Med.*, **1997**, 337(16), 1112-1117.
- 30Plevris, J. N., Schina, M., Hayes, P. C., *Aliment. Pharmacol. Ther.*, **1998**, 12(5), 405-418.
- 31Bond, G. R., Hite, L. K., *Acad. Emerg. Med.*, **1999**, 6(11), 1115-1120.
- 32 Fellous, R., Coulaud, D., El Abed, I., Roques, B. P., Le Pecq, J. B., Delain, E., Gouvette, A., *Cancer Res.*, **1988** 48(22), 6542-9.
- 33 Rawlins, M., Gullichsen, E., Kuttala, K., Peltala, O., Niinikoski, J., *Eur. Surg. Res.*, **1999**, 31(5), 9-18.
- 34 Mikaelian, N. P. *Pathol. Physiol. Exp. Ter.*, **1992**, 1, 19-21.
- 35 Hackenbrock C. R., *J. Cell Biology*, **1968**, 37(2), 345-369.
- 36 Guenthard, J., Wyler, F., Fowler, B., Baumgartner, R., *Arch. Dis. Childh.*, **1995**, 72(3), 233-236
- 37Huang P., Yu T., Yoon Y., *Eur J Cell Biol.*, **2007**, 86 (6), 289-302.
- 38Wilasrusmee, C., Siritheptawee, S., Kanchanapanjapon, S., Sopon, P., Vanichanon, C., Limphong, W., Pongchailerks, P., Lertsithichai, P., Wilasrusmee, S., Kittur, D. S., *J. Hepatobil. Pancreat. Surg.*, **2004**, 11(4), 266-71.
- 39Zamora SA., Pinto A., Scott RB., Parsons HG., *J Inherit Metab Dis.*, **1997**, 20 (4), 509-16.
- 40Guastadisegni, C., Balduzzi, M., Mancuso, M. T., Di Consiglio, E., *J. Toxicol. Environ. Health A.*, **1999**, 57(6), 415-29
- 41Tandler, B., Dunlap, M., Hoppel, C. L., Hassan, M., *Ultrastruct. Pathol.*, **2002**, 26(3), 177-83.
- 42Wakabayashi, T., Horiuchi, M., Sakaguchi, M., Misawa, K., Onda, H., Iijima, M., Allmann, D. W., *Eur J. Biochem.* **1984**, 143(2), 455-65.
- 43Bakeeva, L. E., Manteifel', V. M., Rodichev, E. B., Karu, T. I., *Mol. Biol. (Moscow)*, **1993**, 27(3), 608-17.
- 44Knabe, W., Kuhn, H. J., *Cell Tissue Res.*, **1996**, 285(1), 1-9.

⁴⁵Asano, M., Wakabayashi, T., Ishikawa, K., Kishimoto, H., *Acta Path. Jap.*, **1978**, 28, 205-213.

⁴⁶Navratil, M., Terman, A., Arriaga, E. A., *Exp. Cell Res.*, **2008**, 314(1), 164-72.

⁴⁷Ferri, D., Moro, L., Mastrodonato, M., Capuano, F., Marra, E., Liquori, G. E., Greco, M., *Biol. Cell.*, **2005**, 97(4), 277-88.

⁴⁸Krähenbühl, S., *Pharmacol. Ther.*, **1993**, 60(1), 1-38.

⁴⁹Cheung, E. C., McBride, H. M., Slack, R. S., *Apoptosis*, **2007**, 12(5), 979-92.

Received: 01.05.2013.

Accepted: 18.05.2013.



GIBBS FREE ENERGIES FOR THE SOLVATION OF KClO_3 IN MIXED DMF- H_2O SOLVENTS AT 301.15 K

Esam A. Gomaa^[a], Elsayed M. Abou Elleef^[b] and E. A. Mahmoud^[a]

Keywords: Gibbs free energy, solvation, potassium chlorate, aqueous dimethylformamide

The Gibbs free energies for KClO_3 were evaluated in mixed dimethylformamide (DMF)- H_2O solvents at 301.15 K from the experimental solubility measurements. From the experimental the ionic radii ratio of potassium to chlorate ions, the total free energy of the salt is divided into its individual contribution in the mixtures used. Liberation Gibbs free energy for moving KClO_3 from standard gas state to standard solution state was calculated according to specific cycle for the solvation process using the solubility product. Also the lattice energy for solid KClO_3 (cr) was also calculated and used for further evaluation. The conventional Gibbs free energies for the cation (K^+) and the anion (ClO_3^-) were estimated theoretically and also the Gibbs free energy of ClO_3^- gas was evaluated and all values were discussed.

* Corresponding Authors

E-Mail: eahgomaa65@yahoo.com

[a] Chemistry Department, Faculty of Science, Mansoura University, 35516-Mansoura, Egypt.

[b] Delta Higher Institute for Engineering and Technology, Basic Science Department, Mansoura, Egypt.

absolute values by the value for the absolute Gibbs solvation free energy of the proton.

The conventional Gibbs free energies of solvation for anions are shifted by an equal amount in the opposite direction.

Introduction

For neutral species experimental solvation Gibbs free energies have been tabulated large number of solutes in both aqueous¹⁻⁷ and non-aqueous^{7,8} solvents. Typically, these solvation free energies are determined experimentally⁸ and their uncertainty is relatively low (~ 0.8 kJ/mol).⁹

Determining accurate values for the Gibbs free energies of ionic solutes like KClO_3 is important than that of neutral solutes. Understanding the partitioning of single ions between different liquid phases is important in many areas of biology. For example, the electrical signals sent by nerve cells are activated by changes in cell potential that are caused by the movement of various ions across the neuronal membrane.¹⁰ The division of thermodynamic Gibbs free energies of solvation of electrolytes into ionic constituents is conventionally accomplished by using the single ion solvation Gibbs free energy of one reference ion, conventionally, the proton, to set the single ion scales.^{11,12} The aim of this work is to estimate the single ion Gibbs free energies for K^+ and ClO_3^- ions in mixed DMF- H_2O solvents at 301.15 K.

Sums of solvation free energies of cations and anions are well defined through the use of thermochemical cycles involving calorimetric or electrochemical measurements.¹³⁻¹⁷ A number of different extra thermodynamic approximations have been used¹⁸⁻²⁵ to partition the sums of cation and anion Gibbs free energies into single ion contribution.

Relative and conventional solvation free energies of ions:

The Gibbs solvation free energies of ions as relative free energies by setting the free energy of solvation of some reference ion equal zero.²⁶ Proton was chosen as reference ion. For ions, this result in a set of conventional free energies of solvation that the cations are shifted from their

Conventional Gibbs free energies from reduction potentials

When the convention for the absolute Gibbs free energy of the proton is followed, the solution-phase free energy change associated with the half cell for reduction of hydrogen gas is equal to zero. Reduction potentials following this convention for hydrogen electrode are referred as standard reduction potentials. From the half cell reaction for the reduction of metal cation to crystalline phase and the half reduction reaction of hydrogen gas, the redox reaction can be illustrated through the use of thermochemical cycle.¹² This last procedure can be used to estimate the gas free energy of formation for ClO_3^- ion, to explain the ionic behaviour.

Experimental

Potassium chlorate KClO_3 Griffin Kamp and N-N, dimethylformamide (DMF) from Merck Co, were used.

Saturated solutions of KClO_3 were prepared by dissolving different amounts of the salt in closed test tubes containing different DMF- H_2O mixtures. These mixtures were then saturated with nitrogen gas as inert atmosphere. The tubes were placed in a shaking thermostat (Model Gel) for a period of four days till equilibrium reached. The solubility of KClO_3 in each mixture was measured gravimetrically by evaporating 1 ml of the saturated solution in small cup using I. R. lamp. The measurements were done by three readings for each solution at 301.15 K.

Results and Discussion

The molar solubility (S) for KClO_3 was measured gravimetrically in mixed DMF- H_2O solvents at 301.15 K. The solubility values with an average number of the second

number often comma are cited in Table (1). The (S) value in water agreed well with that in literature values.²⁷ The activity coefficients were calculated by the use of Debye-Hückel equation.^{28, 29}

$$\log \gamma_{\pm} = -0.5062 I^{0.5} \quad (1)$$

where I is the ionic strength calculated from S values. These data ($\log \gamma_{\pm}$) were tabulated also in Table 1.

The solubility product was calculated by the use of equation (2).³⁰

$$\text{p}K_{\text{sp}} = -2\log S + 2\log \gamma_{\pm} \quad (2)$$

The solubility product ($\text{p}K_{\text{sp}}$) data are given in Table (1). From solubility products the Gibbs free energies of solvation and the transfer Gibbs free energies from water to mixed solvents were calculated by using Eqns. (3) and (4). Their values are tabulated also in Table 1:^{31,32}

$$\Delta G = 2.303 RT \text{p}K_{\text{sp}} \quad (3)$$

$$\Delta G_t = \Delta G_s - \Delta G_w \quad (4)$$

where s and w denote solvent and water, respectively.

It was concluded that the Gibbs free energies of transfer (ΔG_t) increases in negativity by increasing the mole fraction of DMF in the mixed DMF- H_2O solvents. This is due to more solvation behaviour in the mixed solvents than that of water (see Fig. 1).

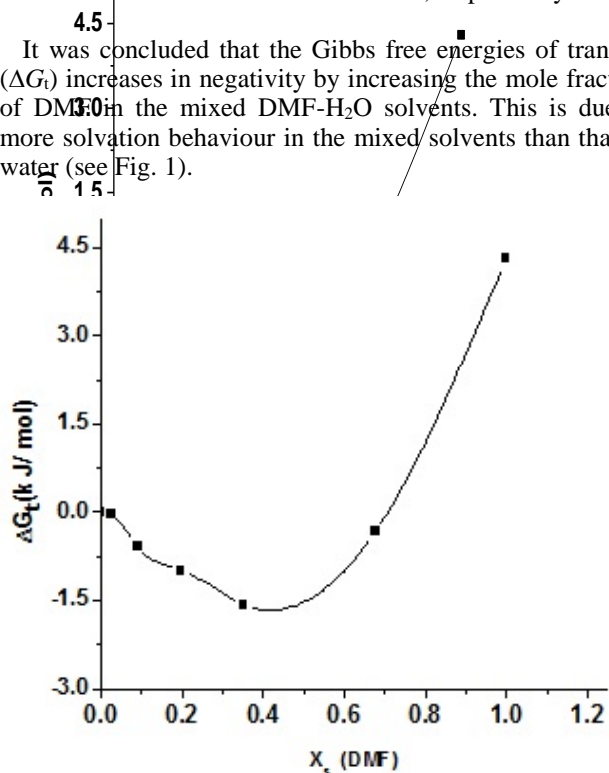


Figure 1. Gibbs free energies of transfer for KClO_3 versus the mole fraction of DMF at 301.15 K.

Single ion Gibbs free energies and convention free energies for K^+ and ClO_3^- ions

It was well known that the preferential single ion thermodynamic parameters depend on the ionic radii of two ions (cation and anion). Therefore the ionic radii ratio between K^+ and ClO_3^- were evaluated from exact radii values given in literature³³ and found to be 0.2788.

Multiply this ratio by the Gibbs free energies of KClO_3 we get the ionic free energies for K^+ ion. This last value was subtracted from the KClO_3 Gibbs free energy we obtain the Gibbs free energies for ClO_3^- anion in KClO_3 . The obtained values for single ions are presented in Table 2. The conventional Gibbs free energies $\Delta G_s^{\text{con}}(\text{K}^+)$ for potassium ion in solvents are shifted from their absolute values by the absolute free energy of the proton³⁴ according to Eqn. (5). And for ClO_3^- anion is shifted by an equal amount in the opposite direction (Eqn. 6):

$$\Delta G_s^{\text{con}}(\text{M}^+) = \Delta G_s^0(\text{M}^+) - \Delta G_s^0(\text{H}^+) \quad (5)$$

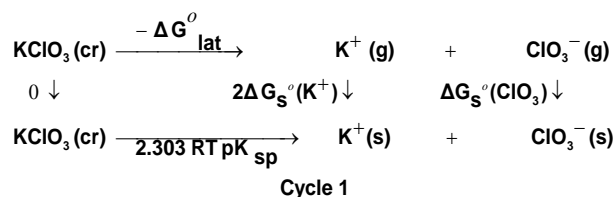
$$\Delta G_s^{\text{con}}(\text{X}^-) = \Delta G_s^0(\text{X}^-) + \Delta G_s^0(\text{H}^+) \quad (6)$$

where $\Delta G_s^0(\text{M}^+)$, $\Delta G_s^0(\text{X}^-)$ and $\Delta G_s^0(\text{H}^+)$ are the Gibbs free energies of solvation for cation, anion and proton in solvents, respectively.

From the mean values of proton solvation free energies in water and other solvents in literature^{12,35,36} relation between these values and the diameter for each solvent taken from,³⁷ straight line was obtained. From this line the proton solvation free energies in pure water and DMF were obtained and found to be 1523 and 1561 kJ mol^{-1} , respectively. Multiplying these value by the mole fraction of each solvent and then sum the results. The mixed solvent proton free energies in DMF- H_2O mixtures were obtained and their values are given in Table 2. Apply Eqns. (5) and (6) we get the conventional Gibbs free energies for the cation and anion and their values are given also in Table 2. Cation conventional free energy values are negative indicating exothermic character and anion values are positive indicating endothermic character. Both values increase with increase in the mole fraction of DMF due to more solvation and the sum of them gives the values for the neutral salt.

Liberation Gibbs free energies for KClO_3 in mixed DMF- H_2O solvents

The liberation Gibbs free energies for KClO_3 in mixed DMF/ H_2O solvents at 301.15 K were calculated following thermochemical cycle 1 as done before¹² for silver salts following solubility product concept:



where ΔG_{lat}^0 is the lattice free energy in kJ mol^{-1} , (g) and (s) denote the gas and solution cases. The lattice energy was calculated following Bartlett's relationship following equation (7).³⁸

Table 1. Solubility and Gibbs free energies for KClO₃ in mixed DMF-H₂O solvents at 301.15 K.

X _s DMF	S, mol L ⁻¹	log γ ±	pK _{sp}	ΔG kJ mol ⁻¹	ΔG _f kJ mol ⁻¹
0	0.244	-0.2514	1.7282	9.8647	0
0.0253	0.246	-0.2524	1.7229	9.8356	-0.0291
0.0909	0.290	-0.2741	1.6234	9.2675	-0.5971
0.3527	0.326	-0.2906	1.5547	8.8756	-0.9891
0.6773	0.391	-0.3183	1.4522	8.2904	-1.5742
0.6773	0.266	-0.2609	1.6720	9.5451	-0.3196
1.0	0.080	-0.1439	2.4816	14.1668	4.3021

Table 2. Single ion Gibbs free energies for K⁺, ClO₃⁻ and their conventional energies at 301.15 K. in mixed DMF-H₂O solvents (in kJ mol⁻¹).

X _s DMF	ΔG(K ⁺)	ΔG(ClO ₃ ⁻)	ΔG _s ^{*con} (K ⁺)	ΔG _s ^{*con} (ClO ₃ ⁻)	ΔG _s ^{*(H⁺)}
0	2.7502	7.1164	-1520.2	1530.11	1523
0.0253	2.7421	7.0934	-1520.2	1530.09	1523
0.0909	2.5837	6.6837	-1520.2	1525.60	1523
0.1965	2.4745	6.4011	-1526.4	1529.40	1529
0.3529	2.3114	5.9790	-1535.5	1543.90	1538
0.6773	2.5511	6.8839	-1549.32	1558.90	1552
1.0	3.9437	10.2170	-1557.05	1571.20	1561

$$\Delta G_{lat} = \frac{232.8}{\sqrt[3]{V}} + 110 \quad (7)$$

The volume of KClO₃ was calculated by dividing its molecular weight by the density of solid given in literature⁴ and apply it in equation (7) to obtain (168.996 kJ mol⁻¹) as ΔG_{lat} for KClO₃.

$$\Delta G_s(K^+) + \Delta G_s(ClO_3^-) = 2.303RTpK_{sp} - \Delta G_{lat} - 2\Delta G^{0 \rightarrow *}$$

On the use of Eqn. (8) cycle (1), the liberation free energy for KClO₃ was obtained (84.498 kJ mol⁻¹).

The ΔG^{0→*}, the free energy change associated with moving KClO₃ from standard gas phase at 1 atmosphere to solution phase. This free energy change has been referred as “compression” work of the gas or liberation free energy.

Conventional free energies from reduction potentials

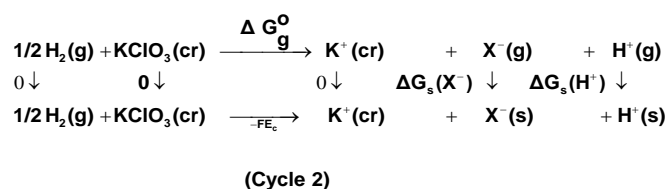
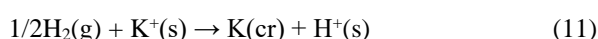
The absolute Gibbs free energy of the proton is followed solution phase free energy change associated with the following half cell.



The half cell reaction for the reduction of cation is:



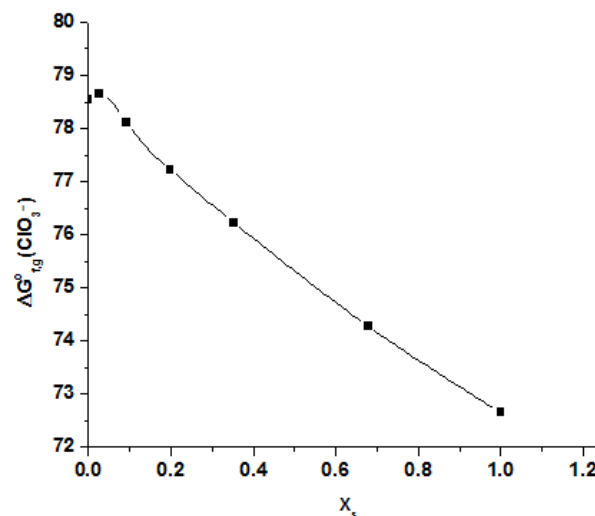
The symbol (cr) denotes the crystalline phase. The sum of the two half cells is:



Through the thermochemical cycle 2, the conventional free energy of K⁺ ion can be written as:

$$\Delta G_s^{*con}(K^+) = \Delta G_f^0(H_g^+) - \Delta G_f^0(K_g^+) - FE_c \quad (12)$$

where ΔG_f⁰(H_g⁺), ΔG_f⁰(K_g⁺) are the gas free energy of formation for H⁺ and K⁺ ions. F is the Faraday's constant, 96.485 kJ per gram equivalent and E_c is the standard reduction potential of K⁺.

**Figure 2.** Relation between ΔG_{f,0}(ClO₃⁻) against the mole fraction of DMF at 301.15 K.

Also the conventional free energy of the chlorate ion can be written following Truhlar¹² explanation as:

$$\Delta G_s^{*con}(\text{ClO}_3^-) = -\Delta G_{f,g}^0 - FE_C - 2\Delta G^{0\rightarrow*} \quad (13)$$

Apply last equation the $\Delta G_{f,g}^0$, gas free energies of formation for the anion ClO₃⁻ and K⁺ estimated in the mixed DMF-H₂O solvents and their values are given in Table 3 and Fig. 2. The $\Delta G_{f,g}^0$ values increase by increase of the mole fraction of DMF favouring less solvation.

Table 3. Gas formation free energy for ClO₃⁻ anion in mixed DMF-H₂O solvents at 301.15 K (in kJ mol⁻¹).

X _s DMF	$\Delta G_{f,g}(\text{ClO}_3^-)$
0	-1731.94
0.0253	-1731.89
0.0909	-1731.49
0.1975	-1731.20
0.3527	-1774.69
0.6773	-1760.59
1.0	-1773.10

References

- Gabani, S.; Gianni, P.; Mollica, V.; Lepori, L, *J. Solut. Chem.* **1981**, *10*, 563.
- Abraham, M. H., Whiting, G. S., Fuchs, R.; Chambers, E. J., *J. Chem. Soc., Perkin Trans. 2*, **1990**, 291.
- Leo, A. J., *Masterfile from Med Chem Software*; Biobytc.: Claremont, C. A., **1994**.
- Physical/Chemical Property Database (PHYSPROP)*; SRC Environmental Science Center: Syracuse, NY, **1994**.
- Yaffe, D., Cohen Y., Espinosa, G., Arenas, A. A., Giralt, F., *J. Chem. Inf. Comput. Sci.*, **2003**, *43*, 85.
- Kelly, C. P.; Cramer, C. J.; Truhlar, D. G., *J. Chem. Theor. Comput.*, **2005**, *1*, 1133.
- Rizzo, R. C.; Aynechi, T., Case, D., A.; Kuntz, I. D., *J. Chem. Theor. Comput.*, **2006**, *2*, 128.
- Thompson, J. D.; Cranier, C. J.; Truhlar, D. G., *J. Phys. Chem. A* **2004**, *108*, 6532.
- Klotz, I. M.; Rosenbery, R. M.; *Chemical Thermodynamics*, 5th ed.; Wiley: New York, **1994**, P459.
- Hodgkin, A. L. *Biol. Rev.*, **1951**, *26*, 339.
- Cramer, C. J.; Truhlar, D. G. In: *Free Energy Calculation in Rational Drug Design*, Reddy, M. R., Eds. Kluwer/Plenum: New York, **2001**.
- Kelly, C. P., Cramer, C. J. and Truhlar, D. G., *J. Phys. Chem. B*, **2007**, *111*(1), 408-422.
- Izmailov, N. A., *Russ. J. Phys. Chem.*, **1960**, *34*, 1142.
- Rossieinsky, D. R., *Chem. Rev.*, **1965**, *65*, 467.
- Pliego Jr. J. R.; Riveros, J. M., *Chem. Phys. Lett.*, **2000**, *332*, 597.
- Llano, J.; Eriksson, L. E., *J. Chem. Phys.*, **2002**, *117*, 10193.
- Bhattacharya, R.; Lahiri, S. C., *Z. Phys. Chem.* **2004**, *218*, 515.
- Conway, B. E., *Annu. Rev. Phys. Chem.*, **1966**, *17*, 481.
- Parker, A., J., *Chem. Rev.* **1969**, *69*, 1.
- Popovych, O., *Crit. Rev. Anal. Chem.* **1970**, *7*, 73.
- Kolthoff, I. M., *Pure Appl. Chem.*, **1971**, *25*, 305.
- Conway, B. E., *J. Solution Chem.*, **1978**, *7*, 721.
- Marcus, Y., *Pure Appl. Chem.*, **1986**, *58*, 1721.
- Krestov, G. A., *Thermodynamics of Solution*; Ellis Horwood; New York, **1991**.
- Coe, I. V., *Int. Rev. Phys. Chem.*, **2004**, *20*, 23.
- Lewis, G. N., Randall, M., Pitzer, K. S., Brewer, L., *Thermodynamics*, 2nd ed.; McGraw-Hill: New York, **1961**, 399.
- Pradyot Patnaik, *Handbook of Inorganic Chemicals*, McGraw-Hill, **2002**, ISBN 049439-8.
- Gomaa, E. A., *Thermochim. Acta*, **1989**, *156*, 91-99.
- Gomaa, E. A., *Eur. Chem. Bull.*, **2013**, *1*(5) 254-261.
- Gomaa, E. A. and Al-Jahdali, *Sci. Technol.*, **2012**, *2*(4) 66-76.
- Gomaa, E. A. and Global Ad. Res. *J. Chem. Mater. Sci.*, **2012**, *1*(2), 35-38.
- Gomaa, E. A., Abu El-Nader, H. M. and Rashed, Sh. E., *Phys. Chem.*, **2012**, *2*(3) 9-17.
- Handbook of Chemistry and Physics*, 91st ed., **2010-2011**.
- Kelly, C. P., Cramer, C. J., Truhlar, J., *Chem. Theor. Comput.*, **2005**, *1*, 1133.
- Marcus, Y., "Ion Properties", Dekker, New York, **1999**.
- Marcus, Y., "Solvent mixtures", Dekker, New York, **2005**.
- Kim, J. I., *Z. Phys. Chem., Neuc Folge*, **1978**, *113*(5), 129-150
- Kelly, C. P., Cramer, C. J., Truhlar, D. J., *J. Phys. Chem. B*, **2006**, *110*, 16066-16081.

Received: 19.04.2013.
Accepted: 18.05.2013.



CORROSION RESISTANCE OF SS 316L ALLOY IN ARTIFICIAL SALIVA IN PRESENCE OF ALMOX 250 DT TABLET

A. Krishnaveni,^[a] S. Rajendran,^{[b,c]*} M. Pandiarajan,^[c] and R. Saranya^[d]

Keywords: corrosion resistance of metals, SS 316L alloy, synthetic saliva, orthodontic wires.

Corrosion resistance of SS316L alloy in artificial saliva, in the absence and presence of a disinfectant tablet, namely, Almox 250 DT has been evaluated by AC Impedance Spectra. It is observed that when 50 ppm of Almox is added to artificial saliva, charge transfer resistance of SS 316 L increases. Similar observation is made in presence of 200 ppm of Almox also. Hence it is concluded that people having orthodontic wires made of SS 316L, can take the Tablet Almox 250 DT without any hesitation, because in its presence corrosion resistance of SS 316L increases.

Corresponding Authors

E-mail: srmjoany@sify.com

[a] Department of Chemistry, Yadava College, Madurai, E.mail:

akveni1972@gmail.com

[b] Department of Chemistry, Corrosion Research centre,RVS School of Engineering and Technology, Dindigul 624005, India.

[c] Corrosion Research Centre, PG and Research Department of Chemistry, GTN Arts College, Dindigul- 624005, India.

E.mail: pandiarajan777@gmail.com,

[d] Department of Chemistry, Jayalakshmi Institute of Technology, Thoppur-636 352, India.E.mail:

senthilkumar944@gmail.com.

Introduction

Over the past two decades, with the accelerated development of tissue engineering, the demand for a variety of synthetic and natural biomaterials has dramatically increased. Biomaterial sales have already exceeded \$240million per year and due to the rapid development of biomaterials, the market will only increase in the years ahead for tissue engineering and artificial organ materials. Specifically, costs related to organ replacement account for 8% of all global healthcare spending and by 2040 as much as 25% of the US gross domestic product (GDP) is expected to be related to healthcare. Such demands require unique, better performing biomaterials for regenerative medicine.

Corrosion resistance of metals and alloys in various body fluids has attracted the attention of many researchers. Corrosion resistance of biomaterials in synthetic body fluids such as blood plasma, urine, Hank solution, Ringer solution and artificial saliva has been extensively studied. The corrosion resistance of metals and alloys in artificial saliva has been reviewed recently. Corrosion resistance of various metals have been investigated in various synthetic (simulated) body fluids such as Ringer's solution,¹⁻⁴ simulated body fluids,^{5,6} Hank solution,^{7,8} blood plasma,⁹⁻¹¹ urine,¹²⁻¹⁴ bovine serum,¹⁵ and artificial saliva.¹⁶⁻²⁰

Various metals and alloys have been used as biomaterials whose corrosion resistance has been investigated in artificial body fluids; various metals and alloys such as Ni-Al-Fe

intermetallic alloys,²¹ titanium alloy,²² NiTi alloy,²³ CoCrMo alloys,^{24,25} magnesium alloy,^{26,27} Cr-Ni stainless steel, Cr-Ni-Mo stainless steel,²⁸ 316L stainless steel.^{29,30} Five non-precious Ni-Co based alloys have been analyzed with respect to their corrosion behavior in artificial saliva.³¹ The effect of different concentrations of eugenol in artificial saliva on titanium corrosion has been investigated by Kinani and Chtaini.³² The corrosion resistance of the commercial metallic orthodontic wires in a simulated intra-oral environment has been evaluated by Ziebowicz et al.³³ The results of corrosion resistance tests of the CrNi, NiTi, and CuNiTi wires showed comparable data of parameters obtained in artificial saliva. The effects of multilayered Ti/TiN or single-layered TiN films deposited by pulse-biased arc ion plating (PBAIP) on the corrosion behavior of NiTi orthodontic brackets in artificial saliva have been investigated by Liu et al.³⁴ The corrosion behavior of various metals and alloys in artificial saliva has been investigated. Rajendran et al., have studied the corrosion resistance of artificial saliva in presence spirulina powder.³⁵ Corrosion behavior of metals in artificial saliva in presence of D-glucose has been investigated.³⁶

Liu, et al have investigated corrosion behavior of nickel-titanium orthodontic wires in presence of Artificial saliva using the methods of continue bending stress thought the 14 days experimental process, they have been findings that bending stress, loading condition with respect to corrosion behavior.³⁷ Koike, et al studied corrosion resistance of Titanium alloy in presence of Artificial Saliva at 37°C using the method of potentiostatic polarization. They have found that all the mechanical properties and corrosion characters were tested³⁸. Anwar et al investigated corrosion behavior of Ti and Ti 6Al4V in presence of artificial saliva using electrochemical methods. They found that as fluoride concentration increases, corrosion resistance is decreased.³⁹ Rajendran et al have studied the corrosion resistance of SS 316 L in Artificial Saliva in presence of electrol.⁴⁰

Ni-Ti alloys have been used by Rondelli and Vincentini⁴¹ and Bahije et al⁴². Krishnaveni et al⁴³ have investigated the corrosion resistance of 18 carat gold in synthetic saliva in presence of Almox 250 DT Tablet.

Dentists recommend the use of orthodontic wires to regulate the arrangement of teeth. After the regulation, people having these orthodontic wires, regulating the arrangement of teeth, have to take orally many tablets. These tablets may corrode the wires in the oral environment, especially saliva. Hence there is a need to investigate the influence of various tablets on the corrosion resistance of orthodontic wires made of many metals and alloys. Can people implanted with orthodontic wires made of SS316L AlmoX 250 DT Tablets orally? To give an answer this question, the following investigation was undertaken. Corrosion resistance of SS 316L gold in artificial saliva (AS) in the absence and presence of AlmoX 250 DT has been investigated by AC Impedance Spectra.

Experimental

SS 316L: The composition of SS 316L⁴⁴ (in wt. %) is the following : Cr-18 %; Ni 12 %, Mo -2.5 %, C-0.03 %, balance – iron. Wire of 1mm diameter was used in the present study.

Artificial Saliva: The composition of artificial saliva⁴⁵ is given as: KCl - 0.4 g L⁻¹, NaCl – 0.4 g L⁻¹, CaCl₂.2H₂O - 0.906 g L⁻¹, NaH₂PO₄.2H₂O 0.690 g L⁻¹, Na₂S.9H₂O – 0.005 g L⁻¹, urea – 1 g L⁻¹.

AlmoX 250DT: The AlmoX 250DT contains 250 mg of Amoxicillin Tri hydrate.

AC impedance spectra: AC impedance spectral studies were carried out in a CHI – Electrochemical workstation with impedance, Model 660A. A three-electrode cell assembly was used. The working electrode was SS316L. A saturated calomel electrode (SCE) was the reference electrode and platinum was the counter electrode. The real part (Z') and imaginary part (Z'') of the cell impedance were measured in ohms at various frequencies. Values of the charge transfer resistance (R_t) and the double layer capacitance (C_{dl}) were calculated.

Results and Discussion

Analysis of AC impedance spectra

AC impedance spectra have been used to detect the formation of film on the metal surface.⁴⁶⁻⁵⁶ If a protective film is formed, the Charge transfer resistance (R_t) increases and double layer capacitance (C_{dl}) value decreases. The impedance value increases.

The AC impedance spectra of SS 316L immersed in various test solutions are shown in (Figs. 1 to 9). The Nyquist plots are given in Figures 1 to 6. The Bode plots shown in [Figs. 7 to 9]. The Corrosion parameters derived from AC impedance spectra are given in Table 4. The charge transfer resistance and double layer capacitance are derived from Nyquist plot. The impedance value and phase angle value are derived from Bode plots.

Table 1. Impedance parameters of SS 316L in artificial saliva in presence of AlmoX (250DT) obtained by AC impedance spectra.

System	R_t ohm cm ²	C_{dl} , F cm ⁻²	Impedance logZ/ohm
Artificial Saliva	5.7458x10 ⁴	8.876048x10 ⁻⁷	5.260
AS+ AlmoX (250DT) 50 ppm	7.0198x10 ⁴	7.265164x10 ⁻⁷	5.265
AS+ AlmoX (250DT) 200 ppm	1.59680x10 ⁵	3.19388x10 ⁻⁷	5.603

SS 316L immersed in Artificial Saliva only

When SS 316L is immersed in artificial saliva the R_t value is 5.7458x10⁴ ohm cm² and C_{dl} value is 8.876048x10⁻⁷ Fcm⁻². (Figs.1 and 2).

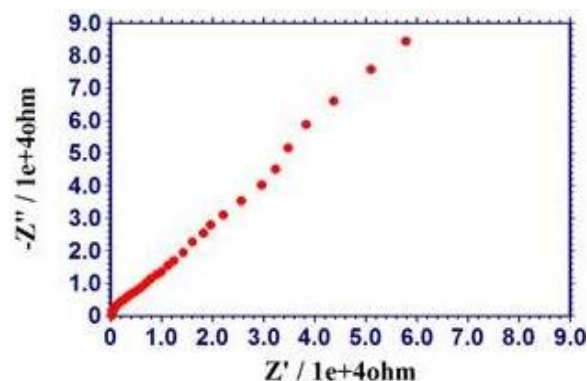


Figure 1. AC impedance spectrum of SS 316L immersed in Artificial Saliva solution (Nyquist Plot)

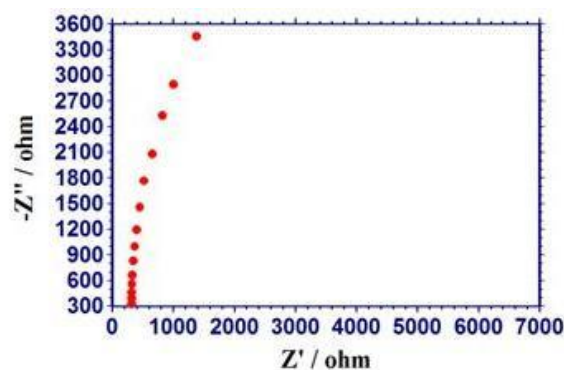


Figure 2. AC impedance spectrum of SS 316L immersed in Artificial Saliva solution (Nyquist Plot Zoomed)

Corrosion behavior of SS 316L in Artificial Saliva in the presence of 50ppm AlmoX 250DT

When 50 ppm AlmoX 250DT is added R_t value increases from 5.7458x10⁴ to 7.0198x10⁴ ohm cm² C_{dl} value decreases from 8.876048x10⁻⁷ to 7.265164x10⁻⁷ F/cm². This indicates that the corrosion resistance of SS 316L increases in presence of 50 ppm AlmoX (250DT) (Figs.3 and 4).

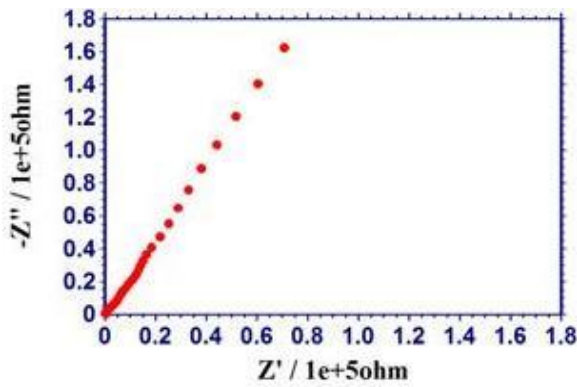


Figure 3. AC impedance spectrum of SS 316L immersed in Artificial Saliva +50 ppm AlmoX 250DT (Nyquist Plot)

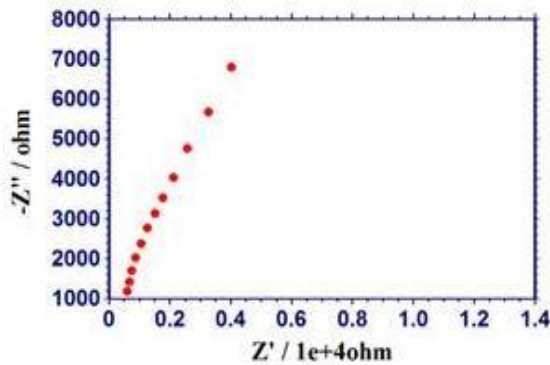


Figure 4. AC impedance spectrum of SS 316L immersed in artificial saliva + 50ppm AlmoX 250DT (Nyquist Plot Zoomed).

Corrosion behavior of SS 316L in Artificial Saliva in the presence of 200ppm AlmoX 250DT

When 200 ppm AlmoX 250DT is added R_t value increases from 70198×10^4 to 159680×10^5 ohm cm^2 C_d value decreases from 7.265164×10^{-7} to 3.19388×10^{-7} Fcm^2 . This is also supported by the increase in impedance value. (Figs 5 and 6).

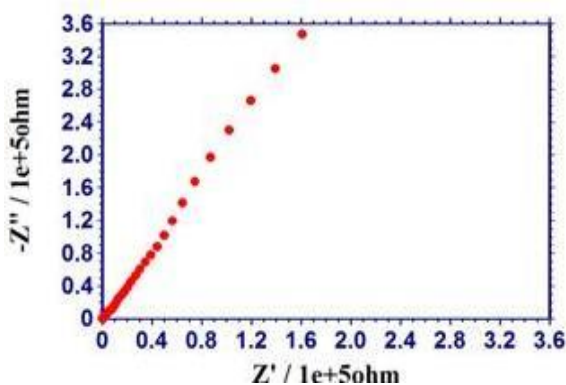


Figure 5. AC impedance spectrum of SS 316L immersed in Artificial Saliva + 200ppm AlmoX 250DT (Nyquist Plot)

When 50ppm of AlmoX 250DT is added the log (Freq/Hz) vs impedance plot [Figure 7,8,9] reveals that the impedance value sharply decreases as frequency increases. The slope of the straight line in the low frequency region is nearly 0.5. This is characteristic of a system having very high protective efficiency.

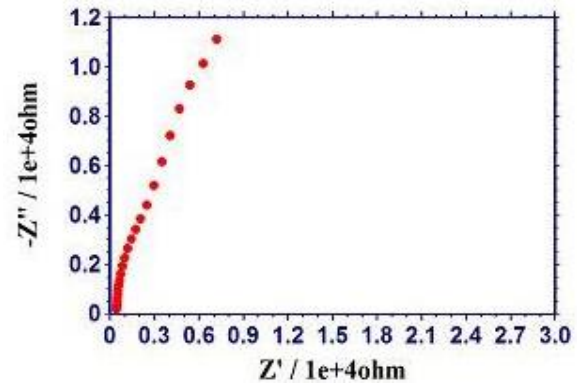


Figure 6. AC impedance spectrum of SS 316L immersed in Artificial Saliva + 200 ppm AlmoX 250DT (Nyquist Plot Zoomed)

Similar observation is made in presence of 200 ppm of AlmoX 250DT also. There is also increase in the phase angle values (65° and 67°) respectively. [Figs. 7, 8 and 9]. Thus AC impedance spectra reveal that in presence of AlmoX 250DT the corrosion resistance of SS 316L increases.

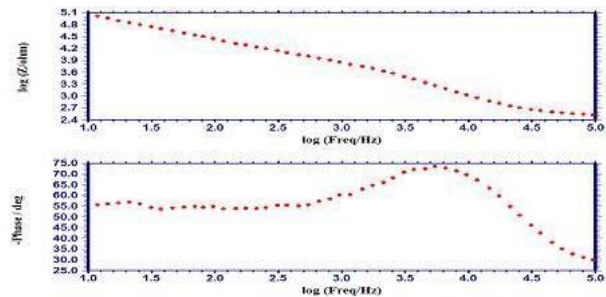


Figure 7. AC impedance spectrum of SS 316L immersed in Artificial Saliva solution. (Bode Plot)

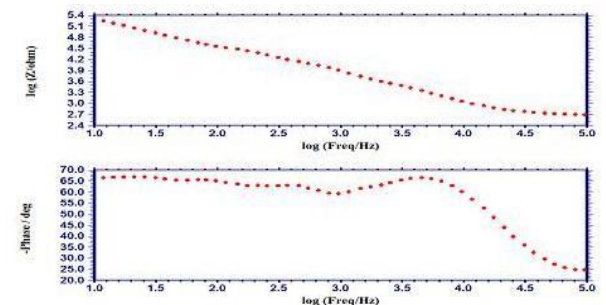


Figure 8. AC impedance spectrum of SS 316L immersed in Artificial Saliva + 50 ppm AlmoX 250DT. (Bode Plot)

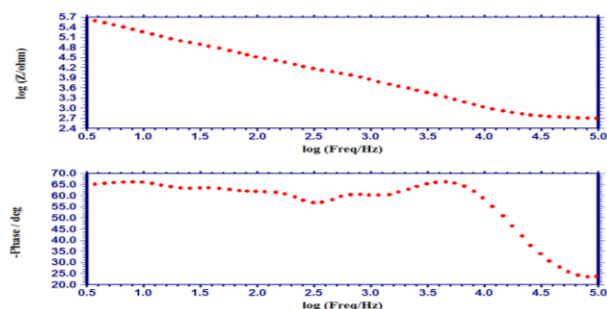


Figure 9. AC impedance spectrum of SS 316L immersed in Artificial Saliva + 200ppm AlmoX 250DT. (Bode Plot)

It is concluded that people having orthodontic wires made of SS316L can take orally AlmoX 250DT without any hesitation

Conclusion

Corrosion Resistance of SS316L in artificial saliva, in the absence and presence of a Tablet, namely, AlmoX 250 DT has been evaluated by AC Impedance Spectra. It is observed that when 50 ppm of AlmoX is added to artificial saliva, Charge transfer resistance of SS 316 L increases, in presence of 50 ppm AlmoX 250 DT. Similar observation is made in presence of 200 ppm of AlmoX also. Hence it is concluded that people having orthodontic wires made of SS 316L, can take the Tablet AlmoX 250 DT without any hesitation, because in its presence corrosion resistance of SS 316L increases.

References

- ¹Vijovic-Alagic, C., Cvijovic, I., Mitrovic, Z., Panic, S., Rakin, V., Ye, M., *Corros. Sci.* **2011**, *53*(2),796.
- ²Singh, R., Kurella, A., Dahotre, N. B., *J. Biomater.Appl.* **2006**, *21*(1), 49.
- ³Popa, M. V., Vasilescu, E., Drob, P., Vasilescu, C., *IFMBEPro.* **2009**, *25*(10), 24.
- ⁴Vasilescu, E., Drob, P., Raducanu, D., Cinca, I., Mareci, D., Calderon Moreno, J. M., Popa, M., Mirza Rosca, J. C., *Corros. Sci.* **2009**, *51*(12), 2885.
- ⁵Castaneda, I. E., Gonzalez-Rodriguez, J. G., Colin, J., Neri-Flores, M. A., *J. Solid State Electrochem.* **2010**, *14*(7),1145.
- ⁶Zhai, W.-J., Zhu, B.-Q., Liu, L.-F., *Mocaxue Xuebao/Tribology.* **2009**, *29*(5), 425.
- ⁷Tamilselvi, S., Raman, V., Rajendran, N., *J. Appl.Electrochem.* **2010**, *40*(2), 285.
- ⁸Wang, Y. B., Li, H. F., Cheng, Y., Wei, S. C., Zheng, Y. F., *Electrochem. Commun.* **2009**, *11*(11), 2187
- ⁹Su, X., Hao, W., Wang, T., Han, F., Zhang, B., He, L., *Cailiao Yanjiu Xuebao.* **2007**, *21*(5), 454.
- ¹⁰Hsu, R. W.-W., Yang, C.-C., Huang, C.-A., Chen, Y.-S., *Mater. Chem. Phys.* **2009**, *93*, 531.
- ¹¹Hsu, R. W.-W., Yang, C.-C., Huang, C.-A., Chen, Y.-S., *Mater. Chem. Phys.* **2004**, *86*(2), 269.
- ¹²Kajzer, W., Chrzanowski, W., Marciniak, J., *Int. J.Microstruct. Mater. Prop.*, **2007**, *2*(2), 188.
- ¹³Przondziono, J., Walke, W., *Arch. Mater. Sci. Eng.* **2009**, *35*(1), 21.
- ¹⁴Walke, W., Przondziono, J., *Solid State Phenomena*, **2010**, *165*, 404.
- ¹⁵Hang, R., Ma, S., Ji, V., Chu, P. K., *Electrochim Acta.* **2010**, *55*(20), 5551.
- ¹⁶Liu, L., Qiu, C. L., Chen, Q., Zhang, S. M., *J. Alloys Compd.*, **2006**, *425*(1), 268.
- ¹⁷Giacomelli, F. C., Giacomelli, C., Spinelli, A., *J. Braz. Chem.Soc.* **2004**, *15*(4), 541.
- ¹⁸Mariano, N. A., Oliveira, R. G., Braga, E. I., Rigo, E. C. S.,*Key Eng. Mater.* **2009**, *396*, 315.
- ¹⁹Popa, M. V., Vasilescu, E., Drob, P., Iordachescu, D.,Cimpean, A., Ionita, D., Vasilescu, C., *Proc. 2006 Int.Conf. Microtechnol. Med. Biol.* **2006**, *81*, Art. no.4281314.
- ²⁰Christopher, M. A., Brett and Ioana Muresan, *Key Eng.Mater.* **2002**, *230*, 459.
- ²¹Castaneda, I. E., Gonzalez-Rodriguez, J. G., Colin, J., Neri-Flores, M. A., *J. Solid State Electrochem.* **2010**, *14*(7),1145.
- ²²Zhou, W., Shen, T., Aung, N. N., *Corros. Sci.*, **2010**, *52*(3),1035.
- ²³Shukla, A. K., Balasubramaniam, R., *Corros. Sci.* **2006**, *48*(7),1696.
- ²⁴Sun, D., Wharton, J. A., Wood, R. J .K., *Tribology Int.*, **2009**, *42*(11), 1595.
- ²⁵Sun, D., Wharton, J. A., Wood, R. J .K., Ma, L., Rainforth, W. M., *Tribology Int.*, **2009**,*42*(1),99.
- ²⁶Daniel, M., Cailean, A., Bolat, G., Crețescu, I., Sutiman, D.*Stud. Univ. Babeş-Bolyai. Chem.*, **2009**, *1*, 93.
- ²⁷Song, Y., Shan, D., Chen, R., Zhang, F., Han, E.-H., *Mater.Sci. Eng C*, **2009**, *29*(3), 1039.
- ²⁸Tutunaru, B., Samide, A. P., Preda, M., *Rev. Chim.* **2007**,*58*(10), 923.
- ²⁹Hsu, R. W.-W., Yang, C.-C., Huang, C.-A., Chen, Y.-S.,*Mater. Chem. Phys.* **2004**, *86*(2), 269.
- ³⁰Peng, P., Kumar, S., Voelcker, N. H., Szili, E., Smart, R. St.C., Griesser, H. J., *J. Biomed. Mater. Res - Part A*, **2006**, *76* (2), 347.
- ³¹Mareci, D., Nemtoi, G. H ., Aelenei, N and Bocanu,C., *Eur. Cells. Mater.* **2005**, *10*, 1
- ³²Kinani, L., and Chtaini, Leonardo, A., *J. Sci.* **2007**, *11*, 33-40.
- ³³Ziebowicz, A., Walke, W., Barucha-Kepka, A., and Kiel, M., *J. Achieve. Mater. Manufact. Eng.* **2008**, *27*, 151-154.
- ³⁴Chenglong Liu, K.Paul, Chu, Guoqiang Lin and Dazhi Yang, , *Corros. Sci.* **2007**, *49*, 3783.
- ³⁵Rajendran, S., Paulraj, J., Rengan, P., Jeyasundari, J and M. Manivannan, *J. Dent. Oral .Hyg.* **2009**, *1*, 1-8.
- ³⁶Rajendran, S., Uma, V., Krishnaveni, A., Jeyasundari, J., Shyamaladevi, B., and Manivannan, M., *Arab. J. Sci. Eng.* **2009**, *34*(2C), 147-158.
- ³⁷Liu, J. K., Lee, T.M., Liu, I. H., *Am. J. Orthodont. Dent. Facial. Orthoped.*, **2011**, *140*,166.
- ³⁸Koike, M., Martinez, K., Guok, L., Chahine, G., Kovacevic, R., Okabe, T., *Mater. Lett.*, **2011**, *27*, 677.
- ³⁹Anwar, E. M., Kherialla, L. S., Tammam, R. H., *Oral Implant.* **2011**, *37*, 309.
- ⁴⁰Rajendran, S., Chitradevi, P., John, M .S., Krishnaveni, A., Kanchana, S., Lydia Christy, J., Nagalakshmi, R., Narayanasamy, B., *Zastit. Mater.* **2010**, *51*, 149.
- ⁴¹Rondelli, G., Vicentini, B., *Biomater.* **1999**, *20*, 785.

- ⁴²Bahije, L., Benyahia, H., El Hamzaoui, S., Ebn Touhami, M., Bengueddour, R., Rerhrhaye Abdallaoui, F., Zaoui, F., *Int. Orthodont.*, **2011**, 9, 110.
- ⁴³Krishnaveni, A., Rajendran, S., Pandiarajan, M., *Eur. Chem. Bull.* **2013**, 2(8), 558.
- ⁴⁴Gurappa, I., *Mater. Character*, **2002**, 49, 73.
- ⁴⁵Saranya, R., Susai Rajendran, Krishnaveni, A., Jeyasundari, J., *Eur. Chem. Bull.*, **2013**, 2(6), 389.
- ⁴⁶Shyamaladevi, B., and Rajendran, S., *Eur Chem Bull.*, **2012**, 1(2), 503-510.
- ⁴⁷Kalaivani, R, Narayanaswamy, B, Selvi, J. A, Amalraj, A J, Jeyasundari J and
- ⁴⁸Rajendran S, *Port. Electrochim. Acta*, **2009**, 27(2), 177-187.
- ⁴⁹Anthony Samy Sahayaraja and Susai Rajendran, *J. Electrochem Sci Eng.*, **2012**, 2, 91-104
- ⁵⁰Manimaran, N., Rajendran, S., Manivannan, M., and Johnmary, S., *Res. J. Chem .Sci.*, **2012**, 2(3), 52-57.
- ⁵¹Sribharathy, V., Susai Rajendran, S., *Res. J. Chem. Sci.*, **2012**, 2(6), 72-81.
- ⁵²Mary Anbarasi, C., Susai Rajendran, Vijaya, N., Manivannan, M., and Shanthi, T., *Open Corros. J*, **2011**, 4, 40-46.
- ⁵³Johsirani, V., Rajendran, S., Sathiyabama, J., Muthumegala, T.S., Krishnaveni, A., Hajarabeevi, N., *Bulg. Chem. Commun.*, **2012**, 44(1), 41-51.
- ⁵⁴Sangeetha, M., Rajendran, S., Sathiyabama, J., Krishnaveni, A., Shanthi, P., Manimaran, Shyamaladevi, B., *Port. Electrochim. Acta*, **2011**, 29, 429-444.
- ⁵⁵Manimaran, N., and Shyamaladevi, B., *Port. Electrochim. Acta*, **2011**, 29(6), 429-444.
- ⁵⁶Rajendran, S., Uma, V., Krishnaveni, A., Jeyasundari, J., Shyamaladevi, Manivannan, M., *Arab. J.Sci.Engg.*, **2009**, 34(2c), 147.

Received: 05.04.2013.

Accepted: 16.05.2013.



ABRAHAM MODEL CORRELATIONS FOR PREDICTING GAS-TO-LIQUID PARTITION COEFFICIENTS AND ACTIVITY COEFFICIENTS OF ORGANIC SOLUTES DISSOLVED IN 1-(2-METHOXYETHYL)-1-METHYLPYRROLIDINIUM TRIS(PENTAFLUOROETHYL)TRIFLUOROPHOSPHATE

Rui Jiang^[a], Jared L. Anderson^[a], Timothy W. Stephens^[b], William E. Acree, Jr.^[b], and Michael H. Abraham^[c]

Keywords: chromatographic retention factors, partition coefficients, linear free energy relationships, ionic liquids.

Chromatographic retention factors were measured for 45 different organic solutes of varying polarity and hydrogen-bonding capability on an anhydrous 1-(2-methoxyethyl)-1-methylpyrrolidinium tris(pentafluoroethyl)trifluorophosphate, ([MeoeMPyrr]⁺[FAP]⁻), stationary phase at both 323 K and 353 K. The experimental retention factor data were combined with recently published thermodynamic data for solutes dissolved in ([MeoeMPyrr]⁺[FAP]⁻) to give the corresponding gas-to-liquid partition coefficients (log *K*). The water-to-anhydrous ([MeoeMPyrr]⁺[FAP]⁻) partition coefficients (log *P*) were also calculated using published gas-to-water partition coefficient data for the solutes studied. The derived partition coefficients were analyzed in accordance with the Abraham model. The Abraham model expressions that were obtained in the present study back-calculate the observed 105 log *K* and 102 log *P* values to within a standard deviation of 0.14 and 0.16 log units, respectively.

* Corresponding Authors

Fax: 1-940-565-4318

E-Mail: Bill.Acree@unt.edu

- [a] Department of Chemistry, The University of Toledo, 2801 W. Bancroft Street MS 602, Toledo, OH 43606 (USA).
 [b] Department of Chemistry, 1155 Union Circle Drive #305070, University of North Texas, Denton, TX 76203-5017 (USA).
 [c] Department of Chemistry, University College London, 20 Gordon Street, London, WC1H 0AJ (UK).

imidazolium cation, [BMIm]⁺, Gonzalez-Miguel *et al.*¹ reported that carbon dioxide solubility increased with decreasing solution temperature, and followed the trend of ([BMIm]⁺[FAP]⁻) > ([BMIm]⁺[Tf₂N]⁻) > ([BMIm]⁺[PF₆]⁻), where [FAP]⁻, [Tf₂N]⁻, and [PF₆]⁻ correspond to the *tris*(pentafluoroethyl)trifluorophosphate, *bis*(trifluoromethanesulfonyl)imide, and hexafluorophosphate anions, respectively.

Introduction

Ionic liquids (ILs) represent a novel class of non-molecular solvents exhibiting unique physical properties including high thermal stabilities, wide viscosity ranges, negligible vapor pressures, and varying solubilizing abilities that result from solvation interactions between the dissolved solute and surrounding solvent ions. The physical properties of ILs can be fine-tuned through judicious selection of the cation-anion pair combination and by introducing select functional groups into the structure of the IL, thus enabling one to design IL solvents for task-specific applications. Ionic liquids are employed numerous commercial manufacturing and engineering applications ranging from reaction solvent media for chemical syntheses, to stationary phases for gas chromatographic chemical separations, to liquid matrices for concentrating/isolating organic compounds in dispersive liquid-liquid micro-extractions, and to absorbent materials for removal of carbon dioxide, sulfur dioxide and ammonia from flue gases. Experimental studies have shown that the IL anion plays an important role in determining carbon dioxide adsorption, with fluorination serving to increase the solubility of CO₂. For three ionic liquid solvents having the common 1-butyl-3-methyl-

The solvation parameter model, developed by Abraham and co-workers^{2,3}, has been used successfully to describe the solubilising properties of traditional organic solvents³⁻⁹, binary aqueous-ethanol solvent mixtures,^{10,11} aqueous-micellar surfactant solutions^{12,13}, and several different classes of ILs¹⁴⁻²⁸. For IL solvents, Sprunger *et al.*¹⁶⁻¹⁸ expressed the logarithm of the water-to-ionic liquid partition coefficient, log *P*:

$$\log P = c_{p,\text{cation}} + c_{p,\text{anion}} + (e_{p,\text{cation}} + e_{p,\text{anion}})E + (s_{p,\text{cation}} + s_{p,\text{anion}})S + (a_{p,\text{cation}} + a_{p,\text{anion}})A + (b_{p,\text{cation}} + b_{p,\text{anion}})B + (v_{p,\text{cation}} + v_{p,\text{anion}})V \quad (1)$$

and logarithm of the gas-to-ionic liquid partition coefficient, log *K*:

$$\log K = c_{k,\text{cation}} + c_{k,\text{anion}} + (e_{k,\text{cation}} + e_{k,\text{anion}})E + (s_{k,\text{cation}} + s_{k,\text{anion}})S + (a_{k,\text{cation}} + a_{k,\text{anion}})A + (b_{k,\text{cation}} + b_{k,\text{anion}})B + (l_{k,\text{cation}} + l_{k,\text{anion}})L \quad (2)$$

to include ion-specific equation coefficients. Numerical values of the two sets of equation coefficients are calculated as a paired cation-anion sum (e.g., $c_{p,cation} + c_{p,anion}$, $e_{p,cation} + e_{p,anion}$, etc.) by regression analyses of experimental $\log P$ and $\log K$ data for solutes having known solute descriptors in accordance with Eqns. 1 and 2. Solute descriptors are the capitalized quantities in the $\log P$ and $\log K$ expressions. To calculate equation coefficients for an individual ion, one must know the equation coefficients for the other ion in the IL. In other words, to calculate $c_{p,cation}$ the value of $c_{k,anion}$ must be known, and *vice versa*. Numerical values of the first sets of ion-specific equation coefficients were obtained by setting the six coefficients of the $[Tf_2N]^-$ anion equal to zero. In many respects this is analogous to setting a reference point for calculating thermodynamic properties of single ions. To date equation coefficients have been published for 21 different cations and 14 different anions.

As noted above the capitalized letters on the right-hand side of Eqns. 1 and 2 are solute descriptors that describe the properties of the partitioned probe molecule. The solute descriptors are defined as follows: **E** denotes the solute excess molar refraction in units of $\text{cm}^3 \text{mol}^{-1}/10$ computed from the solute's refractive index; **S** corresponds to a combined dipolarity/polarizability descriptor; **A** and **B** describe the overall hydrogen-bond donor and acceptor properties of the solute, respectively; **V** is the McGowan characteristic molecular volume in units of $\text{cm}^3 \text{mol}^{-1}/100$; and **L** is the logarithm of the solute's gas-to-hexadecane partition coefficient measured at 298 K. Solute descriptors when multiplied by the complementary solvent equation coefficient quantifies a given type of solute-solvent interaction. For example, the $(a_{p,cation} + a_{p,anion})\mathbf{A}$ and $(a_{k,cation} + a_{k,anion})\mathbf{A}$ terms in Eqns. 1 and 2 describe the hydrogen-bonding interactions between the H-bond donor sites on the solute and the H-bond acceptor sites on the solvent, while the $(b_{p,cation} + b_{p,anion})\mathbf{B}$ and $b_{k,cation} + b_{k,anion})\mathbf{B}$ terms involve interactions between the solute H-bond acceptor sites and solvent H-bond donor sites. Thus far solute descriptors have been determined for several thousand different organic compounds and inert gases from measured water-to-organic solvent partition coefficient data, from measured solubility data in organic solvents, from experimental infinite dilution activity coefficient for solutes dissolved in organic solvents, from measured Henry's law constants, and from experimental gas chromatographic and high-performance liquid chromatographic retention factors. The calculation procedures for determining solute descriptors from available experimental are described in detail elsewhere.^{2,3,29-33}

In the present communication, we report experimental gas-liquid chromatographic retention factor data for a set of 45 chemically diverse organic solutes on a 1-(2-methoxyethyl)-1-methylpyrrolidinium *tris*(pentafluoroethyl)trifluorophosphate, $([\text{MeoeMPyrr}]^+[\text{FAP}]^-)$, stationary phase at 323 K and 353 K. See Figure 1 for the molecular structure of the ionic liquid solvent. Results of the chromatographic measurements are combined with the recently published gas-to-liquid partition coefficient data of Marciniak and Wlazlo³⁴ for volatile organic solutes dissolved in $([\text{MeoeMPyrr}]^+[\text{FAP}]^-)$ to derive Abraham model $\log P$ correlations at 298 K and Abraham model $\log K$ correlations at both 298 K and 323 K. As an information note Marciniak and Wlazlo determined the Abraham model $\log K$ correlations for $([\text{MeoeMPyrr}]^+[\text{FAP}]^-)$ at 318, 328, 338, 348, 358 and 368 K based on 62 probe molecules.

The authors did not report the $\log P$ correlation, nor did the authors give the ion-specific equation coefficients for the 1-(2-methoxyethyl)-1-methylpyrrolidinium cation. To our knowledge no one has yet reported equation coefficients for $([\text{MeoeMPyrr}]^+)$.

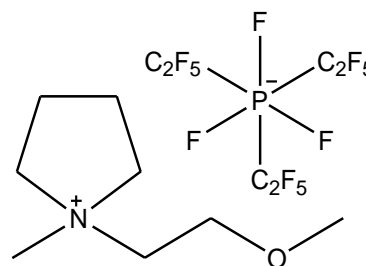


Figure 1. Molecular structure of 1-(2-methoxyethyl)-1-methylpyrrolidinium *tris*(pentafluoroethyl)trifluorophosphate.

We further note that the datasets used in the present communication do contain a more chemically diverse set of probe molecules. The dataset used by Marciniak and Wlazlo³⁴ did not contain the more acidic phenolic and carboxylic acid solutes (solute with larger **A** values) and the lesser volatile organic compounds considered here. An often voiced criticism in using derived $\log P$ and $\log K$ correlations to predict values for additional solutes is that one should not make predictions for solutes whose descriptor values fall outside of the range of chemical space used in determining the equation coefficients.

By including the more acidic and less volatile solutes we were able to increase the expanse of predictive chemical space covered by the $\log P$ and $\log K$ predictive equations.

Experimental Methods and Partition Coefficient Datasets

The sample of 1-(2-methoxyethyl)-1-methylpyrrolidinium *tris*(pentafluoroethyl)trifluorophosphate studied in the present investigation was kindly donated as a gift from Merck KGaA (Darmstadt, Germany). The IL stationary phase was coated onto untreated fused silica capillary columns (5 m x 0.25 mm) purchased from Supelco (Bellefonte, PA). The IL coating solutions were prepared in dichloromethane using a 0.45% (w/v) concentration of $([\text{MeoeMPyrr}]^+[\text{FAP}]^-)$.

Forty-five (45) probe molecules were selected for the characterization of the $([\text{MeoeMPyrr}]^+[\text{FAP}]^-)$ stationary phase. The names of the solutes, along with the chemical purities and suppliers, are given in Table 1. All solute molecules were used as received from the suppliers. The presence of trace impurities in the solutes would in no way affect the experimental results because the main chromatographic peak was easily distinguished from any minor impurity peak by its much larger intensity.

Table 1. List of organic solutes, chemical suppliers, and chemical purities

Solute	Supplier ^a	Purity
Acetic acid	Supelco	99.7%
Acetophenone	Sigma-Aldrich	99%
Aniline	Sigma-Aldrich	99.5%
Benzaldehyde	Sigma-Aldrich	99+%
Benzene	Sigma-Aldrich	99.8%
Benzonitrile	Sigma-Aldrich	99%
Benzyl alcohol	Sigma-Aldrich	99%
1-Bromooctane	Sigma-Aldrich	99%
1-Butanol	Fisher Scientific	99.9%
Butyraldehyde	Acros Organics	99%
2-Chloroaniline	Sigma-Aldrich	98%
1-Chlorobutane	Sigma-Aldrich	99%
1-Chlorohexane	Sigma-Aldrich	99%
1-Chlorooctane	Sigma-Aldrich	99%
<i>p</i> -Cresol	Fluka	99%
Cyclohexanol	J.T. Baker	99%
Cyclohexanone	Sigma-Aldrich	99.8%
1,2-Dichlorobenzene	Sigma-Aldrich	99%
N,N-Dimethylformamide	Fisher Scientific	99.9%
1,4-Dioxane	Sigma-Aldrich	99.8%
Ethyl acetate	Fisher Scientific	99.9%
Ethylbenzene	Eastman Kodak Co	95+%
1-Iodobutane	Sigma-Aldrich	99%
Methyl caproate	Supelco	98%
Naphthalene	Supelco	98%
Nitrobenzene	Sigma-Aldrich	99+%
1-Nitropropane	Sigma-Aldrich	99%
1-Octanol	Sigma-Aldrich	99+%
Octylaldehyde	Sigma-Aldrich	99%
1-Pentanol	Sigma-Aldrich	99+%
2-Pentanone	Sigma-Aldrich	99+%
Phenetole	Sigma-Aldrich	99%
Phenol	Sigma-Aldrich	99+%
Propionitrile	Sigma-Aldrich	99%
Pyridine	Sigma-Aldrich	99.9%
Pyrrole	Sigma-Aldrich	98%
Toluene	Fisher Scientific	99.8%
<i>m</i> -Xylene	Fluka	99.5%
<i>o</i> -Xylene	Fluka	99.5%
<i>p</i> -Xylene	Fluka	99.5%
2-Propanol	Fisher Scientific	99.6 %
2-Nitrophenol	Acros Organics	99%
1-Bromohexane	Sigma-Aldrich	98%
Propanoic acid	Supelco	99%
1-Decanol	Sigma-Aldrich	99+%

^a Acros Organics (Morris Plains, NJ, USA); Eastman Kodak Company (Rochester, NY, USA); Fisher Scientific (Pittsburgh, PA, USA); Fluka (Steinheim, Germany); J.T. Baker (Phillipsburg, NJ, USA); Sigma-Aldrich (St. Louis, MO, USA); and Supelco (Bellefonte, PA, USA).

Chromatographic retention factors, *k*, were determined on a ([MeoeMPyrr]⁺[FAP]⁻) stationary phase at both 323 K and 353 K as part of the present investigation. The percent relative standard deviation (% RSD) in the experimental retention times for all solutes included in the present study was less than 1 %. The stationary phase integrity during the

course of the experimental measurements was verified by periodically monitoring the efficiency and retention factor of the naphthalene separation. The experimental log *k* values are tabulated in the second and third columns of Table 2. The log *k* values are 298 K were obtained from a linear plot of log *k* versus 1/*T* based on the measured data at 323 K and 353 K.

Table 2. Chromatographic retention factor data for solutes on 1-(2-methoxyethyl)-1-methylpyrrolidinium tris(pentafluoroethyl)-trifluorophosphate, ([MeoeMPyrr]⁺[FAP]⁻), stationary phase at 298, 323 and 353 K

Solute	log <i>k</i> , 323 K	log <i>k</i> , 353 K	log <i>k</i> , 298 K
Acetic acid	0.409	-0.124	0.935
Acetophenone	2.110	1.412	2.800
Aniline	2.115	1.407	2.814
Benzaldehyde	1.616	0.992	2.231
Benzene	-0.017	-0.439	0.399
Benzonitrile	1.781	1.152	2.403
Benzyl alcohol	2.094	1.368	2.811
1-Bromooctane	0.830	0.236	1.417
1-Butanol	0.097	-0.379	0.567
Butyraldehyde	0.057	-0.372	0.480
2-Chloroaniline	2.190	1.483	2.889
1-Chlorobutane	-0.554		
1-Chlorohexane	0.028	-0.439	0.490
1-Chlorooctane	0.607	0.038	1.169
<i>p</i> -Cresol	2.078	1.348	2.800
Cyclohexanol	0.865	0.293	1.430
Cyclohexanone	1.341	0.771	1.903
1,2-Dichlorobenzene	0.997	0.441	1.545
N,N-Dimethylformamide	1.869	1.245	2.486
1,4-Dioxane	0.528	0.026	1.024
Ethyl acetate	0.103	-0.360	0.561
Ethylbenzene	0.564	0.026	1.096
1-Iodobutane	-0.123	-0.545	0.295
Methyl caproate	0.957	0.352	1.555
Naphthalene	2.195	1.492	2.889
Nitrobenzene	2.018	1.363	2.665
1-Nitropropane	0.926	0.406	1.439
1-Octanol	1.281	0.614	1.939
Octylaldehyde	1.244	0.612	1.866
1-Pentanol	0.412	-0.104	0.920
2-Pentanone	0.548	0.050	1.040
Phenetole	1.308	0.680	1.928
Phenol	1.769	1.094	2.434
Propionitrile	0.529	0.079	0.973
Pyridine	0.715	0.214	1.210
Pyrrole	1.290	0.688	1.884
Toluene	0.313	-0.172	0.792
<i>m</i> -Xylene	0.639	0.096	1.175
<i>o</i> -Xylene	0.748	0.194	1.294
<i>p</i> -Xylene	0.607	0.068	1.140
2-Propanol	-0.414		
2-Nitrophenol	1.950	1.268	2.624
1-Bromohexane	0.255	-0.231	0.734
Propanoic acid	0.715	0.113	1.309
1-Decanol	1.856	1.074	2.628

The thermodynamic gas-to-ionic liquid partition coefficient, K , can be calculated from isothermal chromatographic measurements through $K = V_N/V_L$, where V_N is the volume of the carrier gas needed to elute the solute, and V_L is the volume of the ionic liquid present as the stationary phase.³⁵ The retention factor, is defined as $k = (t_r - t_m)/t_m$,³⁵ where t_r is the retention time of the solute under consideration and t_m is the “void” retention time for an unretained solute, which in the present study was methane. The corrected retention time, $t_r - t_m$, is directly proportional to the corrected elution volume V_N , hence the gas-to-ionic liquid partition coefficients and retention factors on the ionic liquid stationary phase are related to each other through,

$$K = P^* \cdot k \quad \text{or} \quad \log K = \log P^* + \log k \quad (3)$$

The proportionality constant in Eqn. 3, P^* , is the phase ratio and depends only upon the chromatographic conditions. The numerical value of P^* should remain essentially constant for a given column during the time that it takes to perform the experimental measurements.

Thermodynamic gas-to-liquid partition coefficients are required to compute the proportionality constants needed in Eqn. 3 for converting the observed $\log k$ values in Table 2 to $\log K$ data. Marciniak and Wlazlo³⁴ recently published infinite dilution activity coefficients, γ_{solute}^∞ , and gas-to-IL partition coefficients, K , of water and 61 organic solutes dissolved in ([MeoeMPyrr]⁺[FAP]⁻) at six temperatures from 318 K to 368 K. Experimental uncertainties in the measured values K and γ_{solute}^∞ were reported to be less than 3%. The published experimental data were extrapolated to 298 K and 323 K by assuming linear $\ln K$ versus $1/T$ relationship. There should be very little uncertainty in the extrapolated values because the experimental measurements were performed not too far removed both desired temperatures, less than 20 K in most instances. The proportionality constants needed in the Eqn. 7, $\log P^* = 2.588$ for 298 K and $\log P^* = 2.526$ for 323 K, for ([MeoeMPyrr]⁺[FAP]⁻) were the calculated average between the measured $\log k$ and $\log K$ values for 13 common organic compounds (e.g., benzene, toluene, ethylbenzene, *m*-xylene, *o*-xylene, *p*-xylene, 1-butanol, 1,4-dioxane, ethyl acetate, butyraldehyde, 1,4-dioxane, 2-pentanone, 1-nitropropane, and pyridine) in the IL data set that were studied by both us and Marciniak and Wlazlo. The $\log P^*$ values for each individual solute differed from the average values by less than ± 0.03 log units, further suggesting that the proportionality constants did remain constant during the course of the experimental measurements.

The Abraham model also describes solute transfer between two condensed phases, and in the case of IL solvents it is possible to construct a solute transfer process between water and the anhydrous IL solvent. The transfer process is akin to a partitioning process (or more specifically a hypothetical partitioning process) wherein the ionic liquid and water are not in physical contact with each other. In a direct practical partitioning process the two phases would be in physical contact, and the solute would be distributed between an aqueous phase (saturated with the IL solvent) and an IL phase (saturated with water). For some partitioning systems the organic solvent and water are almost completely immiscible with each other, and the presence of trace water in the organic solvent and trace organic solvent dissolved in water has a negligible affect on

the solute's partitioning behavior. In other words, the direct practical partition coefficient and indirect hypothetical partition coefficient are nearly identical. There has been insufficient experimental studies on ionic liquid solvents to reach any meaningful conclusions at the present time. Hypothetical indirect partition coefficients are still useful in that predicted $\log P$ values can be converted to $\log K$ and γ_{solute}^∞ values through standard thermodynamic relationships

$$\log K = \log P + \log K_w \quad (4)$$

and

$$\log P + \log K_w = \log \left(\frac{RT}{\gamma_{solute}^\infty P_{solute}^o V_{solvent}} \right) \quad (5)$$

where K_w is the solute's gas-to-water partition coefficients, P_{solute}^o is the vapor pressure of the organic solute at the system temperature (T), $V_{solvent}$ is the molar volume of the IL solvent, and R is the universal gas constant. The solutes' gas phase partition coefficients into water (K_w) needed for these calculations are given elsewhere.¹⁵

The calculated $\log K$ and $\log P$ values are compiled in Table 3 for solutes dissolved in ([MeoeMPyrr]⁺[FAP]⁻). $\log P$ values are tabulated only for 298 K as we do not have experimental values for the solutes' gas-to-water partition coefficients, $\log K_w$, at 323 K. The $\log K_w$ values that we have compiled thus far pertain to gas-to-water partitioning at 298 K³⁶ and 310 K.³⁷ We have listed in Table 4 the numerical solute descriptors for the 92 different organic compounds examined in the present communication. The solute descriptors are of experimental origin, and were determined from experimental gas-liquid and high-performance liquid chromatographic retention factor data, from measured solubility data and Henry's law constants, and from observed practical partition coefficient measurements for the equilibrium solute distribution between water and an organic solvent.

Table 3. Logarithm of the gas-to-anhydrous IL partition coefficient, $\log K$ at 298 K and 323 K and logarithm of the water-anhydrous IL partition coefficient, $\log P$, at 298 K for organic solutes dissolved in ([MeoeMPyrr]⁺[FAP]⁻)

Solute	$\log K$, 298 K	$\log K$, 323 K	$\log P$, 298 K
Based on Thermodynamic Data			
Pentane	1.104	0.816	2.804
Hexane	1.449	1.120	3.269
3-Methylpentane	1.416	1.099	3.256
2,2-Dimethylbutane	1.261	0.966	3.101
Heptane	1.797	1.416	3.757
Octane	2.153	1.711	4.263
2,2,4-Trimethylpentane	1.831	1.446	3.951
Nonane	2.483	1.999	4.633
Decane	2.826	2.290	5.146
Cyclopentane	1.480	1.173	2.360
Cyclohexane	1.809	1.460	2.709
Methylcyclohexane	2.006	1.631	3.256
Cycloheptane	2.291	1.886	2.871

Table 3 (cont.)

Cyclooctane	2.733	2.269	3.503	Based on Chromatographic Retention Factor Data			
1-Pentene	1.340	1.032	2.570	Acetic Acid	3.523	2.935	-1.387
1-Hexene	1.703	1.338	2.863	Acetophenone	5.388	4.636	2.028
Cyclohexene	2.119	1.731	2.389	Aniline	5.402	4.641	1.320
1-Heptene	2.046	1.633	3.266	Benzaldehyde	4.819	4.142	1.869
1-Octene	2.393	1.925	3.803	Benzene	2.987	2.509	2.357
1-Decene	3.065	2.501	4.705	Benzonitrile	4.991	4.307	1.901
1-Pentyne	1.874	1.503	1.875	Benzyl alcohol	5.399	4.620	0.539
1-Hexyne	2.223	1.799	2.433	1-Bromooctane	4.005	3.356	4.385
1-Heptyne	2.563	2.094	3.003	Butyraldehyde	3.068	2.583	0.738
1-Octyne	2.902	2.386	3.422	1-Butanol	3.155	2.623	-0.305
Benzene	2.989	2.505	2.359	2-Chloroaniline	5.477	4.716	1.877
Toluene	3.383	2.836	2.733	1-Chlorobutane		1.972	
Ethylbenzene	3.678	3.090	3.098	1-Chlorohexane	3.078	2.554	3.078
<i>o</i> -Xylene	3.894	3.280	3.234	1-Chlorooctane	3.757	3.133	3.947
<i>m</i> -Xylene	3.771	3.171	3.161	<i>p</i> -Cresol	5.388	4.604	0.888
<i>p</i> -Xylene	3.733	3.137	3.143	Cyclohexanol	4.018	3.391	0.008
Styrene	4.064	3.439	3.114	Cyclohexanone	4.491	3.867	0.891
α -Methylstyrene	4.273	3.609	3.313	1,2-Dichlorobenzene	4.133	3.523	3.233
Methanol	2.163	1.788	-1.577	1,4-Dioxane	3.612	3.054	-0.098
Ethanol	2.431	2.003	-1.239	N,N-Dimethylformamide	5.074	4.395	
1-Propanol	2.762	2.292	-0.798	Ethyl acetate	3.149	2.629	0.989
2-Propanol	2.545	2.095	-0.935	Ethylbenzene	3.684	3.090	3.104
1-Butanol	3.143	2.614	-0.317	1-Iodobutane	2.883	2.403	2.703
2-Butanol	2.876	2.373	-0.514	Methyl caproate	4.143	3.483	2.313
2-Methyl-1-propanol	2.973	2.457	-0.327	Naphthalene	5.477	4.721	3.747
<i>tert</i> -Butanol	2.643	2.163	-0.637	Nitrobenzene	5.253	4.544	2.233
Thiophene	3.042	2.554	2.002	2-Nitrophenol	5.212	4.476	1.852
Tetrahydrofuran	2.881	2.417	0.331	1-Nitropropane	4.027	3.452	1.577
1,4-Dioxane	3.614	3.056	-0.096	1-Octanol	4.527	3.807	1.527
Methyl <i>tert</i> -butyl ether	2.233	1.818	0.613	Octylaldehyde	4.454	3.770	2.774
Ethyl <i>tert</i> -butyl ether	2.140	1.721	0.870	1-Pentanol	3.508	2.938	0.158
Methyl <i>tert</i> -amyl ether	2.563	2.108	1.093	2-Pentanone	3.628	3.074	1.048
Diethyl ether	1.883	1.514	0.713	Phenetole	4.516	3.834	2.886
Dipropyl ether	2.374	1.930	1.481	Phenol	5.022	4.295	0.172
Diisopropyl ether	2.079	1.661	1.029	2-Propanol		2.112	
Dibutyl ether	3.012	2.476	2.322	Propionitrile	3.561	3.055	0.741
Acetone	3.037	2.576	0.247	Pyridine	3.798	3.241	0.358
2-Pentanone	3.629	3.072	1.049	Pyrrole	4.472	3.816	
3-Pentanone	3.613	3.060	1.113	Toluene	3.380	2.839	2.730
Methyl acetate	2.881	2.410	0.581	<i>m</i> -Xylene	3.763	3.165	3.153
Ethyl acetate	3.136	2.622	0.976	<i>o</i> -Xylene	3.882	3.274	3.222
Methyl propanoate	3.188	2.664	1.038	<i>p</i> -Xylene	3.728	3.133	3.138
Methyl butanoate	3.467	2.904	1.387	1-Bromohexane	3.322	2.781	3.449
Butyraldehyde	3.055	2.578	0.725	Propanoic acid	3.897	3.241	-0.843
Acetonitrile	3.344	2.877	0.494	1-Decanol	5.216	4.382	2.546
Pyridine	3.804	3.245	0.364				
1-Nitropropane	4.035	3.457	1.585				

Table 4. Abraham model solute descriptors of the organic compounds considered in the present investigation

Solute	<i>E</i>	<i>S</i>	<i>A</i>	<i>B</i>	<i>L</i>	<i>V</i>
Pentane	0.000	0.000	0.000	0.000	2.162	0.8131
Hexane	0.000	0.000	0.000	0.000	2.668	0.9540
3-Methylpentane	0.000	0.000	0.000	0.000	2.581	0.9540
2,2-Dimethylbutane	0.000	0.000	0.000	0.000	2.352	0.9540
Heptane	0.000	0.000	0.000	0.000	3.173	1.0949
Octane	0.000	0.000	0.000	0.000	3.677	1.2358
2,2,4-Trimethylpentane	0.000	0.000	0.000	0.000	3.106	1.2358
Nonane	0.000	0.000	0.000	0.000	4.182	1.3767
Decane	0.000	0.000	0.000	0.000	4.686	1.5176
Cyclopentane	0.263	0.100	0.000	0.000	2.477	0.7045
Cyclohexane	0.305	0.100	0.000	0.000	2.964	0.8454
Methylcyclohexane	0.244	0.060	0.000	0.000	3.319	0.9863
Cycloheptane	0.350	0.100	0.000	0.000	3.704	0.9863
Cyclooctane	0.413	0.100	0.000	0.000	4.329	1.1272
1-Pentene	0.093	0.080	0.000	0.070	2.047	0.7701
1-Hexene	0.078	0.080	0.000	0.070	2.572	0.9110
Cyclohexene	0.395	0.280	0.000	0.090	2.952	0.8204
1-Heptene	0.092	0.080	0.000	0.070	3.063	1.0519
1-Octene	0.094	0.080	0.000	0.070	3.568	1.1928
1-Decene	0.093	0.080	0.000	0.070	4.554	1.4746
1-Pentyne	0.172	0.230	0.120	0.120	2.010	0.7271
1-Hexyne	0.166	0.220	0.100	0.120	2.510	0.8680
1-Heptyne	0.160	0.230	0.120	0.100	3.000	1.0089
1-Octyne	0.155	0.220	0.090	0.100	3.521	1.1498
Benzene	0.610	0.520	0.000	0.140	2.786	0.7164
Toluene	0.601	0.520	0.000	0.140	3.325	0.8573
Ethylbenzene	0.613	0.510	0.000	0.150	3.778	0.9982
<i>o</i> -Xylene	0.663	0.560	0.000	0.160	3.939	0.9982
<i>m</i> -Xylene	0.623	0.520	0.000	0.160	3.839	0.9982
<i>p</i> -Xylene	0.613	0.520	0.000	0.160	3.839	0.9982
Styrene	0.849	0.650	0.000	0.160	3.908	0.9550
α -Methylstyrene	0.851	0.640	0.000	0.190	4.290	1.0960
Naphthalene	1.340	0.920	0.000	0.200	5.161	1.0854
Methanol	0.278	0.440	0.430	0.470	0.970	0.3082
Ethanol	0.246	0.420	0.370	0.480	1.485	0.4491
1-Propanol	0.236	0.420	0.370	0.480	2.031	0.5900
2-Propanol	0.212	0.360	0.330	0.560	1.764	0.5900
1-Butanol	0.224	0.420	0.370	0.480	2.601	0.7310
2-Butanol	0.217	0.360	0.330	0.560	2.338	0.7310
2-Methyl-1-propanol	0.217	0.390	0.370	0.480	2.413	0.7310
<i>tert</i> -Butanol	0.180	0.300	0.310	0.600	1.963	0.7310
1-Pentanol	0.219	0.420	0.370	0.480	3.106	0.8718
1-Octanol	0.199	0.420	0.370	0.480	4.619	1.2950
1-Decanol	0.191	0.420	0.370	0.480	5.610	1.5763
Cyclohexanol	0.460	0.540	0.320	0.570	3.758	0.9040
Benzyl alcohol	0.803	0.870	0.330	0.560	4.221	0.9160
Thiophene	0.687	0.570	0.000	0.150	2.819	0.6411
Tetrahydrofuran	0.289	0.520	0.000	0.480	2.636	0.6223
1,4-Dioxane	0.329	0.750	0.000	0.640	2.892	0.6810
Methyl <i>tert</i> -butyl ether	0.024	0.220	0.000	0.550	2.372	0.8718
Ethyl <i>tert</i> -butyl ether	-0.020	0.160	0.000	0.600	2.720	1.0127
Methyl <i>tert</i> -amyl ether	0.050	0.210	0.000	0.600	2.916	1.0127
Diethyl ether	0.041	0.250	0.000	0.450	2.015	0.7309
Dipropyl ether	0.008	0.250	0.000	0.450	2.954	1.0127
Diisopropyl ether	-0.063	0.170	0.000	0.570	2.501	1.0127

Table 4. (cont).

Dibutyl ether	0.000	0.250	0.000	0.450	3.924	1.2945
Acetone	0.179	0.700	0.040	0.490	1.696	0.5470
2-Pentanone	0.143	0.680	0.000	0.510	2.755	0.8288
3-Pentanone	0.154	0.660	0.000	0.510	2.811	0.8288
Cyclohexanone	0.403	0.860	0.000	0.560	3.792	0.8611
Methyl acetate	0.142	0.640	0.000	0.450	1.911	0.6057
Ethyl acetate	0.106	0.620	0.000	0.450	2.314	0.7466
Methyl propanoate	0.128	0.600	0.000	0.450	2.431	0.7470
Methyl butanoate	0.106	0.600	0.000	0.450	2.943	0.8880
Methyl caproate	0.080	0.600	0.000	0.450	3.874	1.1693
Butyraldehyde	0.187	0.650	0.000	0.450	2.270	0.6880
Acetonitrile	0.237	0.900	0.070	0.320	1.739	0.4040
Pyridine	0.631	0.840	0.000	0.520	3.022	0.6753
1-Nitropropane	0.242	0.950	0.000	0.310	2.894	0.7055
Acetic Acid	0.265	0.640	0.620	0.440	1.816	0.4648
Acetophenone	0.818	1.010	0.000	0.480	4.501	1.0139
Aniline	0.955	0.960	0.260	0.410	3.934	0.8162
Benzaldehyde	0.820	1.000	0.000	0.390	4.008	0.8730
Benzonitrile	0.742	1.110	0.000	0.330	4.039	0.8711
1-Bromohexane	0.349	0.400	0.000	0.120	4.130	1.1290
1-Bromooctane	0.339	0.400	0.000	0.120	5.143	1.4108
Butyraldehyde	0.187	0.650	0.000	0.450	2.270	0.6880
Octylaldehyde	0.160	0.650	0.000	0.450	4.380	1.2515
2-Chloroaniline	1.033	0.920	0.250	0.310	4.674	0.9390
1-Chlorohexane	0.201	0.390	0.000	0.090	3.708	1.0764
1-Chlorooctane	0.191	0.400	0.000	0.090	4.708	1.3582
<i>p</i> -Cresol	0.820	0.870	0.570	0.310	4.312	0.9160
1,2-Dichlorobenzene	0.872	0.780	0.000	0.040	4.318	0.9612
N,N-Dimethylformamide	0.367	1.310	0.000	0.740	3.173	0.6468
1-Iodobutane	0.628	0.400	0.000	0.150	3.628	0.9304
Nitrobenzene	0.871	1.110	0.000	0.280	4.557	0.8906
2-Nitrophenol	1.015	1.050	0.050	0.370	4.760	0.9493
Phenetole	0.681	0.700	0.000	0.320	4.242	1.0569
Phenol	0.805	0.890	0.600	0.300	3.766	0.7751
Propionitrile	0.162	0.900	0.020	0.360	2.082	0.5450
Pyrrole	0.613	0.910	0.220	0.250	2.792	0.5774
Propanoic acid	0.233	0.650	0.600	0.450	2.290	0.6057

Results and Discussion

Ionic liquids can be designed to possess specific physical properties and solubilizing abilities through judicious selection of the cation-anion pair combination and by adding functional groups to the cation alkyl chain. For instance, hydroxy- and ether functionalized ILs have been reported to exhibit especially large abilities in regards to solubilizing SO₂ and CO₂.³⁸ Abraham model Eqns. 1 and 2 provide a mathematical means to estimate how the partitioning behavior of organic compounds and inorganic gases changes as one varies the cation-anion combination in the IL. To estimate the partitioning behavior, however, one does need knowledge of the two sets of equation coefficients which can be obtained by regression analysis of experimental partition coefficient data. Analysis of the log *K* and log *P* values in Table 3 yielded the following three correlation expressions:

$$\log K(298) = -0.145(0.060) + 2.360(0.055)S + 1.248(0.090)A + 0.523(0.088)B + 0.629(0.017)L \quad (6)$$

$$(R^2 = 0.984, SD = 0.137, N = 104, F = 1109)$$

$$\log K(323) = -0.262(0.050) + 2.158(0.046)S + 1.055(0.075)A + 0.442(0.073)B + 0.542(0.014)L \quad (7)$$

$$(R^2 = 0.986, SD = 0.115, N = 106, F = 1773)$$

$$\log P(298) = 0.130(0.089) + 0.168(0.089)E + 0.477(0.103)S - 2.483(0.111)A - 4.245(0.119)B + 3.215(0.077)V \quad (8)$$

$$(R^2 = 0.989, SD = 0.158, N = 102, F = 1778)$$

where the standard error in each coefficient in parenthesis after the coefficient itself. All regression analyses were performed using SPSS Statistics (Version 20) software.

Preliminary analysis showed the $(e_{k,cation} + e_{k,anion})E$ term to be small in $\log K$ correlations at both 298 K, $(e_{k,cation} + e_{k,anion}) = -0.031$, and 323 K, $(e_{k,cation} + e_{k,anion}) = 0.005$, and the standard error in the term were larger than the coefficient. The $(e_{k,cation} + e_{k,anion})E$ term was removed from the final $\log K$ regression analyses. The relevant statistical information is given the respective correlation and is as follows: R^2 refers to the squared correlation coefficient, SD is the standard deviation, N represents the number of data points in the data set, and F denotes the Fisher F -statistic. The number of data points employed in the regression analyses is larger than the number of solutes studied. Remember that there were thirteen solutes common to our dataset and the dataset published by Marciniak and Wlazlo.³⁴ The thirteen common solutes were used to determine the proportionality constant, P^* , needed to convert the measured chromatographic retention factor data to gas-to-liquid partition coefficients. The derived Abraham model correlations given by Eqns. 6 – 8 are statistically quite good and back-calculate the observed partition coefficients to within 0.16 log units.

Figure 2 depicts a plot of $\log K$ (298 K) values back-calculated with Eqn. 6 against experimental values covering a range of approximately 4.373 log units, from $\log K = 1.104$ for pentane to $\log K = 5.477$ for 2-chloroaniline. A comparison of the back-calculated $\log P$ values versus measured $\log P$ data is shown in Figure 3. As expected the deviations in the back-calculated $\log P$ values are slightly larger than those for the $\log K$ correlations because the $\log P$ values contain the additional experimental uncertainty in the gas-to-water data used in the $\log K$ to $\log P$ conversion.

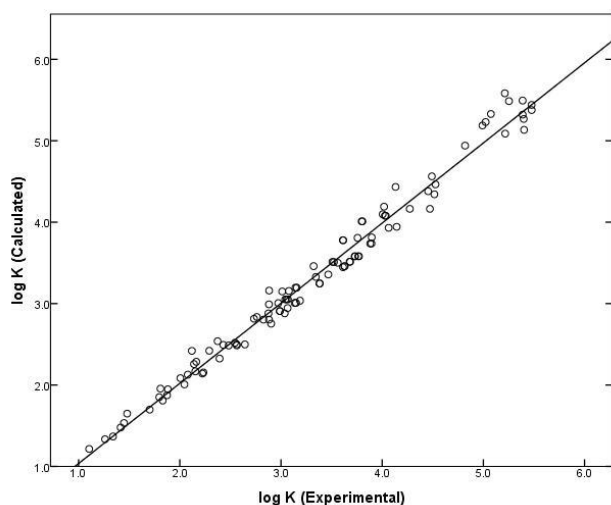


Figure 2. Comparison between experimental $\log K$ (298 K) data and predicted values based on Eqn. 6

The derived $\log K$ (323 K) correlation can be compared to those reported by Marciniak and Wlazlo.³⁴ As noted above the authors determined $\log K$ correlations based on the experimental gas-to-IL partition coefficient data for water and 61 organic solutes dissolved in ([MeoeMPyrr]⁺[FAP]⁻) at six temperatures from 318 K to 368 K. While 323 K was not one of the specific temperatures studied by the authors one should be able to reasonably assume that a $\log K$ correlation for 323 K should fall somewhere between the reported correlations

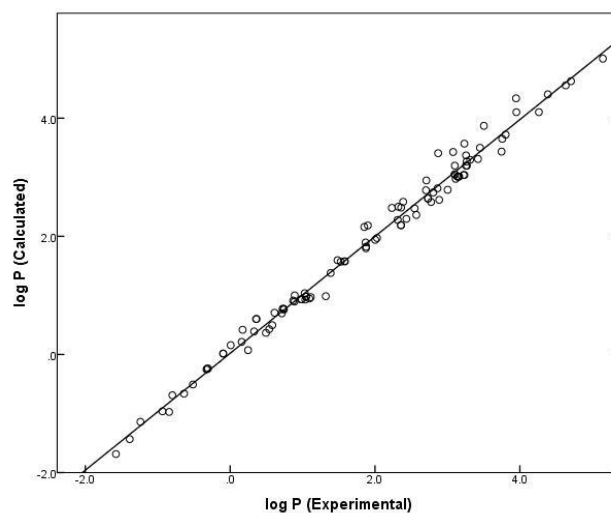


Figure 3. Comparison between experimental $\log P$ (298 K) data and predicted values based on Eqn. 8

$$\log K(318) = -0.355(0.065) - 0.049(0.080)E + 2.37(0.08)S + 1.15(0.12)A + 0.389(0.083)B + 0.580(0.020)L \quad (9)$$

$$\log K(328) = -0.379(0.061) - 0.039(0.074) + 2.28(0.07)S + 1.07(0.11)A + 0.359(0.076)B + 0.552(0.018)L \quad (10)$$

for 318 K and 328 K. Comparison of Eqns. 7, 9 and 10 shows that our calculated equation for the $\log K(323)$ correlation (Eqn. 7) does fall in between Eqns. 9 and 10 when the combined standard errors in the equation coefficients are taken into account. The slight difference between our coefficients and the arithmetic average of the coefficients of Eqns. 9 and 10 likely results for the more diverse set of solutes used in deriving Eqn. 7 and our decision to remove the $(e_{k,cation} + e_{k,anion})E$ term from the derived correlation. Our dataset (see Table 3) contains 104 experimental data points and includes two carboxylic acid solutes (acetic acid and propanoic acid), three phenolic compounds (phenol, 2-nitrophenol and *p*-cresol), two primary amine solutes (aniline and 2-chloroaniline), several halogenated alkanes (1-chlorobutane, 1-chlorohexane, 1-chlorooctane, 1-iodobutane, 1-bromohexane, 1-bromo-octane), and several substituted aromatic benzene derivatives (acetophenone, benzaldehyde, phenetole, benzonitrile, nitrobenzene, phenetole, benzyl alcohol and 1,2-dichlorobenzene). Careful examination of Eqns. 9 and 10 shows that the summed $(e_{k,cation} + e_{k,anion})$ coefficient is small, and that the standard error in the coefficient is larger than the coefficient. Unlike us, Marciniak and Wlazlo³⁴ elected to retain the term in their $\log K$ correlation.

In order to validate and to assess the predictive capabilities and limitations of Eqns. 6 – 8 we performed a training set and test set analysis by allowing the SPSS software to randomly select half of the experimental data values. The selected values became the training sets and the values that were left served as the test sets. By performing regression analyses on the experimental data in the two $\log K$ and one $\log P$ training sets, we obtained the following three mathematical correlations:

$$\log K(298) = -0.257(0.075) + 2.466(0.077)S + 1.469(0.174)A + 0.358(0.127)B + 0.661(0.021)L \quad (11)$$

$$(R^2 = 0.989, SD = 0.117, N = 52, F = 1034)$$

$$\log K(323) = -0.225(0.092) + 2.166(0.080)S + 1.063(0.140)A + 0.407(0.119)B + 0.526(0.028)L \quad (12)$$

$$(R^2 = 0.983, SD = 0.125, N = 53, F = 709)$$

$$\log P(298) = 0.220(0.120) + 0.156(0.117)E + 0.472(0.140)S - 2.496(0.149)A - 4.292(0.158)B + 3.146(0.098)V \quad (13)$$

$$(R^2 = 0.989, SD = 0.148, N = 51, F = 937)$$

Again the $(e_{k,\text{cation}} + e_{k,\text{anion}})E$ term was eliminated from the two log K correlations because the calculated coefficients were small.

Careful examination of Eqns. 6 – 8 and Eqns. 11 – 13 reveals that to within the standard errors in the equation coefficients, the training set equation coefficients are identical to the equation coefficients for the full data sets. The training set expression were then used to estimate the gas-to-IL partition coefficients for the 52 and 53 compounds in the log K test sets, and the water-to-IL partition coefficients of the 51 compounds in the log P test set. For the estimated and experimental values we found: SD values of 0.135, 0.102 and 0.170; average absolute error (AAE) values of 0.116, 0.090 and 0.125; and average error (AE) values of -0.025 , 0.040 and -0.014 for Eqns. 11 – 13, respectively. The small AE values indicate that there is essentially no bias in predicting these log K and log P values. The training set and test set calculations were performed two more times with very similar statistical results.

The derived Abraham model correlations are expected to provide reasonably accurate partition coefficient predictions for additional organic compounds in anhydrous ([MeoeMPyrr]⁺[FAP]⁻) provided that the solute's descriptors values fall with the range of values defined by the compounds listed in Table 4. As an informational note, small gaseous solutes like methane, ethane, ethene, carbon dioxide, sulfur dioxide, etc. would not be included in the above descriptor range because their V and L solute descriptors are too small. We were not able to find gas solubility data for these small solutes dissolved in anhydrous ([MeoeMPyrr]⁺[FAP]⁻). In regards to the log P predictions Eqn. 8 pertains to the hypothetical water-to-anhydrous ([MeoeMPyrr]⁺[FAP]⁻) partitioning process. We do not know how effective the equation will be in predicting practical water-to-([MeoeMPyrr]⁺[FAP]⁻) partition coefficients as there has been very little previous studies comparing direct practical partitioning processes against the indirect hypothetical partitioning processes.

Nakamura *et al.*³⁹ determined the partition coefficients of several substituted benzenes between water and three ionic liquids (1-butyl-3-methylimidazolium bis(trifluoromethylsulfonyl)imide, ([BMIm]⁺[Tf₂N]⁻), 1-butyl-1-methylpyrrolidinium bis(trifluoromethylsulfonyl)imide, ([BMPyrr]⁺[Tf₂N]⁻), and 1-butyl-3-methylimidazolium hexafluorophosphate, ([BMIm]⁺[PF₆]⁻)) for use in liquid-liquid extractions. There is hypothetical indirect partition coefficient data^{18,40} for several of the solutes studied by Nakamura *et al.* in both ([BMIm]⁺[Tf₂N]⁻) and ([BMIm]⁺[PF₆]⁻) based on measured gas-to-IL and gas-to-water partition coefficient data. We have assembled in Table 5 the solutes for which we were able to find both direct and indirect log P values. There is an average difference between the two sets of log P values of 0.072 and

-0.104 log units, respectively, in the case of ([BMIm]⁺[Tf₂N]⁻) and ([BMIm]⁺[PF₆]⁻). For ([BMIm]⁺[Tf₂N]⁻) the direct partition coefficients are slightly larger than the indirect values, and for the ([BMIm]⁺[PF₆]⁻) the indirect values are slightly larger. The water and ([BMIm]⁺[PF₆]⁻) system does exhibit some mutual solubility, the solubility of water in ([BMIm]⁺[PF₆]⁻) is 0.26 mole fraction and the solubility of ([BMIm]⁺[PF₆]⁻) in water is 0.00042 mole fraction.⁴¹ The water and ([BMIm]⁺[Tf₂N]⁻) system exhibits similar mutual solubility. The solubility of water in ([BMIm]⁺[Tf₂N]⁻) is 0.26 mole fraction, while the solubility of ([BMIm]⁺[Tf₂N]⁻) in water is 0.000307 mole fraction.⁴² While there is no published practical partition coefficient data for ([MeoeMPyrr]⁺[FAP]⁻) for us to compare our experimental indirect and predicted indirect log P values against; however there is a reasonable possibility that, like water-to-organic solvent solute partitioning behavior, Eqn. 8 may provide reasonable predictions for direct water-to-([MeoeMPyrr]⁺[FAP]⁻) log P values, provided that the mutual solubility in this partitioning system is not too large.

Table 5. Comparison of practical direct and hypothetical indirect water-to-([MeoeMPyrr]⁺[FAP]⁻) partition coefficients for select organic solutes at 298 K

Solute	log P (direct)	log P (indirect)	Diff.
IL = ([BMIm] ⁺ [Tf ₂ N] ⁻)			
Benzene	2.344	2.253	0.091
Toluene	2.700	2.553	0.147
<i>o</i> -Xylene	3.048	2.977	0.071
<i>m</i> -Xylene	3.060	2.985	0.075
<i>p</i> -Xylene	3.067	2.991	0.076
Acetophenone	1.987	2.011	-0.024
Aniline	1.550	1.478	0.072
Benzyl alcohol	0.940	0.874	0.066
1,2-Dichlorobenzene	3.200	3.290	-0.090
Nitrobenzene	2.257	2.091	0.166
IL = ([BMIm] ⁺ [PF ₆] ⁻)			
Benzene	2.220	2.137	0.083
Toluene	2.480	2.402	0.078
<i>o</i> -Xylene	2.773	2.977	-0.204
<i>m</i> -Xylene	2.775	2.832	-0.057
<i>p</i> -Xylene	2.780	2.739	0.041
Acetophenone	1.924	2.056	-0.132
1,2-Dichlorobenzene	2.960	3.359	-0.399
Nitrobenzene	2.245	2.483	-0.238

As noted above, the equation coefficients represent a cation-anion sum. It is possible to calculate the equation coefficients for an individual cation if the anion values are known, and vice versa. In the present case the [FAP]⁻-specific equation coefficients of $c_{k,\text{anion}} = 0.179$; $e_{k,\text{cation}} = -0.015$; $s_{k,\text{anion}} = 0.063$; $a_{k,\text{anion}} = -1.314$; $b_{k,\text{anion}} = 0.328$ and $l_{k,\text{anion}} = -0.053$ are known from a previous study.⁴³ The above [FAP]⁻-specific equation coefficients pertain to the log K Abraham model correlation for 298 K. The equation coefficients for the [MeoeMPyrr]⁺ cation are obtained by

subtracting the existing [FAP]⁻-specific equation coefficients from the values given in Eqn. 6. Performing the indicated subtractions, the following numerical values are computed: $c_{k,cation} = -0.324$; $e_{k,cation} = 0.015$; $s_{k,cation} = 2.297$; $a_{k,cation} = 2.562$; $b_{k,cation} = 0.285$; and $l_{k,cation} = 0.682$ for the [MeoeMPyrr]⁺ cation. Similarly, numerical values for the [MeoeMPyrr]⁺ cation for the log *P*(298 K) correlation would be calculated by subtracting the published values⁴³ of $c_{p,anion} = 0.132$; $e_{p,anion} = -0.171$; $s_{p,anion} = 0.121$; $a_{p,anion} = -1.314$; $b_{p,anion} = 0.244$; and $v_{p,anion} = -0.107$ for the [FAP]⁻ anion from the coefficients given in Eqn. 8.

Conclusion

The present study increases the number of cations for which we have calculated ion-specific equation coefficients by one, from 21 different cations to 22 different cations, and permits the estimation of log *K* and log *P* values for an additional 14 ILs. We can now predict the partitioning behaviour of organic solutes dissolved in 1-(2-methoxyethyl)-1-methylpyrrolidinium bis(trifluoromethylsulfonyl)imide, 1-(2-methoxyethyl)-1-methylpyrrolidinium tetrafluoroborate, 1-(2-methoxyethyl)-1-methylpyrrolidinium hexafluorophosphate, 1-(2-methoxyethyl)-1-methylpyrrolidinium trifluoroacetate, 1-(2-methoxyethyl)-1-methylpyrrolidinium tetracyanoborate, 1-(2-methoxyethyl)-1-methylpyrrolidinium dicyanamide, 1-(2-methoxyethyl)-1-methylpyrrolidinium tris(pentafluoroethyl)trifluorophosphate, 1-(2-methoxyethyl)-1-methylpyrrolidinium bis(pentafluoroethylsulfonyl)imide, 1-(2-methoxyethyl)-1-methylpyrrolidinium thiocyanate, 1-(2-methoxyethyl)-1-methylpyrrolidinium nitrate, 1-(2-methoxyethyl)-1-methylpyrrolidinium ethylsulfate, 1-(2-methoxyethyl)-1-methylpyrrolidinium octylsulfate, 1-(2-methoxyethyl)-1-methylpyrrolidinium diethylphosphate, and 1-(2-methoxyethyl)-1-methylpyrrolidinium methanesulfonate. Future studies will measure chromatographic retention factors for solutes on more ionic liquid stationary phases in order to determine ion-specific equation coefficients for additional cations and anions.

References

- Gonzalez-Miguel, M., Bedia, J., Abrusci, C., Palomar, J., Rodriguez, F. *J. Phys. Chem. B*, **2013**, *117*, 3398.
- Abraham, M. H. *Chem. Soc. Rev.*, **1993**, *22*, 73.
- Abraham, M. H., Ibrahim, A., Zissimos, A. M. *J. Chromatogr. A*, **2004**, *1037*, 29.
- Abraham, M. H., Smith, R. L., Luchtefeld, R., Boorem, A. J., Luo, R., Acree, W. E. Jr. *J. Pharm. Sci.*, **2010**, *99*, 1500.
- Abraham, M. H., Acree, W. E. Jr. *New J. Chem.*, **2010**, *34*, 2298.
- Saifullah, M., Ye, S., Grubbs, L. M., De La Rosa, N. E., Acree, W. E. Jr., Abraham, M. H. *J. Solution Chem.*, **2011**, *40*, 2082.
- Abraham, M. H., Acree, W. E. Jr. *Thermochim. Acta*, **2011**, *526*, 22.
- Stephens, T. W., Wilson, A., Dabadge, N., Tian, A., Hensley, H. J., Zimmerman, M., Acree, W. E. Jr., Abraham, M. H. *Glob. J. Phys. Chem.*, **2012**, *3*, 9/1.
- Stephens, T. W., De La Rosa, N. E., Saifullah, M., Ye, S., Chou, V., Quay, A. N., Acree, W. E. Jr., Abraham, M. H. *Fluid Phase Equilib.*, **2011**, *308*, 64.
- Abraham, M. H., Acree, W. E. Jr. *J. Solution Chem.*, **2011**, *40*, 1279.
- Abraham, M. H., Acree, W. E. Jr. *J. Solution Chem.*, **2012**, *41*, 730.
- Sprunger, L., Acree, W. E. Jr., Abraham, M. H. *J. Chem. Inf. Model.*, **2007**, *47*, 1808.
- Sprunger, L. M., Gibbs, J., Acree, W. E. Jr., Abraham, M. H. *QSAR Comb. Sci.*, **2009**, *28*, 72.
- Acree, W. E. Jr., Abraham, M. H. *J. Chem. Technol. Biotechnol.*, **2006**, *81*, 1441.
- Abraham, M. H., Acree, W. E. Jr. *Green Chem.*, **2006**, *8*, 906.
- Sprunger, L., Clark, M., Acree, W. E. Jr., Abraham, M. H. *J. Chem. Inf. Model.*, **2007**, *47*, 1123.
- Sprunger, L. M., Proctor, A., Acree, W. E. Jr., Abraham, M. H. *Fluid Phase Equilib.*, **2008**, *265*, 104.
- Sprunger, L. M., Gibbs, J., Proctor, A., Acree, W. E. Jr., Abraham, M. H., Meng, Y., Yao, C., Anderson, J. L. *Ind. Eng. Chem. Res.*, **2009**, *48*, 4145.
- Mutelet, F., Revelli, A.-L., Jaubert, J.-N., Sprunger, L. M., Acree, W. E. Jr., Baker, G. A. *J. Chem. Eng. Data*, **2010**, *55*, 234.
- Revelli, A.-L., Mutelet, F., Jaubert, J.-N., Garcia-Martinez, M., Sprunger, L. M., Acree, W. E. Jr., Baker, G. A. *J. Chem. Eng. Data*, **2010**, *55*, 2434.
- Domańska, U., Królikowska, M., Acree, W. E. Jr., Baker, G. A. *J. Chem. Thermodyn.*, **2011**, *43*, 1050.
- Grubbs, L. M., Ye, S., Saifullah, M., Acree, W. E. Jr., Twu, P., Anderson, J. L., Baker, G. A., Abraham, M. H. *J. Solution Chem.*, **2011**, *40*, 2000.
- Moise, J.-C., Mutelet, F., Jaubert, J.-N., Gubbs, L. M., Acree, W. E. Jr., Baker, G. A. *J. Chem. Eng. Data*, **2011**, *56*, 3106.
- Domańska, U., Królikowska, M., Acree, W. E. Jr. *J. Chem. Thermodyn.*, **2011**, *43*, 1810.
- Acree, W. E. Jr., Baker, G. A., Mutelet, F., Moise, J.-C. *J. Chem. Eng. Data*, **2011**, *56*, 3106.
- Stephens, T. W., Acree, W. E. Jr., Twu, P., Anderson, J. L., Baker, G. A., Abraham, M. H. *J. Solution Chem.*, **2012**, *41*, 1165.
- Twu, P., Anderson, J. L., Stephens, T. W., Acree, W. E. Jr., Abraham, M. H. *Eur. Chem. Bull.*, **2012**, *1*, 212.
- Acree, W. E. Jr., Baker, G. A., Revelli, A.-L., Moise, J.-C., Mutelet, F. *J. Chem. Eng. Data*, **2012**, *57*, 3510.
- Zissimos, A. M., Abraham, M. H., Du, C. M., Valko, K., Bevan, C., Reynolds, D., Wood, J., Tam, K. Y. *J. Chem. Soc., Perkin Trans. 2*, **2002**, 2001.
- Zissimos, A. M., Abraham, M. H., Barker, M. C., Box, K. J., Tam, K. Y. *J. Chem. Soc., Perkin Trans. 2*, **2002**, 470.
- Green, C. E., Abraham, M. H., Acree, W. E. Jr., De Fina, K. M., Sharp, T. L. *Pest Manage. Sci.*, **2000**, *56*, 1043.
- Abraham, M. H., Green, C. E., Acree, W. E. Jr., Hernandez, C. E., Roy, L. E. *J. Chem. Soc., Perkin Trans. 2*, **1998**, 2677.
- Bowen, K. R., Stephens, T. W., Lu, H., Shan, D., Satish, K., Acree, W. E. Jr., Abraham, M. H. *Eur. Chem. Bull.*, **2013**, *2*, 577.
- Marciniak, A., Wlazlo, M. *J. Chem. Thermodyn.*, **2013**, *60*, 57.
- Baltazar, Q. Q., Leininger, S. K., Anderson, J. L. *J. Chromatogr. A*, **2008**, *1182*, 119.
- Abraham, M. H., Andonian-Haftvan, J., Whiting, G. S., Leo, A., Taft, R. W. *J. Chem. Soc., Perkin Trans. 2*, **1994**, 1971.
- Abraham, M. H., Ibrahim, A., Acree, W. E. Jr. *Fluid Phase Equilib.*, **2007**, *251*, 93.

- ³⁸Tang, S., Baker, G. A., Zhao, H. *Chem. Soc. Rev.*, **2012**, *41*, 4030.
- ³⁹Nakamura, K., Kudo, Y., Takeda, Y., Katsuta, S. *J. Chem. Eng. Data*, **2011**, *56*, 2160.
- ⁴⁰Sprunger, L. M., Gibbs, J., Baltazar, Q. W., Acree, W. E. Jr., Abraham, M. H., Anderson, J. L. *Phys. Chem. Liq.*, **2009**, *47*, 74.
- ⁴¹Li, J., Wang, L.-S., Cai, S.-F. *J. Chem. Eng. Data*, **2010**, *55*, 5289.
- ⁴²Freire, M. G., Carvalho, P. J., Gardas, R. L., Marrucho, I. M., Santos, L. M. N. B. F., Coutinho, J. A. P. *J. Phys. Chem. B*, **2008**, *112*, 1604.
- ⁴³Acree, W. E. Jr., Grubbs, L. M., Abraham, M. H., *Selection of Ionic Liquid Solvents for Chemical Separations Based on the Abraham Model in Ionic Liquids: Applications and Perspectives* (Book 2), Kokorin, A. (Editor) INTECH Publishers, 2011, Chapter 13, 273.

Received:04.05.2013.

Accepted:16.05.2013.



PRODUCTION OF CALCIUM MONOHYDROGENPHOSPHATE FROM SEBAIYA PHOSPHATE ORE LEACHED BY NITRIC ACID

Adel A. El-Zahhar,^[a] Mohsen M. Aly,^[a] Ahmed M. Ahmad,^[a] Magdy I. Khalifa,^[b] Ahmed A. El-Asmy^{[b]*}

Keywords: Sebaiya phosphate ore, calcium monohydrogenphosphate production, nitric acid leaching

The production of phosphoric acid and/or calcium monohydrogenphosphate from Sebaiya phosphate ore was investigated by leaching with nitric acid. Various factors affecting the process such as particle size, leaching time, leaching temperature, phosphate rock/HNO₃ ratio and mixing stirring speed and temperature have been studied to estimate the favor phosphate ore dissolution in relation to impurity. These parameters were fixed at a leaching time of 16 min, stirring speed of 400 rpm, temperature of 25 °C, nitric acid concentration of 2.5 % and acid/phosphate ore mass ratio of 25 ml/5 g. The produced aqueous acidic solution was neutralized in such a way that a pure calcium monohydrogenphosphate, CaHPO₄, is precipitated to be used as animal fodder. The production efficiency was 97.2 %.

Corresponding Authors

E-Mail: aelasmy@yahoo.com

[a] Nuclear Chemistry Department, Hot Labs Center, AEA, Cairo, Egypt

[b] Chemistry Department, Faculty of Science, Mansoura University, Mansura, Egypt

The wet process presents 90% of the world current phosphoric acid production. In this process, there are three possible subgroups depending on the mineral acid that is used for the acidification. This may be sulfuric acid,^{5,6} hydrochloric acid^{7,8} or nitric acid.⁹⁻¹¹

Introduction

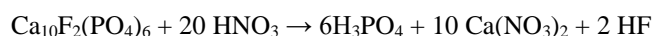
Phosphoric acid (H₃PO₄) is the secondary most important inorganic acid after sulfuric acid produced over the world. It is primarily used for the manufacture of phosphate salts, which are used in fertilizers, animals fodder production and detergents.

The composition of phosphate ores varies from one deposit to another. Therefore, phosphate rocks from different sources are expected to behave differently in acidification processes. Phosphate ores are of two major geological origins, igneous and sedimentary. The phosphate minerals in both types of ore are of the apatite group, of which the most commonly encountered variants are; fluorapatite, Ca₁₀(PO₄)₆(F,OH)₂ and francolite, Ca₁₀(PO₄)₆(CO₃)_x(F,OH)_{2-x}, where fluorapatite predominates in igneous phosphate rocks and francolite predominates in sedimentary phosphate rocks.¹

Phosphate ores occur in Egypt in three main provinces, Western desert, Nile valley, and Red sea. Added to these are some phosphate-bearing sediments present in Wadi Qena, Wadi Araba, Esh El-Mallana range and Sinai.^{2,3}

Phosphoric acid can be prepared by two methods, thermal and wet processes. The acid produced by thermal method is extremely pure; however, it is also expensive. The wet process which is based on the acidification of phosphate ores using any mineral acid is the more popular as a result of the increased demand for high-grade fertilizers, and the energy saving in the wet processes compared with thermal process.⁴

When phosphate rock is treated with nitric acid, phosphoric acid and soluble calcium nitrate are formed according to the following equation:



The process includes first acidulating of crushed phosphate rock in a reaction mixture vessel with excess nitric acid. The nitric acid concentration should be between 40 and 70%. The reaction temperature is at 120 - 130 °C and the reaction time ranges from 1 to 2.5 hrs. The product phosphoric acid contains from 55 - 72 % P₂O₅.¹²⁻¹⁵ Food grade calcium phosphate has successfully produced from phosphoric acid produced by Abu-Zaabal Fertilizers and Chemicals Company by two steps. The first step includes clarification and defluorination of crude phosphoric acid. The second step includes the precipitation of food grade calcium phosphate by using different calcium salts as calcium oxide, calcium hydroxide and calcium carbonate.¹⁶ The production of calcium monohydrogenphosphate for use as animal fodders, by direct acidulation of phosphate rock with mineral acids has long been a goal of the fertilizer industry, since it use much less mineral acid consumption than by conventional other processes.¹⁷⁻²⁰

The aim of the present work is to investigate different conditions as particle size, leaching time, leaching temperature, phosphate rock/HNO₃ ratio and mixing speed (rpm) that affect the production of phosphoric acid and/or the phosphate salt from Sebaiya phosphate ore by attacking with nitric acid to estimate the favor phosphate ore leaching in relation to an impurity and direct production for calcium monohydrogen phosphate (DCP).

Experimental

Materials

HNO₃ (MERCK, Germany), H₂SO₄ (FLUKA, Switzerland) and H₃PO₄ (BDH, England) were chemical reagents grade. CaCO₃ and Ca(OH)₂ from El-Nasr Pharmaceutical Chemicals (ADWIC, Egypt) were used as a source of calcium ions. A composite sample of Sebaiya phosphate ore was delivered from Abu-Zaabal Fertilizers. The chemical analysis of the phosphate rock is shown in Table 1.

Table 1. Chemical analysis of Sebaiya phosphate ore

Constituent	%
P ₂ O ₅	28.6
CaO	47.4
Fe ₂ O ₃	2.3
F	2.9
SiO ₂	6.5
Constituent	mg/kg
Cd	3.30
Pb	25.80
As	30.5

Apparatus

All reactions were carried out in a cylindrical 1 L reactor of 10 cm diameter. It was fitted with Teflon-coated stirrer and placed in thermostatically controlled water bath. The impeller tip speed was adjusted at 400 rpm unless otherwise stated. Filtration was performed using Buchner type filter of 4.6 in. diameter. Polypropylene filter cloth of 80 mesh aperture size was used. A vacuum pump was used for filtration.

Procedure

The phosphate ore sample was crushed with a jaw crusher and sieved using ASTM standard sieves to collect various size fractions for analysis. All the sieved samples were dried in an electric oven at 105 °C, cooled to room temperature and stored in a closed desiccator. These sample fractions were analyzed for P₂O₅ content as shown in Table 2.

For each run 5 g of phosphate sample was transferred with the proper determined amount of nitric acid solution into the reactor. Defoamer (oleic acid) is added when necessary. After the desired reaction time, the leach slurry was immediately separated by filtration. The remaining solids were dried and weighed. In the filtrate the P₂O₅ content was determined by a colorimetric method (spectrophotometer type Shimadzu UV 1208, ammonium molybdate and ammonium metavanadate were used for P₂O₅ analysis).

CaHPO₄ experiments were carried out by adding 4 g of calcium carbonate to the proper amount of acidulate solution into the reactor. After the desired reaction time, the produced CHP was filtrated, dried and weighted. P₂O₅ content was determined in both CHP and the precipitation raffinate solution by colorimetric method (spectrophotometer type Shimadzu UV 1208, ammonium molybdate and ammonium metavanadate were used for P₂O₅ analysis).

Table 2. Sieve analysis and P₂O₅ content of phosphate ore fractions

No.	Fraction			P ₂ O ₅ , wt. %
	Size, μm	Weight, kg	Recovery, %	
1	1180	5.00	100.0	28.60
2	1180–1000	0.519	10.38	26.10
3	750–710	0.731	14.62	28.40
4	600–500	0.741	14.82	29.59
5	420–315	1.000	20.00	29.76
6	315–250	0.764	15.28	30.06
7	250–160	1.215	24.30	30.40

The recovery (φ , in %) of P₂O₅ was calculated by the following equation:

$$\varphi = 100 \times \frac{\text{dissolved P}_2\text{O}_5 \text{ amount}}{\text{total P}_2\text{O}_5 \text{ amount in the rock}}$$

The precipitation efficiency (χ , %) was calculated by:

$$\chi = 100 \times \frac{\text{amount of P}_2\text{O}_5 \text{ in produced DCP}}{\text{total amount of P}_2\text{O}_5 \text{ in the acidulate solution}}$$

Results and Discussion

Nitric Acid Leaching Investigation

The results obtained when Sebaiya phosphate ore was subjected to leaching with nitric acid solution under the following parameters: particle size, reaction time, reaction temperature, nitric acid concentration, HNO₃/phosphate ore mass ratio and stirring speed.

Effect of particle size

The effect of particle size on the phosphate ore leaching process was studied using particle size fractions \leq 1180, 750- 700, 600- 500, 420- 315, 315- 250, 250- 150 and 160- 63 μm. The results in Table 3 relating the P₂O₅ recovery % and particle size clarify that, the phosphate ore fractionation has a slight effect on the P₂O₅ recovery %, where the difference in P₂O₅ recovery % between the largest particle size (\leq 1180 μm) and the smallest (160 – 63 μm) is less than 1 %.

Table 3. Effect of particle size on P₂O₅ recovery % from phosphate ore at 16 min, 25 °C, 400 rpm, 1.0 M HCl and L/S 20 ml/ 5 g.

Fraction, μm	P ₂ O ₅ leaching %
\leq 1180	20.5
1180 - 1000	15.9
750 – 710	17.2
600 – 500	17.5
420 – 315	20.6
315 – 250	20.8
250 – 160	20.9
160 – 63	20.5

Therefore, all investigations were carried out with particle size fractionation $\leq 1180 \mu\text{m}$ to cancel mid cost.

Effect of reaction time

To study the effect of leaching time on phosphate ore leaching by 10 % nitric acid, several experiments were carried at different times (1.0-60 min) at 25 °C; stirring speed of 400 rpm; L/S mass ratio of 25 ml/5 g and particle size $\leq 1180 \mu\text{m}$. The results given in Figure 1 clearly show that, as the time increases from 1.0 to 15 min, the leaching % of P_2O_5 increases from 73.80 to 91.23 % meaning that the reaction is fast. After 15 min, there is a slight increase in the reaction %. Therefore, 15 min is taken as optimum to maximize the phosphate ore leaching by nitric acid.

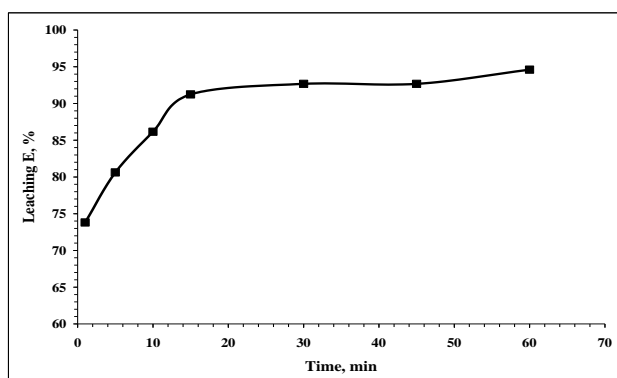


Figure 1. Effect of reaction time on P_2O_5 leaching % from phosphate ore at room temperature, a stirring speed of 400 rpm, an acid concentration of 10 %, L/S mass ratio 25 ml/5 g and a particle size $\leq 1180 \mu\text{m}$.

Effect of acid concentration

The effect of nitric acid concentration on the phosphate ore leaching process was studied at different concentrations (2.5 – 20 %) at 15 min, 400 rpm, 25 °C, particle size fraction of $\leq 1180 \mu\text{m}$, and L/S of 25 ml/5 g. The experimental results (Fig. 2) clarify that, as the acid concentration increases from 2.5 to 10 %, the P_2O_5 recovery increases from 20.63 to 91.23 %; further increase shows slight effect. This may be due to the increase of H^+ concentration increases the number of collisions with PO_4^{3-} or the H^+ ions collisions with PO_4^{3-} , HPO_4^{2-} , H_2PO_4^- in aqueous phase. Therefore, 10 % nitric acid is preferred for the phosphate ore dissolution process.

Effect of reaction temperature

The effect of reaction temperature on the leaching process was investigated at 25 - 60 °C, 15 min, 400 rpm, acid concentration 10%, particle size fraction $\leq 1180 \mu\text{m}$, and L/S mass ratio 25 ml/5 g. The results given in Fig. 3 indicate that the reaction temperature has a slight effect on the reaction rate. Therefore, room temperature (25 °C) is preferred for the leaching process.

Effect of stirring speed

The leaching process was performed using 10 % nitric acid with different stirring speed ranging from 200 to 600 rpm and reaction time of 15 min, L/S mass ratio of 25 ml/5g,

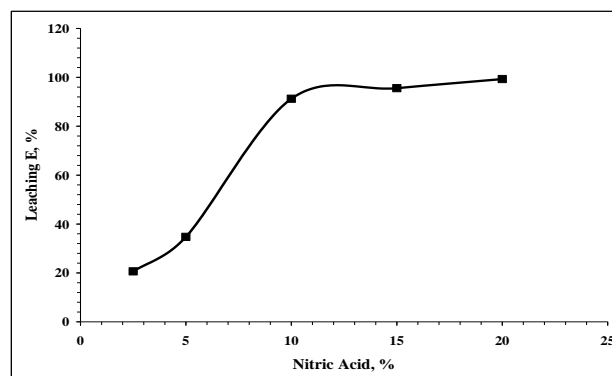


Figure 2. Effect of acid concentration on P_2O_5 leaching % from phosphate ore at a room temperature, for time 15 min, a stirring speed of 400 rpm, L/S mass ratio 25 ml/ 5 g and a particle size $\leq 1180 \mu\text{m}$.

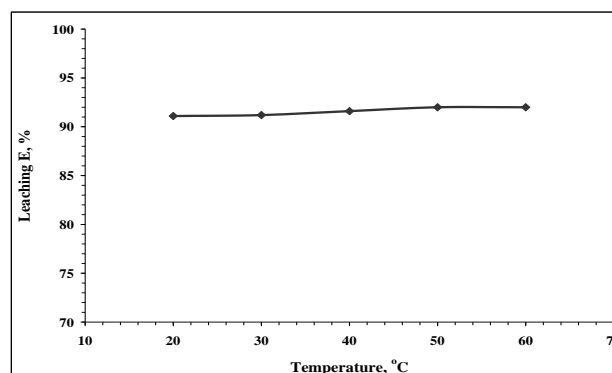


Figure 3. Effect of reaction temperature on P_2O_5 leaching % from phosphate ore for time 15 min, a stirring speed of 400 rpm, an acid concentration of 10 %, L/S ratio 25 ml/ 5 g and a particle size $\leq 1180 \mu\text{m}$.

temperature 25 °C and particle size fraction of $\leq 1180 \mu\text{m}$ to study the effect of mechanical stirring speed on the leaching process. The results in Fig. 4 reflect slight effect. Accordingly, all experiments were carried out at 400 rpm.

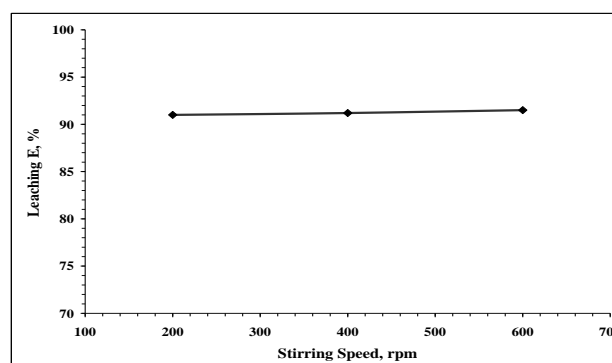


Figure 4. Effect of mixing stirring speed on P_2O_5 leaching % from phosphate ore at L/S mass ratio 25 ml/ 5 g, a room temperature, for time 15 min, an acid concentration of 10%, and a particle size $\leq 1180 \mu\text{m}$.

Effect of HNO_3 /phosphate rock mass ratio

The effect of nitric acid volume to phosphate ore mass ratio was studied within the range from 2 ml/1 g to 6 ml/1 g. Figure 5 shows that, as the liquid/solid ratio increases from 2/1 to 6/1, the recovery % of P_2O_5 increases from 36.21 to 96.50 % meaning that the decrease of bulk density (increase

volume/solid ratio) increases the P_2O_5 leaching %. The volume/solid mass ratio of 6 ml/1 g is the optimum ratio.

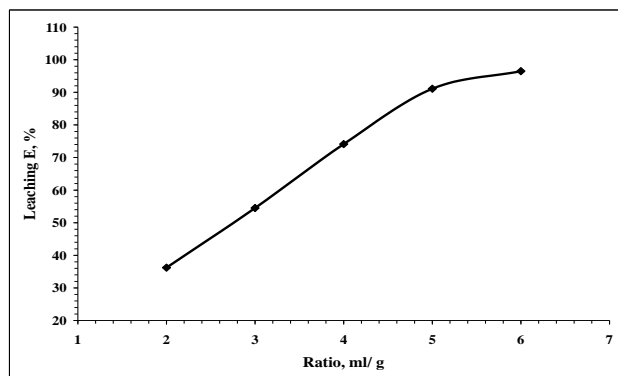


Figure 5. Effect of HNO_3 : phosphate ore ratio on P_2O_5 leaching % from Phosphate ore at mixing stirring speed of 400 rpm, a room temperature, for time 15 min, an acid concentration of 10 %, and a particle size $\leq 1180 \mu\text{m}$.

Specification of leached H_3PO_4

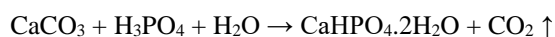
From the aforementioned investigation on leaching Sebaiya phosphate ore by HNO_3 , a leaching experiment was carried out at phosphate ore particle size $\leq 1180 \mu\text{m}$, leaching nitric acid concentration of 10 %, L/S mass ratio 6 ml/1 g, leaching reaction time 15 min, and mixing speed 400 rpm at room temperature. Accordingly, 600 ml of 10% HNO_3 was added to 100 g of phosphate ore of particle size fraction of $\leq 1180 \mu\text{m}$ and stirring for 15 min at room temperature. After filtration, the obtained acidulated solution was analyzed and the results obtained are given in Table 4.

Table 4. The chemical analysis of the produced acidulated phosphoric acid solution

Constituent	Mass, g	Constituent	C, ppm
P_2O_5	27.55	Cd	0.65
Fe_2O_3	1.41	Pb	2.51
F	1.10	As	6.00

Precipitation of Calcium monohydrogenphosphate

Calcium carbonate was used as calcium source to precipitate calcium monohydrogenphosphate from the produced acidic solution according to the following equation:



The parameters affecting the calcium monohydrogenphosphate precipitation efficiency such as mixing time, acidulated solution to calcium carbonate mass ratio, reaction temperature and reaction stirring speed were optimized.

Effect of mixing time

The precipitation of calcium monohydrogenphosphate from the produced acidic solution was studied at different mixing times (1-60 min). The obtained results are given in

Fig. 6 which clarify that as the mixing time increases (1-15 min), the precipitation efficiency increases from 5.6 to 68.1

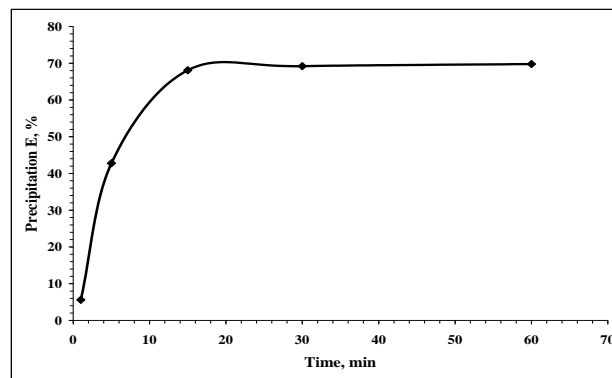


Figure 6. Effect of mixing time on calcium monohydrogen phosphate

and further increase in mixing time has a slight effect on the precipitation efficiency. Therefore, 15 min is preferred for calcium monohydrogenphosphate precipitation process.

Effect of acidulate solution to calcium carbonate mass ratio

The effect of acidic solution/calcium carbonate mass ratio, L/S on calcium monohydrogenphosphate precipitation process was investigated within the range (50 ml/3.0 g-50 ml/6.0 g) at 15 min, stirring speed of 400 rpm, and at room temperature. The results in Fig. 6 indicate that, by increasing the acidic solution/calcium carbonate ratio from 50 ml/3.0 g to 50 ml/6.0 g, an increase in the precipitation efficiency was observed from 22.08 to 99.3 % and by further increase, a slight effect was noticed. The optimum ratio is 50 ml/4.0 g.

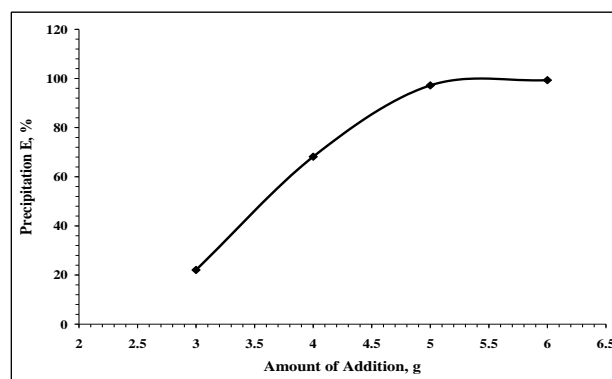


Figure 7. Effect of acidic solution/calcium carbonate mass ratio, L/S on calcium monohydrogen phosphate precipitation%.

Effect of reaction temperature

The process was carried out at different temperatures (20 - 60 °C) for 15 min, stirring speed of 400 rpm and acidulate solution/calcium carbonate mass ratio was 50 ml/4 g. Figure 8 shows a slight effect on the precipitation efficiency (20 - 40 °C) while at 40 - 60 °C, the precipitation efficiency decreases. This could be due to the solubility of calcium

monohydrogenphosphate precipitate again at high temperature. Therefore, room temperature is preferred.

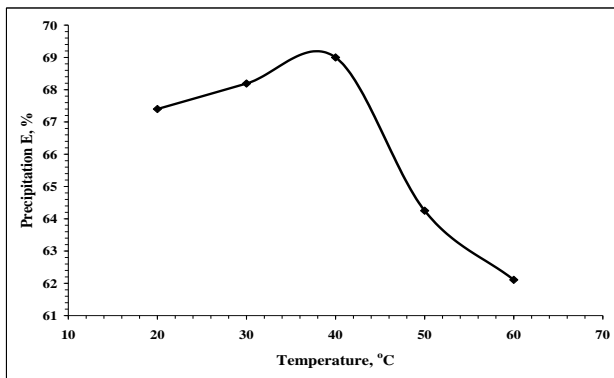


Figure 8. Effect of temperature on calcium monohydrogen phosphate precipitation %

Effect of mixing stirring speed

The effect of mixing stirring speed was assayed in the range of 200 to 800 rpm on the calcium monohydrogenphosphate precipitation. The results in Fig. 9 indicate that, as the speed increases from 200 to 800, the precipitation efficiency increases from 72.5 to 78.60 meaning that the speed has a slight increase in calcium monohydrogenphosphate precipitation %. Accordingly, 400 rpm is suitable.

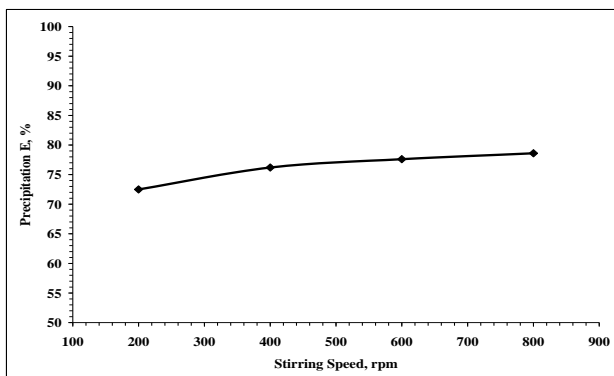


Figure 9. Effect of mixing stirring speed on calcium monohydrogenphosphate precipitation%

Table 5. Calcium monohydrogenphosphate produced from addition of 100 g of calcium carbonate to 1000 ml of acidulate solution for 15 min at room temperature and stirring speed was 400 rpm according to ISO-9001:2000 standard.

* According to ISO-9001:2000 standard.

Characteristic	Produced CHP	Standard*
Solubility in water	Partially insoluble	Partially insoluble
Solubility in 2% citric acid	97 %	97 %
P	17.46 %	18 % min.
Ca	22.5 %	23 % min.
F	0.10 %	0.18 % max.
Cd	< 2 ppm	10 ppm min.
As	4.5 ppm	10 ppm min.
Pb	2.1 ppm	10 ppm min.
Moisture	14.5 %	14.5 %

Developed CHP production flow sheet

Based on the aforementioned investigation, a process for CHP production was developed. In this respect, 1000 ml of the produced acidulate solution was reacted with 100 g of calcium carbonate by mixing at 400 rpm for 15 min at room temperature. The precipitate was filtered and dried at 105 °C for 5 h. Analysis of the product is given in Table 5 together with the standard quality of CHP given in the ISO-9001: 2000. From this table, it is clear that the specification of CHP produced by the developed method is combatable with ISO-9001: 2000 specifications.

Conclusion

The preferred leaching conditions for Sebaiya phosphate ore of particle size ≤ 1180 μm were HNO₃ (10%), temperature (25 °C), HNO₃/Sebaiya phosphate ore mass ratio (6 ml/1 g), stirring speed (400 rpm) and mixing period (15 min). The leaching efficiency was 96.5%. Calcium monohydrogenphosphate from the produced acidulate solution was successfully precipitated using calcium carbonate. The precipitation efficiency was 97.2% using acidulate solution/calcium carbonate mass ration of 10, stirring time of 15 min, stirring speed of 400 rpm and at 25 °C. The specification of the produced CHP is combatable with the ISO-9001: 2000 specifications.

References

- European Fertilizer Manufacturers Association, Booklet No. 4(8) *Production of phosphoric acid*, Belgium, **2000**.
- Zidan, I. H. *Geological and mineralogical studies of Abu-Tartur phosphates western desert-Egypt*, M.Sc. Thesis, Fac. of Sci. Geology Dept., Al-Azhar University, **1998**.
- Al-Wakeel, G. M.. *Int. J. Miner. Process*, **2005**, 75, 101–112.
- Chojnacki, A., Chojnack, K. and Gorecki, H., *J. Chem. Tech. Biotech.*, **2005**, 80, 1331.
- Abdel-Aal E. A. and Amer, A. M., *Bull. Fac. Sci., Alexandria Univ.*, **1991**, 31, 344-359.
- Rashad, M. M. Mahmoud, M. H. H. Ibrahim I. A. and Abdel-Aal, E. A., *J. Cryst. Grow*, **2004**, 267, 372.
- Rashad, M. M., Mahmoud, M. H. H., Ibrahim I. A. and Abdel-Aal, E. A., *J. Cryst. Grow*, **2005**, 40, 741.
- Abdel-Aal, E. A., *Cryst. Res. Technol.*, 39 (2004) 123.
- Mahmoud, M. H. H., Rashad, M. M., Ibrahim I. A. and Abdel-Aal, E. A., *J. Colloid Interface Sci.*, **2004**, 270, 99.
- El-Shafie, A. S. *Studies on the production of phosphoric acid from Abu-Tartur phosphate ore deposits*, M.Sc. Thesis, Fac. of Sci. Chemistry Dept., Zagazig University, **2008**.
- Abdel-Aal, E. A., *Minerals Eng. J.*, **2000**, 13, 223-226.
- De Waal, J. C., US 6183712 B1, **2001**.
- Takhim, M., US 2005-0238558 A1, **2005**.
- Zafar, I. Z. Mahmood, A. T. Mohammad, A. Amin, A. M., *Iranian J. Chem. Chem. Eng.* 2006, 25, 47-57.
- Takhim, M. US 2007-0122326, **2007**
- Khadr, M. E., *Phsico-chemical studies on wet process phosphoric acid*. M.Sc. Thesis, Fac. of Sci., Chem. Dept. Al-Azhar University, **1999**.
- Mizane, A. and Louhi, A., *J. Eng. Appl. Sci.*, **2007**, 2, 1016-1019.

¹⁸Abdel-Aal E.A. and Amer, A. M., *Minerals Eng.*, **1995**, 8 1221-1230.

¹⁹El-Moussaouiti, M. Boistelle, R. Bouhaouss A. and Klein J. P., *Chem. Eng. J.*, **1997**, 68, 123-130.

²⁰Fawzy, M. M. *Purification of wet process phosphoric acid for preparation of dicalcium phosphate*, M.Sc. Thesis, Chemistry Department, Faculty of Science, Benha University, **2006**.

Received: 27.04.2013.

Accepted: 18.05.2013.



THREE OXYACIDS OF PHOSPHORUS: TAUTOMERISM AND OXIDATION MECHANISMS

Raj N. Mehrotra^{[a]*}

Keywords: Oxidation, Hypophosphorous acid, Phosphorous acid, Phenylphosphinic acid, Kinetics, Mechanism.

A review of the chemistry of H_2PO_2 (**P1**), H_3PO_3 (**P3**) and phenylphosphonic acid (**PPA**), and their oxidations by metal and non-metal oxidants is presented.

* Partly presented as a lecture during the award of Acharya P C Ray Memorial Medal of the Indian Chemical Society to the author in 1992
Corresponding Author
Tel: 91-291-2721478
E-Mail: r.n.mehrotra1@gmail.com
[a] Former Professor of Chemistry, JNV University, Jodhpur, 342005. Residence: A-85 Saraswati Nagar, Basni Phase I, Jodhpur 342 005 (Raj) India.

The tribasic orthophosphoric acid, $\text{PO}(\text{OH})_3$, is popularly known as phosphoric acid. It is manufactured by treating the rock phosphate, $\text{Ca}_3(\text{PO}_4)_2$, either in nitric or sulfuric acid. Its main use is in the production of superphosphate fertilizer, $\text{Ca}(\text{H}_2\text{PO}_4)_2 \cdot \text{H}_2\text{O}$ by treating phosphate rock with concentrated phosphoric acid. It is also used in the soft drinks and to produce phosphate compounds. Calcium phosphate is used in tooth paste. Trisodium phosphate (Na_3PO_4) is used as a water softener and cleaning agent. The sodium polyphosphate is used in the production of synthetic detergents. Some condensed phosphates are used in industrial water treatment.

Introduction

Phosphorus was the first element to be discovered in 1669 by Henning Brand in the most unusual manner by boiling 60 buckets of urine. Phosphorus is the combination of two Greek words, *phos* and *phorus* which means light bringing, because it shines in the dark when exposed to the air. Phosphorus does not exist in the elemental form. It is eleventh element in order of abundance in earth's crust because the phosphate rocks, the source of phosphorus, occupy about 0.1% of earth's crust. It is used in the production of insecticides or as additive of industrial oils.

The dibasic phosphorous acid also known as phosphonic acid, $\text{HPO}(\text{OH})_2$, is used in water treatment, and as pesticide in controlling variety of microbial plant diseases. The acid and the phosphite salts are used in the pharmaceutical industry as antioxidant, stabilizer and chelating agent in plastic system, as solvent in paint and as flame retardant on fibres, optical brighteners and in lubricant additives and adhesives. It is also used as corrosion resistant and a review on its inhibitory action has been recently published.¹

The formula, structural formula, basicity, and oxidation state of P in the known oxy acids of phosphorus are as given below. The bold notations for the first three oxy acids have been used throughout the text instead of their names.

The monobasic hypophosphorous acid, $\text{H}_2\text{PO}(\text{OH})$, also named as phosphinic acid, is mainly used in the electro less plating; i.e. deposition of select metal films from solution on a sensitized surface and in pharmaceutical industry.

Name of the oxy acid	Formula	Structural formula	Basicity	Oxidation state of P
Hypophosphorous acid or Phosphinic acid	H_3PO_2 (P1)	$\text{H}_2\text{PO}(\text{OH})$	monobasic	+1
Phosphorous acid or Phosphonic acid	H_3PO_3 (P3)	$\text{HPO}(\text{OH})_2$	dibasic	+3
Phenylphosphinic acid	$\text{C}_6\text{H}_5\text{H}_2\text{PO}_2$ (PPA)	$\text{C}_6\text{H}_5\text{HPO}(\text{OH})$	monobasic	+1
Orthophosphoric acid	H_3PO_4	$\text{PO}(\text{OH})_3$	tribasic acid	+5
Metaphosphoric acid	HPO_3	$\text{O} \leftarrow \text{PO}(\text{OH})$	monobasic	+5
Hypophosphoric acid	$\text{H}_4\text{P}_2\text{O}_6$	$(\text{HO})_2\text{OP}-\text{PO}(\text{OH})_2$	tetrabasic	+5
Pyrophosphoric acid	$\text{H}_4\text{P}_2\text{O}_7$	$(\text{HO})_2\text{OP}-\text{O}-\text{PO}(\text{OH})_2$	tetrabasic	+5

The absence of such tautomeric forms $\text{H}_2\text{P}(\text{O})\text{O}^-$ ion is explained by addition of H^+ or D^+ to the O^- and not to the O of the P=O link, which results in the formation of the normal 'inactive' $\text{H}_2\text{P}(\text{O})\text{OH}$ acid.¹¹

The rate expression from the above mechanism would be as in equation (3).

$$k_{\text{exch}} = k_{\text{H}}[\text{D}^+] + k_{\text{w}} \quad (3)$$

Another study had indicated a dearth of exchange in the P-H links in the 'inactive' form of **P1** because of the extremely slow D-H exchange in the P-H link. However, there was a rapid exchange with D both in the OH groups and in the P-H link of the 'active' form. Since the two forms are in equilibrium, therefore, the added D is distributed among two P-Hs and one O-H link in the 'inactive' form.¹²

The suggested structural requirement for an atom to undergo the D-H exchange was that the atom must have an unshared electron pair and is bonded to the H atom. This explained the lack of D-H exchange in **P3** and its anion because the P atom in either case has no unshared electron pair.¹³

The differing behaviour of **P1** and **P3** toward D-H exchange has been attributed to the decrease in positive charge on P with the increase in the number of attached OH groups to phosphorus. This adversely causes the nucleophilic ability of P to add HO of H_2O . The free negative charges on the O atoms present in the anions have greater effect in this respect. The H_2O -addition mechanism of O exchange is applicable only to those atoms that are capable of octet expansion. It is for this reason that periodates in which I is capable of shell expansion undergo rapid exchange compared to no exchange in perchlorates.¹⁴

Specific studies

Hypophosphorous acid

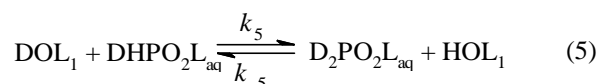
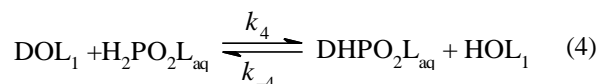
The exchange of tritium between **P1** and H_2O had the rate law: $R = (k_{\text{H}}[\text{H}^+] + k_{\text{P1}}[\text{P1}]) [\text{P1}]$ with $k_{\text{H}} = 0.055 \pm 0.0025$ and $k_{\text{P1}} = 0.0483 \pm 0.0024 \text{ dm}^3 \text{ mol}^{-1} \text{ min}^{-1}$ at 30 °C. R is the rate at which one "undissociable" H atom is exchanged per **P1** molecule. The results were supportive of the existence of normal or 'inactive' and 'active' tautomeric forms in aqueous solution.¹⁵

The tritium (T, radioactive hydrogen) is reported to exchange as T^+ or T_2O with two P-H bonds of **P1**. The reaction $\text{H}_2\text{P}(\text{O})\text{OH} + \text{HTO} \leftrightarrow \text{HTP}(\text{O})\text{OH} + \text{H}_2\text{O}$, and the rate law for the rate limiting P-H fission was $k = k_1[\text{P1}] + k_2([\text{H}^+] + [\text{D}^+])$. The rate coefficients k_1 and k_2 equaled to $0.038 \text{ dm}^3 \text{ mol}^{-1} \text{ min}^{-1}$. The exchange rate was very slow in neutral or alkaline solution. Since the rate expression for the reaction was identical with the rate law for the oxidation of **P1** by various oxidizing agents, therefore the mechanism of exchange was considered similar to that of oxidation reactions.¹⁶

A parallel study of the exchange between D_2O and P-Hs of **P1** was studied using NMR spectroscopy. The rate expression, $k = k_1[\text{P1}] + k_2([\text{H}^+] + [\text{D}^+])$, was similar to that observed by Jenkins and Yost,¹⁶ and referred to the P-H

fission in the rate determining step of the reaction $\text{H}_2\text{POOH} + \text{D}_2\text{O} \rightarrow \text{HDPOOH} + \text{HDO}$. The $k_1 = 0.013 \text{ dm}^3 \text{ mol}^{-1} \text{ min}^{-1}$ and $k_2 = 0.073 \text{ dm}^3 \text{ mol}^{-1} \text{ min}^{-1}$ were reported at 16.5 °C, and were approximately 4 and 12 times larger than the values reported by Jenkins and Yost. Such a large difference in the two values was ascribed to isotope effect.¹⁷

Rate constants for the forward and backward reactions of acid catalyzed reaction of **P1**, equations (4) and (5), where L represents either H or D, were determined.



The equilibrium constants for the reactions (4) and (5) are $K_4 (1.12 \pm 0.08)$ and K_5 are (0.305 ± 0.015) at 25 °C. The rate constants $10^3 k_4 = 4.09$, $10^3 k_{-4} = 1.19$, $10^3 k_5 = 1.87$ and $10^3 k_{-5} = 1.01 \text{ mol dm}^{-3} \text{ s}$ at 25 °C. For the acid-catalyzed, rate-determining tautomerization of 'inactive' $\text{H}_2\text{P}(\text{O})\text{OH}$ to 'active' $\text{HP}(\text{OH})_2$, primary kinetic isotope effects $k_{\text{D}}/k_{\text{H}} = 0.36$ for the forward reaction and 0.24 for the reverse reaction were obtained. The secondary isotope effect was determined to be 1.45. These isotope effects were consistent with a transition state in which proton attachment occurred with a bond order of 0.2. A free energy of tautomerization = 62 kJ was determined using the bond order (0.2) along with the Marcus theory of proton transfer.¹⁸

Phosphorous acid

The exchange reaction $\text{P-H} + \text{D} \leftrightarrow \text{P-D} + \text{H}$ (k_1, k_{-1}) in **P3** was studied in $\text{D}_2\text{O}/\text{H}_2\text{O}$ using stretching vibrations at 2457 and 1793 cm^{-1} for P-H and P-D respectively in the Raman spectrum (the H in O-H exchanged almost instantly). The k_1 and k_{-1} had values of 3.42×10^{-3} and $1.67 \times 10^{-5} \text{ min}^{-1}$ respectively at 23 °C. The rate of exchange increased with increasing acidity (addition of HCl in H_2O , or DCl in D_2O). The exchange rate in $\text{HP}(\text{O})\text{OHO}^-$ and $\text{HP}(\text{O})\text{O}_2^{2-}$ ions was very slow. An isotope effect $k_{\text{H}}/k_{\text{D}} = 5.1$, based on the stretching frequency of P-H and P-D bonds, was predicted. A mechanism similar to the Scheme 1 was proposed except that $3 \rightarrow 4$ was also considered as the rate determining step in addition to the one shown there.¹⁹

A similar study made during the I_2 oxidation of **P3** using NMR spectroscopy reported that the exchange could be observed only in strong acid. The pseudo first order rate constant was $1.97 \times 10^{-3} \text{ min}^{-1}$ at 1.49 mol dm^{-3} and 22 °C.

There are some more exchange studies which were investigated during the oxidation of phosphorous acid. Such studies will be briefly referred to in the section dealing with the oxidation of this acid.

Phenylphosphinic acid

Phenylphosphinic acid, $\text{C}_6\text{H}_5\text{H-P}(\text{O})\text{OH}$, is also named as phenylphosphonous acid. Tautomerism in $\text{C}_6\text{H}_5\text{H-P}(\text{O})\text{OH}$ and its anion was studied using hydrogen isotope exchange

in aqueous and deuterium oxide solutions by infrared. The reaction was both acid and base catalyzed. The termolecular mechanisms involving both acids and bases were not significant. There was negligible exchange in the neutral or near-neutral solution. The rates of exchange of H atoms bound to P and O are different by many orders of magnitude. The acidic H atoms in P-OH groups are known to undergo extremely rapid exchange.¹¹ The exchange in C₆H₅H-P(O)OH resembles more with phosphinic acid H₂P(O)OH, rather more closely with that of dialkyl phosphonates (discussed below) than that of phosphorous acid HP(O)(OH)₂.²⁰

The exchange of P-H bond in C₆H₅H-P(O)OH in D₂O to P-D, studied in acidified EtOH-H₂O mixture and aqueous alkaline solution by following the decreasing intensity of the P-H doublet in NMR spectroscopy, was acid-base catalyzed. The reaction had a first order dependence in H⁺ and OH⁻ ions and C₆H₅H-P(O)OH. The rates in acid solutions were faster than those in alkaline solution. The exchange of O-H to O-D was rapid,¹¹ and no exchange of O-18 between phenylphosphonous acid and H₂O¹⁸ was detected under the conditions in which H exchange was studied. The proposed mechanism of the acid catalyzed exchange was similar to that shown in Scheme I. The OH⁻ ion catalyzed exchange presumably proceeded by direct proton abstraction. The rate law for the acid catalyzed reaction was $k = k_H[H^+] + k_w$ where k_w is the rate coefficient for the acid independent reaction.²¹

Ester of Phosphonic acid

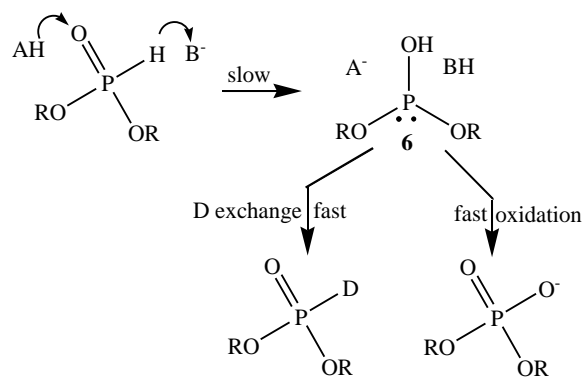
The reactions between dialkyl esters and cuprous halide,²² phenylazide,²³ and diazomethane²⁴ had been suggestive of equilibrium between the pentavalent 'inactive' and trivalent 'active' tautomeric form of the dialkyl esters of phosphorous acid. However, the existence of normal keto or 'inactive' form of the esters was suggested by the Raman,²⁵ ultraviolet,²⁶ NMR and infrared,^{27,28,29} spectral studies.

However, the study of the acid catalyzed exchange of H bonded to P of dimethyl-, diethyl- and di-*n*-propylphosphonate with D in D₂O, followed by the decreasing intensity of the P-H doublet in NMR spectrometer. The exchange reaction was first order in phosphonates and the rate law was: $k = k_H[H^+] + k_w$ where k is the specific rate constant and k_w is the catalytic constant for the spontaneous acid-independent exchange. 10^2k_H ($\pm 10\%$) and 10^3k_w ($\pm 30\%$) at 23 ± 1 °C were 6.6, 8 (dimethyl-), 6,2 (diethyl-) and 5.8,7 (di-*n*-propyl) phosphonate respectively. Although some acid-catalyzed hydrolysis of dialkyl phosphonate was observed but the extent of such hydrolysis was negligible. Since the rate law happened to be identical with the rate law for the oxidation of these esters with iodine,³⁰ it suggested that the phosphite form of the dialkyl phosphonates, **6**, was a common intermediate for both the exchange and oxidation reactions.³¹

Luz and Silver³¹ re-investigated the exchange of the P bonded H with D in D₂O in dimethyl- and diethyl phosphonate in presence of acetate buffer using the same method to follow the reaction. The rate law for the reaction was $k = k_{AcO^-}[AcO^-] + k_{AcOH}[AcOH] + k_w$. The hydrolysis of dialkyl phosphonates under the experimental conditions was negligible.³² The $10^2k_{AcO^-}$ ($\pm 10\%$) = 52 and $7.5 \text{ dm}^3 \text{ mol}^{-1}$

min^{-1} for dimethyl and diethyl phosphonate at 21.5 ± 0.5 °C was much greater than the values of k_H and k_w for the similar phosphonates,³¹ the AcO⁻ ion was considered as the catalyst. Based on the similarity of the rate law with the rate law for the oxidation under similar conditions,³⁰ the Scheme 2 for the catalyzed exchange was suggested. It was further suggested that the substitution of D for the phosphorus bonded H in diethylphosphonate had a negligible effect on the oxidation rate.³³

The infrared study of deuterium exchange between di-*n*-butyl phosphonate and *n*-butylalcohol-*d*, in the presence of acids or bases as well as in neutral solution indicated the existence of mobile prototropic equilibrium between the ester and acidic species present in the reaction mixture. The exchange was catalyzed by both acid and base. In the absence of catalysts, the reaction proceeded in a manner similar to that for acetone.³⁴



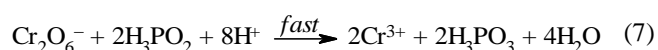
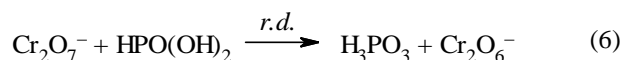
Scheme 2

Oxidation Studies

In this section the kinetics of oxidation of **P1**, **P3** and PhH₂PO₂ (hereafter abbreviated to **P1**, **P3** and **PPA** respectively) are discussed for each metal separately. However, if identical mechanisms were reported for other oxidants then these oxidations have been grouped at one place for brevity. The first order in the oxidant and the oxyacids and negative tests for the free radicals are not mentioned. No mention is made if the oxy-acid reacted in its 'inactive' form.

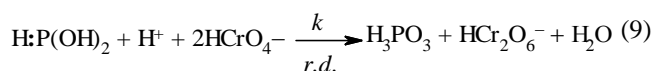
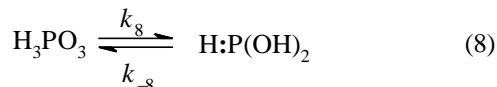
Chromium(VI)

Mitchell, while examining the effect of **P1** on titration of FeSO₄ by K₂Cr₂O₇, probably, for the first time postulated two reactions. The reaction between Cr₂O₇⁻ and HP(O)(OH)₂, the 'active' form, is unimolecular with respect to each and did not involve H⁺ ions. The rate determining (*r.d.*) reaction (6) is followed by the reaction (7). Velocity coefficients varied inversely as the 1/7 power of the initial concentration of the H₂CrO₄.³⁵



The oxidation of **P3** in concentrated solutions of HClO₄, H₂SO₄ and HCl acids is reported without any formal rate law presuming Cr₂O₇²⁻ ion to be the reacting species because it was present in excess.³⁶

The intermediacy of the ‘active form’, H:P(OH)₂, equation (8), and HCr₂O₆⁻ ion, equation (9) was proposed assuming rapid reduction of HCr₂O₆⁻ to Cr(III) in the mechanism. The k_1k_3/k_{-1} had an estimated value of 466 at 25 °C.³⁷

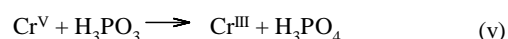
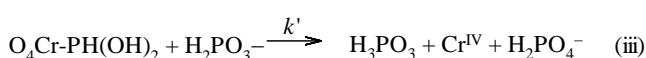
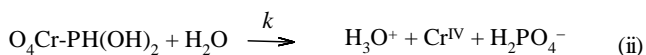
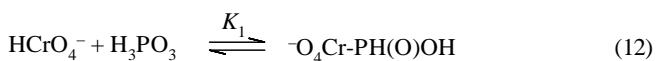


H₂PO₃⁻ was not oxidized in acetate buffer over several days at 25 °C, but it slowly oxidized at 100 °C to H₂PO₄⁻ ion. H-P bond of H₂PO₃⁻ inhibited the oxidation. However, **P3** oxidized fast in 1M H⁺ ion. The spectrometric equilibrium constant *K* for the equation (10) had a value 26. Although the rate law in equation (11) was given, yet the mechanism was not suggested. The values of *k*₁ and *k*₂ were ~10⁻⁴ mol dm⁻³ s⁻¹. Cl⁻ formed CrO₃Cl⁻ which inhibited the reaction.³⁸



$$\text{rate} = \frac{(k_1 + k_2[\text{H}_3\text{PO}_3])[\text{H}_3\text{PO}_3][\text{Cr(VI)}][\text{H}^+]}{1 + K[\text{H}_3\text{PO}_3]} \quad (11)$$

A reinvestigation confirmed almost all the above findings and additionally probed the oxidation of **P1**. A common mechanism for the oxidations of H₂PO₃⁻, **P1** and **P3** was proposed as given in Scheme 3, which depicted the mechanism for **P3** oxidation. The **P3** and HCrO₄⁻ formed an anhydride, equation (12). The abstraction of a proton from the protonated anhydride, protonation could be effected either by H⁺ or **P3**, by bases H₂O and H₂PO₃⁻ were the conjectural rate limiting steps based on analogy with Westheimer mechanisms of alcohol oxidations.³⁹ The derived rate equation (13) was slightly different from the equation (11) with $k_1 = kK_1$ and $k_2 = k'K_1K_a$ where *K*_a is the dissociation constant of the respective acid. A *k*_H/*k*_D = 4 suggested breaking of P-H bond in the rate determining step. H₂PO₂⁻ formed no anhydride at pH 4 nor was oxidized by HCrO₄⁻. The 10³*k*₁ = 1.7, and *K*₁ = 16 were reported for **P3** at 25 °C. The corresponding values for **P1** were 6.0 and 11 respectively.⁴⁰



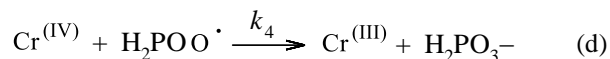
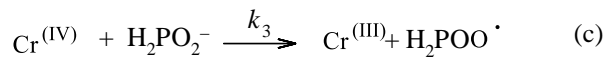
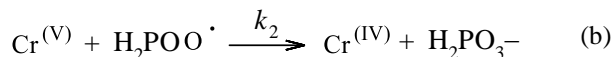
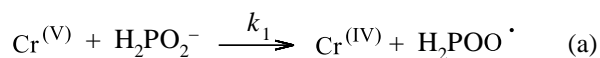
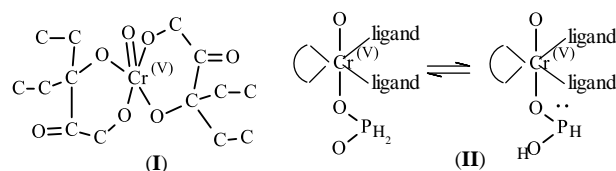
Scheme 3

$$\frac{-d[\text{Cr(VI)}]}{dt} = \frac{(kK_1[\text{H}^+] + k'K_1K_a[\text{H}_3\text{PO}_3])\text{Cr(VI)}[\text{H}_3\text{PO}_3]}{1 + K_1[\text{H}_3\text{PO}_3]} \quad (13)$$

Another study reported *K*₁ = 13 in addition to *K*_a = 0.101 in perchlorate media. Though the results agreed with the above mechanism, yet the rate equation (14) had two new terms, *k*₀ and *k*₂[H⁺]², in addition to the terms appearing in equation (13). The *k*₀ may correspond either to the reaction of unprotonated complex having unknown number of solvent molecules or to abstraction of a phosphinic proton by OH⁻ ion from the neutral protonated complex. The *k*₂[H⁺]² term is attributed to the formation of doubly protonated complex H₄PCrO₆⁺, followed by proton abstraction by water.⁴¹

$$\text{rate} = (k_0 + k_1[\text{H}^+] + k_2[\text{H}^+]^2 + k_3[\text{H}_3\text{PO}_2])[\text{HCrO}_4^-][\text{H}_3\text{PO}_2] \quad (14)$$

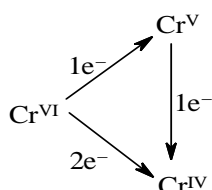
The oxidation of H₂PO₂⁻ by Cr^V chelate (**I**), formed with (C₂H₅)₂C(OH)CO₂H (**lig**), in buffered solution (**buff**) of the **lig** and its Na-salt, to H₂PO₃⁻ and Cr^{III} proceeded through bridged transition state (**II**) in which the mobilization of protons bound to P is favored by strongly acidic Cr^V or Cr^{IV}. The reaction towards the later stages becomes autocatalyzed, which was attributed to Cr^{IV} and had been explained by suggesting the following sequence of the reactions (Scheme 4). The reactions (a) and (b) control the initial stage of the reaction till Cr^{IV} starts getting accumulated when the reaction (c) becomes significant producing more free radical that reacts more rapidly with Cr^V compared to Cr^{IV} in reaction (d). This explains the catalysis of Cr^{IV} in the later part of the reaction. The *k*₁ and *k*₂ had the values (0.049 ± 0.006) and (0.18 ± 0.04) dm³ mol⁻¹ s⁻¹ respectively whereas ratio *k*₂/*k*₄ was (2.32 ± 0.35).⁴²



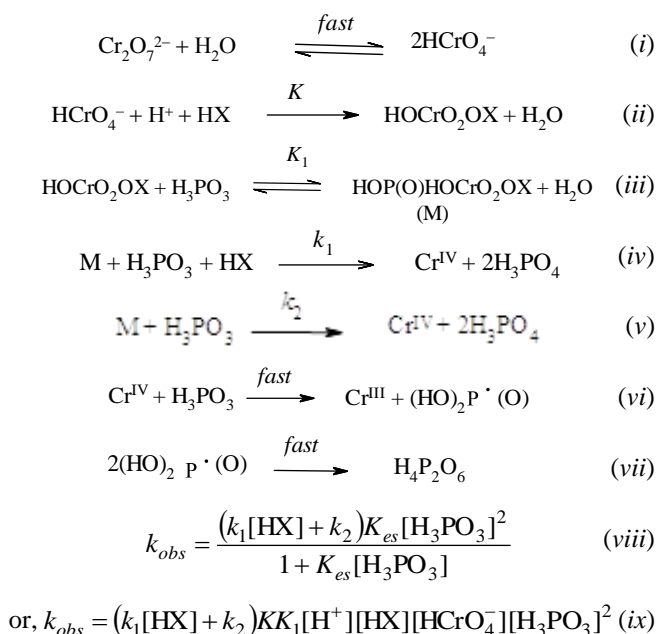
Scheme 4

The oxidation of H₂PO₂⁻ by Cr^{VI}, chelated with the **lig**, in the **buff** at pH 2.7 and excess Cl(NH₃)₅Co²⁺, a scavenger for Cr(II), had shown the parallel formation of Cr^V and Cr^{IV}, stabilized by the **lig**, by competing 1e⁻ and 2e⁻ paths (see below). The reduction of Cr^{VI} to Cr^{IV} and of Cr^{IV} to Cr^{II} involved hydride shifts from H₂PO₂⁻ to the Cr(=O), whereas formation of Cr^V and its reduction to Cr^{IV} involved preliminary coordination of H₂PO₂⁻ to the chromium center,

followed by P-H to O-H tautomerization (see **II**) within the binuclear complex and then transfer of a single-electron from P to the Cr center. The rates of formation of Cr^V and Cr^{IV} from Cr^{VI} were $(25.8 \pm 0.9) \times 10^{-8}$ and $(4.52 \pm 0.08) \times 10^{-8}$ mol dm⁻³ s⁻¹ respectively at 25 °C. The formation of Cr^{IV} had the rate law, $k_{\text{obs}} = (k_1 + k_2[\text{H}^+])[\text{H}_2\text{PO}_2^-][\text{H}^+][(\text{C}_2\text{H}_5)_2\text{C}(\text{OH})\text{CO}_2^-]^2$, with $k_1 = (15.3 \pm 0.2) \text{ M}^{-4} \text{ s}^{-1}$ and $k_2 = (2.5 \pm 0.2) \times 10^4 \text{ M}^{-5} \text{ s}^{-1}$. The $k_{\text{H}}/k_{\text{D}} = 3.9$ and 2.2, $k_{\text{D}_2\text{O}}/k_{\text{H}_2\text{O}} = 2.2$ and 1.7 were observed for generation of Cr^{IV} and Cr^V respectively. The formation of Cr^{II} indicated that the more usual state Cr^{III} was bypassed.⁴³



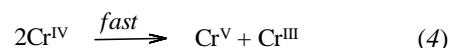
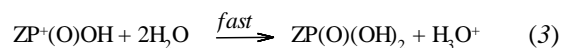
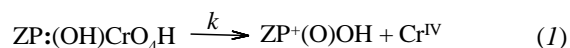
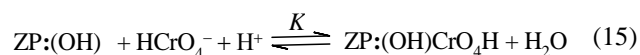
A very confusing paper on the oxidation of P3, which missed on the above mentioned references, mentions that Cr₂O₇²⁻ is the predominant Cr^{VI} species but considers HCrO₄⁻ as the reactive species in the mechanism consisting of reactions (i)-(vii), Scheme 5, where X = HSO₄⁻ or ClO₄⁻. The dimerization of the free radical (OH)₂P·(O) to H₄P₂O₆ was not substantiated. The unsubstantiated formation of higher esters is stated to be more rapid than the rate-limiting formation of the 1:1 ester between HCrO₄⁻ and P3. However, their role in the mechanism was not explained. The reported rate law (viii), where *K_{es}* is perhaps equal to *KK₁*, however, does not match with the rate law (ix) that had been derived without considering the total [P3].⁴⁴



Scheme 5

A single electron transfer was proposed, Scheme 6, in the oxidations of **P1** (Z = H) and **P3** (Z = OH). The formation of the protonated anhydride, equation 15, involved an unlikely tri-body collision of HCrO₄⁻, H⁺ and ZP:(OH)₂ ('active form' of the acid). The rate determining step (1), the

unaided decomposition of anhydride by a base to ZP⁺(O)OH ion and Cr^{IV}, was followed by several fast steps giving the products. The values $\Delta\text{H}(\text{kcal}) = 15 \pm 1$ and 5.2 ± 0.6 and $\Delta\text{S}(\text{eu}) = 50.6 \pm 1.5$ and 16.9 ± 0.8 , indicated that the intermediate with **P1** is stronger than that formed with **P3**. The respective activation energy was 10.4 ± 0.8 and 5.8 ± 0.5 kcal mol⁻¹. The reactions were catalyzed by H⁺ ion, the catalytic effect of pyridine was observed only in **P1** oxidation.⁴⁵



Scheme 6

The oxidation of **PPA** in HClO₄ showed Michaelis-Menten kinetics⁴⁶. The mechanism was similar to that of Scheme 5 (Z = C₆H₅). The activation energy was 7.4 kcal.⁴⁷ Surprisingly, the reaction was reported again by one of the authors with similar results and favoring the same mechanism from amongst few others that were discussed this time. However, the activation energy reported this time was 10.3 ± 1.2 kcal mol⁻¹.⁴⁸

Another investigation substantiated the formation of the anhydride by the rapid scan of the reaction mixture beside the Michaelis-Menten kinetics. The spectrum in Figure 1 is recorded between 302 and 398 nm, selecting the middle wave length at 350 nm, and on an arbitrary scale of 0-1 for the absorbance.

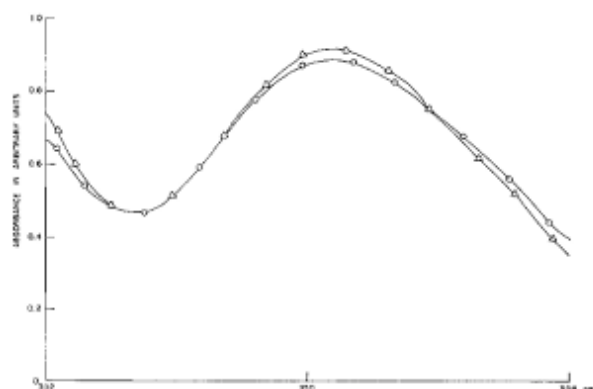


Figure 1. Rapid scan spectra of HCrO₄⁻ (O) and HCrO₄⁻ + PPA (Δ) between the λ 302-398 nm taken between 4.352 and 4.402s after mixing at 25 °C (10⁴[HCrO₄⁻] = 4.0, 10³[PPA] = 4.0, [H⁺] = 1.5 mol dm⁻³).

The HCrO₄⁻ + PPA mixture has a higher absorbance over that HCrO₄⁻ alone suggesting the formation of some new

species which in this case is the anhydride. The study further concluded that **PPA**⁺ is not the reactive species because the deduced rate law conflicted with the observed results. Furthermore, the linear plot between log k_{obs} and $-\text{H}_0$, the Hammett acidity function, with a slope of 1.02 ± 0.02 confirmed that the anhydride is protonated prior to its rate-limiting disproportionation. Because of this it becomes difficult to be specific about the reactive tautomer of **PPA** because the protonation of the anhydride formed by either of the tautomer results in the same intermediate that undergoes the redox reaction. The formation constant for the anhydride formed between **PPA** and HCrO_4^- was almost independent of temperature and had a value ca. $19 \pm 4 \text{ dm}^3 \text{ mol}^{-1}$ and happened to be in agreement with the value $11 \pm 2 \text{ dm}^3 \text{ mol}^{-1}$ over the temperature range 26–46 °C as previously reported in ref. (48).⁴⁹

Chromium(VI) complexes

The oxidations of **P1**, **P3** and **PPA** (hereafter **POA** would represent the combination of three phosphorus oxy-acids) by pyridiniumchlorochromate (**pcc**) were first order both in **pcc** and the substrates. The H^+ dependence was expressed by $k_{\text{obs}} = a + b[\text{H}^+]$. The reaction showed $k_{\text{H}}/k_{\text{D}} = 5.3$ and 6.4 in the oxidation of **P1** and **P3** respectively. The effect of several organic solvents on the rate of the oxidation of **PPA** was analyzed with Kamlet-Taft's and Swain's equations, which indicated that the cation-solvating power of the solvents had a predominant role. The bimolecular reactions of **pcc** and **pccH**⁺ with oxy-acids constituted the parallel rate-determining reactions involving the transfer of a H^- ion from the P-H bond of the 'inactive' specie to **pcc** and **pccH**⁺ giving $\text{RP}^+(\text{O})\text{OH}$ ($\text{R} = \text{H}, \text{OH}$ and Ph) and Cr^{IV} species. $\text{RP}^+(\text{O})\text{OH}$ and Cr^{IV} reacted rapidly to give Cr^{III} and the higher oxy-acids.⁵⁰

The reinvestigated oxidation of **P1** by **pcc**, however, reported Michaelis-Menten kinetics and a different rate law $k_{\text{obs}} = k_1 K_c [\text{P1}][\text{H}^+]/([\text{H}^+] + K_a)(1 + K_c [\text{P1}])$ with $K_c = 1.61 \text{ dm}^3 \text{ mol}^{-1}$ and $k_1 = 6.4 \times 10^{-4} \text{ s}^{-1}$. The rate determining disintegration of the complex to **P3** and Cr^{IV} was followed simultaneously by the rapid reaction similar to reaction (4) in Scheme 6 and the oxidation of **P1** by Cr^{V} to **P3** and Cr^{III} , which was the final reduction product as Cr^{II} could not be detected.⁵¹

The Jodhpur group has repeated the oxidation of **POA** using very similar Cr^{VI} -complexes and nitrogenous oxidizing compounds with almost similar results. The results of these studies would not be repeated unless a different result had been reported.

The oxidation of **POA** by bipyridiniumchlorochromate,⁵² benzyltriethylammoniumchlorochromate,⁵³ morpholiniumchlorochromate,⁵⁴ tetraethylammonium chlorochromate,⁵⁵ pyridiniumbromochromate,⁵⁶ ethyl-N-chlorocarbamate⁵⁷ benzyltrimethylammoniumchlorobromate,⁵⁸ and pyridiniumhydrobromideperbromide⁵⁹ were identical and corresponded to the oxidation by **pcc** described above.⁵⁰ However, in the last two studies, H^+ ions had no effect on the rate.

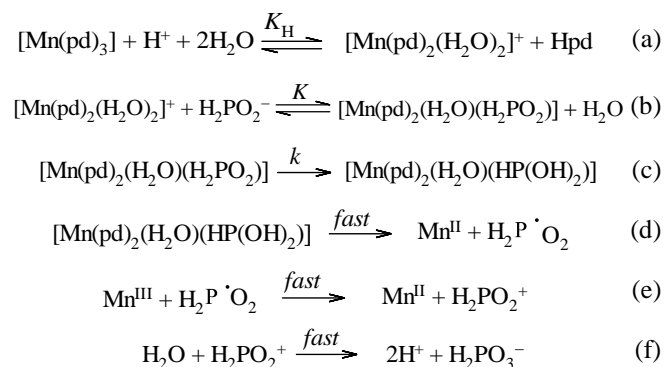
The rates of oxidations of **POA** by pyridinium fluorotrioxochromate,⁶⁰ and hexamethylenetetramine bromine in glacial acetic acid⁶¹ were independent of H^+ ion. The

oxidations by benzimidazoliumdichromate,⁶² butyltriphenylphosphoniumdichromate⁶³ ($k_{\text{H}}/k_{\text{D}} = 5.69$ for **P1**, $k_{\text{H}}/k_{\text{D}} = 5.30$ for **P3**), had first order dependence in H^+ ions varied using *p*-toluenesulphonic acid. The effect of H^+ ions in the oxidations by imidazoliumfluorochromate,⁶⁴ quinoliniumbromochromate,⁶⁵ and quinoliniumfluorochromate⁶⁶ was expressed by the expression $k_{\text{obs}} = a + b[\text{H}^+]$. Michaelis-Menten kinetics was observed in all these studies, and other conclusions were identical to that described in the oxidation of **POA** by **pcc** above.⁵⁰

Manganese

The oxidations of **PPA**,⁶⁷ and those of **P1** and **P3**,⁶⁸ by Mn^{III} in H_2SO_4 had inverse first order dependence in $[\text{H}^+]$ which was explained by assuming MnHSO_4^{2+} , formed from the reversible dissociation of $\text{Mn}^{3+}\text{H}_2\text{SO}_4$ complex, as the reactive species. The mechanism is stated to be explainable by assuming bimolecular reaction between MnHSO_4^{2+} and $\text{Ph}:(\text{OH})_2$ or via the intervention of the complex $\text{MnPhPO}_2\text{H}^{2+}$ formed by Mn^{3+} and $\text{PhHP}(\text{O})\text{OH}$. Formation of $\text{PhP}^+\text{O}_2\text{H}$ is the rate determining step followed by rapid formation of $\text{PhP}^+\text{O}_2\text{H}$ which is finally oxidized to $\text{PhP}(\text{O})(\text{OH})_2$. The complex reacting with H_2O gives $\text{PhP}(\text{O})(\text{OH})_2$ and Mn^{I} , the latter reacts with Mn^{III} giving Mn^{II} .

The oxidation of H_2PO_2^- by $[\text{Mn}(\text{pd})_2(\text{H}_2\text{O})_2]^+$ ($\text{Hpd} = \text{pentane-2,4-dione}$) in perchlorate medium was first order both in the $\text{Mn}(\text{III})$ and the substrate. The rate, however, decreased with increasing pH and Hpd . The proposed inner-sphere mechanism is in Scheme 7. The estimated values of K_{H} , and kK were 1.44×10^5 and $(4.3 \pm 0.1) \times 10^{-4} \text{ mol}^{-1} \text{ dm}^3 \text{ s}^{-1}$ at 40 °C.⁶⁹

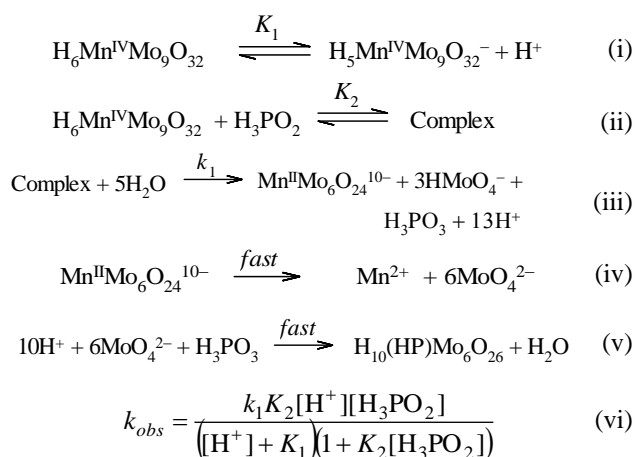


Scheme 7

Oxidations of $\text{RHP}(\text{O})\text{O}^-$ ($\text{R} = \text{H}, \text{OH}, \text{Ph}$) by tris(pyridine-2-carboxylato) Mn^{III} , $\text{Mn}^{\text{III}}(\text{C}_5\text{H}_4\text{NCO}_2)_3$, was studied in picolinate-picolinic acid buffer in the pH 4.63–5.45 range. The oxidations had a common mechanistic pathway in which the substrates could be either six or seven coordinated with the $\text{Mn}(\text{III})$. The breaking of the coordinated complex to a free radical, which subsequently reacted with another $\text{Mn}(\text{III})$ molecule to give the product, was rate-determining. A $k_{\text{H}}/k_{\text{D}} = 4.26$ in the H_2PO_2^- oxidation indicated P-H fission in the rate-determining step.⁷⁰

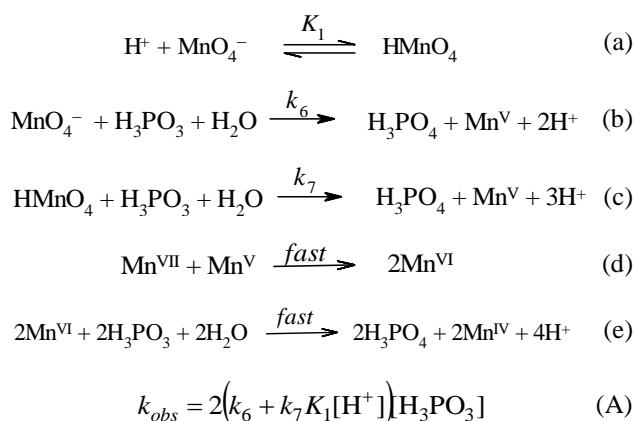
Oxidation of **P1** by $[\text{Mn}^{\text{IV}}\text{Mo}_9\text{O}_{32}]^{6-}$ ion proceeds through an intermediate complex, supported spectrophotometrically,

formed prior to its rate determining decomposition. The H^+ ion is supposed to have a role in an equilibrium marked (i) in the proposed mechanism based on a direct two electron transfer step (iii) shown in Scheme 8, and the rate law is given in (vi).⁷¹

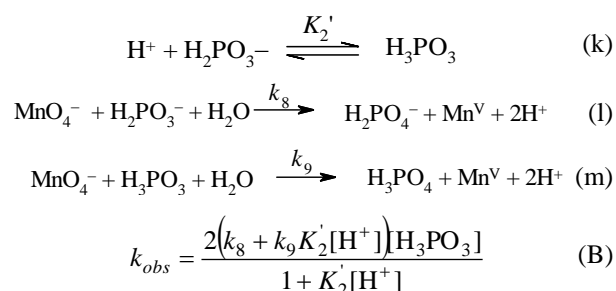


Scheme 8

The H^+ dependence in the MnO_4^- oxidation of P3 had the form $k_{\text{obs}} = a + b[\text{H}^+]$. The interference from Mn^{3+} oxidation was ruled out because F^- had no effect on the rate. The formation of Mn^{IV} in the reaction was indicated by the excellent agreement between the rates measured in terms of MnO_4^- (525 nm) and soluble Mn^{IV} (400 nm). The similar nature of the rate expression for the H^+ dependence in the reaction and that in the exchange reaction suggests that the formation of species similar to the species 3(6) might be rate limiting in the oxidation. But, the fact that the reaction had no zero order dependence on MnO_4^- ion ruled out this possibility. Further, the ratio of $3k_6[\text{MnO}_4^-]/k_w = 265$, and $3k_7K_1[\text{MnO}_4^-]/k_H = 44$ or $3k_9K_2[\text{MnO}_4^-]/k_H = 3.9 \times 10^3$ supported that it is the ‘inactive’ P3 which is oxidized. Yet another argument against the participation of the ‘active’ form in the oxidation is that H_3AsO_3 , H_2SO_3 or HSO_3^- , a pair of electron is available on As or S, can be titrated by MnO_4^- ion at room temperature compared to the slow oxidation of P3. The rate acceleration by the H^+ ion was explained by considering the two mechanisms shown in Schemes 9 and 10.⁷²



Scheme 9



Scheme 10

The reaction of MnO_4^- with P3 and its anions, in presence of $\text{P}_2\text{O}_7^{4-}$ over pH 0-7.2, resulted in Mn^{V} and P^{V} in the rate limiting step. The rate expression is given in equation C. The reaction had a $k_H/k_D = 4.3 \pm 0.2$ at pH 2.2, 7.1 and 12.3. k_1 , k_2 and k_3 are the specific rate constants for P3, H_2PO_3^- and HPO_3^{2-} respectively, and K_1 and K_2 are the first and second dissociation constants of P3.

$$k = \frac{k_1 [\text{H}^+]^2 + k_2 K_1 [\text{H}^+] + k_3 K_1 K_2}{K_1 K_2 + K_1 [\text{H}^+] + [\text{H}^+]^2} \quad \text{(C)}$$

The second order rate constant in the oxidation of monoethylphosphonate was ascribed to the deprotonation equilibrium of the single OH group in acidic media. The Mn^{VII} was reduced to Mn^{IV} in the oxidation of diethylphosphonate both in acidic and neutral solutions. The increasing rate with pH became unmeasurably fast at pH 12. The change over from a first order to a zero-order dependence in Mn^{VII} indicated the formation of an intermediate with a lone pair of electrons on the phosphorus atom, which reacted rapidly with MnO_4^- ion.⁷³

A similar oxidation of P1 and H_2PO_2^- over pH 1-6, had $k_H/k_D = 4.6$ at pH 5.42. The reaction involved a H^- abstraction, probably, *via* a bridged transition state $[\text{O}_3\text{MnO} \cdot \text{H} \cdot \text{PH}(\text{O})\text{OH}]^\ddagger$, formed in the rate determining step, which undergoes a simultaneous ejection of a proton to form the intermediate $[\text{O}_3\text{Mn}^{\text{V}}\text{O} \cdot \text{P}^{\text{III}}\text{H}(\text{O})\text{OH}]^{2-}$ (X). The X rapidly breaks down to Mn^{V} and H_3PO_4 or reacting with another X gives Mn^{IV} , H_3PO_4 and P3. The similarity of k_1 ($80 \text{ dm}^3 \text{ mol}^{-1} \text{ s}^{-1}$, P1) and k_2 ($48.5 \text{ dm}^3 \text{ mol}^{-1} \text{ s}^{-1}$, H_2PO_2^-) at 24 °C suggested that the OH group of P1 was not involved in the rate-determining step.⁷⁴

Michaelis-Menten kinetics is reported in the above reinvestigated reaction in acid perchlorate solution suggesting formation of a weak 1:1 complex on the msec time scale, which enhanced the MnO_4^- spectrum monitored over 10-100 msec (Figure 2). No evidence was found for a radical intermediate or the participation of Mn^{3+} in the rate determining step. The kinetic isotope $k_H/k_D = 4.3$ was observed. The complex between MnO_4^- and H_2PO_2^- appeared stronger than that with P1. The rate dependence on H^+ indicated that the self-decomposition of $[\text{MnO}_4\text{P1}]^-$ to the products in the rate determining step is also assisted by a proton in a simultaneous rate determining step (r). The mechanism is given in Scheme 11 and the observed rate law is given in equation 16.

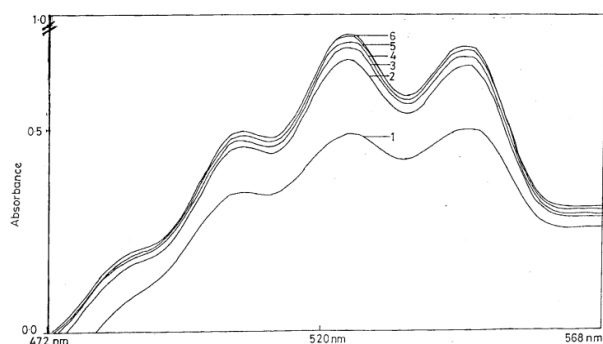
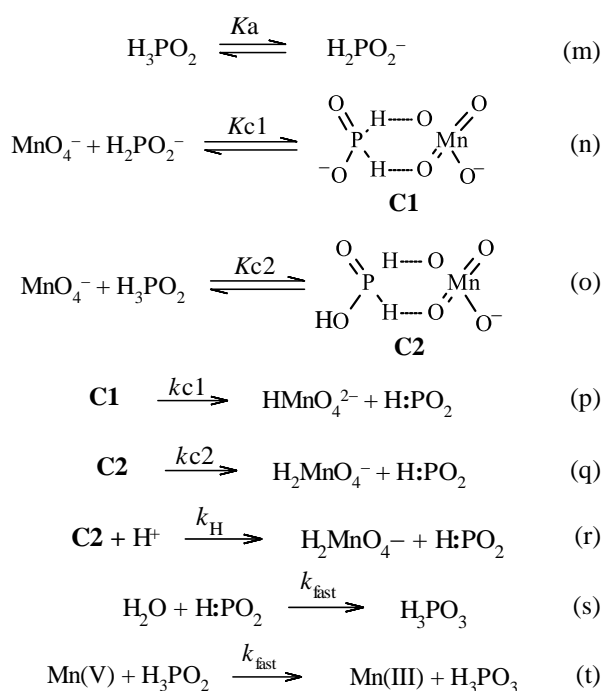


Figure 2. The rapid scans of the reaction mixture, $10^4 [\text{MnO}_4^-] = 5.0$, $10^3 [\text{P1}] = 5.0$, $[\text{H}^+] = 0.1 \text{ mol dm}^{-3}$ at 20°C , recorded at 520 nm. The absorbance is on an arbitrary scale. The lowest spectrum was recorded 2 ms after mixing and the subsequent spectrum were recorded at the same interval. The saturation in the top most spectrum occurred in about 14 ms after mixing.



Scheme 11

$$k_{1\text{obs}} = \frac{(k_{c1}K_{c1}K_a + k_{c2}K_{c2}[\text{H}^+] + k_Hk_{c2}[\text{H}^+]^2)[\text{H}_3\text{PO}_2]_0}{K_a + [\text{H}^+] + (K_{c1}K_a + K_{c2}[\text{H}^+])[\text{H}_3\text{PO}_2]_0} \quad (16)$$

An alternate mechanism in which reactions (n)–(r) are replaced by the rate determining reactions of $\text{MnO}_4^- + \text{H}_2\text{PO}_2^-$, $\text{MnO}_4^- + \text{P1}$ and $\text{MnO}_4^- + \text{P1} + \text{H}^+$ on the consideration that the complexes **C1** and **C2** might be side reactions so that the reaction becomes outer-sphere. The rate law (16) would still hold good.⁷⁵

The oxidation of **PPA** in acid perchlorate solution was similar to the above described reaction of **P1**. However, the values of the specific rate constants, k_{c1} , k_{c2} and k_H , were appreciably lower than the corresponding values in **P1**. The activation parameters also differed widely.⁷⁶

The oxidation of **POA** by bis(2,2'-bipyridyl)copper(II) permanganate (BBCP) was catalyzed by H^+ . The rate was independent of 2,2'-bipyridine but increased with AcOH in the solvent mixture, and exhibited a substantial kinetic isotope effects. The 'inactive' form was the reactive species.⁷⁷

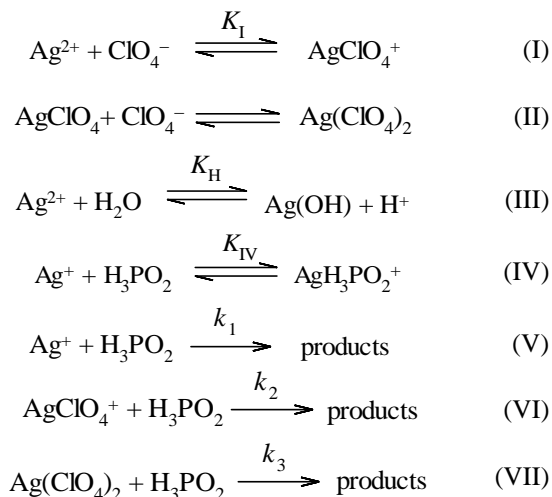
The oxidation of **PPA** by MnHSO_4^{2+} (species in H_2SO_4) proceeds through the rate limiting bimolecular reaction between MnHSO_4^{2+} and **PPA** giving PhHP^+O_2 , which reacting rapidly with MnHSO_4^{2+} gives PhHP^+O_2 . The rapid reaction of the later with H_2O gives the PhH_2PO_3 . The retardation in the rate H^+ ions was due to deprotonation of $\text{MnH}_2\text{SO}_4^{3+}$, the Mn^{III} species in H_2SO_4 .⁷⁸

Silver

The reaction between **P1** and AgNO_3 showed limiting rates with increasing $[\text{H}^+]$ or $[\text{Ag(I)}]$ depending on their ratios. The products Ag^0 inhibited the rate whereas **P3** increased the rate. Formation constants of Ag^+ complexes with H_2PO_2^- ($K_1 = 138 \pm 19 \text{ dm}^3 \text{ mol}^{-1}$) and H_2PO_3^- ($K_2 = 510 \pm 30 \text{ dm}^3 \text{ mol}^{-1}$) were reported. The complex $\text{H}_2\text{PO}_2\text{Ag}$ was considered unreactive in the proposed mechanism. Two mechanisms were considered. The mechanism involving **P1** (inactive form) had a simple rate law whereas the one based on the reaction with H:P(OH)_2 had a complicated rate law the quantitative verification of which was limited.⁷⁹

P3 reacted with Ag^{2+} in HClO_4 through two parallel paths. In one path **P3** is rapidly protonated to H_4PO_3^+ which is dissociated to H^+ from a P-H bond and :P(OH)_3 in the rate determining step (k_1). :P(OH)_3 is rapidly oxidized to H_3PO_4 . The $10^5k_1 = (3.3 \pm 0.3) \text{ sec}^{-1}$ at 3.0 M H^+ and 22°C was in good agreement with the D exchange rate constant $10^5k = 5.2 \text{ sec}^{-1}$ under identical conditions. In the other path Ag^{III} , formed through the reversible reaction $2\text{Ag}^{\text{II}} \leftrightarrow \text{Ag}^{\text{III}} + \text{Ag}^{\text{I}}$, reacted with **P1** in the rate-determining step. However the possibility of the rate determining reaction of Ag^{II} with **P4**, formed by Ag^{II} and **P3** in a rapid reversible reaction, as an alternate to the second path was not ruled out.⁸⁰

The rate law from the mechanism of Ag^{II} oxidation of **P1**, Scheme 12, in HClO_4 solution is given in equation 17, which under certain approximations is reduced to equation 18.



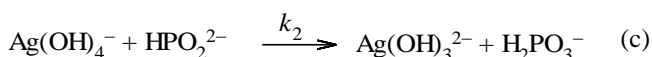
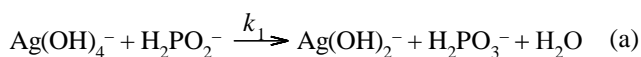
Scheme 12

$$k_{1obs} = \frac{2[H_3PO_2](k_1 + k_2 K_{II}[ClO_4^-] + k_3 K_2 K_3 [ClO_4^-]^2)}{(1 + K_{IV}[Ag(I)])(1 + K_H[H^+]^{-1} + K_2[ClO_4^-] + K_2 K_3 [ClO_4^-]^2)} \quad (17)$$

$$k_{obs} = \frac{2k_2[H_3PO_2]}{1 + K_{IV}[Ag(I)]} \quad (18)$$

k_2 is $(7.6 \pm 0.7) \times 10^2 \text{ M}^{-1} \text{ s}^{-1}$ at 30 °C and K_{IV} is $38 \pm 2.5 \text{ M}^{-1}$. Evidence for the complexes $AgClO_4^+$ and $Ag(ClO_4)_2$ in $HClO_4$ is provided.⁸¹

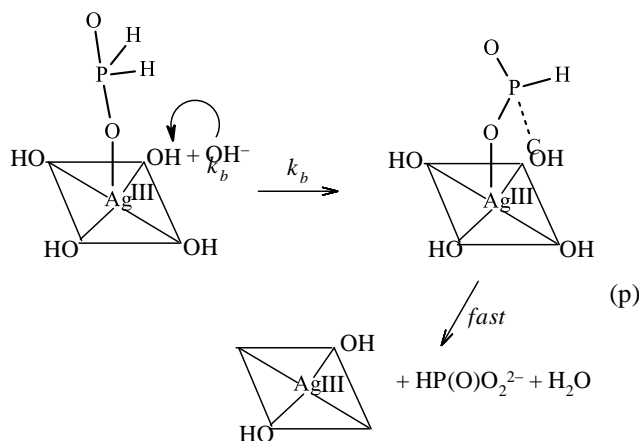
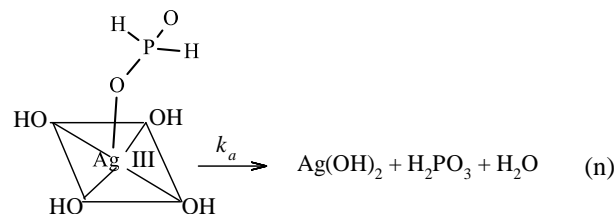
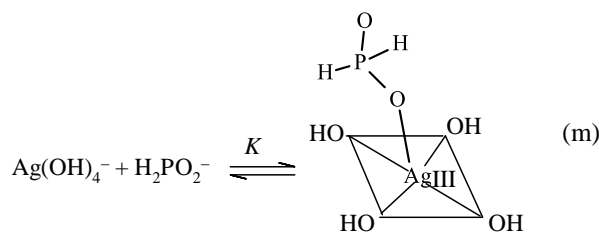
The oxidation of $H_2PO_2^-$ by $Ag(OH)_4^-$ in strong alkaline solution was explained by considering the mechanisms in Scheme 13, based on the fact that there was neither kinetic nor spectrophotometric evidence for the intermediate complex formation, and Scheme 14 which assumed the formation of an intermediate because such intermediates are common for square-planar $Ag(III)$. The absence of an inverse $[OH^-]$ dependence indicated an axial $Ag-O-P$ bridge in which phosphorus accepted an oxygen from the Ag^{III} which then received a pair of electrons directly into the empty $d_{x^2-y^2}$ orbital. The intermediate undergoes redox both by direct internal redox and also assisted by OH^- ion. $D_2PO_2^-$ reacted considerably slower, ($a_H/a_D = 2.46$; $b_H/b_D = 8.2$), indicating that P-H bond is broken in the rate-determining step. The a and b are defined in the rate law $k_{obs} = (a + b[OH^-])$. The ionic strength dependence of the rate reflected competition between the second and third-order paths.⁸²



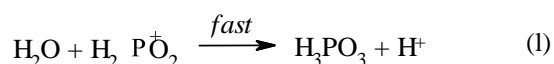
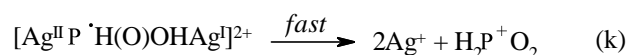
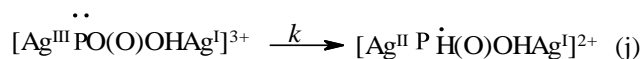
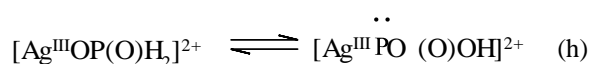
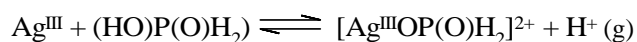
Scheme 13

A coloured intermediate in the Ag^+ catalyzed oxidation of **P1** by [ethylene bis(biguanide)] Ag^3 was formed by Ag^{3+} complex, Ag^+ and $HP:(OH)O^-$ which was tentatively ascribed to some kind of $Ag^+ \rightarrow Ag^{3+}$ charge transfer. The mechanism, Scheme 15, (ionization of **P1** ignored), involved a two-step electron transfer from **P1** to Ag^{3+} via Ag^+ within the intermediate. Free radical was not detected. The second-order rate constant = $6.73 \text{ dm}^3 \text{ mol}^{-1} \text{ s}^{-1}$ was much larger than the second-order rate constant reported⁷⁹ in the corresponding oxidation by Ag^+ ion.⁸³

An alternate mechanism for the above reaction was also proposed in which the order of coordination of Ag species had changed. Thus $H_2PO_2^-$ preferentially coordinated with Ag^+ (d^{10}) rather than to strongly coordinated $[Ag(enbbg)]^{3+}$ (d^8) because the formation constant for the AgH_2PO_2 was $138 \pm 19 \text{ dm}^3 \text{ mol}^{-1}$ (ref. 69). The mechanism would lead to the same rate law with plausible approximations.⁸⁴



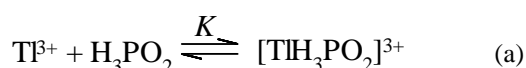
Scheme 14



Scheme 15

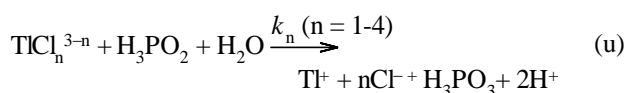
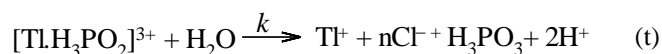
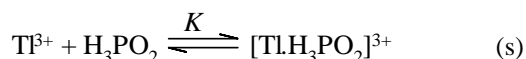
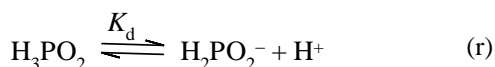
Thallium

The reaction of Tl^{3+} with **P1** in $HClO_4$ solution proceeds through the formation of an intermediate. The intermediate can produce the products through three alternatives. In the first alternative (a) is followed by the rate limiting reaction involving a single-stage two-electron transfer to H_2O . In the second alternative (a) is followed by the rate determining H^- transfer from **P1** to Tl^{3+} to produce $H_3P^+O_2$ which reacted rapidly with H_2O to give **P3**. In the third alternative (a) is followed by its possible rate determining disintegration to Tl^{2+} and $H_2P^+O_2$ because Tl^{2+} had been postulated in several reactions.^{85,86,87} The $H_2P^+O_2$ is rapidly oxidized by Tl^{2+} in presence of H_2O . Thus all these possibilities lead to the common rate law $k_{obs} = kK[P1]/1 + K[P1]$ where K is the formation constant of TlP^{3+} formed in (a).⁸⁸



The investigation of the medium effects, ($\log k = \log k_0 + \beta + \alpha(x)$) where $k = k_0 f_a f_b / f_{\neq}$ and $k_0 =$ rate constant at zero ionic strength, $f =$ activity coefficient, a and b are the reactants forming the intermediate complex (\neq), $\beta = \log(f_a^0 f_b^0 / f_{\neq}^0)$ where $f^0 =$ activity coefficients in the absence of acid in the solution, $\alpha =$ a constant and $(x) = [HClO_4]/([HClO_4] + [NaClO_4])$,⁸⁹ in the above reaction⁸⁸ indicated that $\log k$ did not equal to $\log k_0 + \beta + \alpha(x)$. This indicated that the reaction occurs in 1-step of a 2-electron change as described in the first alternative.⁹⁰

The rate in Cl^- ions catalyzed reaction of Tl^{3+} -**P1** decreased initially reaching a minimum at $[Cl^-]_0/[Tl^{3+}]_0 = 1$, and then starts increasing to a limiting value when this ratio is ~ 50 . The rate increased with H^+ and levels off at about 0.5 M. $H_2P(O)OH$ is the reactive species and the proposed mechanism is in Scheme 16. Equation (w) is the rate law. The reactivity of various Tl^{III} species increased in the order $TlCl_4^- > TlCl_3 > TlCl_2^+ > Tl^{3+} > TlCl^{2+}$. **P1** was the reactive species.⁹¹

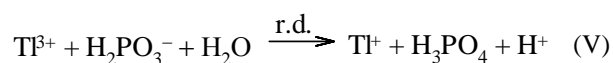
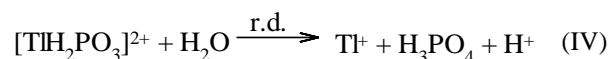
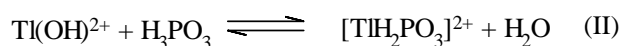


$$-d[Tl(III)]/dt = (kK[Tl^{3+}] + k_1[TlCl^{2+}] + k_2[TlCl_2^+] + k_3[TlCl_3] + k_4[TlCl_4^-])([P1][H^+]/([H^+] + K_d)) \quad (w)$$

Scheme 16

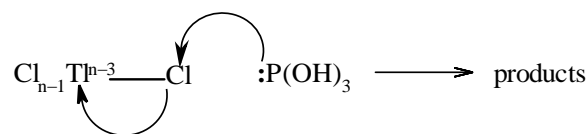
Four mechanisms were proposed in the oxidation of **P3** in view of inverse rate dependence on $[H^+]$ (Scheme 17),

which could be caused either by the dissociation of **P3** or by the hydrolytic equilibrium of Tl^{3+} ion. The complex $[TlH_2PO_3]^{2+}$, involved in the rate determining reaction (IV), could be formed by either of the three equilibrium (I)-(III). In the fourth mechanism, the rate determining reaction (V) followed the dissociation equilibrium of **P3**. All these lead to the common rate law with certain approximations.⁹²



Scheme 17

The reduction of chlorothallium(III) complexes, $TlCl_n^{3-n}$ ($n = 1-4$), by **P3** and $H_2PO_3^-$ indicated that the rate first decreased to a minimum at $[Cl^-]/[Tl(III)] \approx 4$ and then increased with increasing $[Cl^-]$. The Cl^- ion catalysis was explained either by invoking a chloride bridge activated mechanism or by nucleophilic attack of the phosphorus nucleophile $:P(OH)_3$ on chlorine. The preferred later mechanism is shown below.⁹³



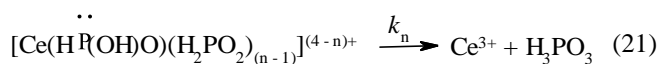
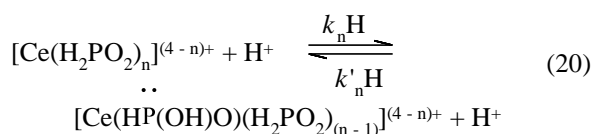
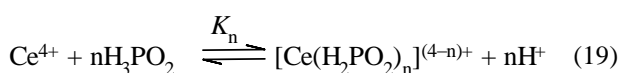
The complex formation between Ru^{3+} and **P3** is envisaged in Ru^{3+} -catalyzed oxidation of **P3** by Tl^{3+} ion in perchlorate solution. The rate law, $k_{obs} = kK_k[Ru^{3+}][P3]/([H^+] + K_h)(1 + K[P3])$, was based on the assumption that the decomposition of a termolecular complex $[TlO^{2+} \cdot u^{III} \cdot {}_3PO_2]$ was rate determining. K and K_h are respectively the formation constant for Ru^{3+} -**P3** complex and hydrolytic constant for the hydrolysis of Tl^{3+} ion. The $HP(O)(OH)_2$ was the reactive species.⁹⁴

The catalysis by $RuCl_3$ in the above reaction had the rate law: $k_{obs} = kK_k[Ru^{3+}][P1]/([H^+] + K_h)(1 + K[P1])$ where K is the equilibrium constant ($17.2 \pm 1 \text{ dm}^3 \text{ mol}^{-1}$ at $(30 \pm 0.1)^\circ\text{C}$) for the envisaged complex formed by Ru^{3+} and **P1** and K_h is the hydrolytic constant for the hydrolysis of Tl^{3+} ion.⁹⁵

Cerium

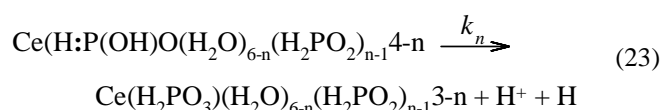
The oxidation of **P1** in $HClO_4$, HNO_3 and H_2SO_4 solutions proceed through the complexes formed by **P1** and Ce^{IV} species, and acceleration of the rate with the acid. The oxidation of **P3** was also studied in H_2SO_4 .

The mechanism in HClO₄ solution is given in equations 19-21, that involved formation of various complexes (n = 1-3) as in equation (19). It was followed by another equilibrium (20) in which one of the coordinated H₂PO₂⁻ was converted to HP:(OH)O⁻ in the presence of H⁺ ion. The complex containing the active form rapidly decomposed to the products as in equation (21). Complexes with n = 1 and 2 were stated to be formed in excess of Ce^{IV}. But at [P1] = 2[Ce(IV)], [Ce(H₂PO₂)₂]²⁺ dominated. However, it was partially converted to [Ce(H₂PO₂)₃]⁺ in excess of P1. The rate expression is in equation (22).⁹⁶



$$-\frac{d[\text{Ce(IV)}]}{dt} = 2[\text{H}^+ \left\{ \begin{array}{l} k_1^H [\text{Ce}(\text{H}_2\text{PO}_2)_3]^{3+} \\ k_2^H [\text{Ce}(\text{H}_2\text{PO}_2)_2]^{2+} \\ k_3^H [\text{Ce}(\text{H}_2\text{PO}_2)]^+ \end{array} \right\}] \quad (22)$$

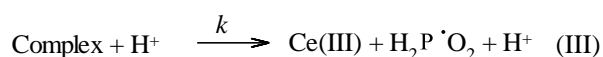
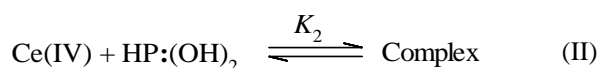
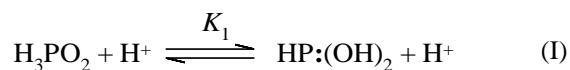
The reinvestigated reaction suggested that complexes with n = 1-6 were formed had similar H⁺ dependence but the formation of [Ce(H₂PO₂)_n]⁽⁴⁻ⁿ⁾⁺ suggested. The neutral Ce(H₂PO₂)₄ complex was stated to be most reactive because HP:(O)O⁻ had the highest probability for its existence, and its interaction with a water molecule in the coordination sphere. Thus the rate determining step is in equation (23).⁹⁷



The Ag⁺ catalysis in the above reaction was investigated. In the uncatalyzed reaction [Ce(P1)_n]⁴⁺ complexes with n = 1-6 were suggested to be initially formed, which was followed by the rapid equilibrium similar to (21). The complex containing HP:(O)O⁻ disintegrated to the products in the rate limiting step.

Two mechanisms were proposed to explain the Ag⁺-catalysis. In one mechanism, Ag⁺ oxidized P1 to P1⁺ in the initial rate determining step, which was followed by the rapid reaction of P1⁺ with another Ag⁺ ion and a water molecule to give P3 and Ag⁰. The Ag⁰ was rapidly reoxidized by Ce(IV) to Ag⁺ ion. In the other mechanism, the initially formed AgP1⁺ reacted rapidly with [Ce(P1)_n]⁴⁺ forming [AgP1Ce(P1)_n]⁵⁺, which reacted rapidly with H⁺ forming [AgP:(OH)₃Ce(P1)_n]⁵⁺. This complex disintegrated in the rate determining step to the products.⁹⁸

The redox in aqueous nitric acid decreased with increasing initial Ce^{IV}, an observation made earlier too but not explained.⁹⁶ This study considered Ce^{IV}-Ce^{IV} dimers⁹⁹ which are unreactive¹⁰⁰ to be responsible for the observation. Formation of a single complex rather than a number of complexes, suggested previously.^{96,98} The suggested mechanism is given in Scheme 5. Ag⁺ catalysis did not affect the order of reaction with respect to [Ce(IV)], and the k_{obs} varied directly with [Ag(I)]. It seemed probable that the Ce(IV)-P1 complex was oxidised by Ag(I).¹⁰¹



Scheme 18

There have been few studies also. The P1 oxidation in H₂SO₄ involved [Ce(SO₄)_nP1]⁽⁴⁻²ⁿ⁾⁺ (n = 0-3) complexes. The disproportionation of the complex with n = 2 was the rate determining step forming H₂PO₂ which reacted rapidly with Ce^{IV} in presence of water to give P3. HP:(OH)₂ was not reactive. The reaction was stated to be catalyzed by Mn²⁺ and Ag⁺ without discussing the mechanism of catalyzed reaction.¹⁰²

The RuCl₃ catalyzed reaction of sulfato-cerium (IV) species with P1 reported complex dependence in P1.¹⁰³

Ce(SO₄)₂ and HCe(SO₄)₃⁻, former being more reactive than the later, reacted with P3 in parallel bimolecular reactions. No evidence either for the formation of an intermediate or the active form of P3 was obtained. The reaction was catalyzed by Ag(I) whereas Mn²⁺ and H⁺ ions had no effect on the rate.¹⁰⁴

Cobalt

A reversible rate determining reaction between HP:(OH)₂ and [CoW₁₂O₄₀]⁵⁻ in HCl resulted in the formation of H₂P[•]O₂, which rapidly reacted with [CoW₁₂O₄₀]⁵⁻ in presence of H₂O to form P3. The probability of the formation of P1⁺ from the reaction of H₂P[•]O₂ with [CoW₁₂O₄₀]⁵⁻ was not excluded from the reaction that was independent of [H⁺].¹⁰⁵

Vanadium

There have been quite a few studies on the oxidation of P1 and P3 by V^V both in HClO₄ and H₂SO₄ solution.

In the oxidation of P1, the rate in H₂SO₄ was faster than that in HClO₄ solution. V(OH)₃²⁺ was the reactive species in H₂SO₄ solution. P1 was oxidized in its reactive form,

HP:(OH)₂, to HP*(O)OH which subsequently reacted with another V^V molecule in presence of H₂O to give **P3**.¹⁰⁶

The formation of VO₂.H₂PO₂ and VO₂.H₃PO₂⁺ complexes were suggested in the reinvestigated oxidation of **P1** in HClO₄. The respective formation constants were 16.6 ± 2.2 and < 1.4 dm³mol⁻¹. The mechanism suggested protonation of the complex VO₂.H₂PO₂ by H⁺ (*k*₀) followed by a tautomerization step in which water abstracts a phosphinic proton. The complexes VO₂(H₂PO₂)(H₃PO₂) (*k*₁) and VO₂(H₂PO₂)(H₃PO₂)₂ (*k*₂) were similarly protonated followed by H⁺ abstraction by water. Thus HP:(OH)₂ intervened in the reaction attended by free radical formation. The *k*₀, *k*₁ and *k*₂ are the specific rate constants for the protonation steps. The Ag⁺ catalyzed reaction had zero order dependence in V(V) indicating that **P1** is oxidized to **P3** primarily by Ag⁺ through H₂PO₂. The catalysis operated through Ag⁺/Ag⁰ cycle.¹⁰⁷

The rate of oxidation of **P3** by V^V was faster in H₂SO₄ than in HClO₄. The reaction had second order dependence in the mineral acid concentration ≤ 5.5M. The reactive species were VO₂.2H₂SO₄⁺ in H₂SO₄ and V(OH)₂³⁺ in HClO₄ solutions. These species reacted with P:(OH)₃ in the slow step to form free radical P*(O)OH.¹⁰⁸ The course followed by the radical is described in the reaction of **PPA** in H₂SO₄ solution (see ref. 112).

The reinvestigated reaction confirmed second order dependence in HA (H₂SO₄ or HClO₄) and the faster rate in H₂SO₄. The intermediate V^V-**P3** complex was formed prior to its decomposition to the free radical H₂P*O₃ as a result of fission of P-H bond, supported by the *k*_H/*k*_D > 1, and not that of H-O bond.^{108,108} The catalysis by Ag⁺ and the change of order from first to zero with respect to V^V was explained by the rate controlling oxidation of **P3** to H₂P*O₃. The Ag⁰ is rapidly oxidized to Ag⁺ by V(V), and H₂P*O₃ could be rapidly oxidized by both V(V) and Ag⁺ in presence of water.¹⁰⁹ The oxidation of **PPA** by V(OH)₃HSO₄⁺ in H₂SO₄ was faster than the oxidation by V(OH)₃²⁺ in HClO₄ solution. The formation of V^V-**PPA** was not detected in either of the acid. The acid catalysis was related to Hammett acidity function -H₀. V(OH)₃HSO₄⁺ is stated to react with **PPA** in the rate limiting reaction to give the free radical PhP*(O)OH which was rapidly oxidized by V^V to PhP⁺(O)OH ion in the following step. V(OH)₃²⁺ acted as a two-electron acceptor forming PhP⁺(O)OH in the slow step. The PhP⁺(O)OH ion reacted rapidly with water molecules giving C₆H₅P(O)(OH)₂.¹¹⁰

Almost entirely different results were reported in the reinvestigated reaction of **PPA** in perchlorate solution. The *k*_{obs} = *a* + *b*[H⁺] prompted the suggestion that VO₂⁺ and V(OH)₃²⁺ ions were the reactive species for the paths that were independent and dependent on H⁺ ions. In the proposed mechanism, VO₂⁺ and V(OH)₃²⁺ reacted bimolecularly with PhP:(OH)₂ and PhHP(O)OH respectively to give a free radical¹¹¹ instead of phosphonium ion,¹¹⁰ thereby suggesting that V^V does not behave as a two-electron oxidant.¹¹⁰

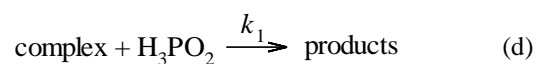
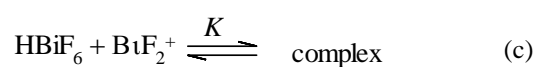
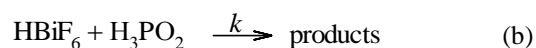
Mercury

The reaction between **P1** and HgCl₂ in HCl, in not too dilute solutions, was catalyzed by H⁺ but independent of HgCl₂. The rate limiting step happened to be the equilibrium

between H₂P(O)OH and HP:(OH)₂ followed by rapid reaction between molecular HgCl₂ (not Hg²⁺ or possible complexes) and two molecules of HP:(OH)₂. The evidence for the rapid reaction is considered strong but not quite conclusive.¹¹²

Bismuth

The redox reaction of Bi^V with **P1**, studied in aqueous mixture of HClO₄ and HF, was catalyzed by BiF₂⁺ ion though the rate was independent of HF and F⁻ ions. The proposed mechanism, Scheme 6, gives the rate law in equation (24).¹¹³



Scheme 19

$$k_{obs} = \left(K_p k + \frac{K_p K k_1 [\text{Bi}^{\text{III}}]}{1 + K [\text{Bi}^{\text{III}}]} \right) [\text{P1}][\text{H}^+] \quad (24)$$

Iridium

In the oxidation of **P1** by IrCl₆²⁻ ions in HClO₄ solution the rate limiting step was the bimolecular reaction between the two reactants resulting in the formation of H₂P*O₂ radical which was rapidly oxidized by another IrCl₆²⁻ ion to **P3**. Cl⁻ and SO₄²⁻ ions accelerate the rate.¹¹⁴

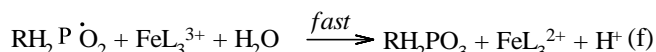
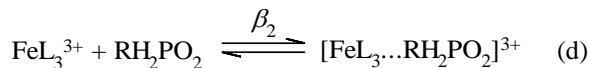
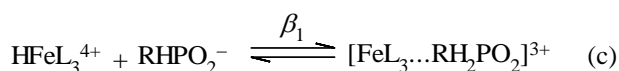
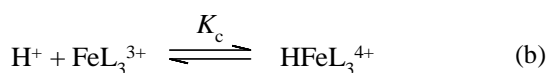
Iron

The oxidation of **P1** and **PPA** by FeL₃³⁺ (L = 1,10-phenanthroline or 2,2'-bipyridine) in HClO₄ solution indicated that **PPA** was more reactive than **P1**, and these reacted in the 'inactive' form. An outer-sphere complex, Scheme 4, formed through paths (l) and (m), decomposed to free radical in the rate determining step. The paths are ambiguous because β₂ = β₁K_aK_c.¹¹⁵

The alkaline oxidation of **PPA** by Fe(CN)₆³⁻ in presence of OsO₄ indicated the formation of a complex between **PPA** and OsO₄ which then reacted with OH⁻ ion in the rate determining step followed by a fast reaction between OsO₄ and Fe(CN)₆³⁻.¹¹⁶

Nitrogen

The details of the mechanism of the oxidation of **P1** by HNO₃ using Raman spectroscopy could not be accessed.¹¹⁷



Scheme 20

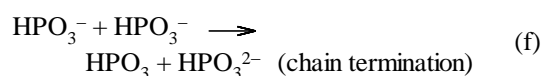
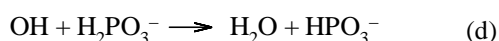
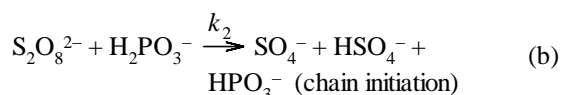
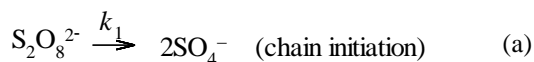
Peroxodiphosphate

The $\text{H}_4\text{P}_2\text{O}_8$ oxidation of **P1** in HClO_4 solution is in fact the oxidation by H_3PO_5 , the hydrolytic product of the former because rate of hydrolysis happens to be larger than the rate of oxidation (k) of **P1** by H_2PO_5^- . The k_{obs} was given by equation (25) where K_1 and K_2 are related to the ionization of H_3PO_2 and H_3PO_5 .¹¹⁸

$$k_{\text{obs}} = \frac{k[\text{H}_3\text{PO}_2][\text{H}^+]}{([\text{H}^+] + K_1)([\text{H}^+] + K_2)} \quad (25)$$

Peroxomon and disulfate

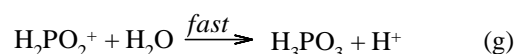
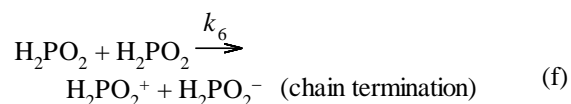
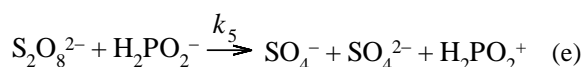
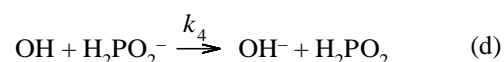
Oxidation of **P3** by $\text{S}_2\text{O}_8^{2-}$ in neutral solution was explained by a chain mechanism which was strongly suggested by the inhibition of the reaction by allyl acetate and fractional order dependence on **P3** and $\text{S}_2\text{O}_8^{2-}$. The reactions in the chain mechanism are in Scheme 5, and the deduced rate law is in equation (26).¹¹⁹



Scheme 21

$$-\frac{d[\text{S}_2\text{O}_8^{2-}]}{dt} = 0.5(k_1 + k_2 \sum \text{P3}) [\text{S}_2\text{O}_8^{2-}]^2 \quad (26)$$

The oxidation of **P1** by $\text{S}_2\text{O}_8^{2-}$ also followed a free-radical chain mechanism in which the steps (a)-(c), Scheme 20 for the oxidation of **P3**, were common but the steps (d)-(g) were different as given in Scheme 9, and a different rate law as given in equation (27). The reaction was independent of acidity up to pH 8 but fell off rapidly with pH > 8 and reached a low plateau at pH 11. O_2 inhibited the reaction, and the effect increased with pH. The reaction was more complex in solutions < pH 2, and had no contribution from $\text{HP}:(\text{OH})_2$.¹²⁰



Scheme 22

$$-\frac{d[\text{S}_2\text{O}_8^{2-}]}{dt} = \left(\frac{k_5^2 k_1}{k_6} + \frac{k_5^2 k_1 [\text{H}_2\text{PO}_2^-]^2}{k_6} \right) [\text{S}_2\text{O}_8^{2-}]^2 \quad (27)$$

The $\text{S}_2\text{O}_8^{2-}$ oxidation of **P1**, induced by irradiation with visible light, in the presence of photocatalyst $\text{Ru}(\text{bipy})_3^{2+}$ followed the rate law in equation (28) where k_0 and k_q are respectively the excitation and quenching rate constants.¹²¹

$$-\frac{d[\text{S}_2\text{O}_8^{2-}]}{dt} = \frac{k_q I_a [\text{S}_2\text{O}_8^{2-}]}{k_0 + k_q [\text{S}_2\text{O}_8^{2-}]} \quad (28)$$

The oxidation of **P1** by peroxomonosulphate ($\text{KHSO}_5 \cdot 0.5\text{KHSO}_4 \cdot 0.5\text{K}_2\text{SO}_4$) in aqueous acidic solution proceeded through the formation of adduct by HSO_5^- and H_3PO_2 prior to its rate determining decomposition to **P3** and HSO_4^- . The possibility of OH^\cdot and $\text{SO}_4^{\cdot-}$ radicals intervening in the reaction was eliminated.¹²² The RuCl_3 -catalyzed oxidation of **P1** by HSO_5^- ion in acetate buffer had also been reported.¹²³

Chlorine and its compounds

The Chloramine T oxidation of **P1** was catalyzed by Cl^- and the rate increased with H^+ and tended to have a limiting value at high concentrations.¹²⁴

$\text{MeC}_6\text{H}_4\text{SO}_2\text{NCl}_2$ was the suggested reactive species in the chloramine oxidation of **P3**, studied in acetate buffers, and the equation 29, where k is the observed third order rate constant, represented the rate law.¹²⁵

$$k = \frac{k_1 K_d [\text{H}^+] + k_2 K_1 K_d + k_3 K_1 K_2 K_d [\text{H}^+]^{-1}}{(4 K_d [\text{RNHCl}] + \text{RNH}_2) ([\text{H}^+] + K_1)} \quad (29)$$

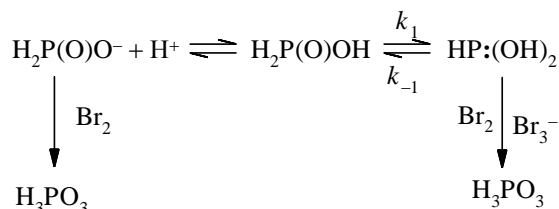
The oxidation of **P1**, **P3** and **PPA** by N-chlorosuccinimide was similar to the oxidation by butyltriphenyl phosphoniumdichromate.⁶³ The $(\text{CC}=\text{O})_2\text{NH}^+\text{Cl}$ was the considered reactive species.¹²⁶

Bromine and its compounds

The earliest report on the reactions of **P3** with Br_2 is in the presence of HBr (or H_2SO_4) and neutral bromides, and with Cl_2 in the presence of HCl and neutral chlorides. The reaction of both H_2PO_3^- and HPO_3^{2-} ions either with Br_2 or Cl_2 was bimolecular in nature, and retarded by H^+ ion and the resulting halide ion. The rate law was given by equation (30) where k_1 and k_2 are the rate coefficients for the bimolecular reaction of X_2 ($\text{X} = \text{Cl}$ or Br) with H_2PO_3^- and HPO_3^{2-} ions respectively, K_1 and K_2 are respectively the first and second dissociation constants of **P3**, K_3 is the association constant for Br_3^- from Br_2 and Br^- , and k_{obs} is the second order rate constant. The dependence on H^+ ruled out the reaction of X_2 with H_3PO_3 .¹²⁷

$$k_{obs} = \frac{k_1 K_1 K_3}{K_1 + [\text{H}^+]} + \frac{k_2 K_1 K_2 K_3}{[\text{H}^+] (K_1 + [\text{H}^+])} \quad (30)$$

The investigation of the corresponding redox with **P1** and H_2PO_2^- reported that the oxidation of **P1** by Br_2 and Cl_2 occurs through the intermediacy of $\text{HP}(\text{OH})_2$, and the latter reacted with X_3^- and probably with X_2 , but not with HOX . However, H_2PO_2^- was oxidized by Br_2 only and not by Br_3^- or HOBr . The H^+ in the range where **P1** mostly existed as H_2PO_2^- had no effect on the rate of the reaction. The mechanism in Scheme 23 was probable for the oxidation by Cl_2 also though the treatment for Br_2 oxidation tended to be more accurate than that by Cl_2 . The $k_1/k_{-1} \sim 10^{-12}$ was reported.¹²⁸



Scheme 23

In the oxidation of **P1**, **P3** and **PPA** by aqueous Br_2 at $[\text{H}^+] = 0.001\text{--}5.0$ M, the Br_2 was the reactive species. The H^+ -dependence indicated that the oxy-anion was oxidized more rapidly than the parent acid. The substantial k_H/k_D in the oxidations of **P1** and **P3** indicated cleavage of the P-H

bond as the rate determining step. A study of $[\text{H}^+]$ variation showed the.¹²⁹

The oxidation of $[\text{Co}(\text{NH}_3)_5\{\text{OP}(\text{H})(\text{O})_2\}]^+$ and phosphite ions by Br_2 was studied over extended pH ranges. The oxidation of $[\text{Co}(\text{NH}_3)_5\{\text{OP}(\text{H})(\text{O})_2\}]^+$ was much faster than the oxidation of $[\text{Co}(\text{NH}_3)_5\{\text{OP}(\text{H})(\text{OH})\text{O}\}]^{2+}$. The reactive oxidant species was Br_2 , and not Br_3^- or HOBr , and the $k_H/k_D = 2.4$ indicated that the redox involved the rate determining fission of P-H bond. The rate law for the reaction was given by equation (31) where k is the specific rate constant for the oxidation, $K_{\text{Br}_3} = [\text{Br}_3^-]/[\text{Br}_2][\text{Br}^-]$, K_a is the acid dissociation constant of $[\text{Co}(\text{NH}_3)_5\{\text{OP}(\text{H})(\text{OH})\text{O}\}]^{2+}$ ion, and $[\text{Phos}] = [\text{Co}(\text{NH}_3)_5\{\text{OP}(\text{H})(\text{O})_2\}]^+ + [\text{Co}(\text{NH}_3)_5\{\text{OP}(\text{H})(\text{OH})\text{O}\}]^{2+}$.

$$k_{obs} = \frac{k K_a [\text{Phos}]}{(K_a + [\text{H}^+]) (1 + K_{\text{Br}_3} [\text{Br}^-])} \quad (31)$$

The Br_2 oxidation of free phosphite ions indicated that HPO_3^{2-} was extraordinarily reactive than H_2PO_3^- , which was the suggested reactive entity in an earlier study.¹²⁹ The $k_H/k_D = 1.7$ supported the fission of P-H bond in the rate determining step. The rate law for HPO_3^{2-} oxidation is given in equation (32), where k is the specific rate constant for the oxidation, K_{a1} and K_{a2} are the first and second dissociation constants of H_3PO_3 and K_{Br_3} is same as defined above. The redox occurred without oxygen exchange, the additional oxygen in the product H_3PO_4 comes from water.¹³⁰

$$k_{obs} = \frac{k K_{1a} K_{2a} [\text{P3}]}{([\text{H}^+]^2 + K_{a1} [\text{H}^+] + K_{a1} K_{a2}) (1 + K_{\text{Br}_3} [\text{Br}^-])} \quad (32)$$

Different rate laws i.e. equations (33) and (34) were respectively proposed for the oxidation of $[(\text{NH}_3)_5\text{CoOP}(\text{H})_2\text{O}]^{2+}$ (**1**) and $\text{H}_2\text{P}(\text{O})\text{O}^-$ by Br_2 along with a cyclic transition state. The oxidation of (**1**) was independent of H^+ ion. $[(\text{NH}_3)_5\text{CoOP}(\text{H})_2\text{O}]^{2+}$ was not detected during the oxidation. In equation (33), k_{Br_2} and k_{Br_3} are the second order rate constants for the reactions effected by Br_2 and Br_3^- respectively and K_{Br_3} has the same meaning as defined in the above reaction.¹³⁰ The reaction with Br_3^- proceeded via a weak $[\text{Co}(\text{NH}_3)_5\text{OP}(\text{H})_2\text{O}]^{2+} \cdot \text{Br}_3^-$ ion-pair.

$$k_{obs} = \frac{(k_{\text{Br}_2} + k_{\text{Br}_3} K_{\text{Br}_3} [\text{Br}^-]) [(\text{NH}_3)_5\text{CoOP}(\text{H})_2\text{O}^{2+}]}{(1 + K_{\text{Br}_3} [\text{Br}^-])} \quad (33)$$

$$k_{obs} = \frac{k_{\text{Br}_2} K_a [\text{H}_3\text{PO}_2]_0}{(K_a + [\text{H}^+]) (1 + K_{\text{Br}_3} [\text{Br}^-])} \quad (34)$$

Br_2 oxidized $\text{H}_2\text{P}(\text{O})\text{O}^-$ whereas H_3PO_2 and Br_3^- were unreactive. A $k_H/k_D = 2.7$ was noted with the implication similar to that stated in the above reaction.¹³⁰ The mechanism envisaged that the attack by O-atom at one end of the polarized Br_2 molecule was synchronous with fission

of P-H bond and substantial transfer of H atom to the other. The transition state is therefore cyclic.¹³¹

Br_3^- ion was the reactive species in the oxidations by tetrabutylammoniumtribromide (**tbatb** in $\text{AcOH-H}_2\text{O}$),¹³² and benzyltrimethylammoniumtribromide (**btmab** in 9:1(vol/vol) acetonitrile-acetic acid.¹³³ The reactive species in the oxidation by benzyltrimethylammonium dichloroiodate (**btaci**) in presence of ZnCl_2 was $[\text{PhCH}_2\text{Me}_3\text{N}^+][\text{Zn}_2\text{Cl}_6^-]2\text{I}^+$.¹³⁴

The oxidation of **POA** by acidic N-bromoacetamide is second order in **POA** and inverse first order in H^+ ions. The oxy-acids reacted in the ‘inactive’ form, with for that indicated the transfer of H^- from the P-H bond to the oxidant in the rate determining step.¹³⁵

In the parallel oxidations by sodium N-bromobenzenesulfonamide in HClO_4 solution, the oxy-acids reacted in the ‘inactive form and $(\text{PhSO}_2\text{NH}_2\text{Br})^+$ was postulated as the reactive species. A substantive $k_{\text{H}}/k_{\text{D}}$ in the oxidation of **P1** and **P3** indicated a rate determining step similar to that described above.¹³⁶

Iodine

An earlier report on the reaction of **P1** and **P3** with I_2 in both acidic and alkaline solution reported an equilibrium between $\text{H}_2\text{PO}(\text{OH})$ and $\text{HP}:(\text{OH})_2$. Alkaline solutions drove the system in the direction of $\text{H}_2\text{PO}(\text{OH})$ which did not react with I_2 , while acidic solution favored the formation of $\text{HP}:(\text{OH})_2$ which reacted with excess of I_2 forming $\text{HP}(\text{OH})_2\text{I}$ and $\text{P}:(\text{OH})_2\text{I}$ (with elimination of HI) when **P1** was in excess. The $\text{HP}(\text{OH})_2\text{I}_2$ is decomposed by H_2O first into $\text{HP}(\text{OH})_4$ and then into $\text{HPO}(\text{OH})_2$. Similarly **P3** existed as $\text{HPO}(\text{OH})_2$ and $\text{P}:(\text{OH})_3$ in solution. The latter reacts with I_2 and H_2O forming H_3PO_4 . The greater stability of $\text{HPO}(\text{OH})_2$ prevents it from forming intermediary compounds with I_2 , the reaction does not go to completion even with an excess of I_2 .¹³⁷

Another report suggested that compounds in which a H^+ ion is bound directly to P, and is in the same state of charge, reacted identically with I_2 . The acidic compounds reacted with I_2 in the neutral state while the univalent anion did not react with I_2 with noticeable speed. The rapid reaction of **P3** with I_2 in slightly acidic solution was studied in various buffer solutions. The appreciable increase in speed of reaction with the pH of the solution was explained by the fact that only the secondary ion reacted with I_2 and considerably more slowly with I_3^- ion. The methyl-, ethyl- and iso-propyl esters exhibited an increased reactivity with I_2 .¹³⁸

The reaction of H_3PO_2 with I_2 involved the general acid catalyzed transformation of $\text{H}_2\text{P}(\text{O})\text{OH}$ to $\text{HP}:(\text{OH})_2$. The former had no detectable reaction with I_2 whereas the latter reacted with I_2 and I_3^- . The study of the reaction in phosphate, arsenate and phthalate buffers (pH 6-8) indicated that H_2PO_2^- also reacted directly with I_2 .¹³⁹

The corresponding reaction of **P3**, studied in the pH range 2-9 indicated that HPO_3^{2-} ions reacted directly with I_2 . The reaction of H_3PO_3 at $\text{pH} < 1$ was subject to general acid-base catalysis, similar to that shown in Scheme 2, forming

$\text{P}:(\text{OH})_3$ which was oxidized by both I_3^- and I_2 . The reaction $\text{H}_2\text{PO}_3^- + \text{I}_2$ was negligibly small to be detectable.¹⁴⁰

The exchange rate of the P-H bond of **P3** in D_2O increased with DCI . The oxidation was acid catalyzed and tautomerism played a role in the oxidation only above $\sim 1\text{N}$ HCl . The proposed mechanism had similarity with the Scheme 2. A $k_{\text{H}}/k_{\text{D}} \approx 3.6$ was observed in the oxidation. The oxidation at pH 8.6 (borate buffer) was consistent with a mechanism involving the attack of I_2 on $\text{HP}(\text{O})\text{O}_2^{2-}$ ions. The oxidation of $\text{HP}(\text{O})\text{OHO}^-$ was much slower than that of $\text{HP}(\text{O})\text{O}_2^{2-}$ ion.¹⁴¹

The oxidation of **P1** involved an equilibrium between $\text{H}_2\text{P}(\text{O})\text{OH}$ and $\text{HP}:(\text{OH})_2$ where the conversion to $\text{HP}:(\text{OH})_2$ is rate determining. $\text{HP}:(\text{OH})_2$ is rapidly oxidized by IO_3^- ion. It is probable that the reaction of IO_3^- with $\text{HP}:(\text{OH})_2$ might be at a much slower rate than do other substances conforming to this rate law.¹⁴²

The reactions of H_2PO_2^- and **P1** with ICl and ICl_3 in HCl solutions and with ICl_4^- in aqueous solution were in conformity with the existence of $\text{H}_2\text{P}(\text{O})\text{OH}$ and $\text{HP}:(\text{OH})_2$. The oxidation reaction of **P1** with I_2 occurred with preliminary addition of I to the acid.¹⁴³

Hydrogen peroxide

The catalytic effect of Ti^{IV} in the oxidation of **P1** by H_2O_2 in H_2SO_4 was ascribed to the formation of $\text{TiO}_2(\text{SO}_4)_2^{3-}$ as an intermediate formed through the reactions $\text{HO}_2 + \text{TiO}_2(\text{SO}_4)_2^{2-} \rightarrow \text{H}^+ + \text{O}_2(\text{TiO}_2(\text{SO}_4)_2)^{3-}$ or $\text{H}_2\text{PO}_3 + \text{TiO}_2(\text{SO}_4)_2^{2-} \rightarrow \text{H}_3\text{PO}_4 + \text{H}^+ + \text{TiO}_2(\text{SO}_4)_2^{3-}$.¹⁴⁴

Acknowledgement

My sincere thanks are due to the Indian Chemical Society for the award of Acharya Praful Chandra Ray Medal in the Year 1992.

Thanks are also due to the Council of Scientific and Industrial Research and the Department of Science and Technology for funding of the research described here.

I am also thankful to the DR. Kótai László for the invitation to write this review.

References

- ¹Kavipriya, K., Rajendran, S., Sathiyabama, J., Prabha, A.S., *Eur. Chem. Bull.*, **2012**, *1*, 366.
- ²Pascal, P., *Compt. rend.*, **1922**, *174*, 457.
- ³Simon, A., Fehér., Schulze, G., *Z. anorg. allgem. Chem.*, **1937**, *230*, 289.
- ⁴Gutowsky, H.S., McCall, D.W., *J. Chem. Phys.*, **1954**, *22*, 162.
- ⁵Lovejoyz, R. W., Wagner, E. L., *J. Phys. Chem.*, **1964**, *68*, 544.
- ⁶Steele, B. D., *J. Chem. Soc., Trans.*, **1907**, *91*, 1641.
- ⁷Mitchell, A. D., *J. Chem. Soc., Trans.*, **1920**, *117*, 1322.
- ⁸Brodskii, A. I., Strazhesko, D. N., Chervyatsova, L. L., *Doklady Akademii Nauk SSSR* **1950**, *75*, 823.

- ⁹ Wilson, J. N., Dickinson, R. G., *J. Am. Chem. Soc.*, **1937**, 59, 1358.
- ¹⁰ Hayward, P., Yost, D. M., *J. Am. Chem. Soc.*, **1949**, 71, 915.
- ¹¹ Brodskii, A. I., Sulima, L. V., *Dokl. Akad. Nauk. SSSR*, **1952**, 85, 1277.
- ¹² Brodskii, A.I., *Izvest. Akad. Nauk S. S. S. R. Otdel. Khim. Nauk.*, **1949**, 3.
- ¹³ A.I. Brodskii, *Zhur. Obshchei Khim.*, **1954**, 24, 413.
- ¹⁴ Brodskii, A. I., *Voprosy Khim. Kinetiki, Katalizai Reaktsionnoi Sposobnosti, Akad. Nauk S.S.S.R., Otdel. Khim. Nauk*, **1955**, 18.
- ¹⁵ Jenkins, W. A., Jr., Yost, D. M., *J. Chem. Phys.*, **1952**, 20, 538.
- ¹⁶ Jenkins, W. A., Yost, D.M., *J. Inorg. Nucl., Chem.*, **1959**, 11, 297.
- ¹⁷ Fratiello, A., Anderson, E. W., *J. Am. Chem. Soc.*, **1963**, 85, 519.
- ¹⁸ Larson, J.W., *Polyhedron*, **1990**, 9 1071.
- ¹⁹ Martin, R. B., *J. Am. Chem. Soc.*, **1959**, 81, 1574.
- ²⁰ Bailey, W. J., Fox, R. B., *J. Org. Chem.*, **1964**, 29, 1013.
- ²¹ Reuben, J., Samuel, D., Silver, B. L., *J. Am. Chem. Soc.*, **1963**, 85, 3093.
- ²² Arbuzov, A. E., *J. Russ. Phys. Chem. Soc.*, **1906**, 88, 293.
- ²³ Kabachnik, M. I., Gilyarnv, V. A., *Dokl. Akad. Nouk SSSR.*, **1956**, 106, 473.
- ²⁴ Kabachnik, M. I., Polikarpov, T. M., *Dokl. Akad. Nouk SSSR.*, **1957**, 115, 512.
- ²⁵ Arbuzov, A.E., Batuev, M.I., Vinogradova, V.S., *Dokl. Akad. Nouk SSSR.*, **1946**, 64, 599.
- ²⁶ Serra, M M., Malateata, P., *Ann. Chem. (Rome)*, **1953**, 43, 568; **1955**, 46, 911.
- ²⁷ Daasch, L.W., *The Structure of Dialkyl Phosphonates and Some of their Salts*, Naval Research Laboratory Report 4945, Washington, D. C., 1957. 116 512 (1987).
- ²⁸ Meyrick, C. I., Thompson, H. W., *J. Chem. Soc.*, **1950**, 225.
- ²⁹ Callis, C. F., Van Wazer, J. R., Shoolery, J. N., Anderaon, W. A., *J. Am. Chem. Soc.*, **1957**, 79, 2719.
- ³⁰ Nylen, P., *Z. Anorg. Allgem. Chem.*, **1938**, 235, 161.
- ³¹ Luz, Z., Silver, B., *J. Am. Chem. Soc.*, **1961**, 83, 4518.
- ³² Nylen, P., *Svensk Kem. Tidskr.*, **1937**, 49, 79.
- ³³ Luz, Z., Silver, B., *J. Am. Chem. Soc.*, **1962**, 84, 1095.
- ³⁴ Bailey, W. J., Fox, R. B., *J. Org. Chem.*, **1963**, 28, 531.
- ³⁵ Mitchell, A. D., *J. Chem. Soc. Trans.*, **1924**, 125, 564.
- ³⁶ Kirson, B., *Bull. Soc. chim. Fr.*, **1948**, 52.
- ³⁷ Kuan, P., Sheng-Hsien, L., *J. Chinese Chem. Soc. (Taiwan)*, **1960**, 7, 75.
- ³⁸ Preer, J., Haight, G. P., Jr., *J. Am. Chem. Soc.*, **1965**, 87, 5256.
- ³⁹ Westheimer, F. H., *Chem. Rev.*, **1949**, 45, 419; Stewart, R., *Oxidation Mechanisms*, W. A. Benjamin, Inc., New York, **1964**.
- ⁴⁰ Haight, G. P., Jr.; Rose, M., Preer, J., *J. Am. Chem. Soc.*, **1968**, 90, 4809.
- ⁴¹ Cooper, J. N., *J. Phys. Chem.*, **1970**, 74, 955.
- ⁴² Ghosh, S. K., Bose, R. N., Laali, K., Gould, E. S., *Inorg Chem.*, **1986**, 25, 4737.
- ⁴³ Chandra, S. K., Gelerinter, E., Gould, E. S., *Inorg. Chem.*, **1995**, 34, 4057.
- ⁴⁴ Khan, Z., Hashmi, A. A., Kabir-Ud-Din, *Transit. Met. Chem.*, **1998**, 23, 147.
- ⁴⁵ Sengupta, K. K., Chakladar, J. K., Chatterjee, A. K., *J. Inorg. Nucl. Chem.*, **1973**, 35, 901.
- ⁴⁶ Michaelis, L., Menten, M., *Biochem. Z.*, **1913**, 49 333.
- ⁴⁷ Sengupta, K. K., *Bull. Chem. Soc. Jpn.*, **1970**, 43, 590.
- ⁴⁸ Sengupta, K. K., Chakladar, J. K., *J. Chem. Soc. Perkin Trans., 2*, **1973**, 929.
- ⁴⁹ Sharma, K., Mehrotra, Raj N., *Transit. Met. Chem.*, **1989**, 14, 48.
- ⁵⁰ Seth, M., Mathur, A., Banerji, K. K., *Bull. Chem. Soc. Jpn.*, **1990**, 63, 3640.
- ⁵¹ Virkar, D.D., Gokavi, G.S., *Oxidn Commun.*, **2002**, 25, 111.
- ⁵² Mathur, D., Sharma, P. K., Banerji, K. K., *Indian J. Chem.*, **1993**, 32A, 961.
- ⁵³ Mishra, M. K.; Sharma, M., Sharma, V., *Int. J. Chem. Sci.*, **2005**, 3, 578.
- ⁵⁴ Bishnoi, G., Sharma, M., Sindal, R. S., Sharma, P. K., *J. Indian Chem. Soc.*, **2007**, 84, 892.
- ⁵⁵ Vadera, K., Sharma, D., Agarwal, S., Sharma, P. K., *Indian J. Chem.*, **2010**, 49A, 302.
- ⁵⁶ Grover, A., Varshney, S., Banerji, K. K., *Indian J. Chem.*, **1994**, 33A, 622.
- ⁵⁷ Asopa, R., Mathur, A., Banerji, K. K., *Indian J. Chem.* **1991**, 30A, 784.
- ⁵⁸ Bhatt, M., Sharma, P. K., Banerji, K. K., *React. Kinet. Catal. Lett.*, **2000**, 69, 247.
- ⁵⁹ Varshney, S., Sharma, P. K., Banerji, K. K., *Proc. Indian Acad. Sci. Chem. Sci.*, **1992**, 104, 603.
- ⁶⁰ Moondra, A., Mathur, A., Banerji, K. K., *J. Chem. Soc. Dalton Trans.*, **1990**, 2697.
- ⁶¹ Mehla, S. K., Kothari, S., Banerji, K. K., *Int. J. Chem. Kinet.*, **2000**, 32, 165.
- ⁶² Kumar, R., Panday, D., Kothari, S., *Prog. React. Kinet. Mech.*, **2011**, 36, 352.
- ⁶³ Kothari, A., Kothari, S., Banerji, K. K., *Oxid. Commun.*, **2000**, 23, 93.
- ⁶⁴ Gilla, M., Meena, A. K., Swami, P., Baghmar, M., Sharma, V., *J. Indian Chem. Soc.*, **2011**, 88, 699.
- ⁶⁵ Prakash, O. M., Sindal, R. S., Sharma, P. K., *Int. J. Chem. Sci.*, **2003**, 1, 411.
- ⁶⁶ Khurana, M., Sharma, P. K., Banerji, K. K., *Oxid. Commun.*, **1999**, 22, 406.
- ⁶⁷ Sengupta, K.K., Sarkar, T., *J. Indian Chem. Soc.* **1975**, 52 248.
- ⁶⁸ Sengupta, K. K., Basu, B., Sarkar, T., *Indian J. Chem.*, **1977**, 15A, 510.
- ⁶⁹ Banerji, R., Das, R., Chakraburty, A.K., *Transit. Met. Chem.*, **1992**, 17, 277.
- ⁷⁰ Sengupta, K. K., Bhattacharjee, N., *Transit. Met. Chem.*, **2000**, 25, 518.
- ⁷¹ Gurame, V.M., Gokavi, G. S., *Polyhedron*, **2008**, 27, 1905.
- ⁷² Mehrotra, Raj N., *J. Chem. Soc. Dalton Trans.*, **1984**, 1531.
- ⁷³ Zahonyi-Budo, E., Simandi, L. I., *Inorg. Chim. Acta*, **1993**, 205, 207.
- ⁷⁴ Zahonyi-Budo, E., Simandi, L. I., *Inorg. Chim. Acta*, **1991**, 181, 149.
- ⁷⁵ Sharma, K., Mehrotra, Raj N., *Indian J. Chem.*, **2000**, 39A, 709.

- ⁷⁶ Sharma, K., Mehrotra, Raj N., *Indian J. Chem.*, **2002**, 41A, 270.
- ⁷⁷ Mohnot, K., Sharma, P. K., Banerji, K. K., *J. Indian Chem. Soc.*, **1997**, 74, 12.
- ⁷⁸ Sengupta, K. K., Sarkar, T., *J. Indian Chem. Soc.*, **1975**, 52, 248.
- ⁷⁹ Indrayan, A. K., Mishra, S. K., Gupta, Y. K., *Inorg. Chem.*, **1981**, 20, 1924.
- ⁸⁰ Viste, A., Holm, D. A., Wang, P. L., Veith, G. D., *Inorg. Chem.*, **1971**, 10, 631.
- ⁸¹ Indrayan, A. K., Mishra, S. K., Gupta, Y. K., *Inorg. Chem.*, **1981**, 20, 450.
- ⁸² Mehrotra, Raj N., Kirschenbaum, L. J., *Inorg. Chem.*, **1989**, 28, 4327.
- ⁸³ Banerjee, R., Das, R., Mukhopadhyay, S., *J. Chem. Soc., Dalton Trans.*, **1992**, 1317.
- ⁸⁴ Solanki, S., Saha, R., Arora, S., Prakash, A., Mehrotra, Raj N., *Indian J. Chem.*, **2001**, 40A, 256.
- ⁸⁵ Ashurst, K. G., Hihhinson, W. C. E., *J. Chem. Soc. A.*, **1953**, 3044.
- ⁸⁶ Jordon, J., Catherino, H.A., *J. Phys. Chem.*, **1963**, 67, 2241.
- ⁸⁷ Warnqvist, B., Dodson, R.W., *Inorg. Chem.*, **1971**, 10, 2624.
- ⁸⁸ Gupta, K. S., Gupta, Y. K., *J. Chem. Soc. Sec. A.*, **1970**, 256.
- ⁸⁹ Bonner, N. A., Hunt, J. P., *J. Am. Chem. Soc.*, **1960**, 82, 3826.
- ⁹⁰ Gupta, K. S., Gupta, Y. K., *Indian J. Chem.*, **1970**, 11, 1001.
- ⁹¹ Gupta, K. S., Gupta, Y. K., *Inorg. Chem.*, **1974**, 13, 851.
- ⁹² Gupta, K. S., Gupta, Y. K., *J. Chem. Soc. Sec. A.*, **1971**, 1180.
- ⁹³ Gupta, K. S., Gupta, Y. K., *Inorg. Chem.*, **1975**, 14, 2000.
- ⁹⁴ Bhasin, M., Dubey, S., Sharma, I., Sharma, P. D., *Indian J. Chem.*, **2000**, 39A, 1036.
- ⁹⁵ Bhasin, M., Bansal, S., Sharma, P. D., *Oxid. Commun.*, **2000**, 23, 515.
- ⁹⁶ Carroll, R. L., Thomas, L. B., *J. Am. Chem. Soc.*, **1966**, 88, 1376.
- ⁹⁷ Treindl, L., Hatala, J., *Collect. Czech Chem Commun.*, **1977**, 42, 2332.
- ⁹⁸ Indrayan, A. K., Mishra, S. K., Gupta, Y. K., *Indian J. Chem.*, **1983**, 22A, 756.
- ⁹⁹ Blaustein, B.D., Gryder, J.W., *J. Am. Chem. Soc.*, **1957**, 79, 540.
- ¹⁰⁰ Dorfman, M.K., Gryder, J.W., *Inorg. Chem.*, **1962**, 1, 799.
- ¹⁰¹ Nagori, R. R., Mehta, M., Mehrotra, Raj N., *J. Chem. Soc. Dalton Trans.*, **1979**, 216.
- ¹⁰² Mishra, S. K., Sharma, P. D., Gupta, Y. K., *J. Inorg. Nucl. Chem.*, **1967**, 29, 1643.
- ¹⁰³ Bansal, S., Dubey, S., Bhasin, M., Sharma, P. D., *Oxid. Commun.*, **2000**, 23, 505.
- ¹⁰⁴ Mishra, S. K., Sharma, P. D., Gupta, Y. K., *J. Inorg. Nucl. Chem.*, **1974**, 36, 1845.
- ¹⁰⁵ Ayoko, G. A., *Transit. Met. Chem.*, **1990**, 15, 421.
- ¹⁰⁶ Sengupta, K. K., Pal, B. B., Mukherjee, D. C., *Z. Phys. Chem.*, (Muenchen), **1970**, 72, 230.
- ¹⁰⁷ Cooper, J. N., Hoyt, H. L., Buffington, C. W., Holmes, C. A., *J. Phys. Chem.*, **1971**, 75, 891.
- ¹⁰⁸ Sengupta, K. K., Pal, B. B., Mukherjee, D. C., *J. Chem. Soc. Dalton Trans.*, **1974**, 226.
- ¹⁰⁹ Mehrotra, Raj N., *J. Chem. Soc. Dalton Trans.*, **1978**, 681.
- ¹¹⁰ Sengupta, K. K., Chakladar, J. K., Pal, B. B., Mukherjee, D. C., *J. Chem. Soc. Perkin Trans. 2*, **1973**, 926.
- ¹¹¹ Mehrotra, Raj N., *Can. J. Chem.*, **1985**, 63, 663.
- ¹¹² Mitchell, A.D., *J. Chem. Soc. Trans.*, **1921**, 119, 1266.
- ¹¹³ Inani, K. M., Sharma, P. D., Gupta, Y. K., *J. Chem. Soc. Dalton Trans.*, **1985**, 2571.
- ¹¹⁴ Sengupta, K. K., Maiti, S., Ghosh, S. P., *Indian J. Chem.*, **1980**, 19A, 869.
- ¹¹⁵ Sharma, K., Prakash, A., Mehrotra, Raj N., *Bull. Chem. Soc. Jpn.*, **1989**, 62, 4009.
- ¹¹⁶ Sengupta, K. K., De, P. C., *J. Indian Chem. Soc.*, **1975**, 52, 252.
- ¹¹⁷ Duisebaeva, K. K., Arynov, K. T., Ushanov, V. Zh., Aueshov, A. P., *Izvestiya Ministerstva Nauki Akademii Nauk Respubliki Kazakhstan, Seriya Khimicheskaya*, **1996**, 14.
- ¹¹⁸ Kapoor, S., Gupta, Y. K., *J. Chem. Soc. Dalton Trans.*, **1977**, 862.
- ¹¹⁹ Ben-Zvi, E., *J. Phys. Chem.*, **1963**, 67, 2698.
- ¹²⁰ Ben-Zvi, E., *Inorg. Chem.*, **1967**, 8, 1143.
- ¹²¹ Bansal, S., Soni, N. K., Khandelwal, C. L., Sharma, P. D., *Oxid. Commun.*, **2007**, 30, 772.
- ¹²² Dubey, S.; Hemkar, S., Khandelwal, C. L., Sharma, P. D., *Inorg. Chem. Commun.*, **2002**, 5, 903.
- ¹²³ Sharma, N., Hemkar, S., Dubey, S., Khandelwal, C. L., Sharma, P. D., *J. Indian Chem. Soc.*, **2003**, 80, 233.
- ¹²⁴ Bhatt, L., Sharma, P. D., Gupta, Y. K., *Indian J. Chem.*, **1982**, 21A, 926.
- ¹²⁵ Sharma, I., Hussain, J., Sharma, P. D., *Oxid. Commun.*, **1994**, 17, 193.
- ¹²⁶ Moondra, A., Mathur, A., Sharma, P. K., Banerji, K. K., *Oxid. Commun.*, **1990**, 13, 99.
- ¹²⁷ Griffith, R. O., McKeown, A., *Trans. Faraday Soc.*, **1933**, 29, 611.
- ¹²⁸ Griffith, R. O., McKeown, A., *Trans. Faraday Soc.*, **1934**, 30, 530.
- ¹²⁹ Agarwal, S., Mathur, A., Banerji, K. K., *J. Indian Chem. Soc.*, **1992**, 69, 433.
- ¹³⁰ Carrington, S. J., Buckingham, D. A., Simpson, J., Blackman, A. G., Clark, C. R., *J. Chem. Soc., Dalton Trans.*, **1999**, 3809.
- ¹³¹ Clark, C. R., Blackman, A. G., *Inorg. React. Mech.*, **2000**, 2, 241.
- ¹³² Sharma, P. K., *Indian J. Chem.*, **2002**, 41A, 1612.
- ¹³³ Rao, P. S., Goel, S., Kothari, S., Banerji, K. K., *Indian J. Chem.*, **1998**, 37B, 1129.
- ¹³⁴ Suri, D., Kothari, S., Banerji, K. K., *Proc. Indian Acad. Sci., Chem. Sci.*, **1997**, 109, 147.
- ¹³⁵ Moondra, A., Mathur, A., Banerji, K. K. *Int. J. Chem. Kinet.*, **1991**, 23, 669.
- ¹³⁶ Moondra, A., Mathur, A., Banerji, K. K., *Indian J. Chem.*, **1990**, 29A, 963.
- ¹³⁷ Orlov, E. I., *Zhur. Russk. Fiziko-Khimicheskogo Obshchestva*, **1914**, 46, 535.
- ¹³⁸ Nylén, P., *Z. Anorg. Allg. Chem.*, **1937**, 230, 385.
- ¹³⁹ Griffith, R. O., McKeown, A., Taylor, R. P., *Trans. Faraday Soc.*, **1940**, 36, 752.
- ¹⁴⁰ Griffith, R. O., McKeown, A., *Trans. Faraday Soc.*, **1940**, 36, 766.

¹⁴¹ Silver, B., Luz, Z., *J. Phys. Chem.*, **1962**, 66, 1356.

¹⁴² Hayward, P., Yost, D. M., *J. Am. Chem. Soc.*, **949**, 71, 915.

¹⁴³ Fialkov, Ya. A., Kagan, F. E., *Zhur. Obshchei Khimii*, **1954**, 24, 3.

¹⁴⁴ Muratbekov, M. B., Nazarbekova, S. P., *Khimiya Vysokikh Energii*, **1988**, 22, 317.

Received: 27.03.2013.

Accepted: 18.05.2013.



SIMULATION, SENSITIVITY ANALYSIS AND OPTIMIZATION OF AN INDUSTRIAL CONTINUOUS CATALYTIC NAPHTHA REFORMING PROCESS

Sepehr Sadighi^[a] and S. Reza Seif Mohaddecy^{[a]*}

Keywords: Catalytic Reformer, Simulation, Petro-Sim, Sensitivity Analysis, Optimization

Continuous catalytic regeneration (CCR) is a key process in petroleum refineries to produce high octane gasoline. In this article, a commercial scale CCR plant with the nominal capacity of 22000 bbl day⁻¹ was simulated using Ref-sim module and Petro-sim simulator. The validity of this plant wide simulator was evaluated by actual test runs obtained during 6 months of operation. Simulation results showed that the AAD % of momentous output variables i.e. outlet temperature of reactors, product volume yield, product RON, H₂ purity of recycle gas and coke deposition on the catalyst against actual data were 0.5 %, 0.94 %, 1.098 %, 0.57 % and 0.347 %, respectively. Then, the optimal values for reactor temperatures, feed flow rate and recycle flow rate were determined using sensitivity analysis approach. After setting these decision variables on the proposed optimal values, the actual RON and volume yield of the CCR plant enhanced from 99.55 and 82.04 % to 99.67 and 82.4 %, respectively.

Corresponding Authors

E-Mail: Seifsr @ripi.ir

[a] Catalysis and Nanotechnology Division, Catalytic Reaction Engineering Department, Research Institute of Petroleum Industry (RIPI), Sadighis@ripi.ir

Introduction

The main objective of the catalytic reforming process is to enhance the octane number of the feed, mainly heavy naphtha. The need to increase the antiknock quality of naphtha as a blending stock for motor fuels is the greatest single reason for installing catalytic reforming units.¹ A large number of reactions occur in catalytic reforming, such as dehydrogenation and dehydroisomerization of naphthenes to aromatics, dehydrogenation of paraffins to olefins, dehydrocyclization of paraffins and olefins to aromatics, isomerization or hydroisomerization to isoparaffins, isomerization of alkylcyclopentanes and substituted aromatics, and hydrocracking of paraffins and naphthenes to lower hydrocarbons.² Some of these reactions are desired because of increasing octane number of gasoline and also purity of the produced hydrogen, and some of them are undesired due to decreasing them. For instance, cyclization and aromatization reactions increase the octane number. They are thus favorite ones. In contrast, coke formation and coke deposition reactions cause the deactivation of the catalyst; consequently, they are undesired reactions.

From the view of the operation, there are three kinds of relevant catalytic reforming units: 1. Semi-regenerative; 2. Continuously catalytic regenerative (CCR), and 3. Cyclic^{1,2}.

The CCR process consists of three or four adiabatic reactors in series with intermediate heaters.² Low octane hydrocarbons, such as paraffin's and naphthenes are converted to high octane aromatics, hydrogen and other light gases through this process.³ In a CCR plant, the reforming reactions take place in a moving bed catalytic reactor from which the catalyst is withdrawn; then it is regenerated and

recycled. The catalyst circulation and regeneration are performed on a continuous basis with full automatic control. Continuous regeneration eliminates the need of shutdown for regeneration of the earlier fixed bed reformers. Additionally, it minimizes the amount of catalyst in the unit, while allowing high gasoline yield and quality.^{4,5} The variables that affect the efficiency of a CCR process are the volume flow of naphtha feed, reactor inlet temperature, hydrogen-to-oil molar ratio and temperature of the separator.⁶

In this research, after simulating a commercial CCR plant using Petro-sim simulator (KBC, 2009), the effect of process variables on the yield of reforming and RON of the product is discussed. Then, the optimal process variables were determined using the sensitivity analysis approach.

Process Description

A commercial CCR unit, called Platformer licensed by UOP cooperation with the nominal capacity of 22000 barrel per day was chosen as a case study. The block flow diagram of the process is shown in Fig. 1. The feed of the plant prior to entering reactors should undergo hydro desulphurization (HDS) reaction in the hydrotreatment unit. Then, the treated feed (Reformate) is passed through filters to remove any particulate matter which may deposit on the welded plates exchanger. The specifications of the feed are presented in Table 1. This feed is mixed with the recycle gas from the recycle compressor, and preheated against the fourth reactor effluent. Before entering to the catalytic reactors, it should be heated to reach the reaction temperature above 500°C. The reactors are radial flow types, so the feed flows through the catalyst bed from the outer circumference towards the center pipe. In the first reactor, the reactions are predominantly endothermic; therefore, the reactor effluent requires reheating in the first inter-heater to the required inlet temperature of second reactor. The reactions in the second reactor are less endothermic, but still require

reheating in other heater before entering the third reactor. The third reactor effluent is reheated in the third inter-heater before entering the fourth reactor. The effluent leaves the fourth reactor at approximately 468-486 °C (depending on position in the cycle) and 3.3 bar.

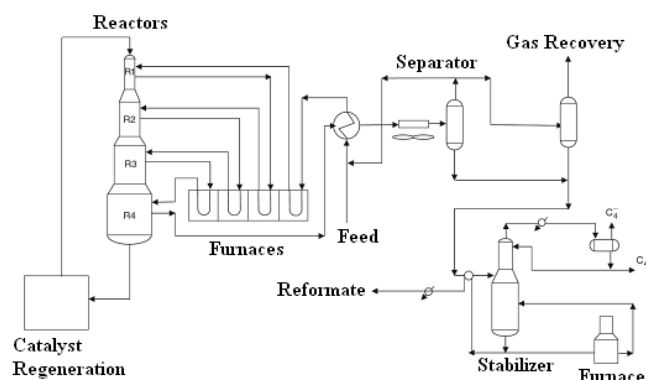


Figure 1. Block flow diagram of the continuous catalytic reforming unit⁷

In all reforming reactors the feed contacts with the reforming catalyst distributed approximately at the ratio of 15/20/25/40 %. In the continuous regeneration process the catalyst circulates continuously:

- In the reactors.
- From one reactor bottom to the top of the next one.
- From the last reactor to the regeneration unit for regeneration.
- From the regeneration unit, the regenerated catalyst returns to the first reactor.

In the regeneration unit, catalyst circulation is achieved either by gravity flow or by gas lift systems. In order to obtaining a good regeneration of the spent catalyst, operations such as coke burning, catalyst oxychlorination, catalyst calcinations, catalyst cooling and catalyst reduction must be carried out. Leaving fourth reactor, the effluent after heat exchange against reactor feed, is cooled by air and water exchange, respectively before entering the separator drum.

Table 1. Feed specifications of the CCR plant studied

Distillation	Case1 Feb. 2011	Case2 April 2011	Case3 May 2011	Case4 July 2011
Method (D86)				
IBP °C	95	92	92	93
10 % vol °C	107	104	104	104
30% vol °C	112	111	109	111
50 % vol °C	118	117	114	117
70 % vol °C	126	127	125	125
90 % vol °C	139	140	137	138
FBP °C	161	164	161	159
PONA Analysis				
Naphthenes vol %	33.2	33.8	33.8	-
Aromatics vol %	12.2	12.4	11.8	-
Density kgm ⁻³	746.5	745	745	744

A portion of the separated gas is compressed by a recycle gas compressor; then, it is recycled to the reactors. Finally, the liquid product leaving the separator is introduced to the gasoline stabilizer in which the LPG and light gases are separated from the gasoline to set the vapour pressure of the gasoline according to the market requirement. The distribution of catalyst between reforming reactors in the CCR plant studied in this work is shown in Table 2. Moreover, the normal operating conditions prevailing in this unit are presented in Table 3.

Table 2. Catalyst distribution in reforming reactors studied

Catalyst	First Reactor	Second Reactor	Third Reactor	Fourth Reactor
Weight (kg)	5880	6754	10545	18984
Distribution (wt %)	14	16	25	45

Table 3. Operating conditions in the CCR plant studied

Process variable	Value
Inlet temperature (°C)	500 - 515
Hydrogen/hydrocarbon ratio (mol mol ⁻¹)	3-7
LHSV (h ⁻¹)	1- 2
Yield (vol %)	70 - 85

Process Simulation

Catalytic reforming process is often modeled and simulated based on the: 1. Number of reactive species, and 2. Type of the used kinetic model.^{8,9,10} Moreover, presence of many components as reactants or intermediate products in the reactive mixture makes a sophisticated situation for modeling and simulating the process. To decrease these complications, reactants in the mixture are classified in certain and limited groups, called pseudo components. The number of selected pseudo components in the mixture is a determinant factor interested in designed models. Additionally, Arrhenius and Langmuir–Hinshelwood kinetics are widely used for kinetic-based catalyst modeling and simulating of the catalytic naphtha reforming process^{11,12}. Petro-sim simulator, developed by KBC, is capable to simulate industrial scale of catalytic reforming units.¹³ This simulator can also simulate the catalytic reforming plants with three or four reactors; so, it enables us to simulate reactors with different catalyst weights and different sizes.^{14,15} In this research, Petro-sim has been used to simulate and analysis of the CCR plant studied.

To simulate the catalytic naphtha reforming process using Petro-sim, external calibration in order to determining the kinetic parameters is essentially needed. For this unit, Ref-sim module is applied to provide these factors^{15,16}. It should be mentioned that for generating these parameters i.e. frequency factors, activation energies and decay constants, actual test runs from the under study unit should be gathered. These parameters mainly consist of inlet and outlet reactor temperatures, catalyst weight, specification of feed and products, operating pressures, flow rates of makeup hydrogen, recycle rates and flow rates of all gaseous and

liquid products. After preparing test runs and running Ref-sim module, calibration factors are sent to the Petro-sim environment in order to simulating and optimizing the under study plant. The algorithm to tune and simulate CCR process studied in this research is shown in Fig. 2.

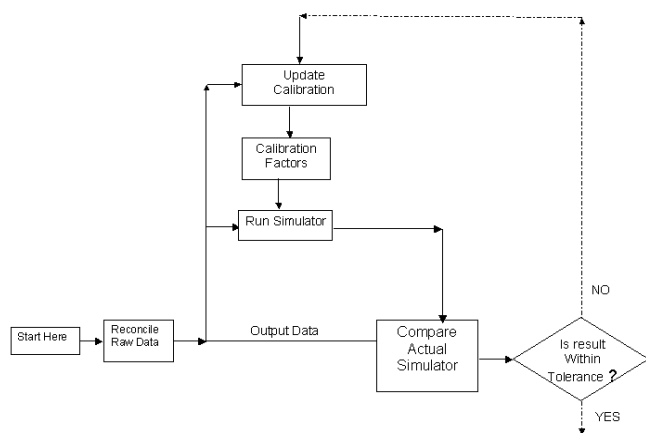


Figure 2. Algorithm of tuning and the CCR plant using Ref-sim module

Results and discussions

Actual test runs were gathered from the CCR unit described in the earlier sections. The data used for the calibration should be selected from the normal condition when no abnormalities, such as tower flooding, emergency depressurization and pump or compressor shut down were happen in the operation. Before using these data to estimate the tuning parameters, it was necessary to validate them. If a reasonable overall mass balance ($\pm 5\%$) cannot be calculated, the validity of test run was compromised. Additionally, from Table 1, it was found that the variation in feed specification was not considerable, and its effect on the yield and RON of the CCR plant can be ignored. The calibration parameters were then generated by Ref-sim module, and they were exported to the Petro-sim simulator to create the wide simulator of the CCR plant studied. The flow sheet of CCR wide simulator developed in Petro-sim environment is shown in Fig. 3. To evaluate and validate the simulation, the significant simulated variables i.e. outlet temperature of 1st, 2nd, 3rd, and 4th reactors, product volume yield, product RON, H₂ purity in recycle gas and coke deposition on the catalyst were compared against the actual data points.

Comparison of these momentous process variables for four data sets obtained during 6 months of study are shown in Tables 4 and 5. From these tables, it can be concluded that the average AAD % of the calculated outlet temperatures using the CCR simulator was less than 0.5 % for all data sets. In addition, the AAD % of simulation for yield, RON of product, H₂ purity in recycle gas and coke deposition on catalyst were 0.94 %, 1.098 %, 0.57 % and 0.347 %, respectively.

From the AAD% of the simulation, the validity of wide simulator was confirmed during 6 months of operation; therefore, it is reliable to study the under study CCR plant.

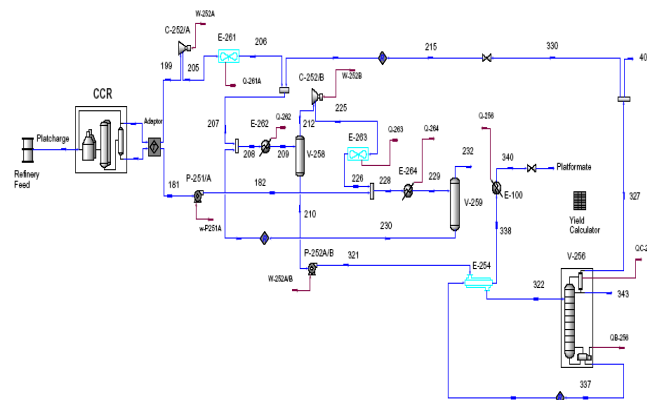


Figure 3. Wide simulation of CCR plant studied

After validating the CCR simulator, it was applied to sensitivity analysis of RON and yield of the produced gasoline. Fig. 4 and Fig. 5 show the sensitivities of RON and volume yield of the gasoline (or Reformate) to the temperature of reactors in the CCR plant studied.

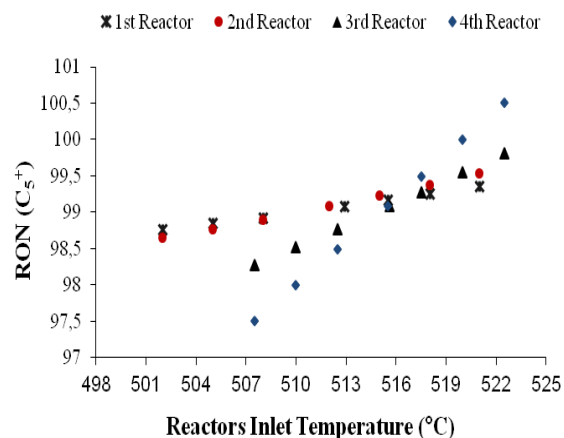


Figure 4. Effect of reactors inlet temperature on product RON

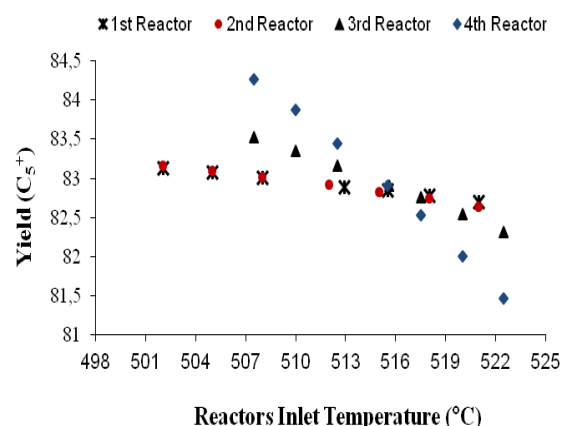


Figure 5. Effect of reactors inlet temperature on product volume yield

As observed in Figures 4 and 5, the RON of product was enhanced by increasing the temperature of reforming reactors. In contrast, the yield of the gasoline dropped by increasing the temperature.

Table 4. Comparison of outlet temperature of 1st to 4th reactors of the CCR plant studie

Variable	Unit	Test run 1		Test run 2		Test run 3		Test run 4		AAD %
		A	S	A	S	A	S	A	S	
1st reactor	° C	393.1	395.1	395.8	397.0	393	392	396.7	394.3	0.417
2nd reactor	° C	446.1	444.2	448.35	448.3	445.9	446.3	448.7	449.9	0.197
3rd reactor	° C	464.3	461.6	465.8	462.1	464.4	465.3	465.6	465.6	0.396
4th reactor	° C	480.8	476.65	480.9	475.8	479.9	479.7	480.9	479.6	0.558

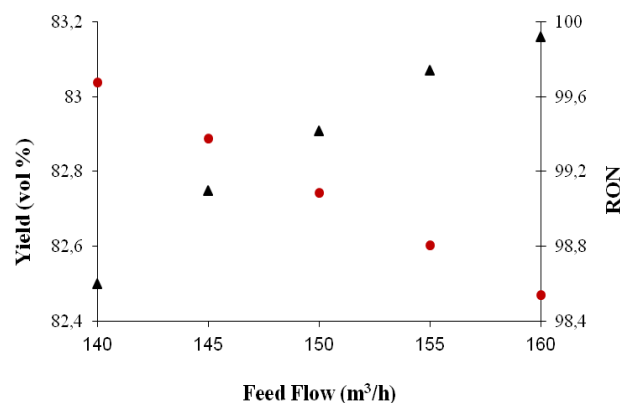
A: Actual, S: Simulation, AAD: Absolute Average Deviation

Table 5. Comparison of product yield, product RON, hydrogen purity in recycle gas and coke on catalyst of the CCR plant studied

Variable	Unit	Test run 1		Test run 2		Test run 3		Test run 4		AAD%
		A	S	A	S	A	S	A	S	
Yield	vol %	84.48	83.8	81.59	81.76	81.5	82.29	81.69	82.51	0.94
RON	-	99.1	97.54	98.73	97.44	98.88	98.1	98.8	98.14	1.087
H ₂ purity	mole %	89.27	89.49	88.48	88.87	88.3	88.95	88.37	89.13	0.57
Coke	wt %/	4.5	4.48	5.6	5.57	4.3	4.29	4.5	4.48	0.347

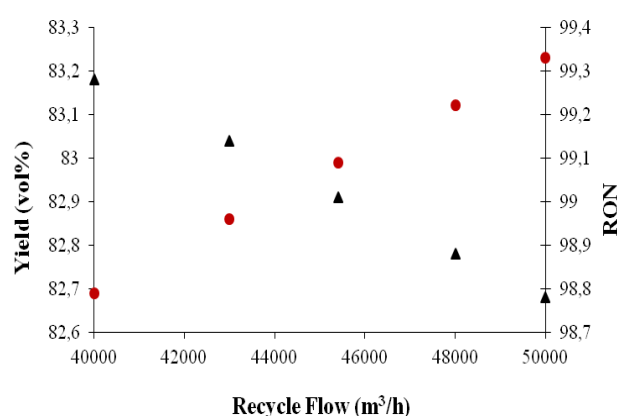
It may be supposed that the hydrocracking reactions are promoted more than the cyclization of paraffins, in consequence with increasing RON of the product, and also decreasing the volume yield. From Fig. 5, the optimum inlet temperature for all reactors is determined about 515 °C.

The effects of feed (heavy naphtha) and recycle flow rates on the RON and volume yield of gasoline are shown in Fig. 6 and 7. In these figures, for all cases, the left y-axis and (▲) points show the volume yield and the right y-axis and (●) points show the RON of the product.

**Figure 6.** Effect of feed flow rate on product RON and volume yield

As illustrated by the (▲) points in Fig.6, by increasing the feed flow rate, the yield of the process (left y-axis) increases, but the right y-axis and (●) points show that increasing the feed flow rate drops the RON of the reformat. Since the inverse of the feed flow rate divided by the amount of catalyst is linked with the residence time of the reactor, it affects directly the kinetic of the reforming reactions. Decreasing the feed flow rate increases residence time in consequence with higher severity, hence it increases product RON, and decreases

product yield. According to this figure, optimal feed flow rate of 148 m³ h⁻¹ is determined. As illustrated by the (▲) points in Figs.7, increasing the recycle flow rate decreases the yield of the process (left y-axis), but the right y-axis and (●) points show that increasing this decision variable increases RON of the reformat. In fact, increasing the recycle flow rate elevates H₂ to hydrocarbon ratio; therefore, hydrocracking reactions are strongly promoted. Enhancing hydrocracking reactions in reforming reactors increases RON of product, and decreases product volume yield. According to this figure, optimal recycle flow rate of 45000 m³ h⁻¹ can be determined.

**Figure 7.** Effect of recycle flow rate on product RON and volume yield

Finally, to evaluate the optimal determined point for the CCR plant, reactor temperature of all reactors, feed flow rate and recycle flow rate were manipulated from 512.9°C, 150 m³ h⁻¹ and 45400 m³ h⁻¹ to the estimated optimal point i.e. 515°C, 148 m³ h⁻¹ and 45000 m³ h⁻¹, respectively. It was observed that the actual RON and volume yield of the CCR plant were enhanced from 99.55 and 82.04 % to 99.67 and 82.4 %, respectively.

Conclusion

In this work, a commercial scale continuous catalytic reformer, a key process for producing high octane gasoline, was simulated. Operating data was obtained from a commercial scale CCR plant for calibrating the simulator using Ref-sim module; then, the wide simulator of CCR unit was created in Petro-sim environment. Results showed that for four data sets gathered during 6 months of study, the average AAD % of the simulated outlet temperatures, volume yield, RON of product, H₂ purity and coke deposition on the catalyst against actual data were about 0.5 %, 0.94 %, 1.098 %, 0.57 % and 0.347 %, respectively.

After validating the simulation, sensitivity analysis showed that the RON of product increased by elevating the temperature of the reactors, but the yield of the gasoline dropped. Moreover, it was found that increasing the feed flow rate increased the yield of the process, but the RON of the gasoline decreased by increasing that. In contrast, increasing recycle flow rate increased the product RON, but it decreased the volume yield.

According to this analysis, the optimal inlet temperature for all reactors, feed and recycle flow rates were 515°C, 148 m³ h⁻¹ and 45000 m³ h⁻¹, respectively. After setting the process variables on these optimal values, it was observed that the actual volume yield and RON of gasoline increased to 99.67 and 82.4 %, respectively. Therefore the efficacy of the presented optimization approach was confirmed.

References

- ¹Antos G.J., Aitani A.M., *Catalytic Naphtha Reforming*, CRC Press, New York, USA, Feb 1, 2004
- ²Zahedi G., Mohammadzadeh S., Moradi G., *Energy Fuels*, **2008**, 22, 2671–2677.

- ³Ancheyta J., Villafuerte E., *Energy Fuels*, **2000**, 14, 1032–1037.
- ⁴Gyngazova M. S., Kravtsov A. V., Ivanchina E. D., Korolenko M. V., Nikita V., *Chem. Eng. J.*, **2011**, 176–177, 134–143.
- ⁵Weifeng H., Hongye S., Shengjing M., Jian C., *Chin. J. Chem. Eng.*, **2007**, 15(1), 75–80
- ⁶Sa'idi M., Mostoufi N., Sotudeh R., *Int. J. Appl. Eng. Res.*, **2011**, 2(1), 115–124.
- ⁷Weifeng H., Hongye S., Yongyou H., Jian C., *Chin. J. Chem. Eng.*, **2006**, 14(5), 584–591.
- ⁸Shakoor Z. M., *Diyala J. Eng. Sci.*, **2011**, 4(2), 86–104.
- ⁹Arani H. M., Shirvani M., Safdarian K., Dorostkar E., *Braz. J. Chem. Eng.*, **2009**, 26(4), 723–732.
- ¹⁰Mohaddeci, S. R., Sadighi, S., Zahedi, S., Bonyad, H., *Petrol. Coal*, **2006**, 48(3), 28–35.
- ¹¹Mohadesi M., Mousavi H.S., *Chem. Prod. Process Model.*, **2012**, 7, 1–25.
- ¹²Arani H. M., Shokri S., Shirvani M., *Int. J. Chem. Eng. Appl.*, **2010**, 1(2), 159–164.
- ¹³*Petro-Sim User Guide*, KBC Advanced Technologies, KBC Profimatic, **2012**
- ¹⁴Ke-min, L., Hai-yan, G., Shie-wei, P., *J. Zhejiang Univ. Sci.*, **2005**, 590–596.
- ¹⁵Seif Mohaddecy S. R., Sadighi S., Bahmani M., *Petrol. Coal J.*, **2008**, 50(2), 60–68.
- ¹⁶Askary A., Karimi H., Rahimi M. R., *Farayandno J. Natl. Iranian Refining*, **2012**(37), 39–55

Received: 27.04.2013.
Accepted: 23.05.2013.



ONE POT THREE-COMPONENT MANNICH REACTION PROMOTED BY IRON(III) PHOSPHATE

Farahnaz K. Behbahani^{[a]*} and Leili Mohammadi Ziarani^[a]

Keywords: β-aminocarbonyl compounds, iron (III) phosphate, catalytic synthesis, one pot three component Mannich reaction

β-Aminocarbonyl compounds are selectively synthesized in high yields under extremely mild conditions via the condensation of aromatic aldehydes, aryl amines and ketones using catalytic amount of iron (III) phosphate under solvent free conditions. The use of readily available iron (III) phosphate as a reusable and recyclable catalyst makes this process quite simple, convenient, and environment-friendly.

Corresponding Authors

Tel: +98 026 34418145

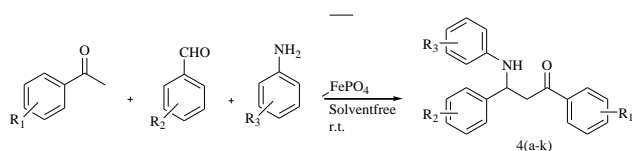
Fax: +98 026 34418156

E-Mail: Farahnazkargar@yahoo.com

[a] Department of chemistry, Karaj Branch, Islamic Azad University, Karaj, Iran.

Introduction

The Mannich reaction is an important carbon–carbon bond-forming process for the preparation of β-aminocarbonyl compounds and 1,2-amino alcohols.^{1,2} Several methods to improve and modify this three-component reaction^{3,4} have been reported such as the use of microwaves,^{5,6} or ultrasound irradiation,⁴ Lewis acids,⁷⁻¹⁰ Lewis bases,¹¹ Bronsted acids,^{12,13} rare and transition metal salts,¹⁴⁻¹⁶ or organo catalysts.¹⁷⁻²⁰ However, most catalysts are difficult to remove, and some of them are corrosive and volatile and often cause environmental problems. Hence, there is increased interest in the development of environmentally benign reactions and atom-economical catalytic processes for the synthesis of β-aminocarbonyl compounds. Herein, we report the three-component Mannich reaction of acetophenone derivatives with a variety of aromatic aldehydes and aromatic amines at room temperature catalyzed by anhydrous FePO₄ (Scheme 1).



R₁ = H, 4-NO₂, 4-MeO

R₂ = H, 4-NO₂, 3-NO₂, 4-Cl, 3-Cl, 2,5-diMeO, 2,6-diCl, 2,3-diMeO

R₃ = H, 4-Br, 4-NO₂, 4-MeO, 2,4-diF, (2-Cl)-4-F, 3,4-diMeO

Results and discussion

To the best of our knowledge, the direct one-step Mannich reaction catalyzed by anhydrous ferric phosphate (FePO₄) has not been reported previously. Although the reaction may be performed under solvent-free conditions on a small scale, it may also be carried out in ethanol; hardly any reaction occurred in methylene

chloride, THF, ether or water. Although they accelerate the rate and shorten the reaction time, higher temperatures (100°C) also promote side reactions and oxidation of the amines and of the aldehydes; thus the reaction in ethanol was performed at room temperature. From a green chemistry standpoint, solvent-free conditions are best and were chosen in the present investigation.

Initially, optimized conditions for the reaction of acetophenone, benzaldehyde and aniline in the presence of a catalytic amount of anhydrous iron(III) phosphate (5 mol %) were investigated under solvent-free conditions and at room temperature (Table 1). Various aromatic aldehydes, acetophenones and arylamines were used with catalytic amounts of FePO₄ to define the scope of this new protocol. Aldehydes bearing either electron-withdrawing groups (–Cl and –NO₂) or electron-donating group (–OCH₃) at the *m*- or *p*-positions were all suitable. The position of the substituents on the aromatic ring of amines has no obvious effect on this conversion. Other aromatic ketones such as propiophenone and desoxybenzoin, and aliphatic ketones such as cyclohexanone failed to give any product. The method is not applicable to aliphatic aldehydes (hexanal) and amines (cyclohexylamine).

It is likely that FePO₄ activates the aldehyde²⁷⁻³⁰ toward attack by the amine and also promotes the enolization of the acetophenones. Condensation of the amine with the aldehyde to the aldimine followed by nucleophilic attack by the enolized ketone on the aldimine would account for the formation of the observed product (Scheme 2).

Experimentals

Mps were measured in capillary tubes on an Electro Thermal 9200 apparatus and are uncorrected. IR spectra were recorded as on a KBr pellets Perkin Elmer FT-IR spectrometer. ¹H NMR and ¹³C-NMR spectra were obtained on Bruker DRX-300MHZ NMR instrument in CDCl₃. Chemical shifts are reported in parts per million (δ) relative to tetramethylsilane (δ 0.0) as an internal standard. Elemental analyses were performed by Elemental analyzer Vario EL. All starting materials were purchased from Merck Co. and used without further purification.

Table 1. FePO₄-catalyzed Mannich Reaction of Acetophenone with Aromatic Aldehydes and Aromatic amines under solvent-free conditions.

Product	R ₁	R ₂	R ₃	Time, min	Yield, %	M.p., °C	
						Found	Reported
4a	H	H	H	30	95	170-171	169-70 ²³
4b	H	4-NO ₂	H	15	90	90-95	89-91 ²⁴
4c	H	4-NO ₂	4-Br	20	90	180-186	Table 2
4d	H	3-NO ₂	4-Br	20	93	84-88	Table 2
4e	H	4-Cl	H	30	91	114-115	114-115 ²³
4f	4-NO ₂	H	H	45	87	169-171	170-171 ²⁵
4g	H	3-Cl	H	30	93	139-141	140-141 ²⁶
4h	4-MeO	4-NO ₂	4-MeO	25	94	100-101	Table 2
4i	H	H	4-NO ₂	45	85	184-186	185-186 ¹⁸
4j	H	2,5-(MeO) ₂	H	20	93	125-127	126-128 ²⁵
4k	4-MeO	H	H	300	95	123-126	123-125 ²⁶
4l ^a	H	2-Cl	H	300	75	135-137	134-136 ³¹
4m ^a	H	H	2-Cl	300	60	111-113	113-115 ³²
4n ^a	H	2-Cl	2-Cl	300	-	-	-
4o ^a	H	4-Me ₂ N	H	300	60	200-201	202-230 ²¹
4l	H	2,6-Cl ₂	H	60	68	125-127	126-128 ²⁶
4m	H	H	2-Cl,4-F	60	70	162-163	163-165 ²⁶
4n	H	H	2,4-F ₂	60	50	175-176	174-176 ²⁶
4o	H	H	3,4-(MeO) ₂	40	92	144-146	145-146 ²⁸
4p	H	2,3-(MeO) ₂	H	45	91	123-125	126-127 ³¹

a) The reaction was stirred in ethanol.

Table 2. M.p.'s, color, and elemental analysis data of 4c, 4d, 4h

Product	Mol. Formula	M.p., °C	Color	Elemental Analysis (Calcd)		
				C	H	N
4c	C ₂₁ H ₁₇ BrN ₂ O ₃	180-186	yellow	59.02 (59.31)	4.01 (4.03)	6.51 (6.59)
4d	C ₂₁ H ₁₇ BrN ₂ O ₃	84-88	yellow	59.02 (59.31)	4.02 (4.03)	6.50 (6.59)
4h	C ₂₃ H ₂₂ N ₂ O ₅	100-101	white	67.88 (67.97)	5.24 (5.46)	6.76 (6.89)

Table 3. FT-IR, ¹H NMR and mass spectroscopic data of 4c, d, h

No.	IR(KBr, cm ⁻¹)	¹ H NMR(δ: ppm)	GC/Mass
4c	3458.9(-NH stretching of secondary amine), 2978(-CH, stretching of aliphatic), 1690(C=O stretching of aromatic ketone), 1583, 1409.8(C=C-stretching of aromatic ring);	8.28 (2H, d, J=8.6Hz, ArH), 8.02 (2H, d, J=8.6Hz, ArH), 7.89 (2H, d, J=8.7Hz, ArH), 7.44 (1H, d, J=7.4Hz, ArH), 7.35 (1H, t, J=7.6Hz, ArH), 7.16 (1H, t, J=7.8Hz, ArH), 7.02 (2H, d, J=8.6Hz, ArH), 6.78 (1H, t, J=7.1 Hz, ArH), 6.66 (1H, d, J=7.8Hz, ArH), 5.07(1H, t, J=6.2Hz, NCH), 3.61 (2H, t, J=5.0Hz, COCH ₂);	425(M ⁺) 427(M+2) ⁺
4d	3434.8(-NH stretching of secondary amine), 2928(-CH, stretching of aliphatic), 1684(C=O stretching of aromatic ketone), 1563, 1353(C=C-stretching of aromatic ring)	8.00 (2H, d, J=9.1Hz, ArH), 7.88 (2H, d, J=7.2Hz, ArH), 7.60 (1H, t, J=7.2Hz, ArH), 7.51 (1H, s, ArH), 7.44 (2H, t, J=7.6Hz, ArH), 7.35 (1H, d, J=7.2Hz, ArH), 7.28 (1H, d, J=8.0HZ, ArH), 7.18 (1H, t, J=8.0Hz, ArH), 6.60 (2H, d, J=9.2Hz, ArH), 5.58 (1H, d, J=6.4Hz, NH), 5.02 (1H, q, J=6.0Hz, NCH), 3.48 (2H, d, J=6.0Hz, COCH ₂)	425(M ⁺) 427(M+2) ⁺
4h	3466(-NH stretching of secondary amine), 3077(-CH, stretching of aromatic), 1692(C=O stretching of aromatic ketone), 1587, 1295(C=C-stretching of aromatic ring)	8.00 (2H, d, J=9.1Hz, ArH), 7.88 (2H, d, J=7.2Hz, ArH), 7.60 (1H, t, J=7.2Hz, ArH), 7.51 (1H, s, ArH), 7.44 (2H, t, J=7.6Hz, ArH), 7.35 (1H, d, J=7.2Hz, ArH), 7.28 (1H, d, J=8.0Hz, ArH), 7.18 (1H, t, J=8.0Hz, ArH), 6.60 (2H, d, J=9.2Hz, ArH), 5.58 (1H, d, J=6.4Hz, NH), 5.02 (1H, q, J=6.0Hz, NCH), 3.48 (2H, d, J=6.0Hz, COCH ₂)	406(M ⁺)

General Procedure for the Synthesis of β -Aminocarbonyl Compounds

A mixture of an aromatic aldehyde (5 mmol), an aromatic amine (5 mmol), the acetophenone (5.5 mmol) and FePO₄ (0.0375 g, 5.0 mol%) was ground using a mortar and pestle at room temperature for the indicated times in Table 1. After completion of the reaction (monitored by TLC, eluent: *n*-hexane/ethyl acetate: 4/1), ethyl acetate (10 ml) was added to the reaction mixture. After the catalyst was filtered off, 10 ml of a saturated NaHCO₃ solution was added, and the organic layer was separated using a separatory funnel and dried over MgSO₄. The crude product obtained after evaporation of solvent was purified by recrystallization from ethanol or ethanol/water 3:2 (v/v) to give the pure compounds. The pure products were identified by comparison of their mp, IR, ¹H NMR with those of authentic samples⁵. Tables 2 and 3 provide the color, melting points, elemental analysis and spectroscopic data of new compounds **4c**, **4d**, **4h** respectively.

The reaction (entry 1, Table 1) was run in larger-scale using benzaldehyde (21.2 g, 200 mmol), aniline (18.6 g, 200 mmol) and acetophenone (25.2 g, 210 mmol) and FePO₄ (1.5 g, 200 mol%) in 150 ml of ethanol at room temperature for 5.0 h. After completion of the reaction, ethanol was removed and the product was obtained 57.2 g in 95%.

At the end of the reaction, the catalyst was recovered by gravity filtration and recycled after washing with ethyl acetate and could be subjected to five additional runs and after five runs the yield was reduced only slightly.

Conclusion

In summary, the present work has reported a general, efficient, convenient, catalytic and green reaction medium for the selective synthesis of β -aminocarbonyl compounds by the Mannich condensation of acetophenones with aromatic aldehydes and aromatic amines in the presence of anhydrous FePO₄ catalyst. This general, simple, rapid and clean protocol does not require the organic solvent and energy and is atom-economical.

References

- ¹Kobayashi, S. and Ishitani, H., *Chem. Rev.*, **1999**, 99, 1069.
- ²Cordova, A. *Acc. Chem. Res.*, **2004**, 37, 102.
- ³Syamala, M. *Org. Prep. Proced. Int.*, **2005**, 37, 103.
- ⁴Syamala, M., *Org. Prep. Proced. Int.*, **2009**, 41, 1.
- ⁵N. E. Leadbeater, H. M. Torenus and H. Tye, *Mol. Divers.*, **7**, 135 (2003).
- ⁶Aberg, V., Almstedt, H., Westermarck, A. and Almqvist, F. *J. Org. Chem.*, **2004**, 69, 7830.
- ⁷Hu, D. Y., Song, B. A., Zhang, G. P., Yang, S., He, W., Wu, Y. L., Hong, Y. P., Jin L. H. and Liu, G., *Chin. J. Org. Chem.*, **2005**, 25, 845.
- ⁸Loh, T. P., Liung S. and Wei, L. L. *Tetrahedron Lett.*, **2000**, 39, 323
- ⁹Komoto I. and Kobayashi, S., *Chem. Commun.*, **2001**, 1842.
- ¹⁰Yang, Y. Y., Shou W. G. and Wang, Y. G., *Tetrahedron*, **2006**, 62, 10079.
- ¹¹Takahashi, E., Fujisawa H. and Mukaiyama, T., *Chem. Lett.*, **2004**, **33**, 936.
- ¹²Yi, L., Lei, H. S., Zou J. H. and Xu, X. J. *Synthesis*, **1991**, 717.
- ¹³Iimura, S. Nobutou, D. Manable K. and Kobayashi, S. *Chem. Commun.*, **2003**, 1644.
- ¹⁴L. Wang, J. Han, J. Sheng, H. Tian and Z. Fan, *Catal. Commun.*, **2005**, 6, 201.
- ¹⁵Chen, X. M., Li X. S. and Chan, A. S. C., *Chin. Chem. Lett.*, **2009**, 20, 407. *Chem. Abstr.*, **2009**, 151, 491365x.
- ¹⁶Dai, Y. Li, B. D. Quan H. D. and Lü, C. X. *Chin. Chem. Lett.*, **2010**, 21, 31.
- ¹⁷Yi, W. B. and Cai, C., *J. Fluorine Chem.*, **2006**, 127, 1515.
- ¹⁸Rodriguez, B. and Bolm, C., *J. Org. Chem.*, **2006**, 71, 2888.
- ¹⁹List, B., Pojarliev, P., Biller W. T. and Martin, H. J., *J. Am. Chem. Soc.*, **2002**, 124, 827.
- ²⁰Ibrahim, I., Casas J. and Cordova, A., *Angew. Chem. Int. Ed.* **2004**, 43, 6528.
- ²¹Li, Z., Ma, X. L., Liu, J., Feng, X., Tian G. Q. and Zhu, A. G., *J. Mol. Catal. A. Chem.*, **2007**, 272, 132.
- ²²Shen, W., Wang L. M. and Tian, H., *J. Fluorine Chem.*, **2008**, 129, 267.
- ²³Khan, A. T., Parvin T. and Choudhury, L. H., *Eur. J. Org. Chem.*, **2008**, 834.
- ²⁴Shailaja, M., Manjula A. and Rao, B. V., *Indian J. Chem.*, **2010**, 49, 482.
- ²⁵Jafari, A. A., Moradgholi F. and Tamaddon, F., *Eur. J. Org. Chem.*, **2009**, 1249.
- ²⁶Wang, R., Li, B. G., Huang, T. K., Shi L. and Lu, X. X., *Tetrahedron Lett.*, **2007**, 48, 2071.
- ²⁷Behbahani, F. K., Yektanezhad T. and Khorrami, A. R., *Heterocycles*, **2010**, 81, 2313.
- ²⁸Heravi, M. M., Behbahani, F. K., Zadsirjan V. and Oskooie, H. A., *Heterocycl. Commun.*, **2006**, 12, 369.
- ²⁹Behbahani, F. K. and Homafar, M., *Synth. React. Inorg. M.*, **2012**, 42, 291.
- ³⁰Behbahani, F. K. Ziaei, P., *Chinese J. Chem.*, **2012**, 30, 65.
- ³¹Wu, H. Shen, Y. Fan, L.-Y. Wan, Y. Zhang, P. Chen C.-F. and Wang, W.-X., *Tetrahedron*, **2007**, 63, 2404.
- ³²Wang, M., Song, Z.-G., Wan, X., Zhao, S., *Monatsh. Chem.* **2009**, 140, 1205.

Received: 07.04.2013.

Accepted: 29.05.2013.



QUASI-CHEMICAL REACTIONS IN IRRADIATED SILICON

Temur Pagava^[a], and Levan Chkhartishvili^{[a]*}

Keywords: radiation defects in crystals, quasi-chemical reactions, silicon.

There are described the quasi-chemical reactions that take place between radiation defects and impurities in irradiated silicon. It has been experimentally investigated single-crystalline n- and p-type silicon doped, respectively, with phosphorus or boron, irradiated with high-energy electrons or protons and subjected to the high-temperature isochronous annealing. Rates of quasi-chemical reactions are found to be dependent on the charge-states of reactants and then controllable by varying the irradiation conditions – beam-intensity, irradiation temperature and IR light exposure during the irradiation, as well as temperature of annealing of the previously irradiated samples. It is shown that the quasi-chemical reactions can serve as effective tools for tuning the electronic properties of silicon, the basic material of micro- and nanoelectronics.

* Corresponding Author's

E-Mail: chkharti2003@yahoo.com

[a] Department of Physics, Georgian Technical University, 77 Merab Kostava Avenue, Tbilisi, 0175, Georgia

Introduction

As is known, structural imperfections and chemical impurities presented in a crystalline lattice can react quasi-chemically with each other resulting in new defect-complexes. In particular, some of quasi-chemical reactions in semiconductors lead the formation of electrically active defects those are thermally stable and, therefore, significantly affect electronic properties of the material. For this reason, the control utilizing quasi-chemical reactions should be considered as an important tool to obtain new crystalline semiconductor materials with predetermined set of desired electronic properties.

A series of our previous studies (see, e.g., papers¹⁻¹⁰) devoted to single-crystalline silicon, basic material of modern ICs, irradiated with high-energy particles has revealed a number of quasi-chemical reactions involving radiation-induced defects, which significantly affect semiconducting properties of this material. Here our purpose is to describe and systemize quasi-chemical reactions that take place in irradiated silicon, as well as identify their potential applications. The paper is organized as follows.

After present Introduction we give the Experimental part describing the samples studied and the measuring methods applied. Following section characterizes the quasi-chemical reactions, which occur with primary radiation defects in silicon at low (room) temperature and low intensity of irradiation.

Rate and even possibility of a quasi-chemical reaction are essentially determined by the charge-states of reactants as the strength of electrostatic attraction between oppositely charged defects and/or impurities and repulsion between like-charged ones, respectively, favors or hampers the reaction. But, charge-states of radiation-defects depend on the conditions of irradiation. It is a reason why special sections are devoted to the influence on quasi-chemical reactions in crystalline silicon of factors such as irradiation intensity and lightening or heating in process of irradiation.

It should be borne in mind that the quasi-chemical reactions take place not only during the irradiation but also the aging of an irradiated sample in ambient conditions or its isochronous annealing at elevated temperatures. For this reason, the influence of annealing on the quasi-chemical reactions in irradiated silicon is presented by the special section as well.

At the end of the paper we summarize obtained results and briefly outline their Prospects for practical applications.

Experimental

We have mainly investigated single-crystalline zone-melted silicon (Si) containing background impurity oxygen (O) in concentration of $\sim 10^{16}\text{cm}^{-3}$ as it was determined from the IR absorption spectrum. The density of growth dislocations in test samples estimated from the etching pits does not exceed $4 \cdot 10^4\text{cm}^{-2}$. In addition, it has been studied several samples grown by Czochralski method, i.e. with significantly higher oxygen content: $\sim 10^{18}\text{cm}^{-3}$. Samples of both origins contain $\sim 10^{16}\text{cm}^{-3}$ of background impurity carbon (C). It has been investigated samples of n- and p-type conduction doped with phosphorus (P) or boron (B) at concentrations of $\sim 10^{13}$ – 10^{14} and $\sim 10^{14}\text{cm}^{-3}$, respectively. The samples were prepared in form of bars of sizes of $1\text{mm} \times 3\text{mm} \times 10\text{mm}$.

These samples were irradiated with 2 and 8MeV electrons or 25MeV protons. Irradiation carried out in the direction perpendicular to the samples largest faces (111). Irradiation doses, $1.0 \cdot 10^{14}$ – $5.0 \cdot 10^{15}$ for electrons, and $2.7 \cdot 10^{12}$ and $8.1 \cdot 10^{12}\text{cm}^{-2}$ for protons, were adjusted so that at nitrogen boiling point (77K) the concentration of majority charge carriers trapped by radiation defects did not exceed the dopants concentration. Used intensities of electron- and proton-beams were of $\sim 10^{12}$ – 10^{13} and $\sim 10^{11}\text{cm}^{-2}\cdot\text{s}^{-1}$, respectively. Irradiations were carried out both at room (300K) and elevated temperatures during heating in the range 20–400°C. It has been also studied the effect of IR-lightening during irradiation on the kinetics of defects formation. From levels corresponding the different radiation defects, electrons were excited into the conduction band by the IR monochromatic light with photons energy of $h\nu=0.2$ – 0.5eV . The samples were annealed isochronously in the temperature range of 80–600°C with steps of 10°C for 10min at a fixed temperature.

To identify the nature of electrically active defects resulting from quasi-chemical reactions accompanying irradiation and heat treatment, from Hall-measurements it was determined their ionization energies and thermal stabilities, i.e., annealing temperatures. Ohmic contacts necessary in such measurements were prepared by rubbing aluminum (Al) on surfaces of test samples. Temperature-curves of majority carriers' Hall-concentration $N-T$ were taken from 77 to 300K. In order to illustrate, some of these characteristics are shown in Figure 1. Methodology of determining the concentration of defects in irradiated silicon from the curves $N-T$ and $N-T_{\text{ann}}$, where T_{ann} is the annealing temperature, had been described in details in above cited papers.

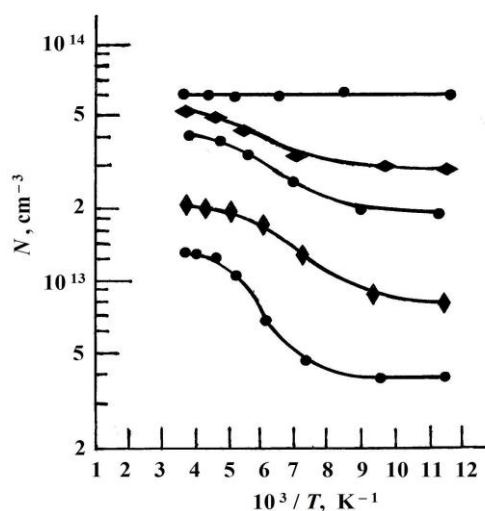


Figure 1. Temperature-dependence of electron concentration in n-Si crystals 1 – before irradiation, 2 – after electron-irradiation with dose of $1.5 \cdot 10^{14} \text{cm}^{-2}$ at 300K, and 3–5 – after annealing at temperatures 100, 150 and 300°C

Effectiveness of introduction of various radiation-induced defects $\eta = \partial N_{\text{RD}} / \partial \Phi$, where N_{RD} is the concentration of defects of given type and Φ is the irradiation dose, measured after cycles of irradiation accompanied with IR lightening or isochronous annealing. For this purpose, we used the method of local irradiation followed by the measuring the bulk photo-emf U_{ph} along the irradiated part of the sample. These measurements were carried out at a fixed dose and, therefore, photo-emf was proportional of the effectiveness of introduction of radiation defects: $U_{\text{ph}} \sim \eta$. The relative errors of all these measurements do not exceed $\sim 10\%$.

Results and Discussion

Charge-states of vacancies and interstitials at their formation in process of low-intensity irradiation at room temperature

As is known,¹¹ the irradiation of silicon with beams of elementary particles forms primary radiation defects – vacancies and interstitials, so-called Frenkel pairs. Some of them experience mutual annihilation or recombination at crystal surfaces. The remaining nonequilibrium Si-interstitials are more mobile than vacancies and, therefore, rapidly form complexes with background impurity O and/or

C. Although, concentrations of these complexes are extremely low. The majority of interstitials tend to form clusters¹² which substantially do not interact with other structural defects or impurity atoms. As for the non-equilibrium (radiation) vacancies remaining in the bulk, they are also quite mobile and participate in different quasi-chemical reactions forming radiation defects of high-orders. Many of these vacancy-complexes are electrically active and hence largely determine electrical parameters of the semiconducting material.

In the quasi-chemical reactions occurring in irradiated n-Si crystals, it can be formed following electrically active vacancy-complexes: A-center (background impurity oxygen + vacancy: OV), E-center (dopant atom, usually, phosphorus + vacancy: PV), divacancy V_2 (or complex VV), etc. In p-Si crystals, there are formed complexes BV (dopant atom, usually, boron + vacancy), B/OV (interstitial boron atom + background oxygen + vacancy), OCV₂ (background oxygen and carbon + divacancy), etc.

In order to determine the sign of electric charge of vacancies in n-Si crystals, we irradiated them with 25MeV protons at 300K. It turned out that in initial samples in almost the entire temperature range of measurements, $N-T$ dependence corresponds to ionization of shallow donors associated with P: $N \approx 6 \cdot 10^{13} \text{cm}^{-3} \approx \text{const}$ (Figure 2, Curve 1). The temperature-dependence of the electron concentration measured after proton irradiation with the dose of $2.7 \cdot 10^{12} \text{cm}^{-2}$ corresponds to depletion of centers with electron energy level at $E_C - 0.17 \text{eV}$ (Figure 2, Curve 6).

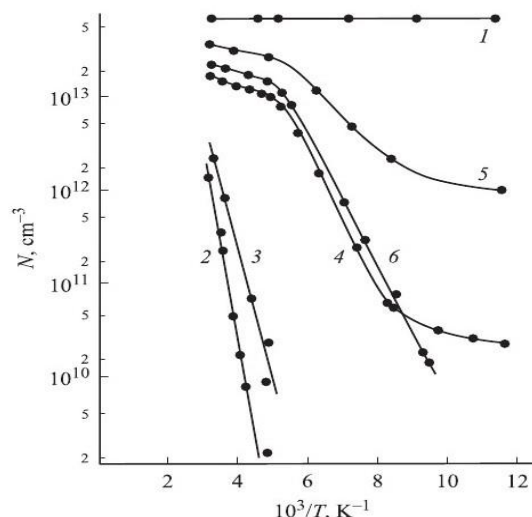
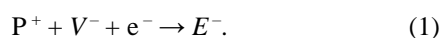


Figure 2. Temperature-dependence of electron concentration in n-Si crystals 1 – before irradiation, after irradiation at 300K by 25MeV protons with doses of 2–5 – $8.1 \cdot 10^{12}$ and 6 – $2.7 \cdot 10^{12} \text{cm}^{-2}$, and annealed at temperatures 4 – 150 and 5 – 300°C

As a result of irradiation with dose of $8.1 \cdot 10^{12} \text{cm}^{-2}$, $N-T$ curves reveal straight-line sections those correspond to depletion of centers at $E_C - 0.42 \text{eV}$ (Figure 2, Curve 3) or are associated with centers with energy levels placed at $E_C - 0.54 \text{eV}$ (Figure 2, Curve 2). As is known,¹² the level $E_C - 0.17 \text{eV}$ is attributed with A-centers, the level $E_C - 0.42 \text{eV}$ with E-centers and divacancies V_2 (or reveals their superposition), and, finally, the level $E_C - 0.54 \text{eV}$ with

centers whose nature remains uncertain (the assumption¹² that it belongs to divacancies has been questioned). Curves 4 and 5 in Figure 2 correspond to depletion of *A*-centers and are obtained by measuring the samples irradiated with the dose of $8.1 \cdot 10^{12} \text{cm}^{-2}$ followed by annealing at 150 and 300°C.

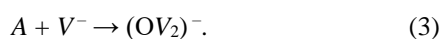
Usually, in n-Si crystals irradiated with ~2MeV electrons at room temperature, formation efficiency of *E*-centers is somewhat higher than that for *A*-centers, notwithstanding the fact that the concentration of background O is about 3 orders of magnitude higher compared to that of dopant P. The high efficiency of introduction of *E*-centers must be due to the negative charge-state of vacancies, namely, their Coulomb attraction by ionized donors P^+ . Thus, the quasi-chemical reaction of formation of *E*-centers should be accompanied by the capture of an electron from the conduction band:



At room temperature *A*-centers with level at $E_C - 0.17 \text{eV}$ are not filled and, therefore, are in electrically neutral state. On the other hand, as noted above in silicon background oxygen is electrically inactive as well. From this we conclude that formation of an *A*-center from the negatively charged vacancy should be accompanied by excitation of an electron:



However, note that electron formed in this reaction, probably, does not move freely in the conduction band, but is captured by a deep center. As for the formed electrically neutral *A*-center, it can join with another (negatively charged) vacancy:



At room temperature, this oxygen–divacancy complex with deeper level at $E_C - 0.50 \text{eV}$ is negatively charged and due to the electrostatic repulsion further joining with negatively charged vacancies highly unlikely. Since at room temperature the *E*-centers with electron level at $E_C - 0.44 \text{eV}$ are negatively charged, the formation of similar divacancy-complexes is impossible as well. Joining of negatively charged vacancy V^- directly with the divacancy is hampered because its level $E_C - 0.39 \text{eV}$ is too deep enough and, therefore, at room temperature divacancy is negatively charged: V_2^- . It should be noted that the formation of divacancies V_2 by diffusion mechanism during the irradiation at room temperature from pairs of negatively charged monovacancies is unlikely. It is assumed that divacancies are formed as primary radiation defects (along with Frenkel pairs).

The reality of above listed quasi-chemical reactions is proved by the Figure 2, which shows that in n-Si during the irradiation at room temperature there are formed *A*- and *E*-centers, divacancies and OV_2 -complexes. Note that the level $E_C - 0.50 \text{eV}$ corresponding to the complex OV_2 we could not detect directly.

However, the existence of such a defect can be argued indirectly, by the increase in electrons concentration in process of isochronous annealing in the temperature range $\geq 500^\circ\text{C}$.

Since impurity B-atom in silicon crystals creates the shallow acceptor level, then at room temperature B-atoms are ionized by capturing of electrons from the valence band: B^- . Therefore, the dopant atoms in p-Si could not join with vacancies if they are negatively charged (like n-Si). On the other hand, in p-Si crystals produced by doping with boron and irradiated with electrons at room temperature there are found secondary radiation defects BV with the energy level at $E_V + 0.45 \text{eV}$. This is a deep level capable to capture a hole from the valence band, what will lead to a positively charged defect-complex. Thus, $(BV)^+$ complex should be formed by the following reaction:



Applying the method of local irradiation followed by the bulk photovoltage measurements, we have experimentally demonstrated^{1,5} that at room temperature and absence of any external influences the charges of primary radiation defects in n-Si crystals are of different sign of charge carriers, while in p-Si are of same sign. Therefore, we conclude that interstitials at the time of formation at room temperature both in n-Si and a p-Si should be charged positively.

Influence of irradiation intensity on efficiency of introduction of radiation defects

Influence of irradiation intensity φ on the efficiency of introduction of radiation defects η in n-Si has been studied for the series of three zone-melted samples doped to levels of $1 \cdot 10^{13}$, $6 \cdot 10^{13}$ and $2 \cdot 10^{14} \text{cm}^{-3}$ irradiated with 2MeV electrons at the dose of $5 \cdot 10^{15} \text{cm}^{-2}$. Measurements performed at room temperature, i.e. in the region of depletion of *A*-centers. Hence, the potential barrier between irradiated and non-irradiated parts of a sample was determined by changes in concentrations of radiation defects with deeper levels: *E*-centers and divacancies V_2 . It has been found that in certain interval the efficiency of introduction of radiation defects versus electron-beam intensity $\eta(\varphi)$ achieves the maximum that with increasing in electron concentration N moves towards higher values of φ . In crystals with above levels of doping, the critical values of intensity, respectively, are $2 \cdot 10^{12}$, $5 \cdot 10^{12}$ and $1 \cdot 10^{13} \text{cm}^{-2} \cdot \text{s}^{-1}$ (see Figure 3).

The $\eta(\varphi)$ curve having the maximum, position of which on φ -axis depends on N , suggest that there is satisfied an optimal relation between rate of creation of primary radiation defects, on the one hand, and changes in free charge carriers concentration, on the other hand. For small values of φ , all nonequilibrium vacancies become negatively charged and creation of divacancies by diffusion mechanism is unlikely because of strong electrostatic repulsion between vacancies. Under these conditions, high efficiency of formation of monovacancy defects, i.e. *E*-centers, according to the reaction (1) is expected. With increasing in the irradiation intensity not all the formed vacancies have a time to become negatively charged before joining with each other.

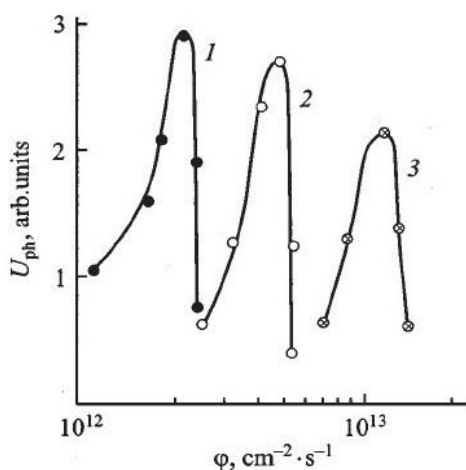


Figure 3. Bulk photo-emf versus electron-beam intensity in locally irradiated n-Si crystals. Energy of incident electrons is 2MeV and dose is $5 \cdot 10^{13} \text{cm}^{-2}$. Concentration of electrons is: 1 – $1 \cdot 10^{13}$, 2 – $6 \cdot 10^{13}$ and 3 – $2 \cdot 10^{14} \text{cm}^{-3}$

Accordingly, it increases the efficiency of formation of divacancies in the reaction,



which leads to the increase in share of divacancy complexes in the total concentration of radiation-induced defects.

But, this also reduces the total concentration of defects. Accordingly, photovoltage U_{ph} decreases and $U_{ph}(\eta)$ curve reveals a maximum. In crystals with different electron concentrations, the recharging of non-equilibrium vacancies occurs at different irradiation intensities that cause the different displacements of the maximum along the ϕ -axis.

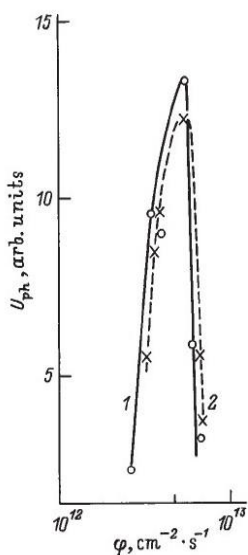


Figure 4. Bulk photo-emf versus electron-beam intensity in locally irradiated p-Si crystals. Energy of incident electrons equals to 2MeV and dose is $5 \cdot 10^{15} \text{cm}^{-2}$. 1 – without electric field and 2 – with biasing electric field of strength of 110V cm^{-1} .

Influence of the intensity of irradiation with 2MeV electrons on the defects formation in silicon has been also investigated for p-type material. It has been found that the

shape and position of the maximum is not changed substantially upon application of a constant electric field to the sample during its irradiation (Figure 4). Consequently, a part of reagents would be unchanged. This result is consistent with above interpretation that in such conditions there are mainly formed charged complexes $(BV)^+$. It is clear that such a product cannot be obtained via quasi-chemical reaction between oppositely charged reagents. Complex $(BV)^+$ is formed from the neutral complex of ionized dopant plus current carrier, $B^- + e^+$, and charged vacancy V^+ .

Influence of IR illumination in process of irradiation on defects formation

To study the effect of IR illumination on the kinetics of defects formation in silicon during 2MeV electron irradiation at room temperature, it has been studied n-Si samples, in which electrons from different levels of radiation defects are excited into the conduction band by monochromatic IR illumination with appropriate photon energies.

Isochronous annealing of irradiated crystals were performed at 200, 300 and 600°C, which are sufficient for complete annealing, respectively, E-centers, divacancies and complex-defects with high thermal stability – PV_2 , O_2V_2 , etc.¹²

As can be seen from Figure 5, the $\eta_E(h\nu)$ dependence has two minima at $h\nu_1=0.28\text{eV}$ and $h\nu_2=0.44\text{eV}$ (Curve 1); $\eta_A(h\nu)$ has the sharp maximum at $h\nu_1$ and it passes through the minimum at $h\nu_2$ (Curve 2); the $\eta_{TSC}(h\nu)$ has two maxima at $h\nu_1$ and $h\nu_2$ (Curve 3). As for the $\eta_{V_2}(h\nu)$ dependence, it has the single maximum at $h\nu_1$ (Curve 4).

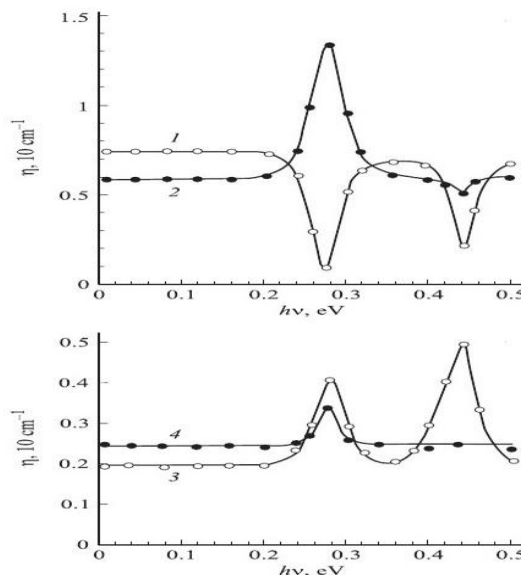
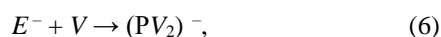


Figure 5. Efficiency of introduction of radiation-induced defects in n-Si versus energy of quantum of IR illumination in process of electron-irradiation: 1 – E-centers, 2 – A-centers, 3 – defects with high thermal stability, 4 – divacancies

As noted above, at 300 K in n-Si crystals primary radiation defects – interstitial atom and vacancy – are charged oppositely: I^+ and V^- . Therefore, in dark the rate of

their recombination should be too high. On the other hand, it is known¹³ that monovacancy in the charge state V^- corresponds to the energy level located at $E_C-0.28\text{eV}$. When samples during irradiation are exposed by monochromatic IR light with quanta energy of $h\nu_1=0.28\text{eV}$, the vacancies are transferred into the neutral charge state and, accordingly, the rate of self-recombination of positively charged interstitials and neutral vacancies decreases. It takes also the place the increase in the concentration of non-equilibrium neutral vacancies, what leads to an increase in the efficiency of introduction of majority of secondary radiation defects. Although, in view of reducing in electrostatic attraction between ionized, i.e. positively charged, P atom and neutral vacancy the efficiency of introduction of E -centers decreases. In addition, some of the generated E -centers participating in quasi-chemical reactions with neutral vacancies are rebuilt in form of divacancy-defects,

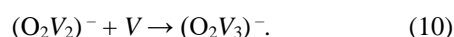
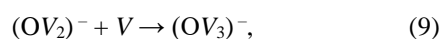
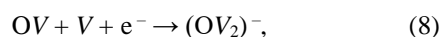


It leads to an additional decrease in η_E and the deep minimum on $\eta_E(h\nu)$ curve (Figure 5).

Non-equilibrium neutral vacancies that were not captured by positively charged P atoms are trapped by neutral O-atoms, the concentration of which is almost 3 orders of magnitude greater:



As a result, $\eta_A(h\nu)$ curve reveals the sharp peak at $h\nu_1=0.28\text{eV}$. For a neutral vacancy it will also be easier to interact with other deep and, therefore, negatively charged at room temperature complexes, what makes it possible the following series of conversions:¹²



Defect-complexes formed in reactions (6–10) are characterized by high thermal stability and lead to an increase in η_{TSC} (Figure 5, Curve 3). It should be noted that complexes OV_2 and O_2V_2 exist in low concentrations and, therefore, complexes OV_3 and O_2V_3 formed at their basis can be found in negligible concentrations. Hence, in the vicinity of $h\nu_1$ the value of η_{TSC} is mainly determined by the concentration of complexes PV_2 .

The cascade mechanism of formation of divacancies prevails over the diffusion mechanism, i.e. divacancies are mostly formed as primary radiation defects. The small increase in η_{V_2} at $h\nu_1$ (Figure 5, Curve 4) can be attributed to the increased probability of formation of divacancies from a pair of neutral monovacancies by diffusion mechanism:



As a result of all these processes in n-Si crystals irradiated with electrons under the IR illumination with photon energy of $h\nu_1=0.28\text{eV}$, the total concentration of radiation-induced defects, and, hence, the efficiency of their introduction remains essentially unchanged: it increases only ~1.2-times.

Note for comparison that the doping with germanium (Ge) perhaps more than 7-fold increases the radiation resistance of silicon due to practically complete eliminating the formation of A -centers even in crystals with elevated concentration of oxygen.¹⁴⁻¹⁷

When n-Si crystal in process of irradiation is exposed to the light with energy of quanta of $h\nu_2=0.44\text{eV}$, negative E -centers become neutral. And due to the weakening in the electrostatic interaction between a neutral E -center and a negative vacancy the probability of formation of PV_2 complexes increases:



If we assume that the irradiation produces only monovacancy defects, then the concentrations of radiation-induced defects N_{RD} and primary vacancies N_V are the same: $N_{RD}=N_V$. But, if in parallel with monovacancies there are formed divacancies then $N_{RD}<N_V$. This inequality explains the observed decrease in η_E and η_A (Figure 5, Curves 1 and 2), appearance of the peak on $\eta_{V_2}(h\nu)$ curve (Figure 5, Curve 3) and the slight (~1.2-fold) decrease in the number of radiation-induced defects in n-Si crystals irradiated under the IR illumination with photon energies of $h\nu_2=0.44\text{eV}$.

Thus, our studies have shown that IR illumination with suitable photon energy can significantly alter the efficiency of introduction of various radiation-induced defects in crystalline silicon, but the total efficiency will remain almost unchanged.

Influence of irradiation temperature on efficiency of defects introduction

The change in the charge-state of radiation defects occurs not only under the IR illumination, but also due to changes in irradiation temperature T_{irr} . Effect of the T_{irr} on the defects kinetics in silicon we have investigated for n-type crystals doped with phosphorus. Namely, we used zone-melted single crystals with electrons concentration of $6 \cdot 10^{13}\text{cm}^{-3}$. Figure 6 shows the efficiency of defects introduction versus the irradiation temperature. As one can see, at 150°C $\eta_E=0$, and $\eta_A(T_{irr})$ and $\eta_{TSC}(T_{irr})$ pass through maxima (Curves 1 and 4). In the region $100\text{--}150^\circ\text{C}$, Curve 2 passes through the minimum and in the region $170\text{--}440^\circ\text{C}$ efficiency decreases monotonically. This means that $\eta_{TSC} \approx \eta_{PV_2} + \eta_{OV_2} + \eta_{O_2V_2} + \eta_{OV_3}$.

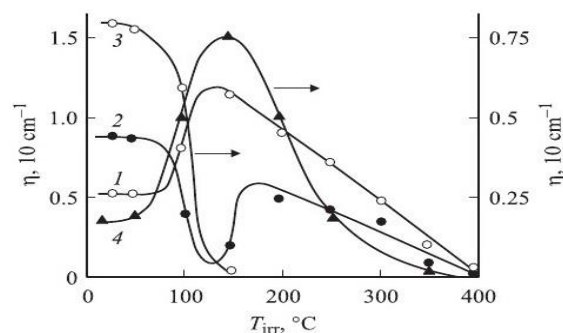
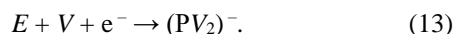


Figure 6 of defects introduction versus irradiation temperature in . Efficiency n-Si crystals irradiated by 2MeV electrons: 1 – A -centers, 2 – divacancies, 3 – E -centers, 4 – defects with high thermal stability

The η_E decreases with increasing T_{irr} up to 100–150°C, apparently, due to two processes: dissociation of a PV complex into P and V and transformation of a neutral E-center into more complex and more stable defect PV₂:



Certain part of the non-equilibrium vacancies that have not been captured by neutral E-centers can be used for the formation of A-centers, on the basis of which the OV₂ complexes are formed in subsequent reaction



Within the band gap, OV₂ complexes correspond to the level of $E_C - 0.50\text{eV}$.¹² Consequently at room temperature these complexes are negatively charged like the monovacancies and the electrostatic repulsion hampers extension of the reaction (14) to form the complex OV₃.

Non-monotonic $\eta_{V_2}(T_{\text{irr}})$ curve can be explained by changes in the charge-state of monovacancies. At low irradiation temperatures (20–80°C), with the accumulation of E-centers and the removal of electrons from the conduction band, up to the temperature of deionization of E-centers, the deal of neutral vacancies increases and crystal saturation by the vacancies is avoided by forming the divacancies V₂. Dissociation of E-centers increases the deal of negative vacancies. In corresponding region, dependence of the efficiency of introduction of negative divacancies on irradiation temperature passes through the minimum (Figure 6, Curve 2), probably, due to electrostatic repulsion of charged vacancies those in more extent are spent on the formation of A-centers. Further increase in T_{irr} shifts the Fermi level to the middle of band gap and it starts recharging of vacancies: $V^- \rightarrow V + e^-$. The deal of neutral vacancies and η_{V_2} again increase. These processes can explain the existence of peaks in the vicinity of 150°C in the Figure 6 (Curves 1 and 4). At higher temperatures, $T_{\text{irr}} \geq 150\text{--}300^\circ\text{C}$, the dissociation of A-centers dominates and V₂ and OV₂ form more stable defect-complexes:



and



which are annealed at 410 and 470°C, respectively.¹²

When $T_{\text{irr}} = 400^\circ\text{C}$, there is satisfied the approximate equations: $\eta_E = \eta_A = \eta_{\text{TSC}} \approx 0$ (Figure 4, Curves 1 and 2), despite the fact that the annealing temperature for these complexes $\geq 400^\circ\text{C}$. This fact indicates that they are formed on the basis of the E- and A-centers according to reactions (13–16). In the range 20–150°C, efficiency of introduction of radiation defects with high thermal stability η_{TSC} increases due to the formation of PV₂ complexes on the basis of neutral E-centers, while in the range of 150–400°C it reduces what can be attributed to the decrease in η_E and η_A , i.e. rates of formation of E- and A-centers, which are formed on the basis of thermal-stable complexes PV₂, OV₂, O₂V and OV₃. Last is annealed at $\geq 400^\circ\text{C}$.

Summarizing the results we can conclude that the increase in the irradiation temperature of silicon doped with phosphorus leads to the increase in efficiency of introduction multi-vacancy phosphorus- or oxygen-containing radiation defects.

Quasi-chemical reactions in irradiated silicon in process of isochronous annealing

When the annealing temperature increases, products of dissociation of relatively less stable defect complexes increasingly come into quasi-chemical reactions with impurity atoms or structural imperfections of the structure. The result is the formation of new more stable complexes, the increase in the concentration of some existing defects or their conversion into different type defects. In electron-irradiated zone-melted n-Si crystals with relatively low content of oxygen, $9 \cdot 10^{15}\text{cm}^{-3}$, formed complexes mainly are A- and E-centers and divacancies V₂.

For test samples irradiated with 2MeV electrons at room temperature and annealed in the range of 80–400°C, it has been shown that E-centers are annealed in the range 100–150°C, V₂ – 250–300°C, and A-centers – around 300°C (Figure 7, Curves 1, 2 and 3). As can be seen from Figure 7, during the annealing of E-centers the concentration of A-centers increases (Curves 1 and 2). Presumably, one of the decay products of E-centers – monovacancy – participates into quasi-chemical reaction with impurity atom of oxygen that results in the effect observed at 150°C:

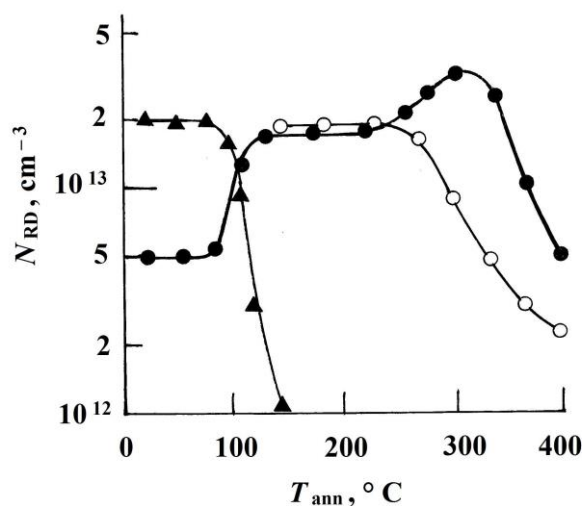
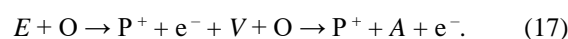


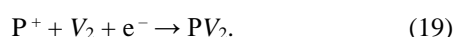
Figure 7. Changes in concentrations of 1 – E-centers, 2 – A-centers (2) and 3 – divacancies in electron-irradiated zone-melted n-Si versus isochronous annealing temperature

The increase in the concentration of A-centers is also observed due to conversion of V₂ in the range 250–300°C:



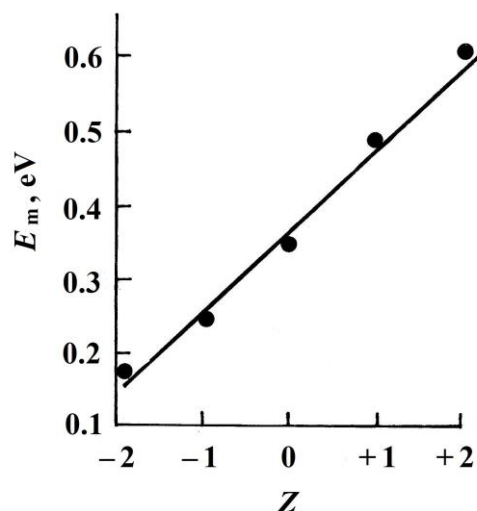
As can be seen from Figure 7, after the conversion of divacancies with concentration of $2 \cdot 10^{13}\text{cm}^{-3}$ there are formed A-centers with concentration of $1 \cdot 10^{13}\text{cm}^{-3}$ (Curves 2 and 3). The decay of V₂ means the formation of a

pair of vacancies. And for the formation of a single A-center it is sufficient only single vacancy. It turns out that the formation of A-centers consumed about a quarter of the annealed V_2 . Apparently, other divacancies are annealed by conversion into other defects such as complexes OV_2 , which in the silicon crystalline lattice are situated near the Si–O–Si bonds. At the first stage, it forms A-center via reaction $O + V \rightarrow A$ (formation mechanism of such a center is easy to analyze for the structure of silicon dioxide¹⁸). And after that, a second vacancy is added: $A + V \rightarrow OV_2$. The OV_2 complexes correspond to the energy level at $E_C-0.50\text{eV}$ and they are annealed at 350°C . It is possible that annealing of V_2 occurs by partially converting them into phosphorus-containing complexes PV_2 . These complexes in n-Si crystals are formed during a long exposure or isochronous annealing of irradiated samples.¹⁹ Under these conditions divacancies are transferred into the neutral charge-state and PV_2 complexes are formed by the reaction:



It is known¹⁴ that in silicon crystals grown by Czochralski method, i.e. with high oxygen content, the dominant radiation defect is A-center – OV complex. If isochronous annealing is conducted at $\geq 300^\circ\text{C}$, a significant part of these centers is transformed into O_2V . With increasing annealing temperature O_2V transforms into O_3V (450°C), then O_3V into O_4V ($450-485^\circ\text{C}$), etc. The O_2V complexes are formed via capturing diffusing A-centers by interstitial oxygen, while the centers with higher content of oxygen are formed via capturing of diffusing oxygen by the complexes O_2V , O_3V , O_4V , etc.¹⁴

Figure 8. Activation energy of vacancy migration in silicon versus its charge-state



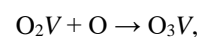
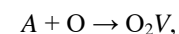
For p-Si crystals obtained by the Czochralski method and irradiated with 8MeV electrons at the dose of $5.0 \cdot 10^{15}\text{cm}^{-2}$, we identified (see the characteristics below) the values of the activation energy of migration E_m for vacancies in the charge-states of 0 and +2 as 0.35 and 0.60eV, respectively. These results, together with available data²⁰ are shown in Figure 8. As one can see, the activation energy of vacancy migration is linearly increasing function of the charge number Z of the defect. Therefore, it seems natural to

assume the same behavior for O_nV complexes ($n=1,2,3,\dots$). With increasing in the annealing temperature it changes their charge state: they lose electrons and become positively charged. Consequently, the activation energy of migration of O_nV complexes increases. When this value exceeds the activation energy of migration of interstitial oxygen atoms (2.54eV^{12}), complexes of higher order are formed mainly in the process of capture of diffusing background oxygen by the already existing oxygen–vacancy complexes.

A minority of A-centers has to be annealed at 300°C by the dissociation reaction:



and rest of these centers is annealed by conversion. Produces are higher order radiation defects,

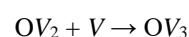
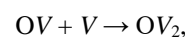


and



respectively, at 300, 450 and 485°C .

Simultaneously with the formation of O_nV complexes, there are also formed OV_n complexes ($n=1,2,3,\dots$). As noted above, in n-Si the level $E_C-0.28\text{eV}$ corresponds to nonequilibrium vacancy and, therefore, at room temperature they are charged negatively. In these conditions, reactions (2) and (3) form only A-centers and OV_2 . However, annealing at $\geq 500^\circ\text{C}$ transforms negative vacancies to the neutral state and then it starts the formation of radiation-induced defects in the high-order reactions:

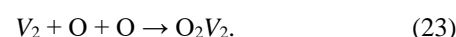


and



respectively, at 20, 300 and 450°C .

Annealing of A-centers at 350°C makes it possible the conversion



The concentration of O_2V_2 complexes should be very low because most of oxygen atoms return to interstitials, the normal position for this impurity in silicon lattice. At 400°C , the capture of vacancy or A-center by O_2V_2 complex transforms it, respectively, into complexes O_2V_3 or O_3V_3 :



Figures 9 and 10 show the changes in the concentration of major carriers depending on the measurement temperature and annealing temperature; and concentrations of major carriers and various radiation defects depending on the temperature of isochronous annealing in p-Si crystals doped up to level of $6 \cdot 10^{13} \text{cm}^{-3}$ and irradiated with 8MeV electrons. The sharp increase in the hole concentration in the range of $T_{\text{ann}}=170\text{--}200^\circ\text{C}$ is due to the annealing of defects with the level at $E_V+0.45\text{eV}$ and concentration of $5 \cdot 10^{12} \text{cm}^{-3}$. This level belongs to the complex of dopant impurity B with a vacancy, i.e. BV .¹²

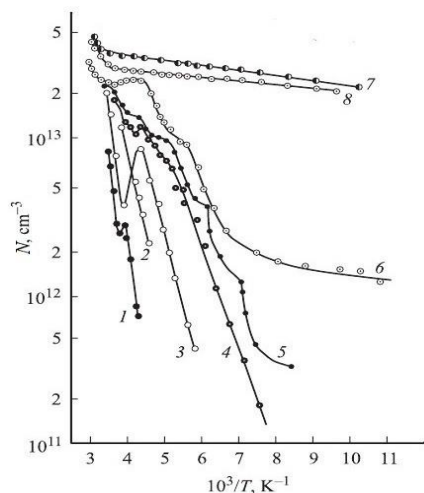


Figure 9. Temperature-dependence of hole concentration in p-Si crystals irradiated with 8MeV electrons at the dose of $5.0 \cdot 10^{15} \text{cm}^{-2}$: 1 – before annealing and after annealing at 2 – 100, 3 – 170, 4 – 240, 5 – 270, 6 – 300, 7 – 400 and 8 – 500°C

In the range $T_{\text{ann}}=260\text{--}300^\circ\text{C}$, there are annealed defects with the energy level at $E_V+0.28\text{eV}$ and concentration of about $8 \cdot 10^{12} \text{cm}^{-3}$ (Figure 9, Curve 3). Judging from annealing temperature and the energy level, these centers are divacancies.¹² Annealing of divacancies lead to a sharp increase in the concentration of defects with the energy level at $E_V+0.22\text{eV}$, so-called *H*-centers (Figure 9, Curve 4). Concentrations of divacancies broken by thermal treatment in the range $270\text{--}290^\circ\text{C}$, on the one hand, and formed centers with level at $E_V+0.22\text{eV}$, on the second hand, are equal within the measurements error limits. From this we can conclude that *H*-centers contain divacancies. On the stepped Curve 5 of Figure 9, third step corresponds to the transition of electrons from the valence band to the level at $E_V+0.22\text{eV}$, what leads to the increase in the hole concentration. As seen from Figure 9, the process ends at temperature of about 220K. Naturally, at higher (e.g., room) temperature electrons cannot return to the valence band causing compensation of holes.

Like a P-atom in n-Si, which forming *E*-center together with a vacancy, takes its fifth valence electron from the conduction band, in p-Si divacancy forming the level at $E_V+0.22\text{eV}$ takes an electron from the valence band. Therefore, annealing should increase the hole concentration. Although, in the range of $T_{\text{ann}}=270\text{--}290^\circ\text{C}$ the hole concentration remains almost unchanged (Figure 10, Curve 1). The explanation lies in the fact that the complexes formed during annealing of divacancies should contain

dopant B-atoms. Concentrations of boron atoms blocked by the formation of *H*-centers and major carriers formed during the annealing of divacancies are equal. Therefore, in the range $270\text{--}290^\circ\text{C}$ there are no changes in concentration of holes. These results confirm the previously expressed view on the existence in irradiated p-Si crystals complexes of boron dopants with divacancies, BV_2 , which are annealed at higher temperatures, in the range of $350\text{--}400^\circ\text{C}$.

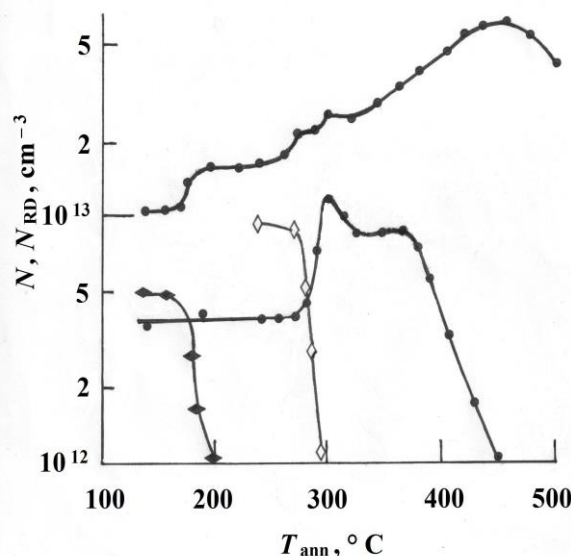


Figure 10. Concentrations of 1 – holes and 2–4 – some of radiation defects in p-Si crystals irradiated with 8MeV electrons at dose $5.0 \cdot 10^{15} \text{cm}^{-2}$ versus isochronous annealing temperature

The activation energy of the migration of divacancies is about 1.30eV, while the binding energy of this defect is higher: 1.47eV.^{12,21} Therefore, in the crystal divacancies can migrate without dissociation. It is also known that the BV complexes are annealed at 180°C (Figure 10, Curve 2) and thus they cannot participate in the formation of BV_2 complexes in higher temperature range of $270\text{--}290^\circ\text{C}$. From the above it can be assumed that BV_2 complexes are formed by conversion of divacancies,



rather than sequential capture by B-atoms of vacancies *V* generated by irradiation, as it had been assumed previously.

As seen from Figure 10, *H*-centers are annealed in two stages: at $300\text{--}320$ and $360\text{--}440^\circ\text{C}$. The initial concentration of *H*-centers is $3.5 \cdot 10^{12} \text{cm}^{-3}$ and the same concentration of centers is annealed at the first stage. The concentration of decayed centers at second stage coincides with the concentration of divacancies formed during annealing of complexes BV_2 ($3.5 \cdot 10^{12} \text{cm}^{-3}$). These results suggest that the so-called *H*-center with the energy level at $E_V+0.22\text{eV}$ actually is the superposition of two defects, H_1 - and H_2 -centers, of different types with different annealing temperature intervals: $300\text{--}320$ and $360\text{--}440^\circ\text{C}$, respectively. At the first stage, there is annealed a center of currently unknown nature, and at the second stage – BV_2 complexes, which are formed during conversion of divacancies at $270\text{--}290^\circ\text{C}$ by joining with substituting B-atoms. After annealing at 300°C the change in the hole concentration may be due to

dissociation or formation of O_2V_2 complexes, so-called *K*-centers ($O + C + V_2$),²² and other deep and thermally stable centers.

Conclusion - Prospects for practical applications

Conducted investigation has shown that the variation in the parameters of irradiation by beams of elementary particles – temperature, intensity, IR illumination of crystals during irradiation – affects the quasi-chemical reactions that occur in silicon during irradiation and isochronous annealing of the irradiated material.

Control over quasi-chemical reactions allows obtaining of crystals with different sets of radiation-induced defects, i.e. crystals with certain electrical, optical or recombination properties. It is also possible to change the type of the dominant defect. In this regard, we note that most of the oxygen-containing complexes formed with high-temperature annealing of irradiated silicon are optically and electrically active and can significantly affect the characteristics of the silicon-based electronic devices.

Another example of this type is associated with changes in the charge-state of nonequilibrium vacancies formed in the process of irradiation, which react quasi-chemically with already existing defects. With this process it is possible to stimulate the formation of defects, such as multi-vacancy complexes OV_n , PV_n , etc ($n=1,2,3,\dots$). But, the more primary radiation defects, in particular, vacancies are spending per complex defect, the higher is the radiation resistance of the material. If, for example, instead of PV complexes (*E*-centers) there are formed PV_4 complexes it is possible to expect the 4-fold increase in the radiation resistance of crystalline silicon doped with phosphorus in regard to the concentration of majority charge carriers, i.e. electrons.

Quasi-chemical reactions also can control formation of “dielectric” and “metallic” nano-inclusions in the irradiated silicon and, hence, the electronic properties of this material.

References

- ¹Bashaleishvili, Z. V., Pagava, T. A., *Semiconductors*, **1999**, 33, 845.
²Pagava, T. A., *Semiconductors*, **2002**, 36, 1079.
³Pagava, T. A., Chkhartishvili, L. S., *Ukr. J. Phys.*, **2003**, 48, 232.

- ⁴Pagava, T. A., Bashaleishvili, Z. V., Kutelia, E. R., Maisuradze, N. I., *Ukr. J. Phys.*, **2003**, 48, 435.
⁵Pagava, T. A., Bashaleishvili, Z. V., Garnik, V. S., Kutelia, E. R., Maisuradze, N. I., *Ukr. J. Phys.*, **2003**, 48, 576.
⁶Pagava, T. A., *Semiconductors*, **2004**, 38, 639.
⁷Pagava, T. A., Maisuradze, N. I., *Semiconductors*, **2010**, 44, 151.
⁸Pagava, T. A., Maisuradze, N. I., Beridze, M. G., *Semiconductors*, **2011**, 45, 572.
⁹Pagava, T. A., Beridze, M. G., Maisuradze, N. I., *Semiconductors*, **2012**, 46, 1251.
¹⁰Pagava, T., Chkhartishvili, L., *Am. J. Mater. Sci.*, **2013**, 3, 29.
¹¹Bourgoin, J., Lanoo, M., “*Point Defects in Semiconductors*,” Springer-Verlag, Berlin, **1983**.
¹²Vavilov, V. S., Kiselev, V. F., Mukhashev, B. N., “*Defects in Silicon and on Its Surface*,” Nauka, Moscow, **1990**.
¹³Luk'yanitsa, V. V., *Semiconductors*, **2003**, 37, 404.
¹⁴Pomozov, Yu. V., Sosnin, M. G., Khirunenko, L. I., Yashkin, V. I., Abrosimov, N. V., Schröder, B., Höhne, M., *Semiconductors*, **2000**, 34, 989.
¹⁵Varentsov, M. D., Gaydar, G. P., Dolgolenko, A. P., Litovchenko, P. G., *Nuclear Phys. Energy (Yadern. Fiz. Energ.)*, **2006**, 17, 60.
¹⁶Dolgolenko, A. P., Litovchenko, P. G., Varentsov, M. D., Lastovetskiy, V. F., Gaydar, G. P., Litovchenko, A. P., *Phys. of Radiat. Damages Radiat. Mater. Sci.*, (*Fiz. Radiats. Povrezhd. i Radiats. Materialoved.*), **2006**, 89, 171.
¹⁷Dolgolenko, A. P., Gaydar, G. P., Varentsov, M. D., Litovchenko, P. G., *Phys. of Radiat. Damages Radiat. Mater. Sci.*, (*Fiz. Radiats. Povrezhd. i Radiats. Materialoved.*), **2009**, 93, 151.
¹⁸Kajihara, K., Skuja, L., Hosono, H., “*Radiation Synthesis of Materials and Compounds*,” **2013**, CRC Press, Boca Raton, 101.
¹⁹Lugakov, P. F., Luk'yanitsa, V. V., *Semiconductors*, **1981**, 18, 345.
²⁰Emtsev, V. V., Mashovets, T. V., “*Impurities and Point Defects in Semiconductors*,” *Radio i svyaz'*, Moscow, **1981**.
²¹Lugakov, P. F., Lukashevich, T. A., *Phys. Status Solidi A*, **1984**, 85, 441.
²²Barabanenkov, M. Yu., Leonov, A. V., Mordkovich, V. N., Omelyanovskaya, N. M., *Semiconductors*, **1999**, 33, 821.

Received: 11.05.2013.
 Accepted: 31.05.2013.



MANAGEMENT OF PETROPORPHYRINS IN A CRUDE OIL POLLUTED ENVIRONMENT

Ozioma Achugasim^{[a]*}, Chukwunonye Ojinnaka^[a] and Leo Osuji^[a]

Keywords: Vanadyl porphyrins; Fenton's reagent; potassium permanganate; potassium persulfate; tar balls

The ability of three chemical oxidants (Fenton's reagent, Potassium permanganate and Potassium persulfate) to degrade one of the recalcitrant non-hydrocarbon components of crude oil- the porphyrins at three different pH media was investigated in this work and the results showed that the oxidants removed less than 10% of the porphyrins on the average, after two months of treatment. The porphyrins were found to experience degradation of 5%, 7% and 4% on the average for the acidic, neutral and basic soils respectively for the vanadyl (VO^{2+}) porphyrins and a reduction of 7%, 15% and 7% on the average for the acidic, neutral and basic soils respectively for the Nickel (Ni^{2+}) porphyrins. This highlighted the recalcitrant nature of porphyrins, but also showed that they are not perfectly so in the presence of chemical oxidants.

Corresponding Authors*

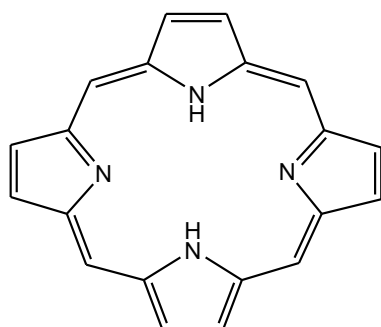
Tel: +2348033770425

E-Mail: Ozioma.Achugasim@uniport.edu.ng

[a] Department of Pure and Industrial Chemistry, University of Port Harcourt.

Introduction

The largest source of hydrocarbons is crude oil. Crude oil contains different types of hydrocarbons – aliphatic (saturated and unsaturated) and aromatic (isolated rings and condensed ringed) hydrocarbons. Some crude oil components are non-hydrocarbon and are highly recalcitrant, remaining essentially undegraded many years after crude oil spillage. Prominent among these degradation-resistant components of crude oil are the porphyrins or more specifically the petroporphyrins or metalloporphyrins. They are highly conjugated heterocyclic organometallic compounds found in crude oil. The porphyrins consists of four pyrrole rings joined at α -carbon atoms by four methine bridges to give a highly conjugated macromolecule.



A porphyrin molecule

They are aromatic and can form intensely coloured complexes with metals at the centre of the molecule called metalloporphyrins. For example, in association with iron they form a metalloporphyrin called haem, a component of haemoglobin found in red blood cells. When they complex with magnesium they form a derivative of chlorophyll, the green colouring matter in plants that is used in photosynthesis. In combination with cobalt, they form vitamin B₁₂ complex and when they combine with vanadium

and nickel, they form complexes called petroporphyrins because they are found in abundance in coals, bitumen and heavy crude oils.^{1,2}

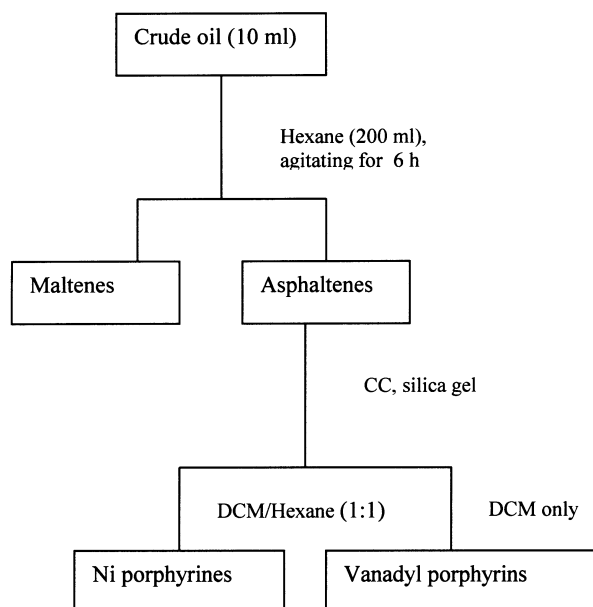
The petroporphyrins are stable and resistant to weathering and biodegradation unlike chlorophyll and haem. In fact, they have been said to be the products of haem and chlorophyll transformation. They are the last to degrade in petroleum among the petroleum residues. They are responsible for the formation of tar balls and other degradation resistant deposits at coastal shores long after oil spills. Thus, they are always used as biomarkers in the study of the origin/source and migration of petroleum residues.³ They exist predominantly as vanadyl (VO^{2+}) and nickel (Ni^{2+}) compounds of two structural types; deoxyphyloerythroetioporphyrins (DPEP) and etioporphyrins (ETIO).⁴

Their highly conjugated nature makes it possible for them to be studied using u.v/visible spectroscopy.⁵⁻⁷ Studies on the degradation and stability of petroleum products and components cannot be complete without these compounds. They are very resistant to degradation by microorganisms and do not volatilize from crude oils. A good understanding of their nature and behaviour will be very useful in the management of crude oil polluted soils and waters. The use of chemical oxidants in the remediation of crude oil / hydrocarbon polluted environments is an emerging trend that has received international acclaim.^{8,9} Its advantages cannot be overemphasized. Researches in this area is ongoing and is yielding good results.

Experimental

Ten millilitres of vacuum distilled crude oil (500 °C) in ten 50 ml volumetric flasks are treated with three oxidants (Fenton's reagent, potassium permanganate and potassium persulfate) at different pH ranges and left to stand for two months. An untreated sample exposed to the same conditions was made to act as control. Subsequently the samples were separated into the soluble maltenes and the insoluble asphaltenes. This was done by dissolving the samples in hexane, agitating them in a mechanical shaker for six hours and allowing it to stand overnight. The

dissolved samples are then filtered with a sintered glass funnel and a 342-whatman filter paper using a vacuum pump. The residue (asphaltenes) are then eluted with dichloromethane (DCM) and hexane in a glass column (50 ml x 1 cm) packed with silica gel according to the outline in Scheme 1.



Scheme 1. Steps involved in the extraction of the vanadyl and nickel porphyrins from the crude oil sample.

The different porphyrins are determined using uv-visible spectrophotometer at (550 nm-570 nm). The concentration of the nickel and vanadylporphyrins calculated using coefficient of extinction of 2.7×10^4 and $2.9 \times 10^4 \text{ L}^{-1}(\text{mole}\cdot\text{cm})$ respectively.^{7,10}

Results and discussion

The results of the absorbance of nickel and vanadyl porphyrins are presented in Tables 1 and 2 respectively. The results show that the porphyrins decreased in concentration after two months of treatment with the oxidants. This supports the generally accepted view that porphyrins are recalcitrant or resistant to degradation.¹¹ It is worthy of note that this reduction in the amount of porphyrins was noticed after the sample was treated with the oxidants for two months. Thus, it might be that after a prolonged period of time, the effect may become pronounced. Porphyrins have been fingered as the main constituents of tar balls – a dark and hard ball deposited at shore lines after incidents of oil spillage in rivers and oceans.⁷ Therefore oil spillage in water bodies managed with chemical oxidants like Fenton's reagent and potassium permanganate may prevent formation of tar balls.

Table 1. Absorbance of the VO^{2+} porphyrins from the oil samples treated with the different oxidants at the different pH media.

Oxidant	pH=5	pH=7	pH=9
Fenton's reagent	0.004	0.001	0.004
$\text{K}_2\text{S}_2\text{O}_8$	0.041	0.038	0.041
KMnO_4	0.002	0.002	0.003
Untreated	0.051	0.055	0.052

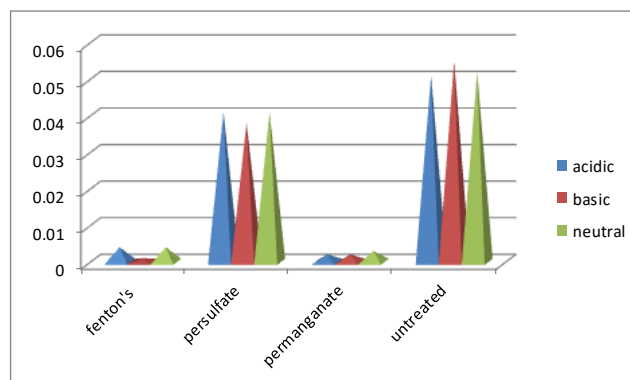


Figure 1. Chart showing the effect of the different oxidants on the VO^{2+} porphyrin concentration at the different pH media

Table 2. Absorbance of the Ni^{2+} porphyrins from the oil samples treated with the oxidants at different pH media

Oxidant	pH=5	pH=7	pH=9
Fenton's reagent	0.003	0.004	0.002
$\text{K}_2\text{S}_2\text{O}_8$	0.037	0.043	0.005
KMnO_4	0.003	0.003	0.003
Untreated	0.061	0.054	0.058

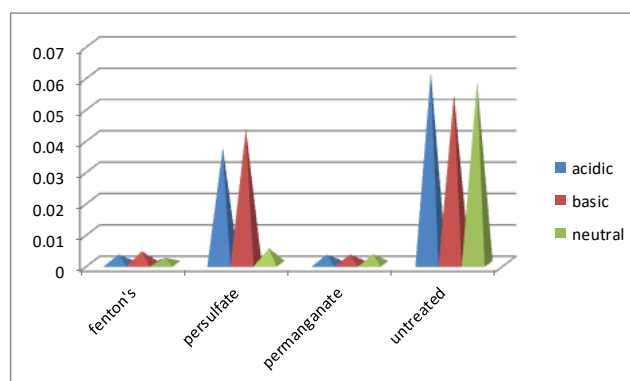


Figure 2. Chart showing the effect of the different oxidants(Fenton's reagent, potassium persulfate and potassium permanganate) on the Ni^{2+} porphyrin concentration at the different pH media

Although all the oxidants used had a slight effect on the amount of the porphyrins, the inactivity is more pronounced in the use of persulfate as oxidant (Tables 1 and 2). This seems to explain why persulfate were ineffective in the removal of the PAHs from the soil samples at all pH media.¹² Since PAHs and porphyrins dominate asphaltic crude oils, it implies that persulfates may not be the right oxidants for the remediation of asphaltic crude oils.

Conclusion

This study has shown that even though the petroporphyrins are recalcitrant in the environment, they can be removed with time using Fenton's reagent and potassium permanganate as chemical oxidants.

The study also revealed that potassium persulphates may not remove petroporphyrin when used as oxidants even after a long period of time.

Acknowledgements

The authors are grateful to the Nigerian National Petroleum Company (N.N.P.C) for the provision of the vacuum distilled crude used for this study. We are also very thankful to Dr Ofodile S.E. of the Department of Pure and Industrial Chemistry University of Port Harcourt for his expert advice/contribution that helped in the successful completion of this work.

References

- ¹Ali, M. F., Perzanowaski, H., Bukhari, A. A. and Al Haji, A. A. *Energy Fuel*, **1993**, 7, 179-184.
- ²Olajire, A. A. and Oderinde, R. A. *Pak. J. Sci. Ind. Res.* **1994**, 37(9), 349.
- ³Rivaro, P. and Frache, R. *Env. Sci. Technol.* **1977**, 11 (5), 502.
- ⁴Baker, E. W. and Louda, J. W. *Org. Geochem.* **1984**, 6, 183-192.
- ⁵Yadi, Z. and Peter, C. U. *J. High. Resol. Chromy.* **1994**, 17(4), 223-229.
- ⁶Sudihara, J. M. and Bean, R. M. *J. Chem. Eng. Data*, **1962**, 7(2), 269-271.
- ⁷Koichi, S., Hideaki, T. and Yazhi, Z. *Anal. Sci.* **2001**, 17, 23-25.
- ⁸Ozioma, A., Ojinnaka, C. and Osuji, L. *Env. Monit. Ass.*, **2012**, 184(11), 6527-6540.
- ⁹Ozioma, A., Ojinnaka, C. and Osuji, L. *Eur. Chem. Bull.* **2013**, 2(4), 226-230.
- ¹⁰Golovko, A. K., Gurkov, N. K., Mozzhelina, T. K. and Soboleva, Y. F. *Petrol. Chem.* **1993**, 33(6), 505-508.
- ¹¹Ikan, P. *Natural Products-A Laboratory Guide*. Academic Press. San Diego. **1991**, 317-319.

Received: 23.03.2013.

Accepted: 18.05.2013.



SOME UNCOMMON REACTIONS OF 1-PHTHALIMIDO-METHYL-4(3H) PHTHALAZIN-4-ONE

Dalal B. Guirguis

Keywords: phthalimides, phthalazinones, Grignard reagents, triazoles, quinazolinones, bond cleavage

A new series of phthalazin-4-one derivatives have been synthesized from the phthalazinone **1** as starting material with some active methylene compounds, Grignard reagents, acetylation, benzoylation and Mannich reaction. A triazolo derivative was also obtained via chlorination of **1** and addition of propionic hydrazide. A C-N bond cleavage occurred accompanied by a good leaving of the phthalimide nucleus upon subjecting **1** to Mannich reaction. A gentle competition between the phthalimide and the phthalazine nuclei was also observed specially upon treatment of Grignard reagent. The structures of the newly synthesized derivatives were confirmed by their elemental analysis, IR, ¹H-NMR as well as mass spectral studies of the synthesized compounds were discussed.

* Corresponding Authors

E-Mail: dalal.guirguis@hotmail.co.uk

[a] Department of Organic Chemistry, Faculty of Science, Ain Shams University, Cairo, Egypt 11566 Abbasseya, Cairo, Egypt

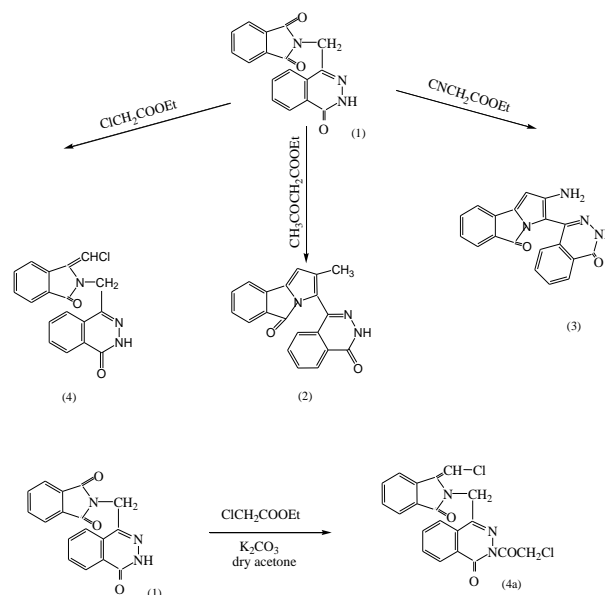
Introduction

Phthalazinone derivatives have found application in clinical medicine¹ due to their pronounced antipyretic, analgesic, and tuberculostatic activity and also vasodialator and antihypertensive properties.^{2,3} Also, they possess anticonvulsant,⁴⁻⁶ cardiotoxic,⁷ antitumor,⁸⁻¹¹ and antidiabetic.¹² It was reported that phthalazine-1(2H)-ones bearing a substitution at C-4 represent key intermediates in the synthesis of various compounds with highly interesting pharmacological properties.¹³ Therefore, the phthalazinone nucleus has been proved to be a versatile system in medicinal chemistry. The present paper studies the synthesis of some phthalazinone derivatives. Also, it studies the behavior of some reactions using variable conditions.

Results and Discussion

The previously obtained phthalazinone compound (**1**) namely, 2-(4-oxo-3,4-dihydrophthalazine-1-ylmethyl)-1H-isindole-1,3(2H)-dione was allowed to react with a variety of some active methylene compounds namely ethyl acetoacetate and ethyl cyanoacetate in n-butanol afforded **2** and **3**.¹³ The structures of **2** and **3** were illustrated from their analytical as well as spectral data. The ¹H NMR spectrum of **2** (DMSO-d₆) showed signal at δ 1.07 (s, 3H, CH₃) as well as correct mass ion peak at *m/z* 327 (4 %), also the IR showed the disappearance of one C=O of the phthalimide. The IR of **3** showed absorption frequencies at 3166 and 3427 cm⁻¹ attributed to νNH₂ and νNH respectively. Also its ¹H NMR spectrum (DMSO-d₆) showed signal at δ 12.0 (s, 2H, NH₂ exchangeable with D₂O). In the case of using ethyl chloroformate, the reaction products depended on the reaction conditions, i.e. in the case of refluxing the reactant in n-butanol **4** was obtained while upon using anhydrous potassium carbonate in dry acetone with ethyl chloroacetate

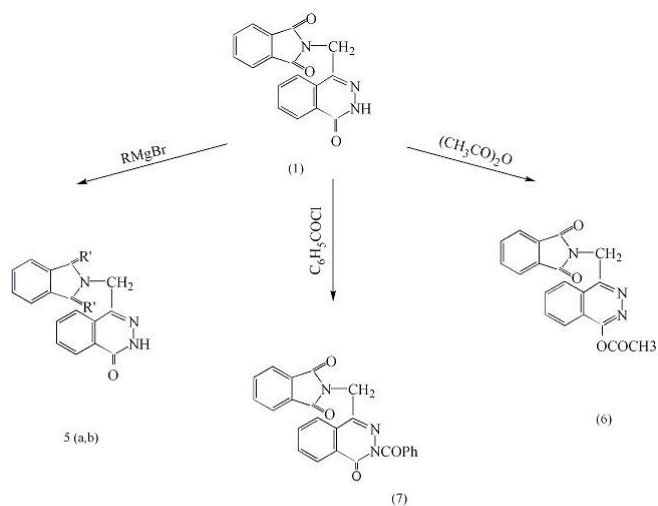
4a was obtained with *m/z* (M⁺+ 4) 406 (4 %), IR spectrum showed a characteristic bands at γ1641 cm⁻¹ and γ1602 cm⁻¹ corresponding to C=O and C=N, respectively (Scheme 1).



Scheme - 1 -

It was reported that when the phthalazinones were submitted to Grignard reagents, phthalazine derivatives were formed.^{14,15} However, in our case, upon the addition of the Grignard reagents (methyl and/or ethyl bromide in THF) to the phthalazinone **1**, the phthalazinones **5a** and **5b** were formed due to the loss of a water molecule from the phthalimide nucleus. The phthalazinones **5a** and **5b** were confirmed from their IR, which shows a complete disappearance of the two γC=O of the phthalimide and the remaining of the γC=O at 1660 cm⁻¹ of the phthalazinone.

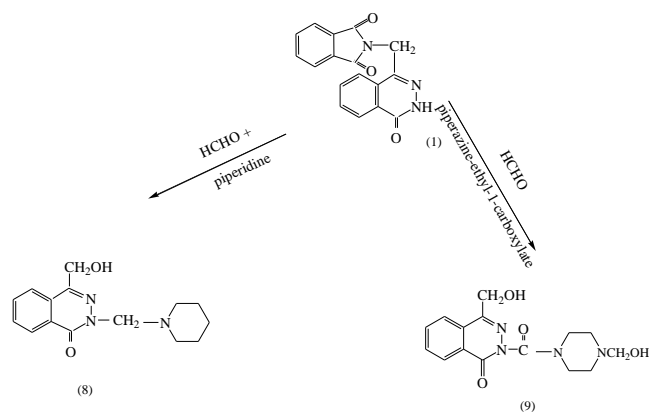
Also, acetylation and benzoylation using acetic anhydride and benzoyl chloride took place, giving **6** and **7** respectively. The IR of **6** showed a characteristic band of νC=O at 1737 cm⁻¹, characteristic of νOCO (Scheme 2).



a) R=Me, R'=CH₂, b) R=Et, R'=CHCH₃

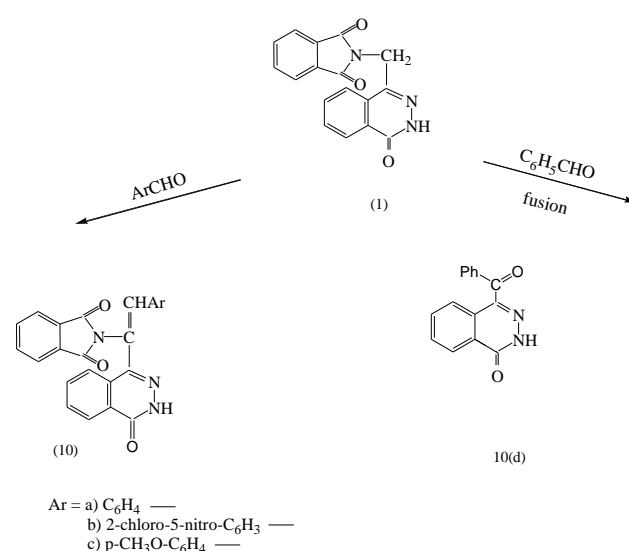
Scheme - 2 -

Extending the study of **1**, Mannich reaction was tried using piperidine and ethyl piperazine-1-carboxylate in the presence of formaldehyde and HCl in methanol to afford **8** and **9**, respectively with a good leaving of the phthalimide nucleus i.e. cleaving of the C-N bond (Scheme 3).



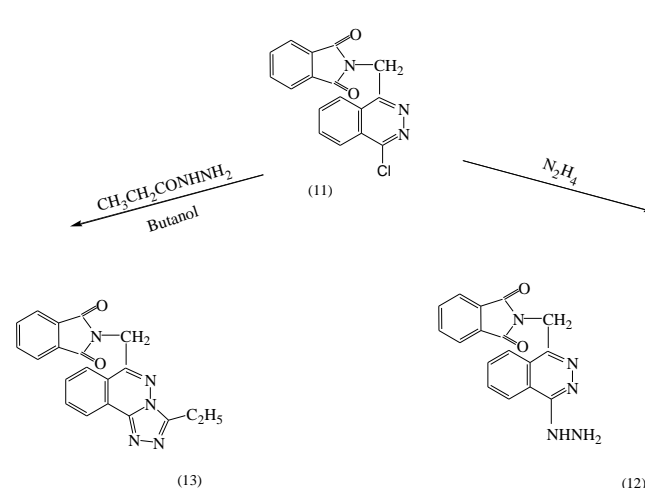
Scheme - 3 -

On the other hand, upon treatment of **1** with different aldehydes namely benzaldehyde, 2-chloro-5-nitrobenzaldehyde, and anisaldehyde in acetic anhydride and acetic acid afforded **10a-c** respectively, while upon fusion of **1** with benzaldehyde **10d** was achieved with m/z 236 which may have the following structure with also a cleavage of the phthalimide nucleus (Scheme 4).



Scheme - 4 -

On the other hand, upon treatment of **1** with a mixture of POCl₃ and PCl₅ on a water bath for 3 h, afforded the chlorophthalazinone **11** which on turn reacted with hydrazine hydrate giving the hydrazinophthalazinone **12** via S_N2 mechanism on the electron deficiency center of [C(1) in phthalazine nucleus which was activated by the adjacent nitrogen atom] and also gave the triazolo derivative **13** upon treatment with propionic hydrazide with m/e 357 (Scheme 5).^{13,15,16}



Scheme - 5 -

Experimental

All melting points are uncorrected and were measured on an electrothermal melting point apparatus. Elemental analyses were performed using a Heraeus CHN Rapid analyzer at the Microanalytical unit, Cairo University. Thin-layer chromatography (TLC) was performed on Merck TLC

aluminium sheets silica gel 60 F₂₅₄ with detection by UV quenching at 254 nm. IR spectra were measured on a Unicam SP-1200 spectrophotometer using KBr wafer technique. ¹H NMR spectra were measured in DMSO-d₆ on a Varian plus instrument (300 MHz). Mass spectra were recorded on a Shimadzu GC-MS QP 1000 EX instrument operating at 70 eV in EI mode.

Preparation of 2-methyl-3-[(4-oxo-3,4-dihydrophthalazin-1-yl)]pyrrole[2,1-a]isoindole-5-one (2), 2-amino-3-[(4-oxo-3,4-dihydrophthalazin-1-yl)]pyrrole[2,1-a]isoindole-5-one (3), and 3-chloromethylene-2-[(4-oxo-3,4-dihydrophthalazin-1-yl)methyl]-1H-isoindole-1-one (4)

A mixture of (0.01 mol) of (1) and (0.01 mol) of ethyl acetoacetate, ethyl cyanoacetate and/or ethyl chloroacetate in n-butanol was refluxed for 3 h, a ppt. was formed after evaporation of the solvent containing a mixture of 2, 3, and 4 respectively. **2**: Pale yellow crystals, 40 % yield, m.p. 230-232 °C, crystallized from n-butanol. ¹H NMR (DMSO-d₆) δ: 1.07(s, 3H, CH₃), 7.85-7.89 (m, 4H, Ar-H), 7.91-8.08 (m, 4H, ArH) 11.24 (s, 1NH, exchangeable with D₂O); IR (KBr) γ_{max}: 3474 (NH), 1660, 1640 (C=O), (C=N) cm⁻¹; MS *m/z* (%) 327, M⁺(4), 312 (40), 181 (64), 153 (52), 105 (28), 77 (100). Anal. calcd for C₂₀H₁₃N₃O₂ (327): C 73.39, H 3.9, N 12.8; found: C 74.0, H 4.2, N 13.1. **(3)**: Pale yellow crystals, 35 % yield, m.p. 115-117 °C, crystallized from butanol. ¹H NMR (DMSO-d₆) 1.34 (s, 1H, =CH), 7.86-7.89 (m, 4H, Ar-H), 7.9-8.08 (m, 4H, Ar-H), 11.4 (s, 2H, NH₂ exchangeable with D₂O); IR (KBr) γ_{max}: 3327, 3280 (NH₂), 3166 (NH), 1602 (C=N), 1660 (C=O) cm⁻¹; MS *m/z* (%) 328 (M⁺ (2), 311 (4), 167 (66), 105 (100). Anal. calcd for C₁₉H₁₂N₄O₂ (328): C 69.5 H 3.65, N 17.0; found: C 69.12, H 4.2, N 17.3. **(4)**: Grey crystals, 40 % yield, m.p. 200-202 °C, crystallized from n-butanol. ¹H NMR (DMSO-d₆) δ: 1.88 (s, 1H, =CH), 6.09 (s, 2H, CH₂), 7.87-7.89 (m, 4H, Ar-H), 7.9-8.1 (m, 4H, Ar-H), 11.2 (s, 1NH, exchangeable with D₂O); IR (KBr) γ_{max}: 3323 (NH), 1657 (C=O), 1556 (C=N) 788 (C-Cl). Anal. calcd for C₁₈H₁₂ClN₃O₂ (337.5): C 64.0, H 3.5, N 12.4; found: C 64.6, H 3.1, N 11.9.

Preparation of 4a

A mixture of (0.01 mol) of 1, (0.2 moles) of ethyl chloroformate and dry potassium carbonate in dry acetone was refluxed for 24 h. After evaporation of acetone and washing with water, solid **4a** was obtained 50% yield, m.p. 160-162 °C, crystallized from ethanol. IR (KBr) γ_{max} 3423 (NH), 1657 (C=O), 1602 (C=N), 788 (C-Cl) cm⁻¹; MS *m/z* (%) 406 (M⁺ 4)

Preparation of 2-[(4-oxo-3,4-dihydrophthalazin-1-ylmethyl)]isoindole-1,3-bis(ethylidene) (5a) and 2-(4-oxo-3,4-dihydrophthalazin-1-ylmethyl)isoindole-1,3-bis(methylidene) (5b).

To a suspension of 1 (0.01 mol) in THF, a solution of Grignard reagents (0.03 mol) (methyl iodide and/or ethyl iodide) was added. The reaction mixture was refluxed on a water bath for 4 h, poured on crushed ice and HCl, a solid

was separated giving **5a** and **5b** respectively. **5a**: 30 % yield, m.p. 220-222 °C, crystallized from methanol. ¹H NMR (DMSO-d₆) δ: 1.09 (s, 4H, 2 CH₂), 6.2 (s, 2 H, CH₂), 7.85-8.04 (m, 8H, Ar-H), 11.7(s, 1H, NH, exchangeable with D₂O); IR (KBr) γ_{max} 3165, 3018 (NH), 1661(C=O), 1602 (C=N) cm⁻¹. Anal. Calcd for C₁₉H₁₅N₃O (301): C 75.7, H 4.9, N 13.9; found: C 75.5, H 5.2, N 13.5. **5b**: 30 % m.p. 300-302 °C, crystallized from methanol. ¹H NMR (DMSO-d₆) δ: 1.18 (s, 6H, 2CH₃), 1.23 (s, 2 H, 2CH), 6.7 (s, 4H, 2CH₂) 7.85-8.04 (m, 8H, Ar-H), 11.7 (s, 1H, NH, exchangeable with D₂O); IR (KBr) γ_{max}: 3165 (NH), 1661 (C=O), 1601 (C=N) cm⁻¹. Anal. calcd for C₂₁H₁₉N₃O (329): C 76.5, H 5.7, N 12.7; found: C 77.0, H 5.9, N 13.1.

Preparation of 2-[4-acetoxy-3H-phthalazin-1-ylmethyl]-1H,3H-isoindole-1,3-dione (6)

A mixture of (0.1 mol) of 1 and (0.1mole) of acetic anhydride in glacial acetic acid was refluxed for 3 h. The mixture was poured on water to give **6**. **6**: yellow crystals, 40 % yield, m.p. 260- 262 °C crystallized from ethanol. IR (KBr) γ_{max}: 1737 (OCO), 1769, 1701(C=O), 1600 (C=N) cm⁻¹. Anal. calcd for C₁₉H₁₃N₃O₄ (347): C 65.7, H 3.7, N 12.1; found: C 66.0, H 4.1, N 11.9.

Preparation of 2-[3-benzoyl-3,4-dihydrophthalazin-1-ylmethyl]-1H,3H-isoindole-1,3-dione (7)

A mixture of (0.01 mol) of (1) and (0.01 mol) of benzoyl chloride in ethanol was refluxed for 3 h, a precipitate was formed after cooling and evaporation of solvent to give **7**. **7**: grey precipitate, 25 % yield, m.p. 190-192 °C crystallized from ethanol. ¹H NMR (DMSO-d₆) δ: 5.9 (s, 2H, CH₂), 7.8-8.1 (m, 13H, Ar-H); IR (KBr) γ_{max}: 1764, 1672 (C=O), 1600 (C=N) cm⁻¹, MS, *m/z* (%), M⁺ 409 (40), 146 (10), 104 (100), 77 (51). Anal. calcd for C₂₄H₁₅N₃O₄ (409): C 70.4, H 3.6, N 10.2; found: C 71.0, H 3.2, N 10.5

Preparation of 4-hydroxymethyl-2-(piperidin-1-ylmethyl)-1-oxo-1,2-dihydrophthalazine (8), and 4-hydroxymethyl-2-(4-hydroxymethylpiperazin-1-ylcarbonyl)-1-oxo-1,2-dihydrophthalazine (9)

A mixture of (0.01 mol) of 1 with (0.01 mol) of (piperidine or piperazine ethyl 1-carboxylate), few drops of formaldehyde and few drops of HCl in methanol was refluxed for 3 h, and cooled at room temperature. The resultant solid was filtered and crystallized from the proper solvent giving **8** and **9**. **(8)**: Pale yellow ppt, 20% yield, m.p. 287-288 °C, crystallized from methanol. IR (KBr) γ_{max}. 3169 (OH), 1672 (C=O), 1600 (C=N) cm⁻¹; MS, *m/z* (%), M⁺ 273 (0.5), 256 [(2), M⁺-H₂O], 130 (27), 104 (100), 97 (8). Anal. Calcd for C₁₅H₁₉N₃O₂ (273): C 65.9, H 6.9, N 15.3; found: C 66.2, H 6.8, N 15.4. **(9)**: Beige ppt, 25% yield, m.p. 318- 320 °C, crystallized from methanol. ¹H NMR (DMSO)-d₆ δ: 2.49 (s, 2H, CH₂), 2.50 (s, 2H, CH₂), 3.35 (s, 8H), (7.85-8.04, m, 4H, Ar-H), 11.5 (s, 2H, 2OH, exchangeable with D₂O); IR (KBr) γ_{max} , 3438, 3318 (OH), 1660, 1603 (C=O), 1600 (C=N) cm⁻¹; MS, *m/z* (%); M⁺, 318 (5), 162 (42), 104 (100). Anal. Calcd for C₁₅H₁₈N₄O₄ (318): C 56.6, H 5.6, N 17.6; found: C 56.5, H 5.4, N 17.8.

General procedure for the condensation of (1) with different aldehydes. 2-[(4-Oxo-3,4-dihydrophthalazine-1-yl(phenyl)methylene]-1H,3H-isoindole-1,3-dione (**10a**), 2-[4-oxo-3,4-dihydrophthalazine-1-yl(2-chloro-5-nitrophenyl)methylene]-1H,3H-isoindole-1,3-dione (**10b**), and 2-[4-oxo-3,4-dihydrophthalazine-1-yl(4-methoxyphenyl)methylene]-1H,3H-isoindole-1,3-dione (**10c**)

A mixture of (0.01 mol) of **1** and (0.01 mol) of different aldehydes namely benzaldehyde, 2-chloro-5-nitrobenzaldehyde, and anisaldehyde in a mixture of acetic anhydride and acetic acid was refluxed for 3 h, a ppt. was formed giving rise to **10a-10c**. **10a**: yellow crystals, 30 % yield, m.p. 164-166 °C crystallized from ethanol. ¹H NMR (DMSO-d₆) δ: 2.9(s, 1H, =CH), 7.8-8.1 (m, 13H, Ar-H), 11.6 (s, NH, exchangeable with D₂O); IR (KBr) γ_{max}: 3440, 3168 (NH), 1764, 1672 (C=O), 1600 (C=N) cm⁻¹. Anal.: calcd for C₂₄H₁₅N₃O₃ (393): C 73.2, H 3.8, N 10.6; found: C 72.9, H 3.5, N 10.2. **10b**: yellow crystals, 52 % yield, m.p. 190-192 °C, crystallized from ethanol. ¹H NMR (DMSO-d₆) δ: 2.9 (s, 1H, =CH), 7.8-8.1 (m, 11H, Ar-H), 11.6 (s, NH, exchangeable with D₂O); IR (KBr) γ_{max}: 3440, 3168 (NH), 1764, 1672 (C=O), 1600 (C=N), 770 (C-Cl) cm⁻¹. Anal. Calcd for C₂₄H₁₃ClN₃O₅ (472.5): C 60.9, H 3.17, N 11.8; found: C 61.2, H 2.9, N 12.2. **10c**: grey crystals, 30 % yield, m.p. > 320 °C. IR (KBr) γ_{max}: 3440, 3168 (NH), 1764, 1672 (C=O), 1600 (C=N) cm⁻¹. Anal. Calcd for C₂₅H₁₇N₃O₄ (423): C 70.9, H 4.0, N 9.92; found: C 70.5, H 4.4, N 10.1.

Preparation of 1-phenylacetylene-4-oxo-3,4-dihydrophthalazine (10d)

(0.01 mol) of **1** was fused with (0.01 mol) of benzaldehyde. The reaction was poured on water giving **10d** 20% yield, m.p. > 260 °C, crystallized from acetic acid; IR (KBr) γ_{max} cm⁻¹, 3168 (NH), 1714, 1661 (C=O), 1602 (C=N) cm⁻¹. MS, m/z (%), M⁺ 236 (71).

2-[(4-Hydrazinophthalazin-1-yl)methyl]-1H-isoindole-1,3(2H)-dione (12)

A mixture of (0.01 mol) of **11** and (0.02 mol) of hydrazine hydrate were fused. The product was diluted with water giving a dark brown precipitate **12**: 35% yield, m.p. > 320 °C, crystallized from acetic acid. IR (KBr) γ_{max}: 3338, 3290 (NH₂), 3210 (NH), 1715 (C=O), 1645, 1630 (C=N) cm⁻¹. Anal.: calcd for C₁₇H₁₃N₅O₂ (319): C 67.2, H 4.2, N 19.6; found: C 67.5, H 4.3, N 19.5.

1-(1,3-Dioxo-1H,3H-isoindolin-2-ylmethyl)-4-ethyl-1,2,4-triazolo[1,2-b]phthalazine (13)

A mixture of (0.01 mol) of **11** and (0.02 mol) of propionic hydrazide in n-butanol was refluxed for 4 h giving brown precipitate **13**: 45% yield, m.p. 228-230 °C. ¹H NMR (DMSO-d₆) δ: 0.09 (q, 3H, 2CH₃), 1.30 (t, CH₂) 6.3(s, 2 H, CH₂), 7.85-8.04 (m, 8H, Ar-H); IR (KBr) γ_{max}: 3171, (NH), 1720, 1670 (C=O), 1612 (C=N) cm⁻¹.

MS, m/z (%), M⁺ 357 (33), 147 (44), 105 (44), 77 (100). Anal. calcd. for C₂₀H₁₅N₅O₂ (357): C 63.9, H 4.0, N 21.9; found: C 64.2, H 3.7, N 21.6.

Conclusion

This work showed several reactions which were carried out on the phthalazinone **1**. A gentle competition was found between the phthalimide and the phthalazinone nuclei leading in some cases to the departure of the phthalimide nucleus depending on the reaction conditions.

References

- Bavin, E. M., Drain, D. J. Seiler, M., Seymour, D. E., *J. Pharm. Pharmacol.*, **1952**, 4, 844.
- Demiryak, S., Karaburun, A. C., Kayagil, I., Erol, K., Sirmagul, B., *Arch. Pharm. Res.*, **2004**, 27, 13.
- Vega, A. M., Aldana, I., Alvarez, E. F., *Eur. J. Med. Chem.*, **1978**, 13, 573.
- Grasso, S., Desarro, G., Micale, N., Zappala, M., Puia, G. Baraldi, M., Demicheli, C., *J. Med. Chem.*, **2000**, 43, 2851.
- Kornet, M., Shackelford, G., *J. Heterocycl. Chem.*, **1999**, 36, 1095.
- Sivakumar, R., Gnanasam, S. K., Ramachandran, S., Leonard, J., *Eur. J. Med. Chem.*, **2002**, 37, 793.
- Nomoto, Y., Obase, H., Takai, H., Teranishi, M., Nakamura, J., Kubo, K., *Chem. Pharm. Bull.*, **1990**, 38, 2179.
- Cockcroft, X., Dillon, K.J., Dixon, L., Drzewiecki, J., Everseley, P., Gomes, S., Hoare, J., Kirrigan, F., Nalthews, I., Menear, K. A., Martin, N. M., Newton, R., Paul, J., Smith, G. C., Vile, J., Whitter, A., *J. Bioorg. Med.*, **2006**, 16, 1040.
- Cockcroft, X., Dillon, K. J., Dixon, L., Drzewiecki, J., Kirrigan, F., Loh, V. M., Martin, N. M., Menear, K. A., Smith, G. C., *Bioorg. Med. Chem. Lett.*, **2005**, 15, 2235.
- Kim, J. S., Lee, H., Suh, M., Choo, H. P., Lee, S.K., Park, H. J., Kim, C., Park, S.W., Lee, C., *Bioorg. Med. Chem.*, **2004**, 12, 3683.
- Haider, N., Kabicher, J., Kaferbock, J., Plenck, A., *Molecules*, **2007**, 12, 1900.
- Madhavan, G. R., Chakrabarti, R., Kumar, S. K., Misra, P., Mamidi, R. N., Balarzu, V., Ksiram, K., Babu, R. K., Suresh, J., Lohray, B. B., Lohray, V. B., Iqbal, J., Raiagopalan, R., *Eur. J. Med. Chem.*, **2001**, 36, 627.
- Salvi, V. K., Bhambi, D., Jat, J. L. Talesara, G. L., *Arctov*, **2006**, 14, 133.
- El-Sawy, A. A., Donia, S. G., Essawy, S. A. Eissa, A. M. F., *J. Chem. Soc. Pak.*, **1989**, 11(2), 116
- El-Hashash, M. A., and El-Badry, Y. A., *J. Chem. Pharm. Res.*, **2012**, 4(5), 2354.
- El-Hashash, M. A., Soliman, A.Y., El-Shamy, I. E., *Turk J. Chem.*, **2012**, 36, 374

Received: 27.03.2013.
Accepted: 21.05.2013.



CATALYTIC ACTIVITY OF CETYLTRIMETHYLAMMONIUM BROMIDE (CTAB) IN THE REACTION OF NINHYDRIN AND ZINC GLYCYLTYROSINE COMPLEX

Mohd. Akram^{[a]*}, Dileep Kumar^[a] and Kabir-ud-Din^[a]

Keywords: glycyl tyrosine dipeptide, ninhydrin, micelle, $[Zn(II)\text{-Gly-Tyr}]^+$, cetyltrimethylammonium bromide, CTAB

The kinetics of interaction between ninhydrin and zinc-dipeptide (glycyl-tyrosine), $[Zn(II)\text{-Gly-Tyr}]^+$ complex have been studied in aqueous and in micelles formed by the cationic surface active material, cetyltrimethylammonium bromide (CTAB) at 80 °C and pH 5.0. The reaction follows first- and fractional- order kinetics with respect to $[Zn(II)\text{-Gly-Tyr}]^+$ and [ninhydrin], respectively, both in the absence and presence of cationic CTAB micelles. The catalytic role of [CTAB] can be related to the extent of incorporation or association of the $[Zn(II)\text{-Gly-Tyr}]^+$ complex and ninhydrin into the micelles. CTAB micelles decrease the activation enthalpy and make the activation entropy less negative. The micellar catalysis is explained in terms of the pseudo-phase model of the micelles. Binding constants K_s for $[Zn(II)\text{-Gly-Tyr}]^+$ and K_N for ninhydrin with micelles are calculated with the help of observed kinetic data.

Corresponding Author*

Tel: +91 571 2703515

E-Mail: drmohdakram@rediffmail.com

[a] Department of Chemistry, Aligarh Muslim University, Aligarh-202002, India

Introduction

Surfactants, due to containing both hydrophilic and hydrophobic properties in the same molecule, are amphipathic. The different interaction of these two moieties with water is an important cause for surfactants to self-aggregate into micelles and other nanometer scale structures in aqueous solution.^{1a} The nature of a surfactant plays a very important role in micellar catalysis. A little change in structure of surfactant can induce changes in the surface properties and rigidity of the micelle which remarkably affect the reactivity of substances. Because of widespread uses and application of surfactants as well as their micellar aggregates in chemical, biochemical, pharmaceutical, and industrial fields, detailed investigations on the fundamentals of aggregation of existing conventional and newer amphiphiles are in progress.^{1b} Cationic surfactants are useful as antifungal, antibacterial, and antiseptic agents and have attracted recently more attention with reference to their interaction with DNA and lipids,² whereas the nonionic surfactants are useful as detergents, solubilizers, and emulsifiers.³ The size, nature, and position of the head group and the length of the hydrophobic chain are all important factors.

Chemical reactivity in ionic colloidal self-assemblies (e.g., micelles, microemulsion droplets, and vesicles) has obtained importance owing to similarities in action with the enzymatic reactions (e.g., shape and size, polar surfaces, and hydrophobic cores). Micelles are known to provide different microenvironment for different parts of the reactant molecules; i.e., a non-polar hydrophobic core can provide binding energy for similar groups while the outer shell interacts with the reactant's polar groups. These properties of micelles play an important role in influencing the rates of reactions. In micellar solutions, reactions can be both

accelerated and inhibited compared to that in pure water.^{4,5} Such studies are expected to provide information: (i) to further understand factors that influence the rates of reactions; (ii) to gain additional insight into the exceptional catalysis of enzymatic reactions; and (iii) to explore the utility of micellar systems for the purpose of synthesis.

Various kinetic studies have examined the following types of micellar catalysis: (1) reactions in which the micelles are reagents; (2) reactions in which interactions between the micelles and the reacting species affect the kinetics; and (3) reactions in which the micelles carry catalytically active substituents.⁶ The present studies were undertaken to provide experimental evidence of catalytic effect of cationic CTAB micelles on the reaction of $[Zn(II)\text{-Gly-Tyr}]^+$ complex with ninhydrin. Ninhydrin has been well recognized for the detection and quantitative estimation of amino acids/peptides from biological fluids.⁷ It has been used also in bio-analytical work for visualization of fingerprints in forensic science. It has been established that metal ions preserve the colored product of ninhydrin-amino acids/peptides reaction. Order of mixing of metal ions also plays an important role as colors vary depending upon the order of mixing of reactants.⁸ Metal ion complex formations are among the prominent interactions in the nature. Metal coordination also plays an important role in biological processes involving metal-enzyme systems, considerable research has been carried out on modeling binary and mixed ligand complexes.⁹⁻¹¹

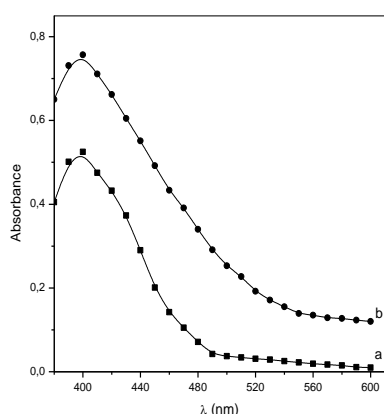
Experimental Section

Materials and Methods

All the solutions were prepared in double-distilled and deionized water (specific conductance $(1-2) \cdot 10^{-6} \text{ ohm}^{-1} \text{ cm}^{-1}$). CTAB (Merck, 99.0%), ninhydrin (Merck, 99.0%), Gly-Tyr (SRL, 99.0%), acetic acid (Merck, 99.0%), sodium acetate (Merck, 99.0%) and zinc sulphate heptahydrate (Merck, 99.0%) were used as supplied. An acetate buffer of pH 5.0

was used as solvent for preparing all the stock solutions. The pH measurements were performed using ELICO LI-122 pH meter in conjunction with a combined glass and calomel electrode.

Spectra of the reaction mixture containing [ninhydrin] ($6.0 \times 10^{-3} \text{ mol dm}^{-3}$) and $[Zn(II)\text{-Gly-Tyr}]^+$ ($3.0 \times 10^{-4} \text{ mol dm}^{-3}$) recorded using UV-visible spectrophotometer (SHIMADZU-model UV mini 1240) in the aqueous and in the presence of CTAB micelles, are shown in Figure 1. The spectra of the product consists of $\lambda_{\text{max}} = 400 \text{ nm}$ in both the media (although the absorbance is higher in presence of



CTAB, which may be due to strong association between the product and CTAB micelles).

Figure 1. Spectra of the reaction product of ninhydrin with $[Zn(II)\text{-Gly-Tyr}]^+$ in buffer solution at pH = 5.0, [ninhydrin] = $6.0 \times 10^{-3} \text{ mol dm}^{-3}$, $[Zn(II)\text{-Gly-Tyr}]^+ = 3.0 \times 10^{-4} \text{ mol dm}^{-3}$ and temperature = $80 \text{ }^\circ\text{C}$: (a) in the absence of CTAB, and (b) in presence of CTAB = $30 \times 10^{-3} \text{ mol dm}^{-3}$.

The composition of the reaction product between $[Zn(II)\text{-Gly-Tyr}]^+$ complex and ninhydrin was determined by Job's method of continuous variations in aqueous and in CTAB micellar media. It was found that one mole of $[Zn(II)\text{-Gly-Tyr}]^+$ complex associates with one mole of ninhydrin to give the reaction product.

Kinetic Studies

Under the conditions used in our studies, zinc(II) forms a 1:1 complex with glycyl-tyrosine. A 1:1 solution ($3 \times 10^{-4} \text{ mol dm}^{-3}$) of the two reactants was therefore taken in a graduated standard flask, boiled for 1 min and heated in a controlled manner at 90°C for 1 h (the flask was fitted with a double-surface condenser to prevent evaporation). After reaction, the flask was brought to room temperature and loss in volume, if any, was maintained with the buffer. The complex was then stored in dark. For each set of kinetic experiments, the requisite quantities of violet $[Zn(II)\text{-Gly-Tyr}]^+$ complex and buffer solution were taken in a three-necked reaction vessel. The mixture was allowed to attain the desired temperature. Pure nitrogen gas (free from CO_2 and O_2) was bubbled through the mixture for stirring and maintaining an inert atmosphere. The reaction was then initiated by adding appropriate amount of ninhydrin; the zero-time was taken when half of the ninhydrin solution had

been added. During the kinetic experiments pseudo-first-order conditions were maintained by using ≥ 10 -fold excess of [ninhydrin] over $[Zn(II)\text{-Gly-Tyr}]^+$. In the present investigations, the progress of reaction was followed spectrophotometrically by pipetting out aliquots at regular time intervals and monitoring the absorbance at $\lambda_{\text{max}} (= 400 \text{ nm})$. The pseudo-first-order rate constants in aqueous (k_{obs} , s^{-1}) and in micellar medium (k_{Ψ} , s^{-1}) were calculated up to completion of 80% of the reaction by using a computer programme. More details related to kinetic measurements can be found elsewhere in the literature.¹²⁻¹⁴

Critical Micellar Concentration (cmc) Measurements

The critical micellar concentration (cmc) determinations by conductivity measurements were carried out by using a Systronic conductivity meter 306 (cell constant = 0.10 cm^{-1}). First the conductivity of the solvent was measured and then conductivity was recorded every time after addition of small volumes of cationic cetyltrimethylammonium bromide (CTAB) solution ensuring complete mixing with and without reactants (i.e., ninhydrin and $[Zn(II)\text{-Gly-Tyr}]^+$) under different experimental conditions. The specific conductance was calculated by applying solvent correction. The cmc values of surfactant in absence and presence of reactants were obtained from break points of nearly two straight line portions of the specific conductivity vs. concentration plots.¹⁵ The experiments were carried out at $30 \text{ }^\circ\text{C}$ and $80 \text{ }^\circ\text{C}$ under varying different experimental conditions of solvent, i.e., water, water + ninhydrin, water + $[Zn(II)\text{-Gly-Tyr}]^+$, water + ninhydrin + $[Zn(II)\text{-Gly-Tyr}]^+$ and the respective cmc values are: ($\times 10^3$) 0.91, 0.89, 0.92 and 0.93 (at $30 \text{ }^\circ\text{C}$); 1.37, 1.28, 1.05 and 1.04 mol dm^{-3} (at $80 \text{ }^\circ\text{C}$).

Results and Discussion

Spectra of the product of $[Zn(II)\text{-Gly-Tyr}]^+$ -ninhydrin reaction has a absorption maximum at $\lambda_{\text{max}} = 400 \text{ nm}$ in the absence and presence of CTAB micelles. As no change in the absorption maximum ($\lambda_{\text{max}} = 400 \text{ nm}$) occurred in the absence as well as the presence of CTAB surfactants, we can conclude that the same product is formed in the two systems.

The kinetic studies of $[Zn(II)\text{-Gly-Tyr}]^+$ ($3.0 \times 10^{-4} \text{ mol dm}^{-3}$) and [ninhydrin] ($6.0 \times 10^{-3} \text{ mol dm}^{-3}$) interaction were made in the pH range 4.0 to 6.0 under both the conditions, i.e., aqueous and CTAB micellar media ($[CTAB] = 30 \times 10^{-3} \text{ mol dm}^{-3}$) at $80 \text{ }^\circ\text{C}$. It was found that the value of rate constant increased sharply in pH up to 5.0 and thereafter became almost constant in both the media. Consequently, all the subsequent measurements were made at pH 5.0 (Table 1).

To see the role of $[Zn(II)\text{-Gly-Tyr}]^+$ complex on the reaction rate, the kinetic experiments were carried out with different concentrations of $[Zn(II)\text{-Gly-Tyr}]^+$ varying from $2.0 \times 10^{-4} \text{ mol dm}^{-3}$ to $4.0 \times 10^{-4} \text{ mol dm}^{-3}$ at fixed [ninhydrin] ($6.0 \times 10^{-3} \text{ mol dm}^{-3}$), temperature ($80 \text{ }^\circ\text{C}$) and pH (5.0) (Table 1). It was found that the order of the reaction with respect to $[Zn(II)\text{-Gly-Tyr}]^+$ complex is unity in both the systems (i.e., aqueous and micellar media) as the

Table 1 Dependence of pseudo-first-order rate constants (k_{obs} or k_{Ψ}) on [Zn(II)Gly-Tyr]⁺, pH and [ninhydrin] for the reaction of [Zn(II)Gly-Tyr]⁺ with ninhydrin at 80 °C.

10 ⁴ [Zn(II)Gly-Tyr] ⁺ , mol dm ⁻³	10 ³ [ninhydrin], mol dm ⁻³	pH	10 ⁵ k_{obs}^a , s ⁻¹	10 ⁵ k_{Ψ}^b , s ⁻¹
3.0	6	4.0	2.0	8.5
3.0	6	4.5	3.1	22.4
3.0	6	5.0	8.8	36.7
3.0	6	5.5	12.5	38.3
3.0	6	6.0	14.2	39.2
2.0	6	5.0	8.4	36.3
2.5	6	5.0	8.5	36.7
3.0	6	5.0	8.8	36.7
3.5	6	5.0	8.7	36.8
4.0	6	5.0	8.5	36.9
3.0	6	5.0	8.8	36.7
3.0	10	5.0	17.0	40.4
3.0	15	5.0	22.7	44.5
3.0	20	5.0	26.0	47.6
3.0	25	5.0	30.0	49.5
3.0	30	5.0	32.5	51.1
3.0	35	5.0	35.2	52.2
3.0	40	5.0	37.5	53.0

^aAbsence of CTAB, ^b[CTAB] = 30 × 10⁻³ mol dm⁻³

value of rate constant is independent of the initial concentration of the complex. Therefore, the rate law is given as Eq. (1):

$$\text{rate} = \frac{d[P]}{dt} = (k_{\text{obs}} \text{ or } k_{\Psi}) [\text{complex}] \quad (1)$$

The effect of ninhydrin concentration was determined by carrying out the kinetic experiments with different [ninhydrin] ranging from 6 to 40 × 10⁻³ mol dm⁻³ at constant values of [Zn(II)-Gly-Tyr]⁺ (3.0 × 10⁻⁴ mol dm⁻³), temperature (80 °C) and pH (5.0) (Table 1). The plots of rate constants vs. [ninhydrin] are non-linear and pass through the origin (Figure 2), that indicates the order to be fractional with respect to [ninhydrin] under both the conditions.

Activation parameters were evaluated from the linear Eyring plots by studying the reaction at varying temperature (Table 2).

Reaction in Aqueous Medium

It is well known that lone pair electrons of amino group are necessary for nucleophilic attack on the carbonyl group of ninhydrin.¹⁶⁻¹⁹ In complex ([Zn(II)-Gly-Tyr]⁺), this lone pair is not free, and therefore, nucleophilic attack is not possible. The reaction, therefore, proceeds through condensation of coordinated carbonyl group of ninhydrin (Nin) within the coordinated coordination sphere of Zn(II). The coordination of both reactants (ninhydrin and Gly-Tyr) with the same metal ion (Zn(II)) is an example of template mechanism.^{8b}

On the basis of the above results and previous observations, the mechanism shown in Scheme 1 has been proposed for the reaction of [Zn(II)-Gly-Tyr]⁺ complex with ninhydrin. According to this Scheme, the rate equation is given as Eq. (2):

$$\frac{d[P]}{dt} = k \frac{K [\text{Nin}] [\text{complex}]}{1 + K [\text{Nin}]} \quad (2)$$

On the basis of Eq. (1) and Eq. (2) we can write:

$$k_{\text{obs}} = k \frac{K [\text{Nin}]}{1 + K [\text{Nin}]} \quad (3)$$

where [Nin] is the total concentration of ninhydrin. Eq. (3) can be written as Eq. (4):

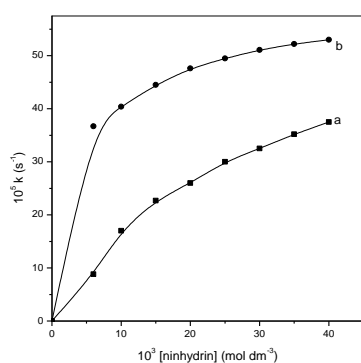
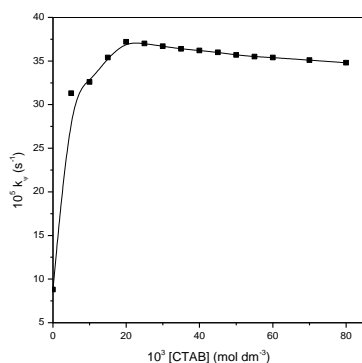
$$\frac{1}{k_{\text{obs}}} = \frac{1}{k} \left(1 + \frac{1}{K [\text{Nin}]} \right) \quad (4)$$

Thus, a plot of 1/ k_{obs} vs. 1/[Nin] should yield a straight line with an intercept (1/ k) and a positive slope (1/ kK). Indeed, it was found so and the values of k and K were found to be 5.0 × 10⁻⁴ s⁻¹ and 44.2 mol⁻¹ dm³, respectively, in aqueous medium. The calculated values of rate constants (k_{cal}), obtained by substituting k and K in Eq. (3), are in close agreement with the k_{obs} , which supports the proposed mechanism and confirms the validity of Eq. (3).

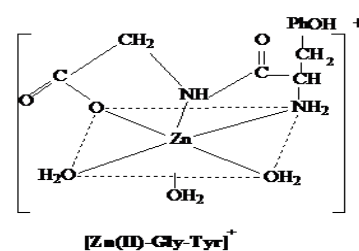
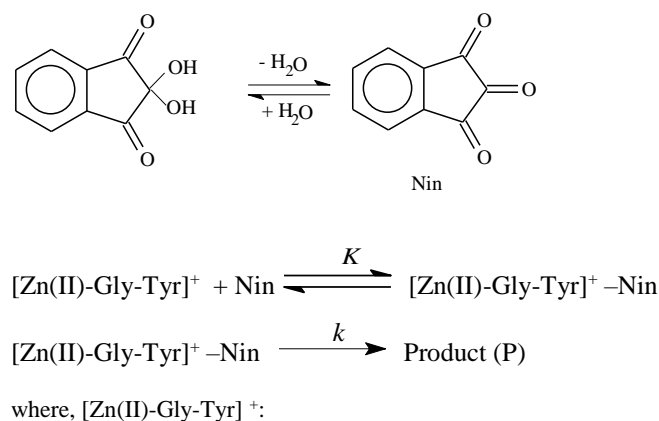
Table 2 Pseudo first-order rate constants, activation parameters, and binding constants for the reaction of $[Zn(II)Gly-Tyr]^+$ and [ninhydrin] in absence and presence of CTAB ($30 \times 10^{-3} \text{ mol dm}^{-3}$)^c.

Temperature, °C	$10^5 k_{obs}, s^{-1}$	$10^5 k_{\psi}, s^{-1}$
70	4.3	24.3
75	7.4	30.3
80	8.8	36.7
85	18.0	46.8
90	31.3	49.1
Parameters		
E_a (kJ mol ⁻¹)	115.1	44.3
ΔH^\ddagger (kJ mol ⁻¹)	112.2	41.4
$-\Delta S^\ddagger$ (J K ⁻¹ mol ⁻¹)	307.0	309.0
$10^3 k_m$ (s ⁻¹) ^d	-	14.1
$10^5 k_w$ (mol ⁻¹ dm ³ s ⁻¹) ^d	-	8.8
K_S (mol ⁻¹ dm ³) ^d	-	24.0
K_N (mol ⁻¹ dm ³) ^d	-	58.9
$10^4 k_2^m$ (mol ⁻¹ dm ³ s ⁻¹) ^d	-	2.0

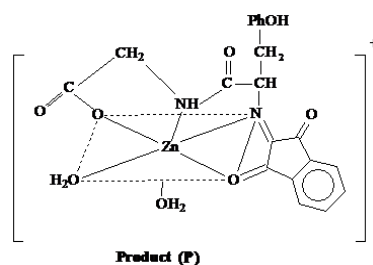
^c $[Zn(II)Gly-Tyr]^+ = 3.0 \times 10^{-4} \text{ mol dm}^{-3}$, [ninhydrin] = $6.0 \times 10^{-3} \text{ mol dm}^{-3}$, pH = 5.0. ^dAt 80 °C

**Figure 2.** Plots of rate constant (k) vs. [ninhydrin] for the reaction of ninhydrin with $[Zn(II)-Gly-Tyr]^+$ at pH = 5.0, temperature = 80 °C, and $[Zn(II)-Gly-Tyr]^+ = 3.0 \times 10^{-4} \text{ mol dm}^{-3}$: (a) in the absence of CTAB, and (b) in presence of CTAB = $30 \times 10^{-3} \text{ mol dm}^{-3}$.**Figure 3.** Effect of CTAB on the rate constant (k_{ψ}) for the reaction of ninhydrin with $[Zn(II)-Gly-Tyr]^+$ at pH = 5.0, temperature = 80 °C, [ninhydrin] = $6.0 \times 10^{-3} \text{ mol dm}^{-3}$, and $[Zn(II)-Gly-Tyr]^+ = 3.0 \times 10^{-4} \text{ mol dm}^{-3}$.**Reaction in CTAB Micellar Medium**

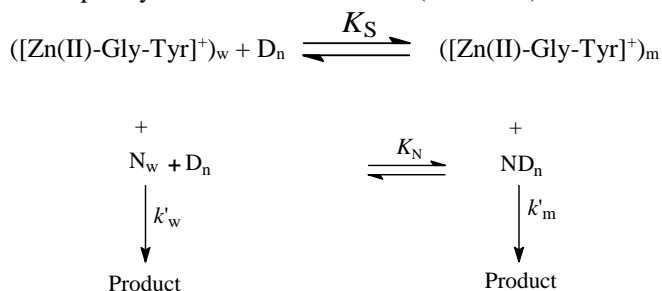
Preliminary experiments indicated that the absorbance of the end product increased as the concentration of CTAB micelles increased, but the wave length of maximum absorbance remained unchanged. It is inferred that there is no change in the products of the two systems. To find out the behaviour of cationic CTAB micelles on the reaction rate, the effect of CTAB was examined by varying amount of CTAB at fixed concentration of reactants (i.e., [ninhydrin] = $6.0 \times 10^{-3} \text{ mol dm}^{-3}$, $[Zn(II)-Gly-Tyr]^+ = 3.0 \times 10^{-4} \text{ mol dm}^{-3}$, temperature = 80 °C and pH = 5.0 (Table 3). The first-order rate constant (k_{ψ}) increased from 8.8 to $37.2 \times 10^{-5} s^{-1}$ on increasing [CTAB] from 0 to $20 \times 10^{-3} \text{ mol dm}^{-3}$ but further increment in [CTAB] had a decreasing effect on the reaction rate (Figure 3). The plot of k_{ψ} vs. [CTAB] is perfectly general being common characteristic of bimolecular reactions catalyzed by micelles.²⁰ The order of reaction with respect to [complex] was found first-order kinetics which shows that rate does not depend upon the initial [complex]. The plot of k_{ψ} -[ninhydrin] shows that the reaction rate increases on increasing [ninhydrin] but non-linearly (Figure 2). The above studies confirm that the order of reaction with respect to [complex] and [ninhydrin] is the same as that in aqueous medium.



and product (P):

**Scheme 1.** Ninhydrin- $[Zn(II)-Gly-Tyr]^+$ reaction mechanism.

The observed enhancement in the reaction rate is quantitatively treated on the basis of the pseudo-phase model (Scheme 2), proposed by Menger and Portnoy,²¹ and developed by Bunton⁴ and Romsted²² (Scheme 2).



Scheme 2. Ninhydrin-[Zn(II)-Gly-Tyr]⁺ reaction mechanism in CTAB micellar medium.

Although several kinetic equations based on the general Scheme have been produced, the most successful seems to be that of Romsted²² who suggested an expression (Eq.(5)), which takes into account the solubilization of both the reactants into the micelles as well as the mass action model:

$$k_{\Psi} = \frac{k_w[\text{Nin}] + (K_S k_m - k_w) M_N^S [D_n]}{1 + K_S [D_n]} \quad (5)$$

In the above equation, k_w and k_m are the second order rate constants, referring to bulk and micellar pseudophases, respectively. K_S and K_N are the binding constants of [Zn(II)-Gly-Tyr]⁺ complex and ninhydrin to cationic micells, M_N^S being the molarity of ninhydrin bound to the micellar head group, $[D_n]$ represents micellized surfactant ([CTAB]-cmc) and ND_n and $([\text{Zn(II)-Gly-Tyr}]^+)_m$ are micellized ninhydrin and complex, respectively.

Table 3 Effect of [CTAB] on pseudo-first-order rate constant (k_{Ψ}) for the reaction of [Zn(II)-Gly-Tyr]⁺ ($3.0 \times 10^{-4} \text{ mol dm}^{-3}$) with ninhydrin ($6.0 \times 10^{-3} \text{ mol dm}^{-3}$) at 80 °C and their comparison with calculated values ($k_{\Psi\text{cal}}$).

$10^3 [\text{CTAB}]$, mol dm^{-3}	$10^5 k_{\Psi}$, s^{-1}	$10^5 k_{\Psi\text{cal}}$, (s^{-1})	$\left(\frac{k_{\Psi} - k_{\Psi\text{cal}}}{k_{\Psi}} \right)$
0	8.8	-	-
5	31.3	30.5	+0.03
10	32.6	33.0	-0.01
15	35.4	35.9	-0.01
20	37.2	37.6	-0.01
25	37.0	36.8	+0.01
30	36.7	37.1	-0.01
35	36.4	36.3	0.00
40	36.2	37.0	-0.02
45	36.0	36.4	-0.01
50	35.7	35.3	+0.01
55	35.5	34.7	+0.02
60	35.4	34.8	+0.02
70	35.1	35.6	-0.01
80	34.8	35.0	-0.01

To find out K_S and k_m , the non-linear least squares technique was used for Eq. (5). This process gave the value

of least squares; i.e., $\sum d_i^2$ ($d_i = k_{\Psi\text{obsi}} - k_{\Psi\text{cali}}$) at i^{th} K_S . The calculation was repeated for different values of K_S and the best value was the one for which $\sum d_i^2$ was minimum. The K_S , thus obtained, was used to obtain the value of k_m .

As pointed out earlier, the micellar pseudo-phase has different properties. Therefore, it is not possible to precisely locate the exact site of the reaction but at least localization of the reactants can be considered. The reactant ninhydrin, having the π -electrons, enhances the possibility of its partitioning between water and cationic charged micelles.²³ The micellar surface can attract or repel ionic species due to electrostatic interactions whereas hydrophobic interactions can bring about the incorporation of the reactants into micelles. Thus, overall increment of rate occurs due to the increased concentration of both ninhydrin and [Zn(II)-Gly-Tyr]⁺ complex in the Stern layer of micelle (Figure 4). The slow decrease in rate constant (k_{Ψ}) beyond [CTAB] = $20 \times 10^{-3} \text{ mol dm}^{-3}$ can be explained as follows. At [CTAB] > $20 \times 10^{-3} \text{ mol dm}^{-3}$, practically all the substrate has been incorporated into the micellar phase. When bulk of the substrate is incorporated into the micelles, addition of more CTAB generates more cationic micelles, which simply take up the ninhydrin molecules into the Stern layer, and thereby deactivate them, because a reactant molecule in one micelle could not react with the other in another micelle.²⁰ Another reason of decrease in k_{Ψ} could be a result of counter ion inhibition.

General

The rate constants k_m (whose unit is reciprocal seconds) in the micellar pseudo-phase cannot be compared directly with the second-order rate constant in water k_w ($\text{mol}^{-1} \text{ dm}^3 \text{ s}^{-1}$), because the k_m is calculated by taking concentration as a mole ratio, M_N^S . To compare k_m with k_w , Bunton and others^{4,20,24} used the volume element for reaction within the micellar pseudo-phase. Stern layer volume of one mole of CTAB is about 0.14 mol dm^{-3} . The second-order rate constant (k_2^m , $\text{mol}^{-1} \text{ dm}^3 \text{ s}^{-1}$) for reaction in the Stern layer is then given as $k_2^m = 0.14 k_m$. For bimolecular reactions, in general, $k_w > k_2^m$.^{25,26} In the present case, the two values are comparable. Micellar surfaces are water rich but are less polar than pure water and do not provide a uniform reaction medium because micelle is a porous cluster with a rough surface and deep water filled cavities. On the other hand, the variations in k_w/k_2^m are not related in any obvious way to estimate polarities of micellar surfaces.

Activation Parameters

In order to learn more about the microenvironments of submicroscopic assemblies, a series of kinetic experiments were made at constant [Zn(II)-Gly-Tyr]⁺ ($3.0 \times 10^{-4} \text{ mol dm}^{-3}$), [ninhydrin] ($6.0 \times 10^{-3} \text{ mol dm}^{-3}$) and pH 5.0 in the temperature range 70 °C to 90 °C presence of surfactant (Table 2). The values of energy of activation (E_a), enthalpy of activation (ΔH^\ddagger) and entropy of activation (ΔS^\ddagger) are given in Table 2. On comparing the values of these parameters to those of aqueous medium, we observe a large decrease in energy of activation and enthalpy of activation with substantial negative entropy which suggests the formation of a well-structured activated state in which the reactive groups are closely associated with less degree of freedom.

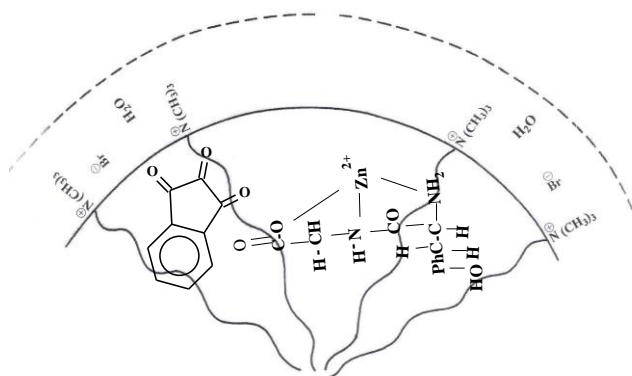


Figure 4. Schematic model representing probable location of reactants for the cationic micellar catalyzed condensation reaction between $[Zn(II)\text{-Gly-Tyr}]^+$ complex and ninhydrin.

Conclusions

Kinetic runs were carried out spectrophotometrically at fixed concentrations of $[Zn(II)\text{-Gly-Tyr}]^+$ (3.0×10^{-4} mol dm^{-3}), [ninhydrin] (6.0×10^{-3} mol dm^{-3}), temperature (80°C) and pH 5.0 at $\lambda_{\text{max}} = 400$ nm, in the absence and presence of CTAB micellar media. The presence of CTAB micelles do catalyze the reaction and provide new path of the ninhydrin reaction and thus enhance the sensitivity of the technique/reaction.

Acknowledgement

Authors are thankful to UGC (India) for financial assistance (to DK) and UGC-BSR Faculty Fellowship (to KU).

References

- ¹(a)Lawrence, C.A., "Cationic Surfactants", Jurgerman, E. (ed.), Marcel Decker, New York, **1979**, p 491. (b) "Recent Trends in Surface and Colloid Science", Statistical Science and Interdisciplinary Research, vol. 12, Paul, B.K. (ed.), World Scientific, Singapore, 2012.
- ²Moulik, S., Dutta, P., Chatteraj, D.K. and Moulik, S.P. *Colloids Surf.*, **1998**, *11*, 1.
- ³Sulthana, S.B., Rao, P.V.C., Bhat, S.G.T., Nakano, T.Y., Sugihara, G. and Rakshit, A.K. *Langmuir*, **2000**, *16*, 980.
- ⁴Bunton, C.A. *Catal. Rev. Sci. Eng.*, **1979**, *20*, 1.
- ⁵Engberts, J.B.F.N., *Pure Appl. Chem.*, **1992**, *94*, 1653.
- ⁶Morawetz, H., *Adv. Catal.*, **1969**, *20*, 341.
- ⁷Joullie, M.M., Thompson, T.R. and Nemeroff, N.H., *Tetrahedron*, **1991**, *47*, 8791.
- ⁸(a) Khan, Z., Gupta, D. and Khan, A.A., *Int. J. Chem. Kinet.*, **1992**, *24*, 481. (b) Rafiquee, M.Z.A., Khan, Z. and Khan, A.A., *Trans. Met. Chem.*, **1994**, *19*, 447.
- ⁹Frumen, H.C., *Adv. Protein Chem.*, **1967**, *22*, 257.
- ¹⁰Sigel, H. and Martin, R.B., *Chem. Rev.*, **1982**, *82*, 385.
- ¹¹Herr, U., Spahl, W., Trojadt, G., Steglisch, W., Thaler, F. and van Eldik, R., *Bioinorg. Med. Chem.*, **1999**, *7*, 699 and references therein.
- ¹²Rafiquee, M.Z.A., Shah, R.A., Kabir-ud-Din and Khan, Z., *Int. J. Chem. Kinet.*, **1997**, *29*, 131.
- ¹³Khan, Z., Ali, S.I., Gupta, D. and Khan, A.A., *Indian J. Chem. A*, **1996**, *35*, 320.
- ¹⁴Kabir-ud-Din, Rafiquee, M.Z.A., Akram, M. and Khan, Z., *Int. J. Chem. Kinet.*, **1999**, *31*, 103.
- ¹⁵Mukerjee, P. and Mysels, K.J., "Critical Micelle Concentrations Aqueous Surfactant Systems", NSRDS-NBS 36, Superintendent of Documents, Washington, DC, **1971**.
- ¹⁶Akram, M., Zaidi, N.H. and Kabir-ud-Din, *J. Disp. Sci. Technol.*, **2008**, *29*, 1.
- ¹⁷Akram, M., Zaidi N.H. and Kabir-ud-Din, *Int. J. Chem. Kinet.*, **2007**, *39*, 556.
- ¹⁸Akram, M., Zaidi N.H. and Kabir-ud-Din, *Int. J. Chem. Kinet.*, **2006**, *38*, 643.
- ¹⁹Kabir-ud-Din, Akram, M., and Khan, Z., *Indian J. Chem. B*, **2002**, *41*, 1045.
- ²⁰Bunton, C.A. and Robinson, L., *J. Am. Chem. Soc.*, **1968**, *90*, 5972.
- ²¹Menger, F.M. and Portnoy, C.E., *J. Am. Chem. Soc.*, **1967**, *89*, 4698.
- ²²Romsted, L.S., "Micellization, Solubilization and Microemulsions", vol. 2, Mittal, K.L. (ed.), Plenum Press, New York, **1977**.
- ²³Roberts, J.D. and Caserio, M.C., "Basic Principles of Organic Chemistry", Benjamin, 2nd ed., New York, **1977**.
- ²⁴Bunton, C.A., *J. Mol. Liq.*, **1997**, *72*, 231.
- ²⁵Buist, G.J., Bunton, C.A., Robinson, L., Sepulveda, L. and Stam, M., *J. Am. Chem. Soc.*, **1970**, *92*, 4072.
- ²⁶Bunton, C.A., Rivera, F. and Sepulveda, L., *J. Org. Chem.*, **1978**, *43*, 1166.

Received: 12.04.2013.

Accepted: 02.06.2013.



CORROSION INHIBITION BY POLYMERS – A BIRD'S EYEVUE

R. Kalaivani,^{[a]*} P. Thillai Arasu^[b] and S. Rajendran^{[c]*}

Keywords: adsorption site, active centres, conducting polymers, corrosion inhibition, electron rich, polymers.

Polymers are macromolecules. They have high molecular weight. They cover a large surface area and hence act as effective corrosion inhibitors. They have been used to control corrosion of various metals such as mild steel, copper, aluminium and stainless steel. They have been used in acidic, basic and neutral mediums. Adsorption of polymers on metal surface obeys various isotherm such as Langmuir, Temkin, Freundlich and Frumkin. Methods such as weight loss and electrochemical studies have been used to evaluate the corrosion inhibition efficiency of polymers. Surface analysis techniques such as FT-IR, SEM and AFM have been used to study the surface morphology of the protective films.

* Corresponding Authors

E-Mail: vaniraj21@yahoo.com
srmjoany@sify.com

- [a] Department of Chemistry, Research Scholar, Manonmanium Sundaranar University, Thirunelveli 627 132, Tamilnadu, India.
[b] Department of Chemistry, Kalasalingam University, Srivilliputhur 626 126, Tamilnadu, India.
[c] Corrosion Research Centre, PG and Research Department of Chemistry, GTN Arts College, Dindigul - 624 005, Tamilnadu, India.

Introduction

Macromolecules, also known as polymers, are very high molar mass compounds consisting of several structural units inter-connected by covalent bonds. The molar mass varies from 5,000 to several millions. There are polymers which are soluble in water, ethanol, and chloroform, but insoluble in ether. The use of polymer in corrosion prevention is due to the fact that polymer has excellent film forming, emulsifying, and adhesive properties. It is resistant to oil, grease and solvent. It is odourless and non-toxic. It has high tensile strength and flexibility. It is used as stabiliser and clarifying agent. Due to these properties polymers are used in corrosion resistant materials. Polymers have functional groups such as –OH, –NH₂, –PO₄⁻ and oxygen linkage. These groups interact with metal surface through active centers of polymer. Conducting polymers, due to their inherent nature, offer better inhibition efficiency than organic compounds because of conjugated systems which possess alternate single and double bonds. Rich in electrons it gets effectively adsorbed on metallic surface. It acts as protective film and prevents corrosion.

Metals

Polymers¹⁻¹⁰² have the ability to control the corrosion process of various metals such as mild steel,^{2,15,18,23,26,27,33,36,40,48,61,62,63,65,67,70,71,77,83,84,86,89,90,100} carbon steel,^{1,12,24,32,35,47,51,69,72,75,87,91,95,99} stainless steel,^{4,9,37,39,46,68,97} alumi-

nium,^{10,17,22,31,43,49,56,57,58,60,73,79,92,94,98} iron,^{8,11,13,21,25,28,30,38,44,50,54,64,66,80,93,96} zinc,^{7,14,42,59,76} copper,^{3,5,20,101} brass,^{19,45,88} tin,^{29,52} cadmium,⁷⁸ cerium,³⁴ amorphous alloy,⁵³ gold,^{55,85} and magnesium.⁷⁴

Medium

The inhibition efficiency of polymers in controlling corrosion of metals in various corrosive environment such as acidic medium^{2,3,10-12,16-18,21,23,25,27,29,33-36,38,43-44,46-48,50-52,59-66,68,70-73,77,78,80,82,83,85-86,90-93,95,97,100,} alkaline medium^{19,56,74,88} NaCl medium^{4,6,7,24,31,32,49,54,67,69,76,81,87,99} water^{41,57-58,101}, seawater^{13,15,22,39,94} aqueous medium^{5,9,45,53,55,84,89} surfactant solution,³⁰ ground water¹ borax buffersolution²⁰ acetonitrile medium³⁷ hypochlorite solution⁴⁰ deionised water⁴² and potassium chlorite solution⁹⁶ has been investigated.

Additives

The inhibition efficiency of polymers have increased by addition of halides.^{16,34,36,43,46,100}

Methods

Various methods used to evaluate the inhibition efficiency of inhibitors include weight loss method,^{1,2,10,12,17,18,23,25,26,47,56,57,60,63,69,70,73,83,84,86,93-96,99,100} electrochemical studies,^{2-5,12,15,18,19,21,27-30,33-35,37,38,41,46,47-50,59,61,64,66,67,72,74,77-82,85-88,92,94,97,101}, open-circuit potential,^{3,8,37,39} hydrogen evolution method,^{17,43,100} and cyclic voltammetry.^{2,3,11,52,73,85,90,91,97,98}

Adsorption isotherm

Corrosion inhibition by polymers is mainly due to adsorption of polymers on metal surface. Adsorption on metal surface obey various isotherms such as Langmuir isotherm,^{2,18,25,26,36,59,83,85,95} Freundlich isotherm,⁹³ Temkin isotherm,^{6,17,33,61,62,71,78,86,92} and Frumkin isotherm⁹³.

Table 1. Various polymers used as inhibitors

S. No.	Metal	Medium	Inhibitor	Additives	Method	Findings	Ref.
1	Carbon steel	Ground water	Polyacrylamide	----	Weight loss and polarization studies. The protective film formed on the metal surface characterized using surface morphological studies such as Fourier Transform Infrared spectra (FT-IR) and scanning electron microscopy (SEM)	Protective layer on metal surface	1
2	Mild steel	1 M HCl	Polyethylene glycol – Anthranilic acid composite	----	Weight loss measurements, Potentiodynamic polarisation curves, FT-IR spectra	Langmuir adsorption isotherm	2
3	Copper	0.5 M HCl	Poly(1-vinylimidazole)	----	Open circuit potential(ocp) temporal variation tafel polarisation curves & electrochemical impedance spectroscopy (EIS), SEM & CV	Electrochemical behaviour and anticorrosion properties	3
4	Stainless steel	0.5 M NaCl	Poly(3-octylthiophene)	----	Potentiodynamic polarisation curves, linear polarisation resistance, electrochemical impedance SEM & AFM	Temperature effect in the morphology of the coatings before and after corrosive environment.	4
5	Copper	Marine and aqueous environment	2,2'-bi-thiophene and immobilisation of silver nanoparticles	----	Tafel polarisation curves and electrochemical impedance spectroscopy	Enhance Antibacterial properties	5
6	Copper	3% NaCl	Poly(o-ethylamine)	----	Electrochemical impedance spectroscopy	Ability to protect the copper from corrosion	6
7	Zinc coated steel	Chloride	Plasma polymer coated galvanized steel	----	Scanning electron probe	Resistant to Cathodic deadhesion process	7
8	Iron	0.1 M Na ₂ SO ₄	16-hydroxyhexadecanoate ion OH(CH ₂) ₁₅ CO ₂ ⁻ with 1,2-bis(triethoxysilyl)ethane (C ₂ H ₅ O) ₃ Si(CH ₂) ₂ Si(OC ₂ H ₅) ₃ and octadecyltriethoxy silane C ₁₈ H ₃₇ Si(OC ₂ H ₅) ₃	----	Open circuit potential(ocp) polarisation curves & Electron probe microanalysis(EPMA)	Ultra thin polymer coated	8
9	Stainless steel	Aqueous	Polyaniline	----	Variation of applied field Polymer optical characteristics	Polymer deposition generate negative finger print mark	9
10	Aluminium Alloy	HCl	Polyvinylpyrrolidone and Polyacrylamide	----	Weight loss, hydrogen evolution and thermometric method	Temkin adsorption, El-Awady adsorption & Kinetic thermodynamic parameters	10
11	Iron	1.0 N HCl	5-lithosulphosphoric acid doped poly(aniline-co-2-isopropylamine)	----	FT-IR, UV-visible spectra, NMR, X-ray diffraction, TGA, DSC & cyclic voltametry	Synergistic effect of copolymer composition	11
12	Carbon steel	1N HCl	Poly(o-Methoxy aniline)	----	Weight loss measurement, Electrochemical polarisation techniques, impedance studies, FT-IR, UV-visible spectra	Film formed on carbon steel	12
13	Iron	Sea water	Polymeric scale inhibitors	----	High temperature range, FT-IR,	Molecular stability	13
14	Zinc	Adhesive layer film	Polymer/zincoxide/Zn interface	----	In situ attenuated-total-reflection infrared spectroscopy (ATR-IR) studies, in situ electrochemical scanning Kelvin probe Blister- test studies	Prevent the formation of an extended interfacial electrolyte layer	14
15	Mild steel	Seawater	Poly(glycidyl methacrylate)-polyaniline	----	X-ray photoelectron microscopy, SEM, Tafel polarisation curves, and electrochemical impedance spectroscopy	Antibacterial and anticorrosion capabilities	15

Table 1. (cont.)

S. No.	Metal	Medium	Inhibitor	Additives	Method	Findings	Ref.
16	Mild steel	Acidic (H ₂ SO ₄)	Gumarabic and polyethylene glycol	Halides	Temkin adsorption isotherm	Inhibition efficiency	16
17	Aluminium	HCl	Polyvinylpyrrolidone and Polyacrylamide	----	Weight loss, hydrogen evolution and thermometric method	Freundlich, Flory-temkin adsorption isotherm	17
18	Steel	Acidic (H ₂ SO ₄)	Electroactive co-polymer	----	Weight loss measurements (mg/cm ²) Electrochemical polarisation techniques, SEM	Langmuir adsorption isotherm	18
19	Brass	Alkaline solution containing methanol	Poly(3-amino-1,2,4-triazole)	----	Cyclic polarisation, chronoamperometry, electrochemical impedance studies and SEM	Monomer disappears Insulating film	19
20	Copper	Borax buffer solution	Polyaspartic acid (PASP)	----	Photocurrent response method	p-type photocurrent response	20
21	Iron	0.5 M H ₂ SO ₄	Polyaniline	----	Tafel polarisation curves and electrochemical impedance spectroscopy	Increased electron rich benzenoid groups absorbs effectively	21
22	Aluminium	Water	Amino propylphosphonate	----	FT-IR-RAS, SAM & XPS analysis	Interfacial stabilization	22
23	Mild steel	1N HCl, H ₂ SO ₄ , NaCl	Polynitroaniline	----	Weight loss measurements (mg/cm ²), Electrochemical polarisation techniques, FT-IR & SEM	Stable layer	23
24	Carbon steel	3.5 wt % NaCl	Polypyrrole	----	Doped with organic anions like dihydroxynaphthalene-disulphonate, naphthalenedisulphonate, anthroquinone-disulphonate	Bi-layer polypyrrole film	24
25	Iron	HCl	Polyacrylamide	----	Weight loss measurement Electrochemical impedance techniques	Langmuir adsorption isotherm	25
26	Steel	Phosphoric acid	Poly(vinyl caprolactone-co-vinyl pyridine) and poly(vinyl imidazole-co-vinylpyridine)	----	Weight loss measurement, Electrochemical impedance techniques, potentiometric polarisation techniques	Langmuir adsorption	26
27	Mild steel	Oxalic acid	Polyaniline and polypyrrole	----	Electrochemical impedance techniques, potentiometric polarisation techniques	Stable hostmatrix on steel	27
28	Iron	1M HCl	Poly(p-toluidine)	----	Tafel polarisation curves and electrochemical impedance spectroscopy	Suppressed by anodic and cathodic process	28
29	Tin	Succinic acid	Polyethylene glycol	----	Potentiodynamic anodic polarisation techniques	Physical adsorption	29
30	Iron	Surfactant solution	Polypyrrole	----	Electrochemical technique, SEM, EDAX and IR spectroscopy	Anticorrosion property	30
31	Aluminium	0.5 M NaCl	2,5-dimercapto-1,3,4-thiadiazole (polyDMcT)	----	Corrosive environment couples to a base metal – coatings with a defect	Monomer anion very good oxygen reduction Inhibit at cathode	31
32	Carbon steel	NaCl	Polyaniline	----	Redox condition at different coatings on metal	Delamination	32
33	Mild steel	H ₂ SO ₄	Polyvinyl alcohol and Polyethylene glycol	----	Potentiodynamic polarisation techniques ,Electrochemical technique	Temkin, Freundlich and Langmuir adsorption isotherm	33

Table 1. (cont.)

S. No.	Metal	Medium	Inhibitor	Additives	Method	Findings	Ref.
34	Cerium	0.5 M H ₂ SO ₄	Polyaniline	Halides	Potentiodynamic polarisation curves, linear polarisation resistance, electrochemical impedance	High coverage of complex	34
35	Carbon steel	Acid	Poly(nickel-tetraaminophthalocyanine)	----	Electrochemical impedance, FT-IR spectra	Redox & more conductive behaviour	35
36	Mild steel	H ₂ SO ₄ acid	Polyvinyl alcohol	Halides	Weight loss measurement, gasometric (hydrogen evolution) techniques	Flory-huggins, Freundlich and Langmuir adsorption isotherm	36
37	Stainless steel	Acetonitrile	Polyaniline, poly(2-chloroaniline) and poly(aniline-co-2-chloroaniline)	----	Open circuit potential(ocp), Potentiodynamic polarisation techniques, electrochemical impedance, FT-IR spectra & cyclic voltametry	Film as a passivator and barrier	37
38	Iron	Acid	Polyaniline	----	Potentiodynamic polarisation curves, linear polarisation resistance, electrochemical impedance	Passivation tendency of iron	38
39	Stainless steel	Saline solution	Poly(2,5-dimethoxy aniline) / fluoro polymer	----	X-ray photoelectron spectroscopy, open circuit potential, electrochemical impedance	Super corrosion inhibition	39
40	Mild steel	Sodiumhypochlorite (base)	Polyether	----	Spectroscopic measurements, NMR	Biodegradable under cooling water system	40
41	Any Metal	Oil/water	Cationic polymer with anionic surfactant	----	polarisation techniques, electrochemical impedance	Well covering film	41
42	Zinc	Deionised water	Poly(ethylene glycol) (PEG600), poly(ethylene glycol), bis(carboxymethyl)ether	----	In situ scanning tunnelling microscopy (STM)	Incomplete coverage appearance of pits.	42
43	Aluminium	Acidic	Polyvinyl alcohol and polyethylene glycol	Halides	Hydrogen evolution technique	Freundlich adsorption isotherm	43
44	Iron	1 M HCl	P-Aminobenzoic acid and its polymer	----	Ultraviolet reflection studies	Anodic and cathodic process	44
45	Brass	Aqueous	Phosphonic multipolymer	----	Energy dispersive X-ray analysis (EDAX)	Anodic inhibitor	45
46	Stainless steel	0.5 M H ₂ SO ₄	Nation-polyaniline	Chloride	Potentiodynamic polarisation curves, Open circuit potential (ocp)	Inhibiting pitting corrosion	46
47	Carbon steel	3 N H ₂ SO ₄	Polyethylene glycol	----	Weight loss measurement, Electrochemical, polarisation curves, SEM	Cavitation corrosion inhibition	47
48	Mild steel and silver	Sulphuric and perchlorate solution	Poly(thioflavin)	----	Electrochemical impedance technique, infrared reflectance, SEM	Metal chelation with nitrogen or sulphur	48
49	Aluminium	3.5% NaCl	Intrinsically conducting polymer	----	Polarisation resistance method	Hybrid nanocomposite	49
50	Iron	0.5 M H ₂ SO ₄	Poly (diphenylamine)	----	Potentiodynamic polarisation curves, Electrochemical impedance technique, FT-IR spectra	Increase the passivation	50
51	Carbon steel	H ₂ SO ₄	Polyvinyl acetate	----	Voltametric method	Metal coorodability, solution corrosiveness with time	51
52	Tin	Isobutyric acid	Polyethylene glycol	----	Cyclic voltametric method	Decrease the anodic peak <i>i.e.</i> passivation	52

Table 1. (cont.)

S. No.	Metal	Medium	Inhibitor	Additives	Method	Findings	Ref.
53	Amorphous m alloy(Al-Co-Ce)	Aqueous	Conducting polymer	----	Galvanic-ion exchange method	Sacrificial cathodic protection	53
54	Iron	0.1 M chloride	Ultrathin polymer	----	X-ray photoelectron spectroscopy, FT-IR spectra	Arranged two dimensional polymer film	54
55	Gold	0.1 M aqueous H ₂ SO ₄	Poly(p-phenylenediamine)	----	Scanning electrochemical microscopy (SECM), quartz crystal impedance (PQCI), SEM	Porosity and stability	55
56	Aluminium	Weakly alkaline	Polyacrylic acid	----	Weight loss measurement, polarisation curves, impedance technique and EDAX studies	Mixed type inhibitors	56
57	Aluminium	Water	Polyethylene glycol	----	Weight loss measurement	First order kinetics	57
58	Aluminium	Water	Polystyrene and polymethylmethacrylate	----	FT-IR Spectroscopy, AFM and SEM	Quantify Corrosion in crevice	58
59	Zinc	Acidic	Amidopolyethylamines	----	Galvanostic polarisation curves, Electrochemical technique	Langmuir adsorption isotherm	59
60	Aluminium	HCl	Hydroxyl ethyl cellulose	----	Weight loss measurement, Electrochemical technique	Inhibition efficiency increases with increasing concentration of inhibitor	60
61	Mild steel	10% HCl	Lignin polymer	----	Polarisation curves, impedance technique	Temkin adsorption isotherm	61
62	Steel	15% HCl	Poly furfurylalcohol	----	FT-IR Spectroscopy NMR, polarisation curves	Temkin adsorption isotherm	62
63	Mild steel	Acidic	Polyanthranilic acid	----	Weight loss measurement, polarisation curves, impedance technique	Self doped increases the corrosion efficiency	63
64	Iron	Acidic	Guanidine-urea copolymer	----	Electrochemical impedance technique	Antibacterial activity	64
65	Mild steel	1 M HCl	Copolymer of diallyldimethylammonium chloride and diallyldodecyl ammonium chloride	----	Viscosity determination in presence of CTAB	Conducting Polymer Electrolytes Hydrophobes better inhibitor	65
66	Iron	1 M HCl	Polyaniline-polyelectrolyte (polydimethylammoniumchloride)	----	FT-IR, UV-visible, XRD, AFM and electrochemical techniques	Active inhibitors	66
67	Steel and aluminium alloy	3% and 0.1 M NaCl	Polyaniline,poly-o-methoxyaniline	----	Electrochemical impedance technique	Anodic nature by setting the redox potential in the passive potential of the substrate	67
68	Stainless steel	2 M HCl	Polymeric surfactant (C ₆ H ₄ [MA-(CH ₂ CH ₂ O) ₁₀ -N-(CH ₂ CH ₂ O) ₁₀ -MA-BP]n	----	Chemical and electrochemical technique	Surface morphology of stainless steel by gamma ray radiation	68
69	Carbon steel	Chloride	Polyvinylpyrrolidone	----	Weight loss measurement, pH immersion time, FT-IR, UV-visible	Protective film formed	69
70	Mild steel	1 M HCl	Poly(4-vinylpyridine)and potassium iodide	----	Weight loss measurement, polarisation curves, impedance technique	Inhibitive action of (p4vp+KI)	70

Table 1. (cont.)

S. No.	Metal	Medium	Inhibitor	Additives	Method	Findings	Ref.
71	Mild steel	1 M HCl	Poly(ortho-ethoxyaniline)	----	Spectroscopic properties with molecular weights	Temkin adsorption isotherm, Activation corrosion energy	71
72	Carbon steel	Acidic	Polyvinylbenzyltrimethylammonium chloride and latex	----	Polarisation curves, impedance technique	Anodic inhibitors	72
73	Aluminium	Acidic	Polyethyleneglycol	----	Weight loss measurement, polarisation curves, impedance technique, differential pulse polarography, voltammetry	Study of inhibition efficiency was 94% after 24 hrs	73
74	Magnesium	1 M NaOH	6-dihexylamino-1,3,5-triazine-2,4-dithiol monosodium salts	----	Polarisation curves, impedance technique	Corrosion rate decreases	74
75	Carbon steel	corrosive	Polyaniline and polyortho-methoxy aniline	----	FT-IR, UV-visible, SEM	Protection against dissolution	75
76	Zinc	0.5 M NaCl	Sodiumsilicate and cerium (iii)nitrate- (organosiloxane polymer)	----	X-ray photoelectron spectroscopy Electroprobe-microanalysis	Suppression of pitting corrosion	76
77	Mild Steel	HCl	Poly(styrene sulphonic acid)-doped polyaniline	----	Polarisation curves, impedance technique	Anodic inhibitor	77
78	Cadmium	0.5 M HCl	Polyvinyl alcohol, carboxymethyl cellulose, polyacrylate, polyethylene glycol	----	Polarisation curves, impedance technique	Temkin adsorption isotherm	78
79	Aluminium		Poly(2,5-bis(N-methyl-N-alkylamino)phenylenevinylenes	----	Polarisation curves, impedance technique	Temkin adsorption isotherm	79
80	Iron	0.5M H ₂ SO ₄	Poly (aminoquinone)	----	Polarisation curves, impedance technique	Mixed inhibitor to improve the passivation tendency	80
81	Aluminium	3.5% wt of NaCl	Polyaniline	----	Electrochemical studies, optical microscopy, SEM	Duplex coating	81
82	Iron	1M HCl	Polyaniline (PAni), Poly(diallyldimethylammoniumchloride) (PDDMAC)	----	Electrochemical studies, FT-IR, UV-vis spectra, XRD, AFM	Active inhibitors	82
83	Mild steel	H ₂ SO ₄	Co-polymer of maleic anhydride and N-vinyl-2-pyrrolidone (VPMA)	----	Weight loss measurement, polarisation curves, impedance technique, SEM	Langmuir adsorption isotherm	83
84	Mild steel	Neutral Aqueous environment	Polyacrylamide, Phenyl phosphonate	----	Weight loss measurement, polarisation curves, FT-IR	Inhibit corrosion	84
85	Gold and mild steel	HCl & H ₂ SO ₄	Polyacrylamide	----	Cyclic voltammetry, polarisation curves, impedance technique	Langmuir and FloryHuggins isotherms	85
86	Mild steel	HCl	Poly(styrenesulphonic acid)-doped Polyaniline	----	Weight loss measurements, galvanostatic polarisation studies, electropermeation studies and A.C. impedance measurements	Temkin's adsorption isotherm	86
87	Carbon steel	NaCl	Polyaniline	----	Potentiodynamic polarization techniques	Inhibition rather than passivation	87
88	Brass	Alkaline	Poly(3-amino-1,2,4-triazole)	----	Cyclic polarization, chronoamperometry, electrochemical impedance techniques and scanning electronic microscopy	The protective effect of the film formed on brass	88

Table 1. (cont.)

S. No.	Metal	Medium	Inhibitor	Additives	Method	Findings	Ref.
89	Steel	Aqueous	Polypyrrole	----	DC polarization and Electrochemical impedance spectroscopy (EIS)	The corrosion resistance of polypyrrole coated steel	89
90	Mild steel	0.3 M HCl	Polypyrrole/Polyanilinecoatings	----	Cyclic voltammetric electrochemical impedance spectroscopy, polarization and open-circuit potential measurements	passivity protection	90
91	Carbon steel	Acidic	Poly(nickel-tetraamino)phthalocyanine	----	Cyclic voltammetry, UV-vis spectroscopy, FT-IR spectroscopy and spectroelectrochemistry, electrochemical impedance spectroscopy (EIS)	Inhibition efficiency increases	91
92	Aluminium	Oxalic acid	Polyamide	----	Potentiostatic, potentiodynamic anodic polarisation technique	Temkin adsorption isotherm	92
93	Iron	1M H ₂ SO ₄	Poly(4-vinyl pyridine isopentyl bromide) (P4VPIPBt)	----	Weight loss measurements, potentiodynamic polarization techniques	Frumkin adsorption isotherm	93
94	7075 Aluminium alloy	Water	Poly styrene(PS) and Polymethylmethacrylate(PMMA)	----	Potentiodynamic polarization techniques, FT-IR spectroscopy, SEM	Protective film	94
95	Carbon steel	1 M HCl + 1 M H ₂ SO ₄	Poly ethylene glycol	----	Weight loss measurements, potentiodynamic polarization techniques, Electrochemical impedance spectroscopy (EIS)	Langmuir adsorption isotherm	95
96	Iron	0.1 M KClO ₄	16-hydroxy hexadecanateion OH(CH ₂) ₁₅ CO ₂ ⁻ Octadecyltriethoxysilane C ₁₈ H ₃₇ Si(OC ₂ H ₅) ₃	----	Polarisation measurement & electron-probe microanalysis	Protection of passive film	96
97	Stainless steel	0.5 M H ₂ SO ₄	Polyaniline and poly(o-methoxy aniline)	----	Cyclic voltammetry, impedance spectroscopy, Open circuit potential(ocp)	Polymer film on surface	97
98	Aluminium and steel	-----	Polyaniline, polypyrrole and Polythiophene	----	Electrochemical impedance spectroscopy and electrochemical noise methods	Protective film	98
99	Carbon steel	Neutral chloride medium	Carboxymethyl cellulose	----	Weight loss measurement, potentiodynamic polarization techniques, Electrochemical impedance spectroscopy (EIS), FT-IR spectroscopy, AFM	Formation of film with higher resistance on carbon steel	99
100	Mild steel	1 M H ₂ SO ₄	Polyvinyl pyrrolidone	Halides	Weight loss measurement, Hydrogen evolution methods	Freundlich and Temkin adsorption isotherms	100
101	Copper	Neutral tap water	Sodium triphosphosphate	----	Electrochemical methods, x-ray photoelectron spectroscopy (XPS), and scanning electron microscopy	Film formed on the surface	101
102	Carbon steel	Neutral aqueous solution containing chloride	Polyvinyl alcohol	----	Weight loss measurement, UV-vis spectroscopy, FT-IR spectroscopy	Protective film consist Fe ²⁺ -PVA complex	102

Thermodynamic parameters such as changes in free energy, enthalpy and entropy have been calculated for proposed isotherm. Adsorption occurs through polar atoms such as O, N, P and sulphur present in polymers.

Surface analysis

The protective film formed on the metal surface has been analysed by various surface analysis techniques such as FTIR,^{1,2,11-13,22,30,35,37,50,54,58,62,66,69,75,82,84,91,94,99} uv-visible spectra,^{11,12,44,66,69,75,82} SEM,^{1,3,4,15,19,30,47,48,55,58,75,81,94} EDAX,^{30,45,56} AFM,^{4,58,66,82,99} and X-ray photoelectron spectroscopy.^{11,15,22,39,54,66,76,82,101}

Advantages and limitation

Polymers have high molecular weight. Hence as the size of inhibitor increases inhibition efficiency also increases. Polymers have many active centres compared to monomer. Hence they have excellent inhibition efficiency. However the main disadvantage their low solubility in aqueous medium. They have been used in the cooling water system. Polymers such as carboxymethylcellulose,⁹⁹ polyvinyl-alcohol,^{33,36,43,102} polyacrylamide,^{1,25,84,85} polyvinyl pyrrolidone,^{10,17,69,100} poly-o-ethoxy-aniline^{6,12,71,75} and polyaniline^{9,15,21,27,32,34,37,38,66,67,75,81,82,87,97,98} have been used as corrosion inhibitors. Rajendran et al. have used polymers such as polyacrylamide,^{1,84} polyvinylpyrrolidone⁶⁹ and polyvinylalcohol¹⁰² as corrosion inhibitors.

Conclusion

This review paper will be useful to a researcher who would like to select polymer as inhibitors to control corrosion of metals and its alloys in different kinds of environments.

Acknowledgement

The authors are thankful to their respective managements for their help and encouragement.

References

- Manimaran, N., Rajendran, S., Manivannan, M., John Mary, S., *Res. J. Chem. Sci.*, **2012**, 2, 52.
- Banumathi, N., Subhashini, S., Rajalakshmi, R., *E-J. Chem.*, **2010**, 7, S67.
- Yuvan S., Pehkonen, S.O., Liang, B., Ting, Y.P., Neoh, K.G., Kang, E.T., *Corros. Sci.*, **2010**, 52, 1958.
- Leon-Silva, U., Nicho, M.E., Gonzalez-Rodriguez, J.G., Chacon-ava, J.G., Salinas-Bravo, V.M., *J. Solid State Electrochem.*, **2010**, 14, 1089.
- Wan, D., Yuan, S., Neoh, K.G., Kang, E.T., *ACS Appl. Mat Interface.*, **2010**, 2, 1653.
- Shinde, V., Pati, P.P., *Mat. Sci. Eng. Mat. Adv. Technol.*, **2010**, 168, 142.
- Titz, T., Horzenberger, F., Bergh, K.V.D., Grundmeier, G., *Corros. Sci.*, **2010**, 52, 369.
- Aramaki, K., Shimura, T., *Corros. Sci.*, **2010**, 52, 1.
- Beresford, A.L., Hillman, A.R., *Anal. Chem.*, **2010**, 82, 483.
- Umoren, S.A., *Surf. Rev. Lett.*, **2009**, 6, 831.
- Bhandari, H., Choudhary, V., Dhawan, S.K., *Polym. Adv. Technol.*, **2009**, 20, 1028.
- Sankar, A., Kumaravel, M., Rameshkumar, S., Vijayan, M., *Int. J. Chem Appl.*, **2012**, 4, 137.
- Wang, S., Wylde, J.J., *NACE-Int. Corros. Conf. Series.*, **2009**.
- Posner, R., Giza, G., Vlasak, R., Grundmeier, G., *Electrochem. Acta.*, **2009**, 54, 4837.
- Wan, D., Yuan, S.J., Neoh, K.G., Kang, E.T., *J. Electrochem. Soc.*, **2009**, 156, C266.
- Umeron, S.A., Ogbobe, O., Igwe, I.O., Ebensoe, I., *Corros. Sci.*, **2008**, 50, 1998.
- Umeron, S.A., Ebenso, E.E., *Ind. J. Chem. Technol.*, **2008**, 15, 355.
- Achary, A.G., Naik, Y.A., Kumar, S.V., Venkatesha, T.V., *Appl. Surf. Sci.*, **2008**, 254, 5569.
- Elbakari, M., Touir, R., Ebn Touhami, M., Srhiri, A., Benmessaoud, M., *Corros. Sci.*, **2008**, 50, 1538.
- Zhu, L., Mendoza, L., Marzorati, M., Verstraete, W., *J. Chem. and Eng. (China)*, **2008**, 59, 665.
- Sathyanarayanan, S., Jeyaprabha, C., Venkatachari, G., *Mat. Chem. Phys.*, **2008**, 107, 350.
- Wapner, K., Stratmann, M., Grundmeier, G., *Int. J. Adhes.*, **2008**, 28, 59.
- Sachin, H.P., Achary, G., Naik, Y.A., Venkatesha, T.V., *Mat. Chem. Phys.*, **2007**, 104, 422.
- Kowalski, D., Ueda, M., Ohtsukat., *Corros. Sci.*, **2007**, 49, 3442.
- Chamovska, D., Cvetkovska, M., Grchev, T., *J. Ser. Chem. Soc.*, **2007**, 72, 687.
- Benabdellah, M., Oussilm, A., Hammouti, B., Elidrissi, A., Aouniti, A., Dafali, A., Bekkouch, K., Benkaddour, M., *J. Appl. Electrochem.*, **2007**, 37, 819.
- Yagan, A., Pekmez, N.O., Yildiz, A., *Pro. Org. Coat.*, **2007**, 59, 297.
- Manivel, P., Venkatachari, G., *J. Appl. Polym. Sci.*, **2007**, 104, 2595.
- Foad, E.I., Sherbini, E.E., Moussa, S.O., Abd El-Rehim, S.S., Hamed, E., *J. Appl. Electrochem.*, **2007**, 37, 533.
- Lehr, I.L., Saidman, S.B., *Corros. Sci.*, **2007**, 49, 2210.
- Kendig, M., Kinlen, P., *J. Electrochem. Soc.*, **2007**, 154, C195.
- Gabriel, A., Laycock, N.J., McMurphy, H.N., Williams, G., Cook, A., *ECS Transactions.*, **2006**, 1, 37.
- Umoren, S.A., Ebenso, E.E., Okafor, P.C., Ogbobe, O., *Pigm. Resin. Technol.*, **2006**, 35, 340.
- Jeyaprabha, C., Sathyanarayanan, S., Venkatachari, G., *Appl. Surf. Sci.*, **2006**, 253, 432.
- Maranhao, S.L.A., Toma, F.J., Aoki, I.V., *Electrochem. Acta.*, **2006**, 52, 519.
- Umoren, S.A., Ogbobe, O., Ebenso, E.E., Ekpe, U.J., *Pigm. Resin. Technol.*, **2006**, 35, 284.
- Hur, E., Bereket, G., Sahin, Y., *Prog. Org. Coat.*, **2006**, 57, 149.
- Jeyaprabha, C., Sathyanarayanan, S., Venkatachari, G., *J. Appl. Polym. Sci.*, **2006**, 101, 214.
- Moraga, G.A., SilvaPaniago, R.M., *Synth. Met.*, **2006**, 156, 1036.
- Oyaizu, K., Yamaguchi, A., Hayashi, T., Nakamura, Y., *Polym. J.*, **2006**, 38, 343.

- ⁴¹ Knag, M.J., *Dispersion Sci. Technol.*, **2006**, 27, 587.
- ⁴² Cohen-Hyams, T., Ziengerman, Y., Ein-Eli, Y., *J. Power Sources.*, **2006**, 157, 584.
- ⁴³ Ebenso, E.E., Ekpe, U.J., Umoren, S.A., Jackson, E., Abiola, O.K., Oforika, N.C., *J. Appl. Polym. Sci.*, **2006**, 100, 2889.
- ⁴⁴ Manivel, P., Venkatachari, G., *J. Mat. Sci. Technol.*, **2006**, 22, 301.
- ⁴⁵ Wang, C., Wang, L., Song, C.J., *Univ. Sci. Technol.*, **2006**, 13, 164.
- ⁴⁶ Sazou, D., Kosseoglou, D., *Electrochem. Acta.*, **2006**, 51, 2503.
- ⁴⁷ Ashasssi-Sorkhabi, H., Ghalebsaz-jeddi, N., *Ultrason Sonochem.*, **2006**, 13, 180.
- ⁴⁸ Atta, N.F., *Eur. Polym. J.*, **2005**, 41, 3018.
- ⁴⁹ Iroh, J.O., Kottarath, S., Shah, K., Rajamani, D., *Int. SAMPE Symposium and Exhibition(Proceedings)*, **2005**, 50, 2227.
- ⁵⁰ Jeyaprabha, C., Sathiyarayanan, S., Phani, K.L.N., Venkatachari, G.O., *J. Electro. Chem.*, **2005**, 585, 250.
- ⁵¹ Shukla, J., Pitre, K.S.A., *Ind. J. Chem. Sec A.*, **2005**, 44, 2270.
- ⁵² ElSherbini, E.E.F., *J. Electroanal. Chem.*, **2005**, 584, 167.
- ⁵³ Jakab, M.A., Scully, J.R., *Nature Mater.*, **2005**, 144, 667.
- ⁵⁴ Aramaki, K., Shimura, T., *Corros. Sci.*, **2005**, 47, 1582.
- ⁵⁵ Williams, G., McMurray, H.N., *Electrochem. Solid-state Lett.*, **2004**, 7, B13.
- ⁵⁶ Amin, M. A., Abd El-Rehim, S.S., El-Sherbini, E.E.F., Hazzazi, O.A., Abbsas, M.N., *Corros. Sci.*, **2009**, 51, 658.
- ⁵⁷ Abiola, O.K., Otaigbe, J.O.E., *Corros. Sci.*, **2008**, 50, 242.
- ⁵⁸ Matarredona, O.M., Mach, K., Riger, M.M., Rear, E.A.O., *Corros. Sci.*, **2003**, 45, 2541.
- ⁵⁹ Abdullah, M., ElEtre, A.Y., Moustafa, M.F., *Electrochem. Acta.*, **2009**, 27, 615.
- ⁶⁰ Arukalam, I.O., Obidiegwu, M.U., *Academic Res. Int.*, **2011**, 1, 484.
- ⁶¹ Ren, Y., Luo, Y., Zhang, K., Zhu, G., Tan, X., *Corros. Sci.*, **2008**, 50, 3147.
- ⁶² Vishwanathan, S., Halder, N., *Corros. Sci.*, **2008**, 50, 2999.
- ⁶³ Shukla, S.K., Quraishi, M.A., Parakash, R., *Corros. Sci.*, **2008**, 50, 2867.
- ⁶⁴ Lebrini, M., Bentiss, F., Chihib, N.E., Jama, C., Hornez, J.P., Lagrenee, M., *Corros. Sci.*, **2008**, 50, 2914.
- ⁶⁵ Ali, S.A., El-Shareef, A.M., Al-Muallem, H.A., *J. Appl. Polym. Sci.*, **2008**, 109, 3256.
- ⁶⁶ Prakash, S., Rao, C.R.K., Vijayan, M., *Electrochem. Acta.*, **2008**, 53, 5704.
- ⁶⁷ Huerta-Vilca, D., Siefert, B., Moreassr, Pantoja, M.F., Motheo, A.J., *Mol. Crystal Liquid Crystals*, **2004**, 415, 229.
- ⁶⁸ Migahed, M.A., Aly R.O., Al-Sabagh, A.M., *Corros. Sci.*, **2004**, 46, 2503.
- ⁶⁹ Selvaraj, S.K., Kennedy, A.J., Amalraj, A.J., Rajendran, S., Palaniswamy, N., *Corros. Rev.*, **2004**, 22, 219.
- ⁷⁰ Larabi, L., Harek, Y., Traisnel, M., Mansri, A., *J. Appl. Electrochem.*, **2004**, 34, 833.
- ⁷¹ Mekki Daouadji, M., Chelali, N., *J. Appl. Polym. Sci.*, **2004**, 91, 1275.
- ⁷² Bereket, G., Yurt, A., Turk, H., *Anti. Corros. Methods Mater.*, **2003**, 50, 422.
- ⁷³ Shukla, J., Pitre, K.S., Jain, P., *Ind. J. Chem. Sec. A.*, **2003**, 42, 2784.
- ⁷⁴ Mori, K., Kang, Z., Oravec, J., Oishi, Y., *Mater. Sci. Forum.*, **2003**, 419, 889.
- ⁷⁵ Vera, A.R., Romero, B.H., Ahumada, E., *J. Chilean Chem. Soc.*, **2003**, 48, 35.
- ⁷⁶ Aramaki, K., *Corros. Sci.*, **2002**, 44, 1375.
- ⁷⁷ Manickavasagam, R., Karthick, K.J., Paramasivam, M., Iyer, S.V., *Anti. Corros. Methods Mater.*, **2002**, 49, 19.
- ⁷⁸ Khairou, K.S., El-Sayed, A., *J. Appl. Polym. Sci.*, **2003**, 88, 866.
- ⁷⁹ Zaras, P., Stenger-Smith, J.D., Miles, M.H., *Polymeric materials science and engineering proceedings of the ACS division of polymeric materials science and engineering.*, **2006**, 76, 589.
- ⁸⁰ Jeyaprabha, C., Sathiyarayanan, S., Phani, K. L. N., Venkatachari, G., *Appl. Surf. Sci.*, **2005**, 252, 966.
- ⁸¹ Johansen, H.D., Brett, C.M.A., Motheo, A.J., *Corros. Sci.*, **2012**, 63, 342.
- ⁸² Prakash, S., Chepuri, R.K., RaoVijayan, M., *Electrochem. Acta.*, **2008**, 53, 5704.
- ⁸³ Achary, G., Naik, Y.A., Kumar, S.V., Venkatesha, T.V., Sherigara, B.S., *Appl. Surf. Sci.*, **2008**, 254, 5569.
- ⁸⁴ Rajendran, S., Apparao, B.V., Palaniswamy, N., *Electrochem. Acta.*, **1998**, 44, 533.
- ⁸⁵ Grchev, T., Cvetkovska, M., Stafilov, T., Schultze, J.W., *Electrochem. Acta.*, **1991**, 36, 1315.
- ⁸⁶ Manickavasagam, R., Karthik, K.J., Paramasivam, M., Iyer, S.V., *Anti-Corros. Methods Mater.*, **2002**, 49, 19.
- ⁸⁷ Cook, A., Gabriel, A., Siew, D., Laycock, N., *Current Appl. Phys.*, **2004**, 4, 133.
- ⁸⁸ Elbakri, M., Touir, R., Ebn Touhami, M., Shhiri, A., Benmessaoud, M., *Corros. Sci.*, **2008**, 50, 1538.
- ⁸⁹ Iroh, J.O., Su, W., *Electrochem. Acta.*, **2000**, 46, 15.
- ⁹⁰ Zeng, C.L., Ren, Y.J., *J. Power Sources.*, 2008,182,524.
- ⁹¹ Maranhao, S.L.A., Guedes, I.C., Anaissi, F.J., Toma, H.E., Aoki, H.E., *Electrochem. Acta.*, **2006**, 52, 519.
- ⁹² Abdallah, M., Megahed, H.E., Etre, A.Y., Obied, M.A., Mabrouk, E.M., *Bull. Electrochem.*, **2004**, 20, 277.
- ⁹³ Chetounai, A., Medjahed ,K., Benabadij, K.E., Hammouti, B., Kertit, Mansari, A., *Prog. Org. Coat.*, **2003**, 46, 312.
- ⁹⁴ Matarredona, O.M., Mach, K., Rieger, M.M., O'Rear, E.A., *Corros. Sci.*, **2003**, 45, 2541.
- ⁹⁵ Ghalebsaz-jeddi N., Ashassi-Sorkhabi, H., Modirshahla, N., Bahmani-Azar, M., EUROCORR 2008-European Corrosion Congress: Managing Corrosion for Sustainability, Book of Abstracts, p.85.
- ⁹⁶ Aramaki, K., Shimura, T., *Corros. Sci.*, **2010**, 52, 766.
- ⁹⁷ Kilmartin, P.A., Trier, L., Wright, G.A., *Synth. Met.*, **2002**, 131, 99.
- ⁹⁸ Tallman, D.E., Pae, Y., Chen, G., Bierwaganz, G.P., Reems, B., Gelling, V.J., *Cond. Polym. Plast. Ind. Appl.*, **1999**, 201.
- ⁹⁹ Noreen, A.H., Sherine, B., Rajendran, S., *Arab. J. Sci. Eng.*, **2009**, 35, 41.
- ¹⁰⁰ Umoren, S.A., Eduok, U.M., Oguzie, A.E.E., *Electrochem. Acta.*, **2008**, 26, 533.
- ¹⁰¹ Feng, Y., Siow, K.S., Teo, W.K., Tan K.L., Hsieh, A.K., *Corros.*, **1997**, 53, 546.
- ¹⁰² Rajendran, S., Sridevi, S.P., Anthony, S. N., John Amalraj, A., Sundaravadivelu, M., *Anti-Corros. Methods Mat.*, **2005**, 52, 102.

Received: 28.04.2013.
Accepted: 31.05.2013.



STRUCTURE-REACTIVITY CORRELATION IN THE OXIDATION OF SUBSTITUTED BENZYL ALCOHOLS BY IMIDAZOLIUM FLUOROCHROMATE

Poonam, D. Sharma^[a], P. Panchariya^[a], P. Purohit^[a] and Pradeep K. Sharma^{[a]*}

Keywords: Correlation analysis; halochromates; imidazolium fluorochromate; kinetics; mechanism; oxidation

Oxidation of benzyl alcohol and some *ortho*-, *meta*- and *para*-monosubstituted ones by imidazolium fluorochromate (IFC) in dimethyl sulphoxide (DMSO) leads to the formation of corresponding benzaldehydes. The reaction is of first order with respect to IFC. A Michaelis – Menten type of kinetics were observed with respect to the alcohols. The reaction is promoted by hydrogen ions; the hydrogen-ion dependence has the form $k_{obs} = a + b [H^+]$. Oxidation of α,α -dideuteriobenzyl alcohol (PhCD₂OH) has exhibited a substantial primary kinetic isotope effect ($k_H/k_D = 5.86$ at 298 K). The reaction has been studied in nineteen organic solvents and the effect of solvent analysed using Taft's and Swain's multi-parametric equations. The rates of oxidation of *para*- and *meta*-substituted benzyl alcohols have been correlated in terms of Charton's triparametric LDR equation whereas the oxidation of *ortho*-substituted benzyl alcohols with tetraparametric LDRS equation. The oxidation of *para*-substituted benzyl alcohols is more susceptible to the delocalization effect than that of *ortho*- and *meta*- substituted compounds, which display a greater dependence on the field effect. The positive value of η suggests the presence of an electron-deficient reaction centre in the rate-determining step. The reaction is subjected to steric acceleration by the *ortho*-substituents. A suitable mechanism has been proposed.

Corresponding Authors

E-Mail: drpkvs27@yahoo.com

[a] Department of Chemistry, J N V University, Jodhpur 342 005, India

prepared by the reported method^{13b}. Its isotopic purity, as ascertained by its NMR spectra, was $95 \pm 4\%$. Due to

non-aqueous nature of the solvent, toluene-*p*-sulphonic acid (TsOH) was used as a source of hydrogen ions. Solvents were purified by the usual methods^{13c}.

Introduction

Halochromates have been used as mild and selective oxidizing reagents in synthetic organic chemistry¹. Imidazolium fluorochromate (IFC) is also one of such compounds used as mild and selective oxidizing agent in synthetic organic chemistry². A few reports on the oxidation aspects of halochromates, including IFC are available in the literature³⁻⁶. We have been interested in the kinetic and mechanistic studies of the reactions of chromium (VI) species. In continuation of our earlier work⁷⁻¹⁰, we report in the present article the kinetics of oxidation of some monosubstituted benzyl alcohols by IFC in DMSO as solvent. Attempts have been made to correlate reactivity and structure in this reaction. Oxidation of benzyl alcohols with various oxidants is an important area of chemistry both from kinetics¹¹ and preparative point of views¹².

Product analysis

The product analysis was carried out under kinetic conditions. In a typical experiment, benzyl alcohol (5.4 g, 0.05 mol) and IFC (3.10 g, 0.01 mol) were made up to 50 cm³ in DMSO and kept in the dark for *ca.* 15 h to ensure completion of the reaction. The solution was then treated with an excess (200 cm³) of a saturated solution of 2,4-dinitrophenylhydrazine in 2 mol dm⁻³ HCl and kept overnight in a refrigerator. The precipitated 2,4-dinitrophenylhydrazone (DNP) was filtered off, dried, weighed, re-crystallized from ethanol, and weighed again. The yields of DNP before and after re-crystallization were 2.59 g (91 %) and 2.26 g (79 %) respectively. The DNP was found identical (m.p. and mixed m.p.) with the DNP of benzaldehyde. Similar experiments were performed with other alcohols also. The oxidation state of chromium in completely reduced reaction mixtures, determined by an iodometric method was 3.95 ± 0.1 .

Experimental Section

Materials

IFC was prepared by the reported method² and its purity checked by an iodometric method. The procedure used for the purification of alcohols has been described earlier^{13a}. α,α -Dideuteriobenzyl alcohol (PhCH₂OH) was

Kinetic measurement

The pseudo-first order conditions were attained by maintaining a large excess ($\times 15$ or more) of the alcohol over IFC. The solvent was DMSO, unless specified otherwise. The reactions were followed, at constant temperatures (± 0.1 K), by monitoring the decrease in [IFC] spectrophotometrically at 354 nm. No other

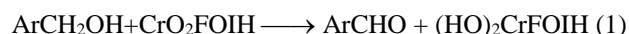
reactant or product has any significant absorption at this wavelength. The pseudo-first order rate constant, k_{obs} , was evaluated from the linear ($r=0.990 - 0.999$) plots of $\log [\text{IFC}]$ against time for up to 80% reaction. Duplicate kinetic runs showed that the rate constants were reproducible to within $\pm 3\%$. The second order rate constant, k_2 , was obtained from the relation: $k_2 = k_{\text{obs}}/[\text{alcohol}]$. All experiments, other than those for studying the effect of hydrogen ions, were carried out in the absence of TsOH.

Results and Discussion

The rates and other experimental data were obtained for all the alcohols. Since the results are similar, only representative data are reproduced here.

Stoichiometry

Oxidation of benzyl alcohols by IFC results in the oxidation of corresponding benzaldehydes. Analysis of products and the stoichiometric determinations indicate the following overall reaction (1).



Thus IFC undergoes a two electron change. This is in accord with the earlier observations with other halochromates⁷⁻¹⁰ also. It has already been shown that both PFC¹⁴ and PCC¹⁵ act as two electron oxidants and are reduced to chromium (IV) species, by determining the oxidation state of chromium by magnetic susceptibility, ESR and IR studies

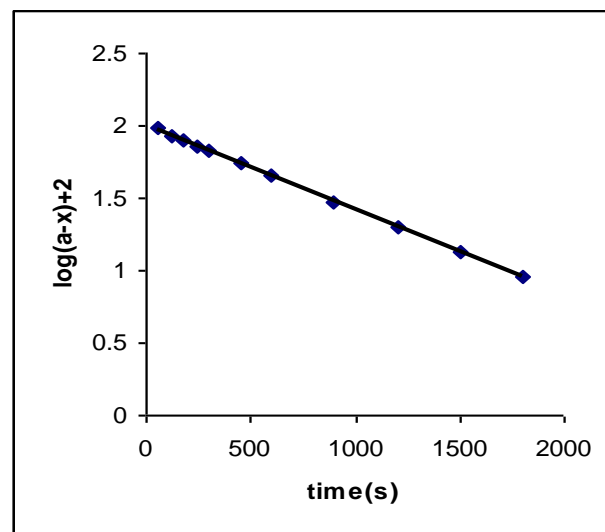
Rate laws

The reactions are of first order with respect to IFC. Figure 1 depicts a typical kinetic run. Further, the pseudo-first order rate constant, k_{obs} is independent of the initial concentration of IFC. The reaction rate increases with increase in the concentration of the alcohols but not linearly (Table 1)..

Table 1. Rate constants for the oxidation of benzyl alcohol by IFC at 298 K

$10^3[\text{IFC}]$, mol dm^{-3}	$[\text{Alcohol}]$, mol dm^{-3}	$[\text{TsOH}]$, mol dm^{-3}	$10^4 k_{\text{obs}}$, s^{-1}
1.0	0.10	0.0	4.62
1.0	0.20	0.0	6.89
1.0	0.40	0.0	9.12
1.0	0.60	0.0	10.2
1.0	0.80	0.0	10.9
1.0	1.00	0.0	11.3
1.0	1.50	0.0	12.0
1.0	3.00	0.0	12.7
2.0	0.40	0.0	10.8
4.0	0.40	0.0	11.7
6.0	0.40	0.0	10.2
8.0	0.40	0.0	10.5
1.0	1.00	0.1	5.46
1.0	1.00	0.2	6.42

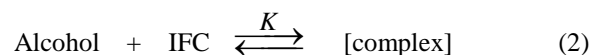
1.0	1.00	0.4	7.84
1.0	1.00	0.6	9.27
1.0	1.00	1.0	12.6
1.0	0.40	0.0	9.72*



*contained $0.001 \text{ mol dm}^{-3}$ acrylonitrile

Figure 1. Oxidation of Benzyl alcohol by IFC: A typical kinetic run

A plot of $1/k_{\text{obs}}$ against $1/[\text{Alcohols}]$ is linear ($r > 0.995$) with an intercept on the rate-ordinate (Figure 2). Thus, Michaelis-Menten type kinetics are observed with respect to the alcohols. This leads to the postulation of following overall mechanism (2) and (3) and rate law (4).



$$\text{Rate} = \frac{k_2 K [\text{Alcohol}][\text{IFC}]}{1 + K [\text{Alcohol}]} \quad (4)$$

The dependence of reaction rate on the reductant concentration was studied at different temperatures and the values of formation constants K and decomposition constants of the complex k_2 were evaluated from the double reciprocal plots. The thermodynamic parameters of the complex formation and activation parameters of the decomposition of the complexes were calculated from the values of K and k_2 respectively at different temperatures (Tables 2 and 3).

Tests for free radicals

The oxidation of benzyl alcohol by IFC, in an atmosphere of nitrogen failed to induce the polymerisation of acrylonitrile. Further, an addition of a

radical scavenger, acrylonitrile, had no effect on the rate (Table 1).

Table 2. Rate constants and activation parameters of oxidation of substituted benzyl alcohols by IFC

Substance	$10^4 k_2, \text{dm}^3 \text{mol}^{-1} \text{s}^{-1}$				$\Delta H^\ddagger,$ kJ mol ⁻¹	$\Delta S^\ddagger,$ J mol ⁻¹ K ⁻¹	$\Delta G^\ddagger,$ kJ mol ⁻¹
	288 K	298 K	308 K	318 K			
H	5.76	13.5	31.5	71.1	61.3±0.6	-95±2	89.3±0.5
<i>p</i> -Me	12.5	28.3	63.0	135	57.9±0.4	-99±1	87.5±0.3
<i>p</i> -OMe	26.1	59.0	126	270	56.6±0.4	-98±1	85.7±0.3
<i>p</i> -F	5.36	12.8	30.6	70.2	62.8±0.6	-90±2	89.5±0.5
<i>p</i> -Cl	3.37	8.19	19.8	46.5	64.1±0.6	-89±2	90.6±0.5
<i>p</i> -NO ₂	0.23	0.64	1.76	4.67	73.9±0.6	-78±2	96.9±0.5
<i>p</i> -CF ₃	0.72	1.87	4.85	12.1	69.2±0.7	-85±2	94.2±0.5
<i>p</i> -COOMe	0.99	2.54	6.45	15.8	67.8±0.6	-87±2	93.5±0.5
<i>p</i> -Br	3.29	8.01	19.4	45.5	64.2±0.7	-89±2	90.6±0.5
<i>p</i> -NHAc	12.6	28.8	64.8	141	58.8±0.6	-97±2	87.5±0.4
<i>p</i> -CN	0.42	1.13	3.02	7.74	71.5±0.2	-81±2	95.5±0.5
<i>p</i> -SMe	14.4	34.6	77.4	162	58.9±0.5	-95±1	87.1±0.1
<i>p</i> -NMe ₂	132	270	531	1080	51.6±0.5	-99±2	82.2±0.4
<i>m</i> -Me	10.4	23.4	52.8	115	58.5±0.6	-99±2	88.0±0.5
<i>m</i> -OMe	10.8	23.7	51.9	108	56.0±0.4	-108±1	87.9±0.3
<i>m</i> -Cl	1.76	4.29	10.4	24.3	64.2±0.6	-95±2	92.2±0.5
<i>m</i> -Br	1.74	4.23	10.3	23.4	63.6±0.4	-96±1	92.2±0.4
<i>m</i> -F	2.16	5.18	12.3	27.9	62.5±0.5	-99±2	91.7±0.4
<i>m</i> -NO ₂	0.18	0.51	1.39	3.67	73.9±0.5	-79±2	97.5±0.4
<i>m</i> -CO ₂ Me	0.95	2.43	6.17	15.3	68.0±0.8	-86±2	93.6±0.6
<i>m</i> -CF ₃	0.65	1.69	4.37	10.8	68.9±0.6	-86±2	94.5±0.5
<i>m</i> -CN	0.33	0.89	2.38	6.12	71.6±0.6	-82±2	96.1±0.5
<i>m</i> -SMe	7.35	16.5	36.9	79.2	57.8±0.5	-82±2	96.1±0.5
<i>m</i> -NHAc	6.51	14.8	33.3	72.9	58.8±0.6	-104±2	89.1±0.4
<i>o</i> -Me	58.5	117	239	468	50.4±0.6	-113±2	83.9±0.5
<i>o</i> -OMe	40.5	81.9	167	324	50.4±0.5	-116±1	84.9±0.4
<i>o</i> -NO ₂	0.61	1.53	3.98	9.81	68.2±0.9	-90±3	94.7±0.7
<i>o</i> -COOMe	4.86	11.2	25.7	56.7	59.9±0.9	-101±2	89.8±0.5
<i>o</i> -NHAc	72.0	142	279	522	47.9±0.3	-120±1	83.5±0.3
<i>o</i> -Cl	12.6	27.0	59.4	124	55.7±0.7	-108±2	87.6±0.5
<i>o</i> -Br	17.1	36.9	77.4	159	54.0±0.4	-111±1	86.9±0.3
<i>o</i> -I	30.2	62.1	126	251	51.2±0.5	-116±1	85.6±0.4
<i>o</i> -CN	1.32	3.24	7.92	18.9	65.0±0.7	-94±2	92.9±0.6
<i>o</i> -SMe	63.0	124	243	459	48.0±0.4	-121±1	83.9±0.3
<i>o</i> -F	6.75	15.3	34.2	74.7	58.5±0.5	-103±2	89.0±0.4
<i>o</i> -CF ₃	13.5	28.7	61.2	126	54.2±0.5	-112±2	87.5±0.4
α, α' -BA	0.94	2.34	5.73	13.7	65.5±0.6	-95±2	93.7±0.5
k_H/k_D	6.12	5.77	5.50	5.19			

Effect of acidity

The reaction is catalysed by hydrogen ions. The hydrogen-ion dependence taking the form: $k_{\text{obs}} = a + b[\text{H}^+]$ (Table 1). The values for *a* and *b* for benzyl alcohol are $4.67 \pm 0.25 \times 10^{-4} \text{ s}^{-1}$ and $8.14 \pm 0.41 \times 10^{-4} \text{ mol}^{-1} \text{ dm}^3 \text{ s}^{-1}$ respectively ($r^2 = 0.9898$)

Kinetic isotope effect

To ascertain the importance of the cleavage of the α -C-H bond in the rate-determining step, oxidation of α, α -di-deuterio benzyl alcohol was studied. Results

showed the presence of a substantial primary kinetic isotope effect (Table 2).

Effect of solvents

The oxidation of benzyl alcohol was studied in 19 different organic solvents. The choice of solvents was limited by the solubility of IFC and its reaction with primary and secondary alcohols. There was no reaction with the solvents chosen. Kinetics were similar in all the solvents. The values of *K* and k_2 are recorded in Table 3.

The correlation between activation enthalpies and entropies of oxidation of the thirty three alcohols is not

very good ($r^2 = 0.9042$). The value of the isokinetic temperature is 593 ± 33 K. However, according to Exner¹⁶, an isokinetic relationship between the calculated values of activation enthalpies and entropies is often vitiated by random experimental errors.

Table 3. Formation constants for the decomposition of IFC–Alcohol complexes and thermodynamic parameters

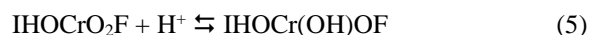
Substance	$K, \text{dm}^3 \text{mol}^{-1}$				$-\Delta H,$ kJ mol^{-1}	$-\Delta S,$ $\text{J mol}^{-1} \text{K}^{-1}$	$-\Delta G,$ kJ mol^{-1}
	288 K	298 K	308 K	318 K			
H	5.85	5.21	4.56	3.88	12.3±0.3	20±1	6.56±0.2
<i>p</i> -Me	5.46	4.82	4.22	3.60	13.0±0.4	23±1	6.37±0.3
<i>p</i> -OMe	5.32	4.70	4.05	3.42	13.7±0.5	25±2	6.29±0.4
<i>p</i> -F	5.56	4.95	4.32	3.65	13.1±0.6	23±2	6.42±0.5
<i>p</i> -Cl	5.90	5.26	4.65	4.03	12.1±0.4	19±1	6.59±0.3
<i>p</i> -NO ₂	6.18	5.53	4.95	4.28	11.7±0.4	17±1	6.72±0.3
<i>p</i> -CF ₃	5.89	5.25	4.65	4.02	12.1±0.4	19±1	6.58±0.3
<i>p</i> -COOMe	5.44	4.82	4.17	3.51	13.6±0.6	25±2	6.35±0.4
<i>p</i> -Br	5.81	5.22	4.50	3.96	12.4±0.4	19±1	6.59±0.3
<i>p</i> -NHAc	6.02	5.40	4.78	4.14	12.0±0.4	18±1	6.65±0.3
<i>p</i> -CN	6.22	5.57	4.95	4.32	11.7±0.4	17±1	6.73±0.3
<i>p</i> -SMe	6.15	5.53	4.90	4.30	11.6±0.3	17±1	6.71±0.3
<i>p</i> -NMe ₂	5.66	5.04	4.41	3.78	12.7±0.4	21±1	6.47±0.4
<i>m</i> -Me	5.73	5.13	4.49	3.87	12.4±0.4	20±1	6.51±0.4
<i>m</i> -OMe	5.45	4.81	4.20	3.53	13.4±0.6	24±2	6.36±0.4
<i>m</i> -Cl	6.13	5.51	4.88	4.23	11.4±0.3	16±1	6.70±0.2
<i>m</i> -Br	5.49	4.86	4.22	3.60	13.2±0.4	23±1	6.38±0.4
<i>m</i> -F	5.99	5.35	4.75	4.12	11.9±0.4	18±1	6.63±0.3
<i>m</i> -NO ₂	6.02	5.40	4.77	4.13	12.0±0.4	19±1	6.65±0.3
<i>m</i> -CO ₂ Me	6.05	5.42	4.80	4.15	12.0±0.4	18±1	6.66±0.3
<i>m</i> -CF ₃	5.98	5.36	4.71	4.06	13.2±0.4	23±1	6.38±0.4
<i>m</i> -CN	60.3	5.41	4.76	4.15	12.1±0.4	19±1	6.60±0.3
<i>m</i> -SMe	5.31	4.70	4.06	3.45	12.0±0.4	18±1	6.65±0.3
<i>m</i> -NHAc	5.94	5.31	4.67	4.06	13.4±0.5	24±2	6.29±0.4
<i>o</i> -Me	5.27	4.65	4.03	3.40	13.6±0.5	25±2	6.27±0.4
<i>o</i> -OMe	6.18	5.56	4.95	4.28	11.7±0.5	17±1	6.72±0.4
<i>o</i> -NO ₂	5.91	5.29	4.65	4.05	12.1±0.4	19±1	6.59±0.3
<i>o</i> -COOMe	5.45	4.82	4.20	3.57	13.2±0.5	23±2	6.36±0.4
<i>o</i> -NHAc	5.92	5.28	4.65	4.05	12.1±0.3	19±1	6.59±0.3
<i>o</i> -Cl	5.61	4.97	4.32	3.75	12.7±0.3	22±1	6.44±0.2
<i>o</i> -Br	5.83	5.21	4.58	3.92	12.5±0.5	21±2	6.55±0.4
<i>o</i> -I	5.79	5.18	4.50	3.93	12.4±0.4	20±1	6.53±0.3
<i>o</i> -CN	6.04	5.40	4.77	4.14	12.0±0.4	19±1	6.65±0.3
<i>o</i> -SMe	5.88	5.22	4.62	4.01	12.2±0.3	19±1	6.57±0.3
<i>o</i> -F	5.86	5.23	4.61	3.95	12.4±0.5	20±2	6.57±0.4
<i>o</i> -CF ₃	5.76	5.13	4.52	3.88	12.5±0.4	20±1	6.52±0.3
α, α' -BA	5.31	4.66	4.03	3.40	13.8±0.5	26±2	6.28±0.4

Exner suggested an alternative method for establishing the isokinetic relationship. Exner's plot between $\log k_2$ at 288 K and at 318 K was linear ($r^2 = 0.9990$) (Figure 3).

The value of isokinetic temperature evaluated from the Exner's plot is 690 ± 37 K. The linear isokinetic correlation implies that all the alcohols are oxidized by the same mechanism and the changes in the rate are governed by changes in both the enthalpy and entropy of activation.

The observed hydrogen-ion dependence suggests that the reaction follows two mechanistic pathways, one acid-independent and another acid-dependent. The acid-catalysis may well be attributed to a protonation of IFC as equation 5 to yield a protonated Cr(VI) species which is a stronger oxidant and electrophile. Formation of a protonated Cr(VI) species has earlier been postulated in the reactions of structurally similar PCC¹⁷.

Reactivity oxidizing species



The rate constants, k_2 , in seventeen solvents (CS₂ was not considered as the complete range of solvent parameters was not available) were correlated in terms

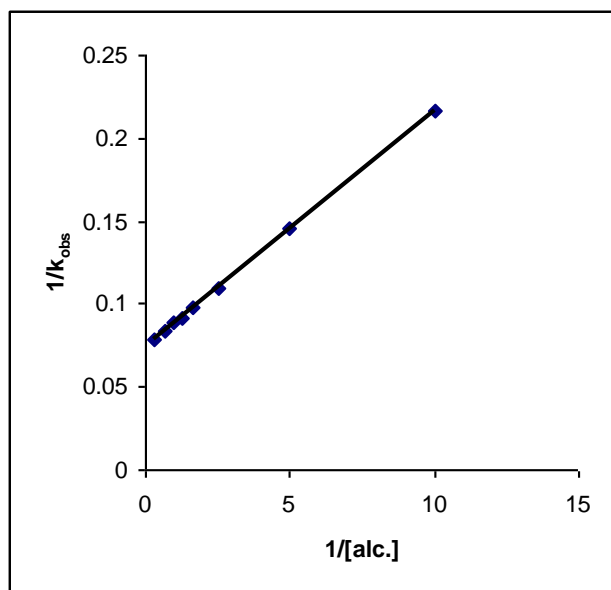


Figure 2. Oxidation of benzyl alcohol by IFC: A double reciprocal plot

$$\log k_2 = A_0 + p\pi^* + b\beta + a\alpha \quad (6)$$

In Eq. (3) π^* represents the solvent polarity, β the hydrogen bond acceptor basicities and α is the hydrogen bond donor acidity. A_0 is the intercept term. It may be mentioned here that out of the 18 solvents, 13 has a value of zero for α . The results of correlation analyses terms of Eq. (3), a biparametric equation involving π^* and β , and separately with π^* and β are given below (equation 7 - 10).

$$\log k_2 = -3.71 + 1.60(\pm 0.21)\pi^* + 0.19(\pm 0.17)\beta + 0.09(\pm 0.16)\alpha \quad (7)$$

$$R^2 = 0.8409; sd = 0.19; n = 18; \psi = 0.44$$

$$\log k_2 = -3.73 + 1.63(\pm 0.20)\pi^* + 0.15(\pm 0.16)\beta \quad (8)$$

$$R^2 = 0.8371; sd = 0.19; n = 18; \psi = 0.43$$

$$\log k_2 = -3.70 + 1.67(\pm 0.19)\pi^* \quad (9)$$

$$r^2 = 0.8271; sd = 0.19; n = 18; \psi = 0.43$$

$$\log k_2 = -3.02 + 0.45(\pm 0.36)\beta \quad (10)$$

of linear solvation energy relationship (Eqn. 6) of Kamlet *et al*¹⁸.

$$r^2 = 0.0878; sd = 0.43; n = 18; \psi = 0.98$$

Here n is the number of data points and ψ is Exner's statistical parameter¹⁹.

Kamlet's¹⁹ triparametric equation explains *ca.* 84 % of the effect of solvent on the oxidation. However, by Exner's criterion the correlation is not even satisfactory (cf. equation 7). The major contribution is of solvent polarity. It alone accounted for *ca.* 83 % of the data. Both β and α play relatively minor roles.

The data on the solvent effect were also analysed in terms of Swain's equation²⁰ of cation- and anion-solvating concept of the solvents equation 11.

$$\log k_2 = aA + bB + C \quad (11)$$

Here A represents the anion-solvating power of the solvent and B the cation-solvating power of the solvent. C is the intercept term. $(A+B)$ is postulated to represent the solvent polarity. The rates in different solvents were analysed in terms of equation (11), separately with A and B and with $(A+B)$.

$$\log k_2 = 0.69 + (\pm 0.05)A + 1.71(\pm 0.03)B - 3.95 \quad (12)$$

$$R^2 = 0.9941; sd = 0.04; n = 19; \psi = 0.08$$

$$\log k_2 = 0.45(\pm 0.57)A - 2.77 \quad (13)$$

$$r^2 = 0.0358; sd = 0.46; n = 19; \psi = 1.01$$

$$\log k_2 = 1.38(\pm 0.13)B - 3.62 \quad (14)$$

$$r^2 = 0.8625; sd = 0.17; n = 19; \psi = 0.38$$

$$\log k_2 = 1.66 \pm 0.13(A+B) - 3.63 \quad (15)$$

$$r^2 = 0.9099; sd = 0.14; n = 19; \psi = 0.31$$

The rates of oxidation of benzyl alcohol in different solvents show an excellent correlation in Swain's equation (12) with the cation-solvating power playing the major role. In fact, the cation-solvation alone accounts for *ca.* 99% of the data. The solvent polarity, represented by $(A+B)$, also accounted for *ca.* 91% of the data. In view of the fact that the solvent polarity is able to account for *ca.*

91 % of the data, an attempt was made to correlate the rate with the relative permittivity of the solvent. However, a plot of $\log(\text{rate})$ against the inverse of the relative permittivity is not linear ($r^2 = 0.0584$, $sd = 0.33$, $\psi = 0.99$).

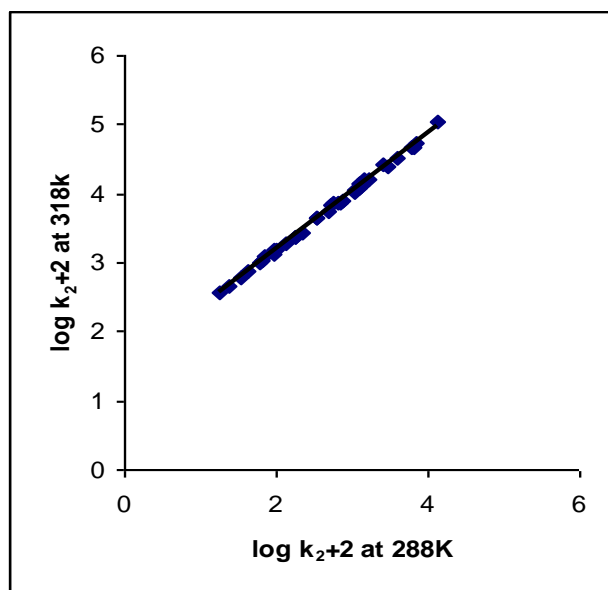


Figure 3. Exner's Isokinetic Relationship in the oxidation of benzyl alcohols by IFC

Correlation analysis of reactivity

The effect of structure on reactivity has long been correlated in terms of the Hammett equation²¹ or with dual substituent-parameter equations^{22,23}. In the late 1980s, Charton²⁴ introduced a triparametric LDR equation for the quantitative description of structural effects on chemical reactivities. This triparametric equation results from the fact that substituent types differ in their mode of electron delocalization. This difference reflected in a different sensitivity to the electron demand for the phenomenon being studied. It has an advantage of not requiring a choice of parameters as the same three substituent constants are reported to cover the range of electrical effects of the substituents. In this work we have applied the LDR equation 16 to the rate constants, k_2 .

$$\log k_2 = L\sigma_1 + D\sigma_d + R\sigma_e + h \quad (16)$$

Here, σ_1 is a localized (field and/or inductive) effect parameter, σ_d is the intrinsic delocalized electrical effect parameter when active site electronic demand is minimal and σ_e represents the sensitivity of the substituent to changes in electronic demand by the active site. The latter two substituent parameters are related by equation (17).

$$\sigma_D = \eta\sigma_e + \sigma_d \quad (17)$$

Here η represents the electronic demand of the reaction site and is given by $\eta = R/D$, and σ_D represents the delocalized electrical parameter of the diparametric LD equation.

For *ortho*-substituted compounds, it is necessary to account for the possibility of steric effects and Charton²⁴, therefore, modified the LDR equation to generate the LDRS equation (15).

$$\log k_2 = L\sigma_1 + D\sigma_d + R\sigma_e + S\nu + h \quad (18)$$

where ν is the well known Charton's steric parameter based on Van der Waals radii.²⁵

Table 4 - Solvent effect on the oxidation of benzyl alcohol by IFC at 298 K

Solvents	K , $\text{dm}^{-3} \text{mol}^{-1}$	$10^4 k_2$, s^{-1}
Chloroform	5.58	41.7
Toluene	5.31	10.7
1,2-Dichloroethane	4.76	51.3
Acetophenone	6.21	60.3
Dichloromethane	4.35	39.8
THF	4.75	19.1
DMSO	5.21	135
t-Butylalcohol	4.38	17.8
Acetone	5.33	44.7
1,4-Dioxane	4.27	20.4
DMF	4.65	64.6
1,2-Dimethoxyethane	5.40	12.3
Butanone	5.85	32.4
CS ₂	4.95	5.25
Nitrobenzene	4.67	47.9
Acetic acid	5.90	7.94
Benzene	6.03	15.5
Ethyl acetate	5.40	16.6
Cyclohexane	5.25	1.51

The rates of oxidation of *ortho*-, *meta*- and *para*-substituted benzyl alcohols show an excellent correlation in terms of the LDR/LDRS equations (Table 4). We have used the standard deviation (sd), the coefficient of multiple determination (R^2), and Exner's¹⁹ parameter, ψ , as the measures of goodness of fit.

The comparison of the L and D values for the substituted benzyl alcohols showed that the oxidation of *para*-substituted benzyl alcohols is more susceptible to the delocalization effect than to the localized effect. However, the oxidation of *ortho*- and *meta*-substituted compounds exhibited a greater dependence on the field effect. In all the cases, the magnitude of the reaction constants decreases with an increase in the temperature, pointing to a decrease in selectivity with an increase in temperature.

All three regression coefficients, L, D and R, are negative indicating an electron-deficient carbon centre in the activated complex for the rate-determining step. The positive value of η adds a negative increment to σ_d ,

reflecting the electron-donating power of the substituent and its capacity to stabilise a cationic species. The positive value of S indicates that the reaction is subject to steric acceleration by an *ortho*-substituent.

Table 5 - Temperature dependence for the reaction constants for the oxidation of substituted benzyl alcohols by IFC

T/K	L	D	R	S	η	R^2	sd	ψ	P_D	P_S	T/K
<i>Para</i> -substituted											
288	-1.71	-1.98	-1.40	-	0.71	0.9999	0.009	0.01	53.7	-	288
298	-1.62	-1.89	-1.36	-	0.72	0.9989	0.001	0.01	53.8	-	298
308	-1.53	-1.80	-1.26	-	0.70	0.9998	0.003	0.02	54.1	-	308
318	-1.43	-1.71	-1.21	-	0.71	0.9998	0.007	0.02	54.5	-	318
<i>Meta</i> -substituted											
288	-1.99	-1.45	-1.16	-	0.80	0.9998	0.002	0.02	42.2	-	288
298	-1.89	-1.35	-1.09	-	0.81	0.9999	0.001	0.01	41.7	-	298
308	-1.80	-1.26	-0.99	-	0.79	0.9999	0.001	0.01	41.2	-	308
318	-1.72	-1.16	-0.94	-	0.81	0.9998	0.004	0.02	40.3	-	318
<i>Ortho</i> -substituted											
288	-1.89	-1.53	-0.79	1.44	0.52	0.9999	0.003	0.01	44.7	25.5	288
298	-1.80	-1.44	-0.70	1.35	0.49	0.9998	0.004	0.02	44.4	25.5	298
308	-1.71	-1.35	-0.65	1.26	0.48	0.9999	0.002	0.01	44.1	25.4	308
318	-1.62	-1.26	-0.55	1.17	0.44	0.9998	0.003	0.02	43.8	25.4	318

To test the significance of localized, delocalized and steric effects in the *ortho*-substituted benzyl alcohols, multiple regression analyses were carried out with (i) σ_1 , σ_d and σ_e (ii) σ_d , σ_e and υ and (iii) σ_1 , σ_e and υ . The absence of significant correlations showed that all the four substituent constants are significant.

$$\log k_2 = -1.52(\pm 0.50)\sigma_1 - 1.53(\pm 0.39)\sigma_d - 3.32(\pm 2.25)\sigma_e - 2.41 \quad (19)$$

$$R^2 = 0.7628; \text{sd} = 0.34; n = 12; \psi = 0.56$$

$$\log k_2 = -1.61(\pm 0.46)\sigma_d - 1.28(\pm 2.87)\sigma_e + 1.06(\pm 0.53)\upsilon - 3.43 \quad (20)$$

$$R^2 = 0.6638; \text{sd} = 0.41; n = 12; \psi = 0.67$$

$$\log k_2 = -2.02(\pm 0.61)\sigma_1 - 0.05(\pm 2.94)\sigma_e + 1.47(\pm 0.55)\upsilon - 2.22 \quad (21)$$

$$R^2 = 0.6457; \text{sd} = 0.42; n = 12; \psi = 0.69$$

Similarly in the cases of oxidation of *para*- and *meta*-substituted benzyl alcohols, multiple regression analyses indicated that both localization and delocalization effects are significant. There is no significant collinearity between the various substituents constants for the three

series. The percent contribution²⁶ of the delocalized effect, P_D , is given by equation (22).

$$P_D = \frac{|D| \times 100}{|L| + |D|} \quad (22)$$

Similarly, the percent contribution of the steric parameter²⁵ to the total effect of the substituent, P_S , was determined by using equation (23).

$$P_S = \frac{|S| \times 100}{|L| + |D| + |S|} \quad (23)$$

The values of P_D and P_S are also recorded in Table 5. The value of P_D for the oxidation of *para*-substituted benzyl alcohols is *ca.* 54% whereas the corresponding values for the *meta*- and *ortho*-substituted alcohols are *ca.* 42 and 44% respectively. This shows that the balance of localization and delocalization effects is different for differently substituted benzyl alcohols. The less pronounced resonance effect from the *ortho*-position than from the *para*-position may be due to the twisting away of the alcoholic group from the plane of the benzene ring. The magnitude of the P_S value shows that the steric effect is significant in this reaction.

The positive value of S showed a steric acceleration of the reaction. This may be explained on the basis high

ground state energy of the sterically crowded alcohols. Since the crowding is relieved in the in the product aldehyde as well as the transition state leading to it, the transition state energy of the crowded and uncrowded alcohols do not differ much and steric acceleration, therefore results.

Mechanism

A hydrogen abstraction mechanism leading to the formation of the free radicals is unlikely in view of the failure to induce polymerization of acrylonitrile and no effect of the radical scavenger on the reaction rate. The presence of a substantial kinetic isotope effect confirms the cleavage of a α -C-H bond in the rate-determining step.

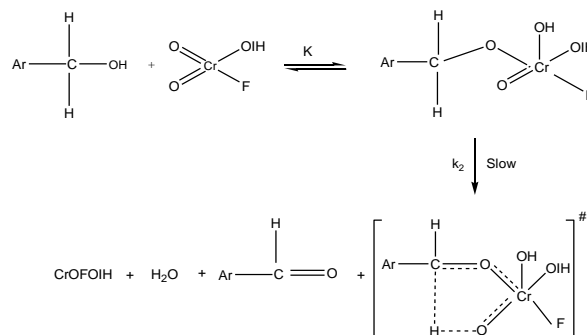
The negative values of the localization and delocalization electrical effects i.e. of L, D and R points to an electron-deficient reaction centre in the rate-determining step. It is further supported by the positive value of η , which indicates that the substituent is better able to stabilise a cationic or electron-deficient reactive site. Therefore, a hydride-ion transfer in the rate-determining step is suggested. The hydride-ion transfer mechanism is also supported by the major role of cation-solvating power of the solvents. The hydride ion transfer may take place either by a cyclic process via an ester intermediate or by an acyclic one-step bimolecular process. Kwart and Nickle²⁶ have shown that a dependence of kinetic isotope effect on temperature can be gainfully employed to determine whether the loss of hydrogen proceeds through a concerted cyclic process or by an acyclic one.

The data for protio- and deuterio-benzyl alcohols, fitted to the familiar expression: $k_H/k_D = A_H/A_D(-\Delta H^*/RT)$ ^{27,28} show a direct correspondence with the properties of a symmetrical transition state in which activation energy difference for protio and deuterio compounds is equal to the difference in the zero-point energy for the respective C-H and C-D bonds ($\approx 4.5 \text{ kJ mol}^{-1}$) and the entropies of activation of the respective reactions are almost equal. Similar phenomena were also observed earlier in the oxidation of benzaldehydes by IFC.²⁹ Bordwell³⁰ has documented a very cogent evidence against the occurrence of concerted one-step bimolecular processes by hydrogen transfer and it is evident that in the present studies also the hydrogen transfer does not occur by an acyclic biomolecular process.

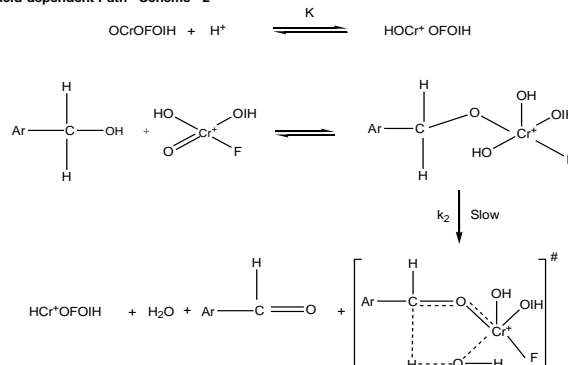
It is well-established that intrinsically concerted sigmatropic reactions, characterised by transfer of hydrogen in a cyclic transition state, are the only truly symmetrical processes involving a linear hydrogen transfer.³¹ Littler³² has also shown that a cyclic hydride transfer, in the oxidation of alcohols by Cr(VI), involves six electrons and, being a Huckel-type system, is an allowed process. Thus, a transition state having a planar, cyclic and symmetrical structure can be envisaged for the decomposition of the ester intermediate. Hence, the overall mechanism is proposed to involve the formation of a chromate ester in a fast pre-equilibrium step and then a decomposition of the ester in a subsequent slow step via a cyclic concerted symmetrical transition state leading to the product (Schemes 1 and 2).

The observed negative value of entropy of activation also supports the proposed mechanism. As the charge separation takes place in the transition state, the charged ends become highly solvated. This results in an immobilization of a large number of solvent molecules, reflected in the loss of entropy.³³

Acid-independent Path - Scheme - 1



Acid-dependent Path - Scheme - 2



Conclusion

The reaction is proposed to proceed through a hydride-ion transfer from alcohol to the oxidant in the rate-determining step. It has also been observed that an α -C-H bond is cleaved in the rate-determining step. Both deprotonated and protonated forms of IFC are the reactive oxidising species.

Acknowledgements

Thanks are due to University Grants Commission, New Delhi for financial support in the form of BSR-One Time Grant, No. F. 4-10/2010 (BSR) dated 07.03.2012.

References

- Corey, E.J., Suggs, W.J. *Tetrahedron Lett.*, **1975**, 2647; Guziec, F.S., Luzio, F.A. *Synthesis*, **1980**, 691; Bhattacharjee, M.N., Choudhuri, M.K., Dasgupta, H.S., Roy, N., Khathing, D.T. *Synthesis*, **1982**, 588; Balasubramanian, K., Prathiba, V. *Indian J. Chem.*, **1986**, 25B, 326;

- Pandurangan, A., Murugesan, V., Palamichamy, P. *J. Indian Chem. Soc.*, **1995**, 72, 479.
- ²Pandurangan A., Rajkumar A., Arabindoo G.A. and Murugesan V. *Indian J. Chem.*, **1999**, 38B, 99.
- ³Kumbhat, R., Prasadrao, P.T.S.R.K., Sharma, V., *Oxid. Commun.*, **2007**, 30 (1) 97.
- ⁴Choudhary, A., Agarwal, S., Sharma, V., *Indian J. Chem.*, **2009**, 48A, 362.
- ⁵Gehlot, M., Gilla, M., Mishra, P., Sharma, V. *J. Indian Chem. Soc.*, **2011**, 88(5) 685.
- ⁶Khatri, J., Choudhary, A., Purohit, P., Kumbhat, R., Sharma, V., *Eur. Chem. Bull.*, **2012**, 1(3 4) 49.
- ⁷Malani, N., Baghmar, M., Sharma, P.K., *Int. J. Chem. Kinet.*, **2009**, 41, 65.
- ⁸Vadera, K., Yajurvedi, D., Purohit, P., Mishra, P., Sharma PK. *Prog. React. Kinet. Mech.*, **2010**, 35, 265.
- ⁹Sharma, D., Panchariya, P., Vadera K., Sharma P.K. *J. Sulfur Chem.*, **2011**, 32(4) 315–326
- ¹⁰ Sharma, D., Panchariya, P., Purohit P., Sharma, P.K. *Oxid. Commun.*, **2012**, 35(4) 821.
- ¹¹Banerji, K. K., *J. Chem. Soc., Perkin Trans. 2*, **1978**, 639; Kumar, A., Sharma, P. K., Banerji, K. K., *J. Phys. Org. Chem.*, **2002**, 15(10), 721–727; Vyas, V. K., Kothari, S., Banerji, K. K., *Int. J. Chem. Kinetics*, **1997**, 29, 9-16; Kothari, S., Banerji, K., *Can. J. Chem.*, **1985**, 63, 2726; Kumar, A., Mishra, P., Kótai L., Banerji, K. K., *Ind. J. Chem.*, **2003**, 42A, 72.
- ¹²Choudhary, V. R., Jha, R., and Jana, P., *Green. Chem.*, **2007**, 9, 267; Bugarcic, Z., Novokmet, S., Kostic, V., *J. Serb. Chem. Soc.*, **2005**, 70(5), 681.; Kotai, L., Kazinczy, B., Keszler, A., Holly, S., Gacs, I., Banerji, K. K., *Z. Naturforsch. B-J. Chem. Sci.*, **2001**, 56(8), 823.
- ^{13a}Banerji, K.K., *Indian J. Chem.*, **1983**, 22B, 413.
- ^{13b}Bunnet, J.F., Devis, G.T., Tanida, H., *J. Am. Chem. Soc.*, **1962**, 84, 1606.
- ^{13c}Perrin, D.D., Armarego, W.L., Perrin, D.R., *Purification of Organic Compounds*, Oxford, Pergamon Press, **1966**.
- ¹⁴Bhattacharjee, M.N., Choudhuri, M.K., Purakayastha S. *Tetrahedron*, **1987**, 43, 5389.
- ¹⁵Brown, H.C., Rao, G.C., Kulkarni, S.U. *J. Org. Chem.*, **1979**, 44, 2809.
- ¹⁶Exner, O. *Collect. Chem. Czech. Commun.*, **1977**, 38, 411.
- ¹⁷Saraswat, S., Sharma, V., Banerji, K.K. *Indian J. Chem.*, **2001**, 40A, 583.
- ¹⁸Kamlet, M.J., Abboud, J L.M., Abraham, M.H., Taft, R.W. *J. Org. Chem.*, **1983**, 48, 2877.
- ¹⁹Exner, O. *Collect. Chem. Czech. Commun.*, **1966**, 31, 3222.
- ²⁰Swain, C.G., Swain, M.S., Powel, A.L., Alunni, S. *J. Am. Chem. Soc.*, **1983**, 105, 502.
- ²¹Johnson, C.D. *The Hammett equation*, University Press, Cambridge, **1973**, 78.
- ²²Dayal, S.K., Ehrenson, S., Taft, R.W. *J. Am. Chem. Soc.*, **1974**, 94, 9113.
- ²³Swain, C.G., Unger, S.H., Rosenquest, N.R., Swain, M.S. *J. Am. Chem. Soc.*, **1983**, 105, 492.
- ²⁴Charton, M., Charton, B. *Bull. Soc. Chim. Fr.*, **1988**, 199 and references cited therein.
- ²⁵Charton, M. *J. Org. Chem.*, **1975**, 40, 407.
- ²⁶Kwart, H., Nickel, J.H. *J. Am. Chem. Soc.*, **1973**, 95, 3394.
- ²⁷Kwart, H., Latimer, M.C., *J. Am. Chem. Soc.*, **1971**, 93, 3770.
- ²⁸Kwart, H., Slutsky, J. *J. Chem. Soc. Chem. Commun.*, **1972**, 1182.
- ²⁹Khatri, J. Choudhary, A., Purohit, P., Kumbhat R., Sharma, V. *Eur. Chem. Bull.*, **2012**, 1(3-4), 49.
- ³⁰Bordwell, F.G., *Acc. Chem. Res.*, **1974**, 5, 374.
- ³¹Woodward, R.W., Hoffmann R. *Angew. Chem. Int. Ed Eng*, **1969**, 8, 781.
- ³²Litler, J.S., *Tetrahedron*, **1971**, 27, 81.
- ³³Gould, E.S. *Mechanism and Structure in Organic Chemistry*, Holt, Rinehart & Winston Inc., NY, **1964**.

Received: 03.05.2013.

Accepted: 05.06.2013.



MAGNETICALLY SEPARABLE CuFe₂O₄ NANOPARTICLES: AN EFFICIENT CATALYST FOR THE SYNTHESIS OF QUINOXALINE DERIVATIVES IN TAP-WATER UNDER SONICATION

Anshu Dandia,^{[a]*} Ruby Singh,^[a] Jyoti Joshi^[b] and Shuchi Maheshwari^[b]

Keywords: Magnetically separable nanoparticles, quinoxaline derivatives, one-pot synthesis, ultrasound irradiation.

A simple and rapid synthetic methodology has been explored exhibiting the use of a magnetically separable copper ferrite (CuFe₂O₄) nanocatalyst in water for the construction of medicinally privileged quinoxalines under sonication. High catalytic activity and ease of recovery using an external magnetic field are additional eco-friendly attributes of this catalytic system.

Corresponding Authors

Tel: +91-941407346; (0141) 2520301

Fax: 0091-141-2523637

E-Mail: dranshudandia@yahoo.co.in

[a] Department of Chemistry, University of Rajasthan, Jaipur, India

[b] Department of Chemistry, Malaviya National Institute of Technology, Jaipur, India

INTRODUCTION

During the last decade, there is a growing emphasis in synthetic chemistry towards the development¹ of sustainable and ecofriendly methodologies. The critical emphasis is towards the growth of green chemistry. The important aspect of green chemistry is the utility of environmentally friendly catalysts with easy recovery of the catalyst after the completion of the reaction.

Considering the above concept, nano catalysts have several benefits over the conventional catalytic systems used.² Although, a significant improvement of catalytic activity can be achieved by utilizing a catalyst in nanometer dimensions due to the increment of its surface area upto many folds. But the recovery of these tiny nanocatalysts from the reaction mixture is not easy. Most of the heterogeneous catalytic systems require a filtration or centrifugation step or a troublesome work-up of the reaction mixture to recover the nanocatalyst. Conventional techniques (such as filtration) are not efficient for the separation of nanocatalyst on account of the nano size of the catalytic particles. This drawback hampers the economics and sustainability of these protocols. To overcome the separation problem of the nano catalysts, magnetically active nano particles have recently emerged as viable alternatives to conventional nanomaterials for catalyst supports.³

Further, the application of sonochemical energy delivery⁴ has become an exciting field of research during the last few years. Ultrasonic irradiation arises from acoustic cavitation, which involves sequential formation, growth and explosive collapse of millions of vaporized bubbles in an irradiated liquid.⁵ Cavitation stimulates very high local temperature to a very large amount of molecules fulfilling their requirement

to attain sufficient active energy for a reaction.⁶ Clearly, reduction in reaction times, improved yields and suppression of side products, less severe reaction conditions,⁷ are some added benefits of this emerging technology making synthetic protocols greener.

Nitrogen-containing heterocyclic molecules are the fundamental structural units studied both by the chemists and biologists. Quinoxalines are one of the important nitrogen-containing heterocyclic compounds which are the core constituents of many pharmacologically active agents.⁸ Quinoxaline drugs CQS (chloroquinoxaline sulfonamide) and XK469 were observed to have anticancer activity against solid tumors. (2-Quinoxalinyloxy)phenoxy propanoic acid derivatives, such as Assure are well known to act as herbicide (Fig. 1).⁹ Quinoxaline structural motif is found in several natural products and antibiotics such as echinomycin, leromycin, and actinomycin,¹⁰ which are known to inhibit the growth of gram-positive bacteria. Compounds with quinoxaline core are used as allosteric dual Akt1 and Akt2 inhibitors,^{11a} human cytomegalovirus polymerase inhibitors,^{11b} Src-Family Kinase p56^{Lck} inhibitors,^{11c} SRPK-1 inhibitors,^{11d} monoamine oxidase A inhibitors.^{11e} Some pyrrolo[1,2-a]quinoxaline derivatives are found to be potent and selective 5-HT₃ ligands.¹² Therefore, these compounds have distinguished themselves as heterocycles with chemical and biological significance. As a result of these significant properties, a variety of synthetic approaches have been reported for the synthesis of quinoxalines.

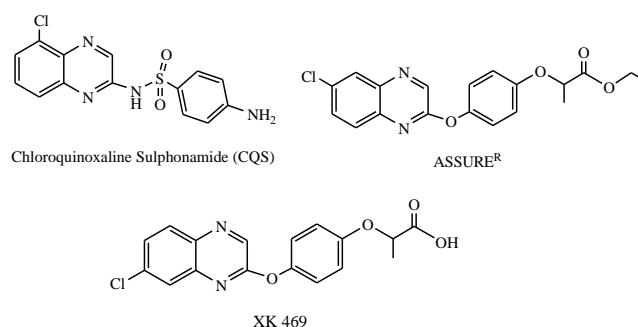


Figure 1. Representatives of quinoxaline ring containing molecules.

The literature survey reveals several reports on the synthesis of quinoxalines using different catalysts such as amidosulfonic acid,^{13a} *p*-TSA,^{13b} Mn octahedral molecular sieves,^{13c} ionic liquid (Hbim)BF₄,^{13d} Ga(OTf)₃,^{13e} SnCl₂,^{13f} montmorillonite K-10,^{13g} DMSO-PdI₂,^{13h} oxalic acid,¹³ⁱ Bi(III),^{13j} Zr(DS)₄,^{13k} ZrO₂ mixed metal oxide,^{13l} silica bonded S-sulfonic acid,^{13m} ZnI₂,¹³ⁿ silica supported SbCl₃,^{13o} NbCl₅,^{13p} amberlyte-15,^{13q} I₂,^{13r} Ru/C,^{13s}.

Recently, several workers have also improved the synthesis of quinoxalines using some modified catalyst and reagent like clayzic,^{14a} silicagel,^{14b} Zr(IV) modified silica gel,^{14c} alumina,^{14d} DABCO,^{14e} Sm(OTf)₂,^{14f} PEG-400 in MW,^{14g} PEG-water,^{14h} glycerol,¹⁴ⁱ silica sulfuric acid in PEG,^{14j} CeCl₃·7H₂O in glycerine,^{14k} FeCl₃ with morpholine,^{14l} triethylamine/O₂,^{14m} Ga(ClO₄)₃,¹⁴ⁿ and graphite^{14o}.

Though the reported methods provide good yields, these methods suffer from several disadvantages such as tedious work-up, harsh and longer reaction times, critical product isolation procedures that limit their use under the aspect of environmentally benign processes. In view of this, there is still need to design a simple and recyclable catalytic system that promotes efficient one-pot synthesis of the functionalized quinoxaline derivatives.

During the course of our studies towards the synthesis of biologically active heterocycles and nanocatalysis,¹⁵ we demonstrated the high catalytic activity of nano crystalline copper ferrite (CuFe₂O₄) for the synthesis of quinoxalines by the reaction of phenanthrenequinone with *o*-phenylenediamine (Scheme-1) in aqueous media for the first time. The method has advantages of ambient reaction condition, environmentally acceptable solvent, high yields, simple work-up and easy catalyst recovery and reusability.

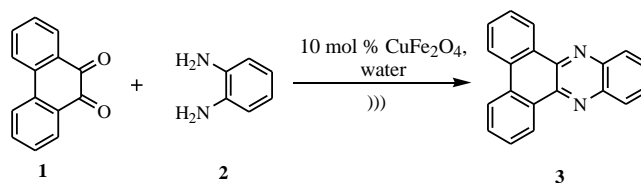
RESULTS AND DISCUSSION

The detailed characterization viz., Transmission Electron Microscopy (TEM), Scanning Electron Microscopy (SEM) and X-ray diffraction (XRD) analyses and synthetic experimental procedure of copper ferrite (CuFe₂O₄) has been published in our previous paper.¹⁶ The quick recovery of the catalyst prompted us to explore its potential use for the synthesis of quinoxalines.

To achieve suitable conditions, the reaction of phenanthrenequinone **1** and *o*-phenylenediamine **2** was chosen as the model reaction to find best conditions for synthesizing **3a** in the presence of catalytic amount of copper ferrite (10 mol %) NPs. In our initial study for the optimization of the reaction conditions, a screening was performed with a variety of different solvents like ethanol, methanol, toluene, acetonitrile and water (Table 1). We noticed that the polar protic solvents afforded better yield than other solvents and the best catalytic activity of nano copper ferrite (10 mol %) was observed in aqueous medium (Table 1). As cavitation in water is most effective as compared to other solvents, the ultrasonic intensity in aqueous solutions is higher because of the low sound absorption coefficient,¹⁷ hence, the effect of nature of solvent on the reactivity is predominant in the present reaction.

The catalytic activity of various catalysts including acidic and nano catalysts such as *p*-TSA, L-proline, sulfamic acid, ZnS and magnetically separable copper ferrite nanoparticles were employed to test their efficacy for the synthesis of **3** using water as solvent under sonication and the results are summarized in Table 2. It was clear that copper ferrite nanoparticles successfully promoted this reaction with high isolated yields. In the absence of catalyst, lower yield of product was obtained under sonication. Therefore, this catalyst appears to be superior to any of the other catalysts tested. Further, to check the role of ultrasound, the reaction was also carried out in boiling water using conventional heating in absence of sonication. In this case, lower yield was obtained with prolonged reaction time. Hence, there is a combined effect of ultrasound and copper ferrite nanoparticles to promote the present reaction.

The quantity of the catalyst plays a vital role for the formation of the desired product. In evaluating the effects of catalyst concentration, the best yields were found in the presence of just 10 mol % copper ferrite NPs. A higher amount of catalyst did not improve the results to an appreciable extent.



Scheme 1: Copper ferrite catalysed synthesis of quinoxalines

Table 1. Effect of different solvents in presence of copper ferrite NPs (10 mol %) under sonication.

Entry	Solvent	Time, min	Yield %*
1.	Water	20	95
2.	Ethanol	60	80
3.	Methanol	60	79
4.	Toluene	60	74
5.	Acetonitrile	60	82

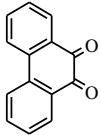
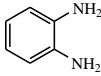
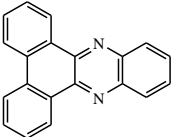
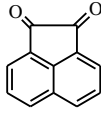
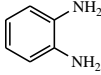
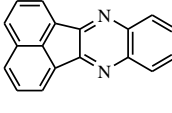
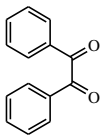
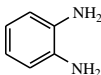
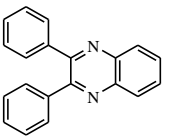
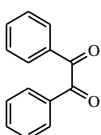
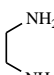
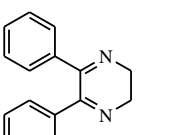
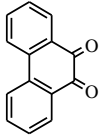
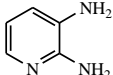
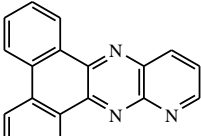
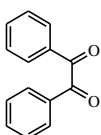
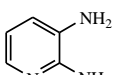
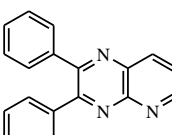
*Isolated Yield

Table 2. Effect of different catalysts in aqueous medium under sonication

Entry	Catalyst	Time, min	Yield %*
1.	-	120	55
2.	<i>p</i> -TSA	60	78
3.	Sulfamic acid	60	83
4.	L-proline	60	61
5.	CuFe ₂ O ₄ NPs (5 mol %)	60	89
6.	CuFe ₂ O ₄ NPs (10 mol %)	20	95
7.	CuFe ₂ O ₄ NPs (20 mol %)	20	95

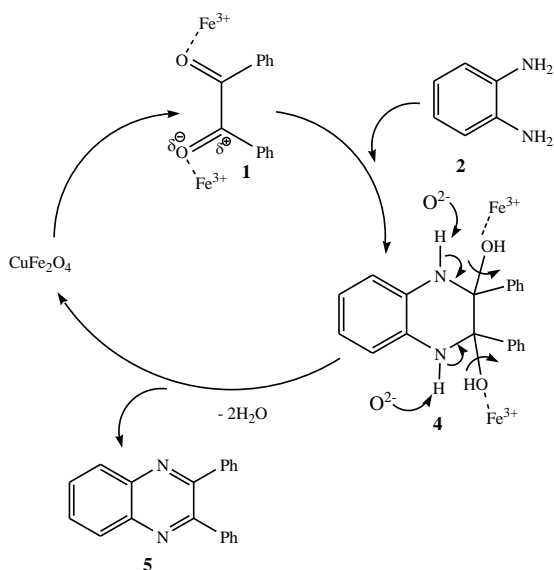
*Isolated yield

Table 3. Synthesis of compounds (3a-f) under sonication

Entry	Carbonyl compound	Amine	Product	Time (min.)	Yield (%) [*]
1				20	95
2				18	93
3				25	91
4				30	89
5				28	92
6				22	90

*Isolated Yield

To generalize the scope and versatility of this protocol, different diketones and diamines are used for the synthesis of substituted quinoxalines (Table 3).

**Scheme 2.** Proposed mechanism for the synthesis of quinoxaline derivatives.

The proposed mechanism for the formation of quinoxaline derivatives is shown in scheme 2. Diketones stabilized by the interaction of Fe³⁺ by partial polarization of carbonyl group reacts readily with *o*-phenylenediamine.

The resultant amino-1,2-diol undergoes base-induced dehydration on account of interaction of O²⁻ to give quinoxaline as the end product.

Here, oxide (O²⁻) of the copper ferrite nanoparticle acts as a Lewis base and Fe³⁺ as a Lewis acid coordinates with the carbonyl oxygen atom of diketones, thus increasing the electrophilicity of the carbonyl carbon.

EXPERIMENTAL SECTION

Melting points were determined on a Toshniwal apparatus. The purity of compounds was checked on thin layers of silica gel in various non-aqueous solvent systems, *e.g.* benzene : ethylacetate (8 : 2), benzene : dichloromethane (9 : 1). ¹H NMR and ¹³C NMR spectra were recorded on Bruker 400 Avance III using DMSO-*d*₆ at 400 and 100 MHz, respectively. TMS was used as internal reference. ESI Mass spectra of representative compounds were recorded on Waters UPLC-TQD Mass spectrometer. The ultrasound-

assisted reactions were carried out using ultrasonic processor probe system (Processor SONOPROS PR-1000MP, OSCAR ULTRASONICS made) operating at 20 KHz, 750 W with 6 mm/12 mm tip diameter probes and provided with an infrared sensor for temperature measurement.

Synthesis of quinoxaline and pyrido[2,3-*b*]pyrazine derivatives (3a-f).

A mixture of appropriate diketone **1** (1.0 mmol) and diamine **2** (1.0 mmol) in water (10 ml) were taken in a flask. The flask was attached to a 12 mm tip diameter probe and the reaction mixture was sonicated for the specified period at 50 % power of the processor at 4 s pulse mode. After the completion of the reaction, TLC was checked and the flask was detached from the probe and the content was transferred into a beaker. The formed product was filtered and washed well with water to afford the pure crystalline product.

Dibenzo[a,c]phenazine (3a)

Yield: 95 %; mp 229-231 °C (lit. 228-229 °C^{13d}); ¹H NMR (400 MHz, DMSO-*d*₆) δ: 7.64 (d, 2H, *J* = 7.2 Hz), 7.89 (dd, 2H, *J* = 5.6, 2.4 Hz), 8.07-8.96 (m, 8H); ¹³C NMR (100 MHz, DMSO-*d*₆) δ: 121.3, 122.4, 122.8, 123.7, 124.6, 125.8, 126.9, 127.7, 128.5, 129.4, 130.6, 131.3, 133.4, 135.1, 141.8, 142.4, 143.2, 143.8; MS (ESI): *m/z* 281[M+H]⁺.

Acenaphtho[1,2-*b*]quinoxaline (3b)

Yield: 92 %; mp 228-230 °C (lit. 224 °C^{14a}); ¹H NMR (400 MHz, DMSO-*d*₆) δ: 7.69-7.92 (m, 6H), 7.83 (dd, 2H, *J* = 6.0, 2.8 Hz), 8.05 (d, 2H, *J* = 7.6 Hz); ¹³C NMR (100 MHz, DMSO-*d*₆) δ: 122.1, 122.7, 123.6, 124.8, 125.2, 125.9, 126.3, 126.8, 127.1, 128.3, 128.7, 130.4, 134.9, 140.2, 141.3, 141.9; MS (ESI): *m/z* 255[M+H]⁺.

2,3-Diphenylquinoxaline (3c)

Yield: 91 %; mp 125-127 °C (lit. 126-127 °C^{14a}); ¹H NMR (400 MHz, DMSO-*d*₆) δ: 7.02-7.19 (m, 6H), 7.26-7.38 (m, 4H), 8.10 (d, 2H, *J* = 7.6 Hz), 8.17 (dd, 2H, *J* = 6.0, 3.2 Hz); ¹³C NMR (100 MHz, DMSO-*d*₆) δ: 124.1, 124.7, 125.2, 125.4, 126.3, 127.0, 128.1, 128.6, 129.7, 130.3, 132.6, 133.9, 134.5, 135.8, 141.7, 142.3, 152.3, 152.9; MS (ESI): *m/z* 283[M+H]⁺.

5,6-Diphenyl-2,3-dihydropyrazine (3d)

Yield: 93 %; mp 162-164 °C (lit. 160-162 °C¹³ⁱ); ¹H NMR (400 MHz, DMSO-*d*₆) δ: 3.56 (s, 4H), 7.08-7.19 (m, 6H), 7.38-7.67 (m, 4H); ¹³C NMR (100 MHz, DMSO-*d*₆) δ: 38.9, 39.4, 125.7, 126.2, 127.4, 127.9, 128.3, 128.8, 129.3, 130.1, 131.2, 158.7, 159.3; MS (ESI): *m/z* 235[M+H]⁺.

Dibenzo[f,h]-pyrido[2,3-*b*]quinoxaline (3e)

Yield: 89 %; mp 226-228 °C (lit. 228-229 °C^{13e}); ¹H NMR (400 MHz, DMSO-*d*₆) δ: 7.07 (d, 1H, *J* = 7.6 Hz), 7.18-7.26 (m, 4H), 7.39-7.47 (m, 4H), 7.86 (d, 1H, *J* = 7.0 Hz),

8.51 (d, 1H, *J* = 7.2 Hz); ¹³C NMR (100 MHz, DMSO-*d*₆) δ: 123.9, 124.2, 127.8, 129.1, 129.8, 130.4, 131.2, 132.5, 137.3, 138.6, 139.1, 141.2, 142.4, 145.0, 145.9, 157.5, 158.2; MS (ESI): *m/z* 282[M+H]⁺.

2,3-diphenylpyrido[2,3-*b*]pyrazine (3f)

Yield: 90 %; mp 136-138 °C (lit. 135-136 °C^{13q}); ¹H NMR (400 MHz, DMSO-*d*₆) δ: 7.18-7.23 (m, 4H), 7.40-7.48 (m, 4H), 7.71 (d, 1H, *J* = 7.6 Hz), 7.83 (t, 1H, *J* = 8.0 Hz), 8.65 (d, 1H, *J* = 7.2 Hz); ¹³C NMR (100 MHz, DMSO-*d*₆) δ: 121.3, 123.6, 124.5, 127.8, 131.6, 131.8, 132.4, 135.7, 136.6, 139.1, 139.4, 139.8, 141.0, 142.3, 153.8, 154.6, 155.7; MS (ESI): *m/z* 284[M+H]⁺.

CONCLUSION

In conclusion, we have developed a novel, efficient and eco-friendly synthetic strategy for the synthesis of quinoxaline derivatives from various 1,2-diketones and 1,2-diamines using magnetically separable copper ferrite (CuFe₂O₄) nanocatalyst. Use of water as a reaction medium rendered this procedure cost-effective and environmentally benign. In addition to its efficiency and simplicity, this method provided high yields of biologically potent quinoxalines in shorter reaction time with the use of ultrasonic irradiation.

ACKNOWLEDGEMENTS

Financial assistance from the C.S.I.R., [CSIR, F. No. 02 (0143)/13/EMR-II], New Delhi is gratefully acknowledged and two of authors also thankful for providing SRA and JRF. We are also thankful to Central Drug Research Institute (CDRI), Lucknow and SAIF, Cochi for spectral analyses.

REFERENCES

- Zonouz, A. M., Eskandari, I., Moghani, D., *Chem Sci Trans.* **2012**, *1*, 91.
- Zhang, Z.-H., Lu, H.-Y., Yang, S.-H., Gao, J.-W., *J. Comb. Chem.* **2010**, *12*, 643 and references therein.
- Polshettiwar, V., Baruwati, B., Varma, R. S., *Chem. Commun.* **2009**, 1837.
- Singh, B. S., Lobo, H. R., Pinjari, D. V., Jarag, K. J., Pandit, A. B., Shankarling, G. S., *Ultrasonics Sonochemistry* **2013**, *20*, 633.
- Gouvêa, D. P., Bareño, V. D. O., Bosenbecker, J., Drawanz, B. B., Neuenfeldt, P. D., Siqueira, G. M., Cunico, W., *Ultrasonics Sonochemistry* **2012**, *19*, 1127.
- Zang, H., Zhang, Y., Zang, Y., Cheng, B.-W., *Ultrasonics Sonochemistry* **2010**, *17*, 495.
- Ocampo, R. A., Koll, L. C., Mandolesi, S. D., *Ultrasonics Sonochemistry* **2013**, *20*, 40.
- Kotharkar, S. A., Shinde, D. B., *Bioorg. & Med. Chemistry. Lett.* **2006**, *16*, 6181 and references therein.
- Kumbhar, A.; Kamble, S.; Barge, M.; Rashinkar, G.; Salunkhe, R. *Tetrahedron Lett.* **2012**, *53*, 2756.
- Meshram, H. M., Kumar, G. S., Ramesh, P., Reddy, B. C., *Tetrahedron Lett.* **2010**, *51*, 2580 and references therein.

- ¹¹(a) Zhao, Z., Robinson, R. G., Barnett, S. F., Jones, D. D., Jones, R. E., Hartman, G. D., Huber, H. E., Duggana, M. E., Lindsley, C. W., *Bioorg. & Med. Chemistry. Lett.* **2008**, *18*, 49; (b) Tanis, S. P., Strohbach, J. W., Parker, T. T., Moon, M. W., Thaisrivongs, S., Perrault, W. R., Hopkins, T. A., Knechtel, M. L., Oien, N. L., Wieber, J. L., Stephanski, K. J., Wathen, M. W., *Bioorg. & Med. Chemistry. Lett.* **2010**, *20*, 1994; (c) Chen, P., Norris, D., Iwanowicz, E. J., Spengel, S. H., Lin, J., Gu, H. H., Shen, Z., Wityak, J., Lin, T. -A., Pang, S., Fex, H. F. D., Pitt, S., Shen, D. R., Doweiko, A. M., Bassolino, D. A., Roberge, J. Y., Poss, M. A., Chen, B. -C., Schievend, G. L., Barrisha, J. C., *Bioorg. & Med. Chemistry. Lett.* **2002**, *12*, 1361; (d) Szekelyhidi, Z., Pato, J., Waczek, F., Banhegyi, P., Barakonyi, B. H., Eros, D., Meszaros, G., Hollosy, F., Hafenbradl, D., Obert, S., Klebl, B., Keri, G., Orfi, L., *Bioorg. & Med. Chemistry. Lett.* **2005**, *15*, 3241; (e) Hassan, S. Y., Khattab, S. N., Bekhit, A. A., Amer, A., *Bioorg. & Med. Chemistry. Lett.* **2006**, *16*, 1753.
- ¹²(a) Campiani, G., Cappelli, A., Nacci, V., Anzini, M., Vomero, S., Hamon, M., Cagnotto, A., Fracasso, C., Uboldi, C., Caccia, S., Consolo, S., Mennini, T., *J. Med. Chem.* **1997**, *40*, 3670; (b) Campiani, G., Morelli, E., Gemma, S., Nacci, V., Butini, S., Hamon, M., Novellino, E., Greco, G., Cagnotto, A., Goegan, M., Cervo, L., Valle, D. F., Fracasso, C., Caccia, S., Mennini, T., *J. Med. Chem.* **1999**, *42*, 4362.
- ¹³(a) Li, Z., Li, W., Sun, Y., Huang, H., Ouyang, P., *J. Heterocyclic. Chem.* **2008**, *45*, 285; (b) Shi, D., Dou, G., *Synth. Commun.* **2008**, *38*, 3329; (c) Sithambaram, S., Ding, Y., Li, W., Shen, X., Gaenzler, F., Suib, S. L., *Green Chem.* **2008**, *10*, 1029; (d) Potewar, T. M., Ingale, S. A., Srinivasan, K. V., *Synth. Commun.* **2008**, *38*, 3601; (e) Cai, J., Zou, J., Pan, X., Zhang, W., *Tetrahedron Lett.* **2008**, *49*, 7386; (f) Shi, D., Dou, G., Ni, S., Shi, J., Li, X., *J. Heterocyclic. Chem.* **2008**, *45*, 1797; (g) Huang, T., Wang, R., Shi, L., Lu, X., *Catal. Commun.* **2008**, *9*, 1143; (h) Mousset, C., Provot, O., Hamze, A., Bignon, J., Brion, J., Alami, M., *Tetrahedron* **2008**, *64*, 4287; (i) Hasaninejad, A., Zare, A., Mohammadzadeh, M. R., Shekouhy, M., *ARKIVOC* **2008**, *xiii*, 28; (j) Yadav, J. S., Reddy, B. V. S., Premalatha, K., Shankar, K. S., *Synthesis* **2008**, *23*, 3787; (k) Hasaninejad, A., Zare, A., Zolfigol, M. A., Shekouhy, M., *Synth. Commun.* **2009**, *39*, 569; (l) Ajaikumar, S., Pandurangan, A., *Applied Catal., A: General* **2009**, *357*, 184; (m) Niknam, K., Saberi, D., Mohagheghnejad, M., *Molecules* **2009**, *14*, 1915; (n) Sangshetti, J. N., Kokare, N. D., Shinde, D. B., *Russ. J. Org. Chem.* **2009**, *45*, 1116; (o) Darabi, H. R., Aghapoor, K., Mohsenzadeh, F., Taala, F., Asadollahnejad, N., Badiei, A., *Catal. Lett.* **2009**, *133*, 84; (p) Hou, J., Liu, Y., Zhang, Z., *J. Heterocyclic Chem.* **2010**, *47*, 703; (q) Liu, J., Liu, J., Wang, J., Jiao, D., Liu, H., *Synth. Commun.* **2010**, *40*, 2047; (r) Bandyopadhyay, D., Mukherjee, S., Rodriguez, R. R., Banik, B. K., *Molecules* **2010**, *15*, 4207; (s) Akkilagunta, V. K., Reddy, V. P., Kakulapati, R. R., *Synlett* **2010**, 2571.
- ¹⁴(a) Dhakshinamoorthy, A., Kanagaraj, K., Pitchumani, K., *Tetrahedron Lett.* **2011**, *52*, 69; (b) Nandi, G. C., Samai, S., Kumar, R., Singh, M. S., *Synth. Commun.* **2011**, *41*, 417; (c) Sharma, R. K., Sharma, C., *Catal. Commun.* **2011**, *12*, 327; (d) Jafarpour, M., Rezaeifard, A., Danehchin, M., *Applied Catal., A: General* **2011**, *394*, 48; (e) Qi, C., Jiang, H., Huang, L., Chen, Z., Chen, H., *Synthesis* **2011**, 387; (f) Raghuvveerachary, P., Devanna, N., *Asian J. Chem.* **2011**, *23*, 1628; (g) Zhang, X., Wang, J., Bai, L., *Synth. Commun.* **2011**, *41*, 2053; (h) Chavan, H. V., Adsul, L. K., Bandgar, B. P., *J. Chemical Sciences* **2011**, *123*, 477; (i) Bachhav, H. M., Bhagat, S. B., Telvekar, V. N., *Tetrahedron Lett.* **2011**, *52*, 5697; (j) Huang, T., Jiang, D., Chen, J., Gao, W., Ding, J., Wu, H., *Synth. Commun.* **2011**, *41*, 3334; (k) Narsaiah, A. V., Kumar, J. K., *Synth. Commun.* **2012**, *42*, 883; (l) Song, W., Liu, P., Lei, M., You, H., Chen, X., Chen, H., Ma, L., Hu, L., *Synth. Commun.* **2012**, *42*, 236; (m) Zhang, C., Xu, Z., Zhang, L., Jiao, N., *Tetrahedron* **2012**, *68*, 5258; (n) Pan, F., Chen, T., Cao, J., Zou, J., Zhang, W., *Tetrahedron Lett.* **2012**, *53*, 2508; (o) Kadam, H. K., Khan, S., Kunkalkar, R. A., Tilve, S. G., *Tetrahedron Lett.* **2013**, *54*, 1003.
- ¹⁵(a) Dandia, A., Jain, A. K., Laxkar, A. K., Bhati, D. S., *Tetrahedron* **2013**, *69*, 2062; (b) Dandia, A., Laxkar, A. K., Singh, R., *Tetrahedron Lett.* **2012**, *53*, 3012; (c) Dandia, A., Jain, A. K., Bhati, D. S., *Tetrahedron Lett.* **2011**, *52*, 5333; (d) Dandia, A., Singh, R., Bhaskaran, S., Samant, S. D., *Green Chem.* **2011**, *13*, 1852; (e) Dandia, A., Singh, R., Bhaskaran, S., *Ultrason. Sonochem.* **2011**, *18*, 1113; (f) Dandia, A., Singh, R., Laxkar, A., *J. Serb. Chem. Soc.* **2011**, *76*, 1339; (g) Dandia, A., Singh, R., Bhaskaran, S., *Ultrason. Sonochem.* **2010**, *17*, 399; (h) Dandia, A., Parewa, V., Gupta, S. L., Rathore, K. S., *Journal of Molecular Catalysis A: Chemical* **2013**, *373*, 61; (i) Dandia, A., Parewa, V., Rathore, K. S., *Catal. Commun.* **2012**, *28*, 90.
- ¹⁶Dandia, A., Jain A. K., Sharma, S., *RSC Adv.* **2013**, *3*, 2924.
- ¹⁷(a) Mason, T. J.; Lorimer, J. P. *Sonochemistry: Theory, Application and Uses of Ultrasound in Chemistry*, John Wiley and Sons, New York **1988**; (b) Mason, T. J. *Ultrason. Sonochem.* **2003**, *10*, 175; (c) Mason, T. J.; Paniwnyk, L.; Lorimer, J. P. *Ultrason. Sonochem.* **1996**, *3*, 253.

Received: 01.05.2013.

Accepted: 07.06.2013.